1-1-2014

Probing Proteasome Inhibition By Metal Copmplexes As A New Route For Anticancer Therapy

Dajena Tomco
Wayne State University,

PROBING PROTEASOME INHIBITION BY METAL COMPLEXES AS A NEW ROUTE FOR ANTICANCER THERAPY

by

DAJENA TOMCO

DISSERTATION

Submitted to the Graduate School

of Wayne State University,

Detroit, Michigan

in partial fulfillment of the requirements

for the degree of

DOCTOR OF PHILOSOPHY

2014

MAJOR: CHEMISTRY (Inorganic)

Approved by:

_____

Advisor Date

_____

_____

_____

DEDICATION

I dedicate this work to my dear parents, Dhimitra and Thomas Tomco, and to my sister Vasiana Tomco. Thank you for all the love and support you have given me through this time and always.

ACKNOWLEDGEMENTS

My greatest appreciation goes to my advisor Prof. Claudio Verani. I would like to thank him for giving me the opportunity to join his lab and allowing me to develop and become the confident scientist I am today. This has truly been a long journey full of challenges and hard work which would have not been possible without his support, encouragement, and constructive criticism. I first joined the Verani Lab as an undergraduate student and was so inspired by his passion for science, teaching, mentoring, and preparing students for real world challenges that I chose to continue my graduate studies in his laboratory. I have learned a tremendous amount from Dr. Verani, and I can honestly say that I will be applying what I've learned from him to my professional career. You are a true inspiration, excellent leader, and role model.

Thank you Dr. Verani!

I would like to express my deepest gratitude to my research committee members: Prof. Stephanie Brock, Prof. Ping Dou, and Prof. Tiffany Mathews. Thank you all for your patience, support, valuable suggestions, and time throughout this program.

I personally thank Prof. Brock for always being highly professional. Her valuable critical comments during my oral exam and pre-defense have greatly served me towards completion of this program. I would also like to thank her for the opportunity to volunteer in the scientific outreach programs of *Go Girls, Go Nano*.

Thank you Dr. Brock, you are truly a great role model to all of the students and faculty!

I extend my appreciation to Prof. Ping Dou for the highly productive collaboration with his lab. Thank you Prof. Dou for allowing me to train in your lab, and providing all of the critical comments on the work that we have published.

I truly appreciate the assistance of Prof. Tiffany Mathews for the valuable comments during my oral exam. I really enjoyed her class during my first semester in the graduate program. Thank you Dr. Mathews for all your support!

Marco Allard is acknowledged for his guidance, help, and criticism when I first joined the Verani Lab as a graduate student. I thank him for his contributions on the computational studies for one of my publications. Thank you Marco!

I appreciate the help and work ethics of Frank Lesh with whom I became friends during graduate school. He taught me that no matter how hard you are hit by cumes, classes, or research, you always have to find the strength to fight back and dominate. I always remembered that, and it kept me positively strong during this program. I thank Frank for his critical suggestions in crystallization techniques and scientific writing. Thank you Frank, you are truly a great friend!

I acknowledge and thank Sara Schmitt for her contributions with the biological studies during this project and her help in training me with the biological assays and protocols in the Dou Lab. She is a second author on two of my published articles.

Sarmad Hindo is acknowledged for training me as an undergraduate student in the Verani Lab, and for being a supportive friend who has provided good advice on career options. I am a third author on two of his publications. I acknowledge Fernando Xavier for his contributions as a second author in the article presented in Chapter 4.

Jeffrey Driscol, a former doctoral student in the Verani Lab, is appreciated for his upbeat spirit, loyal friendship, and positive attitude. Thanks Jeff!

I would like to thank Dr. Rajendra Shakya for his assistance in the lab during this program and the great help he provided me by offering teaching materials.

My group members including Dakshika Wanniarachchi, Rama Shanmugam, Lanka Wickramasinghe, Sunalee Gonawala, and Ryan Thomas have been great colleagues during these years. Thank you for your friendship and support. I would like to thank Debashis Basu, for the great scientific conversations during the lunches at the University Towers.

I would like to thank the three undergraduate students, Matthew Laschuk, Huong Nguyen, and Emily Davis, whom I trained in the Verani Lab during the completion of this work. I wish them all best of luck in their future studies.

Dr. Mary Jane Heeg is acknowledged for her exceptional efforts in solving the X–ray crystallographic structures. I also want to thank Dr. Bashar Ksebati for the NMR training and comments during this program, as well as Dr. Lew M. Hryhorczuk for performing the mass spectrometric analyses of my compounds.

I would like to thank Melissa Barton for her tremendous help during the completion of this work. I appreciate the help and service of Nestor Ocampo, Marty Krol for their assistance with any technical and computer problems. I would like to thank the administrative staff in the chemistry department, including Mary Wood, Jackie Baldyga, Diane Klimas, Diana Kudla, Berny Miesik, Erin Bachert, Debbie McCreless, and Francine Owczarek for their assistance.

I would like to express my greatest appreciation to Prof. Maryfrances Barber for her tremendous support and training during my teaching experience at Wayne State. I appreciate her excellent teaching techniques which I have already implemented in my methods of teaching. I would also like to thank Prof. Regina Zibuck, Prof. Michael Maguire, and Prof. Vladimir Chernyak for their guidance when I was a teaching assistant.

I would like to acknowledge the financial support provided by Graduate School Rumble Fellowship, Summer Dissertation Fellowship, National Science Foundation (NSF), and Karmanos Cancer Institute Pilot Grant, as well as Lumigen Center for all the instrumentations.

TABLE OF CONTENTS

LIST OF FIGURES

LIST OF TABLES

LIST OF SCHEMES

CHAPTER 1

INTRODUCTION

1.1. General Overview

Cancer causes the highest number of deaths worldwide. Each year, over 8 million people perish from this disease.[1] It has been estimated that by 2030 the number of patients dying from cancer will increase by 80%.[2] Prostate cancer is the most common cancer affecting males, while the most common cancer affecting females is breast cancer. According to the American Cancer Society in 2014, approximately 233,000 new cases of prostate cancer are estimated to be diagnosed in males. About 232,670 new cases of breast cancer are projected to be diagnosed in females.[3] In their lifetime, 1 in every 7 American men will be diagnosed with prostate cancer and 1 in every 8 American women will be diagnosed with breast cancer.[3] To date lung and bronchus cancer have the highest death rates with an estimated 159,260 in 2014.[4]

Diagnosis and treatment of cancer has been developed throughout the years. Most of these methods include use of radiation, photodynamic therapies, surgical removal, laser, chemotherapy, and targeted therapy. This later method has been widely successful in the development of organic- and inorganic-based therapeutic drugs that selectively target specific genes, growth factors, and proteins, or interfere with different intracellular pathways that cause cancer. Understanding the chemical mechanism of action of these drugs and their interaction with the intracellular environment has always been a challenge.

In the last four decades, the field of medicinal inorganic chemistry expanded rapidly since metals have proven to be valuable as chemotherapeutic agents for the treatment of various tumors.[5] Ever since the discovery of cisplatin, $[Pt^{II}(NH_3)(Cl)_2]$, in the 1960s[6,7] research has focused on other metal ions including ruthenium,[8] gold,[9] and cobalt[10] as great candidates for

drug development. Although the intracellular molecular target for most of these metal-based drugs is the DNA, other systems such as proteins have proven to be excellent targets in anticancer therapy.

1.2. Proteasome as a Target for Anticancer Therapy

The chemical degradation of biomolecules in cells is performed by two systems including the lysosome and the ubiquitin-proteasome pathway (UPP). Over 80% of the intracellular protein degradation is carried out by the ubiquitin-proteasome system (UPS);[11] the major proteolytic mechanism responsible for degradation of misfolded, oxidized, and damaged cellular proteins in eukaryotes.

In 2004, the Nobel Prize in Chemistry was awarded to Aaron Ciechanover, Avram Hershko, and Irwin Rose for their excellent work on the discovery of UPS.[12,13] The ubiquitin-proteasome pathway involves two major processes: (1) ubiquitination of the damaged or misfolded proteins and (2) proteolysis of such proteins by the 26S proteasome (**Figure 1.2.1**).[14] During ubiquitination, misfolded proteins are appended with ubiquitins (Ub), small proteins of 8.5 kDa which bind to a lysine residue of the substrate.[15] This process is facilitated through a chain of three enzymes: Ub-activating, -conjugating, and -ligating E1, E2, E3, respectively.[16] The degradation process by the 26S proteasome is only performed on the poly-ubiquitinated (four or more ubiquitins attached to the misfolded protein) species. The second process of the ubiquitin-proteasome pathway is proteolysis, an ATP-dependent process, in which ubiquinated proteins undergo peptide bond cleavage in the 26S proteasome.[17] The 26S proteasome is a multicatalytic protein complex with molecular weight of 2500 kDa, composed of the 20S catalytic part and the two regulatory subunits known as 19S.

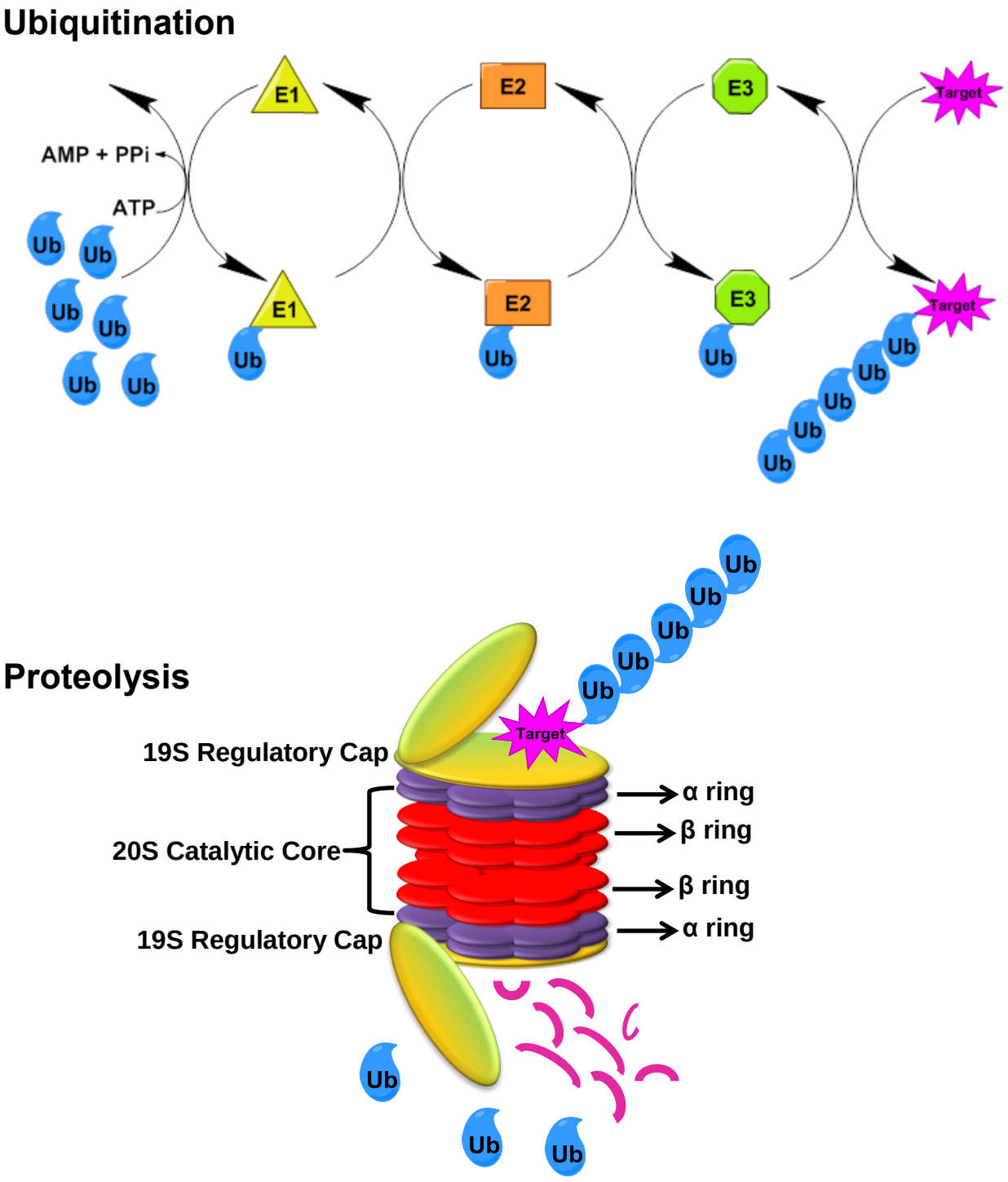

Figure 1.2.1. Degradation of the targeted protein by ubiquitin-proteasome system (adapted from ref. 14).

The catalytic part of the 26S proteasome is flanked between the two 19S regulatory particles and is composed by two α and two β rings (**Figure 1.2.1**). Each of the four rings contains a total of seven subunits.[18] Only three out of the fourteen β subunits are responsible for the catalytic activity of the 20S core and they are known as β_1, β_2, and β_5. The subunit β_1 is responsible for the caspase-like activity and cleaves a peptide bond after acidic amino acids. The β_2 subunit performs trypsin-like activity resulting in a peptide bond cleavage after basic amino acids. The subunit β_5 is responsible for chymotrypsin (CT)-like activity and cleaves a peptide bond after hydrophobic amino acids.[19] Characteristic for the catalytic β subunits is the presence of an N-terminal threonine (Thr) residue which is responsible for the nucleophilic attack during peptide bond cleavage. The α subunits provide structural support to the overall barrel-like core of the 20S proteasome. Parts of the 19S regulatory particles are by two subcomplexes known as the lid and the base.[20] The main function of the lid is to remove the ubiquitin tags from the substrate prior to degradation by the catalytic site,[21] while the base unfolds the targeted substrate and directs it towards the 20S core.[22] Degradation of ubiquitinated proteins through the catalytic chamber of the proteasome results in generation of smaller peptide units comprised of 3 to 22 amino acids.

Besides the degradation of damaged proteins, the ubiquitin proteasome system is also involved in regulation of various nuclear growth factors, signal transduction, and the control of cell apoptosis.[23] Regulation of such cellular growth factors is crucial for normal functioning of the cell. One of these growth factors is NF-κB which promotes DNA transcription. Under normal cell conditions NF-κB is bound to the IκB inhibitor, which blocks the activation of NF-κB.[24] Due to external stimuli, such as stress, the IκB complex will be ubiquinated, thus entering the UPP for degradation and releasing the NF-κB unit. At this point, the NF-κB factor will enter the nucleus

and promote transcription; hence, enhancing cellular proliferation. Cancer cells are characterized by uncontrolled cell growth,[25] due to higher levels of proteasome activity[26] compared to normal cells. Therefore, inhibition activity of the proteasome presents an excellent mechanism in anticancer therapy.

To date, most of the known proteasome inhibitors are designed to inhibit the activity of the catalytic subunits of the proteasome, particularly the chymotrypsin-like activity. Classes of the most common proteasome inhibitors include: peptide aldehydes,[27] boronic acid,[28] vinyl sulfones,[29] and epoxyketones.[30] The most studied 20S proteasome inhibitor is bortezomib (**Figure 1.2.2**, **top**) known as VELCADE or PS341.[31] It is the first FDA approved proteasome inhibitor for treatment of non-Hodgkin lymphoma and various myeloma.[32] The chemical structure of this boronic acid contains the fragment of Pyz-Phe-Leu (pyrazinoic acid-phenylalanine-leucine) which gives this drug highest affinity towards the terminal threonine the β_5 subunit of the catalytic core.[33] The mechanism of inhibition activity of the chymotrypsin-pocket involves formation of a tetrahedral adduct[18] (pharmacophore) with the terminal threonine residue (**Figure 1.2.2**, **bottom**). Even though bortezomib has shown much success with treatment of hematological malignancies, it has failed in treatment of solid tumors.[34] This drug is expensive and exhibits high levels of toxic side effects, including fatigue, nausea, diarrhea, thrombocytopenia, and lymphopenia.[35,36] Hence, there is a quest for the development of other drug candidates with higher potency against solid tumors, and to understanding the mechanisms of action towards the proteasome. Appropriate candidates would be metal-containing drugs which consist of the ligand carrier and the metal ion. The ultimate goal of the current research is to develop novel anti-cancer proteasome inhibitors that display multiple inhibition mechanisms and less toxicity. The advantage of developing metal-containing proteasome inhibitors rests on

the versatility in tuning the coordination number, charge, redox activity, geometry, and intracellular selectivity.

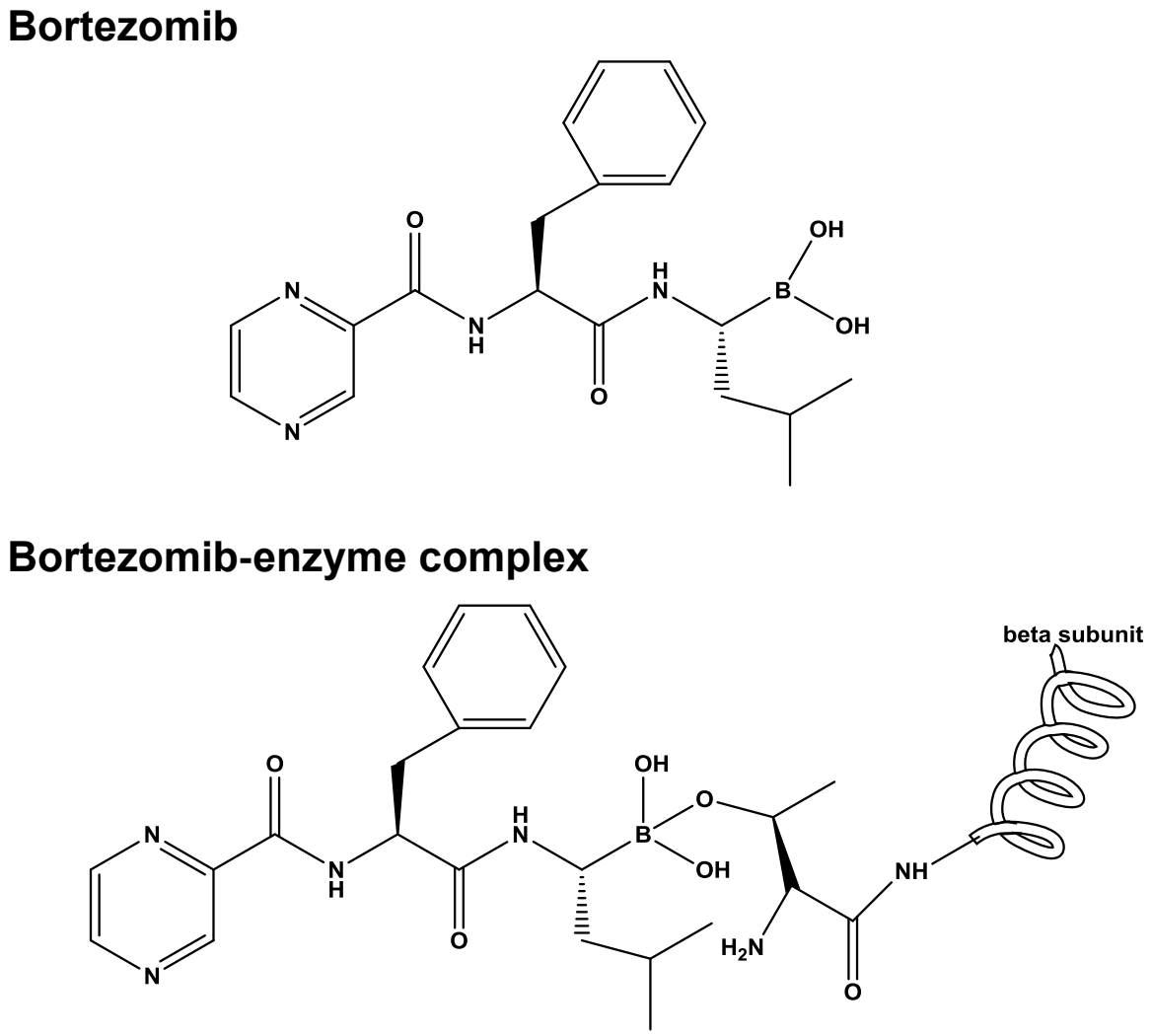

Figure 1.2.2. Chemical structure of bortezomib (top) and tetrahedral adduct (bottom) (adapted from ref. 18).

1.3. Metal Complexes as Potential Pro-Drugs

The first efforts made towards the development of metal-based proteasome inhibitors were presented from the Dou Lab where different ligands including disulfiram,[37] clioquinol,[38] and dithiocarbamate [39] were mixed with copper salts and tested against the inhibition of proteasomal activity in LNCaP, C4-2B, and PC-3 prostate cancer cells,[40] followed by *in vivo* studies.[34] These results showed considerable inhibition activity of the proteasome and induction of cell apoptosis for all complexes. Inspired by these findings, we focused our efforts in the development of novel stochiometrically defined metal-containing anticancer pro-drugs with the aim of understanding the solution-based behavior of these compounds by addressing: (1) the chemical nature of the ligands, (2) the role of metal ions, (3) the appropriate ratio between metal ions and ligands, (4) the chemical structure of the pharmacophore.[41,42]

For the past few years, we have reported on the synthesis and characterization of a series of gallium(III) complexes $[Ga^{III}(L^{X})_2]ClO_4$, where X = methoxy (MeO–), nitro (NO_2–), chloro (Cl–), bromo (Br–), and iodo (I–) occupy the 4th and 6th position of the phenolate ring in the asymmetric NN'O-containing ligand (**Scheme 1.3.1**).[43]

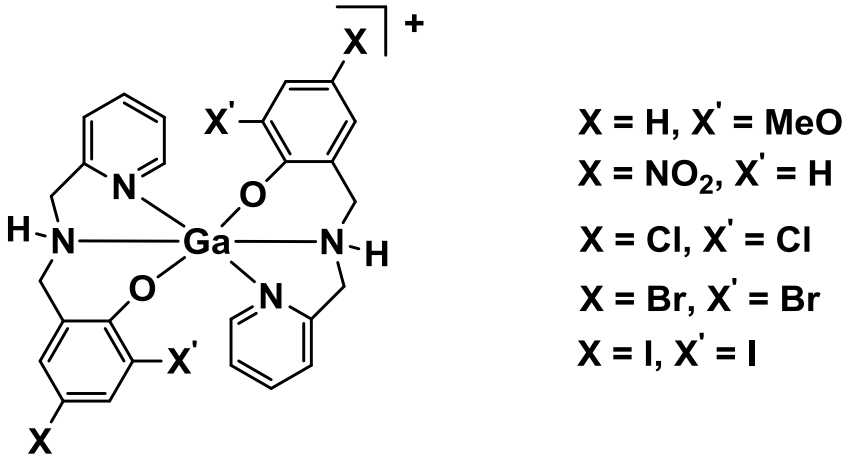

Scheme 1.3.1. Chemical structure of gallium(III)-containing complexes.

Anti-cancer properties of these complexes were tested against the growth of neuroblastoma cells. The halogen-containing species on the phenolate ring possessed superior antineoplastic properties compared to the methoxy- and nitro-containing species. This study concluded that functionalization of the phenolate ring with the halogen groups (I, Br, Cl) enhances the anti-proliferative effects of these gallium complexes. To address the cause of apoptosis induction in cancer cells, the abovementioned five gallium(III) complexes were tested as inhibitors of the activity of proteasome.[41] Results with purified proteasome demonstrated that the halogen-containing gallium(III) complexes were more potent, with the best inhibition shown by the iodo-substituted gallium complex.

Consistent results were obtained when the halogen-containing gallium(III) complexes were tested in various prostate cancer cell lines. The $[Ga^{III}(L^{I})_2]ClO_4$ complex showed the highest inhibitory effects of the CT-like activity of the 26S proteasome with IC_{50} (concentration at 50% cell death) = 17 μM. In addition, this complex showed promising results *in vivo*, by reducing the tumor growth in PC-3 xenografted nude mice by 66% due to proteasome inhibition.[44] This data allowed us to conclude that functionalization of the phenolate ring by iodo-substituents is effective towards the inhibition activity of the proteasome in cancer cells.

In order to address how the stoichiometry of metal to ligand ratio affects the inhibition activity of the proteasome, three copper-containing[47] complexes were synthesized with 1:1 $[Cu^{II}(L^{I})Cl]$, $[Cu^{II}(L^{I})OAc]$ and 1:2 $[Cu^{II}(HL^{I})(L^{I})]OAc$ metal to ligand ratios (**Scheme 1.3.2**), where L is the deprotonated form of (2,4-diiodo-6-((pyridine-2-ylmethylamino)methyl)phenol) ligand. Spectroscopic and spectrometric characterization of these complexes confirmed the four and five coordination arrangement of the Cu(II) (d^9 configuration) ion around the ligand.[42] The anticancer properties of these copper-containing complexes resulted in comparable IC_{50} values of

~4.0 μM against the growth of human leukemia cells.[47] Consistently, inhibition of CT-like activity in C4-2B cancer cells resulted in over 80% at 15 μM for all three copper complexes.

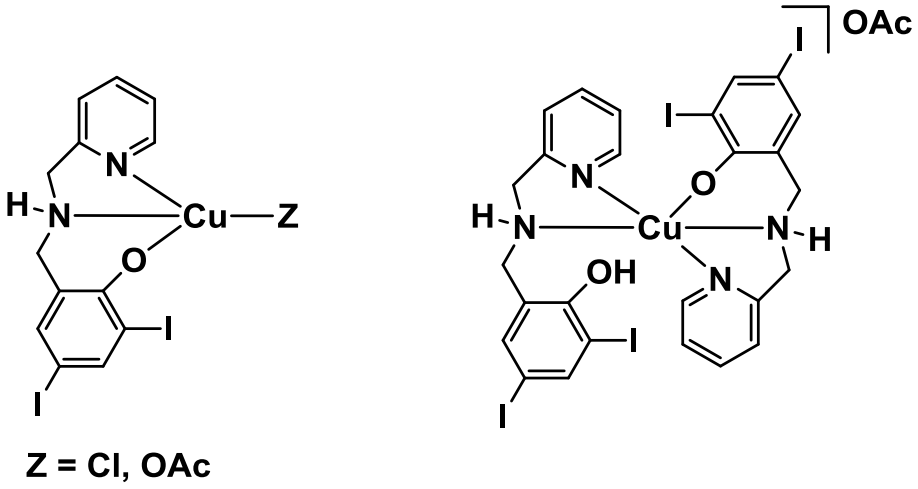

Scheme 1.3.2. Chemical structures of four- and five-coordinate copper(II)-containing complexes.

Due to these pharmacological results, it is suggested that 1:1 metal-to-ligand species is the proposed pharmacophore that could possibly interact with the threonine residue of the chymotrypsin-like activity of 20S core.[45] To evaluate this hypothesis, two complexes $[Zn^{II}(L^{I})_2]$ and $[Ni^{II}(L^{I})_2]$ were synthesized and characterized (**Scheme 1.3.3**).[46]

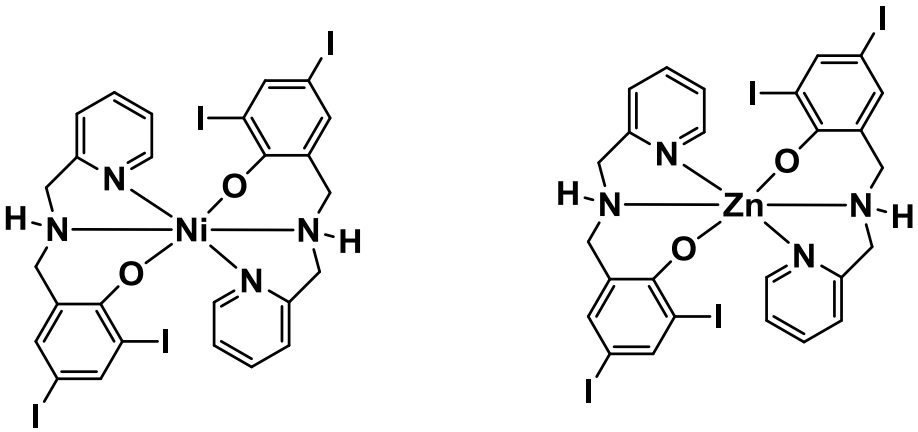

Scheme 1.3.3. Chemical structures of nickel(II)- and zinc(II)-containing complexes.

The pharmacological effects of these species have been investigated *in vitro*, in cultured human cancer cells C4-2B. The zinc-containing complex inhibits the 26S proteasome activity in prostate cancer cells with IC_{50} = 4.4 μM, whereas no such inhibition was observed for the nickel-containing complex. The differences in the cytotoxic effects of these complexes could be possibly explained by the nature of the metal ion. The labile the zinc(II) ion due to lack of ligand-field stabilization energy (LFSE) allows the formation of 1:1 metal-to-ligand species in solution. On the other hand, the inert character of nickel(II) ion due to a non-zero LFSE does not favor the formation of 1:1 metal-to-ligand species.[43] From these studies, we have concluded that the presence of an $[ML^1]^+$ species as the pharmacophore, is necessary for proteasomal inhibition. This observation supports the current hypothesis that ligand dissociation is required in the mechanism to form species capable of interacting with the proteasome (**Figure 1.3**).

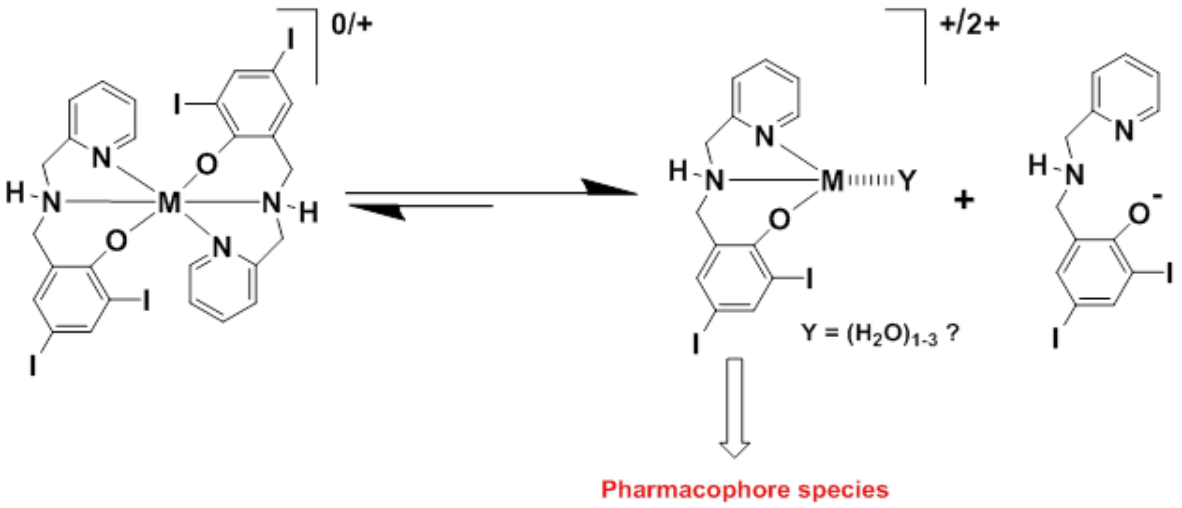

Figure 1.3. Proposed dissociation mechanism of pharmacophore formation.

This dissertation focuses on understanding the fundamental use of transition and main group metal complexes as inhibitors of the 26S proteasome *in vitro*. Our approach involves: (1) the selection of appropriate metal ions in well-understood ligand moieties for interaction with the

proteasome, and (2) ligand optimization that allows for the elucidation of mechanisms of proteasomal inhibition in prostate cancer cell lines, since prostate cancer is classified as an aggressive carcinoma[47] with even higher proteasomal activity. Therefore, prostate cancer cells are expected to be more sensitive against inhibition of the proteasome activity. Some of the factors that promote prostate cancer are related to the environment. For instance, cadmium is a human carcinogen[48] and patients with smoking habits develop more aggressive forms of prostate cancer than non-smokers due to cadmium accumulation in the prostate.[49] Other toxic metals such as mercury[50] and lead[51] have been found to promote prostate cancer. Hence, part of this research investigates whether the toxicity of these heavy metal ions can be correlated with their interaction with proteasome in non-cancerous epithelial prostate cells.

1.4. Research Statements

The principal motivation behind this research project is defined within the scope of the following research statements:

I. To understand the mechanisms of metal-based inhibition of the 26S proteasome by developing metal-containing anticancer pro-drugs for the treatment of prostate cancer. This approach takes advantage of the tunability of the electronic properties and reactivity of the resulting pharmacophores. For this research, we studied the use of transition and main group metal complexes as inhibitors of the 26S proteasome *in vitro*, by: (1) the selection of appropriate metal ions (inert/labile, redox active, charge) in known ligand moieties for interaction with the proteasome and (2) optimization of the ligand that allows for elucidation of mechanisms for proteasomal inhibition.

II. To investigate whether the proteasome is one of the targets for the toxicity of heavy metal ions in non-cancerous epithelial prostate cells. Synthesis and characterization of these complexes along with the biological studies will be evaluated.

These aims will be accomplished via four research objectives presented in the next section.

1.5. Research Objectives

The strategies and different solutions used to address the Research Statements will be presented as the following research objectives, described in **Chapters 3-6**.

Objective #1: ***To interrogate the mechanism of inhibition of the 26S proteasome using inert/labile metal ions coordinated to NN'O tridentate and $N_2N_2'O_2$ hexadentate ligands.*** This aim focuses on the role of the metal ion (kinetically inert or labile) and the nature of the chelating ligands on the inhibition of CT-like activity of the purified proteasome and intact prostate cancer cells. The results of this objective will be introduced in **Chapter 3**. A thorough analysis of synthetic and chemical characterization procedures will be discussed, as well as an extensive evaluation of the biological testing in purified proteasome and prostate cancer cells.

Objective #2: ***To investigate chemical reduction as a viable mechanism for the generation of pharmacophore species involved in the inhibition of the 26S proteasome.*** This aim focuses on evaluating the viability of ligand dissociation in order to form the active pharmacophore $[ML^1]^+$ species of an inert cobalt(III) complex as an inhibitor of the chymotrypsin-like activity of the 26S proteasome. **Chapter 4** details the investigation of the electrochemical behavior of this complex in solution.

Objective #3*: To probe the effect of the ion charge towards the inhibition activity of 20S proteasome.* In order to advance this objective a new series of gallium(III) and zinc(II) ions coordinated to a hexadentate $N_2N_2'O_2$ ligand were

prepared and the activity of these complexes towards purified proteasome and prostate cancer cells are studied. These findings are discussed in **Chapter 5**.

Objective #4: ***To evaluate the effect of aluminum and heavy metal ions on the inhibition activity of the 20S and 26S proteasome in non-cancerous prostate cells.*** In this study we are interested in the comparison of the activity of the proteasome in CRL2221 transformed human prostate epithelial cells, which mimic the behavior of normal prostate cells treated with complexes containing toxic metal ions; such as, Al(III), Cd(II), Hg(II), Pb(II), and Sn(IV). A detailed discussion on the purpose of this study is provided in **Chapter 6** and includes validation of the potential role of such heavy metal species towards the inhibition activity of the proteasome.

1.6. References

1 Statistical analysis on cancer: http://progressreport.cancer.gov

2 http://www.cdc.gov/cancer/dcpc/resources/features/worldcancerday/

3 http://www.cancer.org

4 http://seer.cancer.gov/statfacts/html/all.html

5 Goodman, L. S.; Gilman, A. *Macmillan* **1985**.

6 Rosenberg, B.; Van Camp, L.; Krigas, T. *Nature* **1965**, *205*, 698.

7 Rosenberg, B.; Van Camp, L.; Trosko, J. E.; Mansour, V. H. *Nature* **1969**, *222*, 385.

8 Jakupec, M. A.; Galanski, M.; Arion, V. B.; Hartinger, C. G.; Keppler, B. K. *Dalton Trans.* **2008**, 183.

9 Milacic, V.; Fregona, D.; Dou, Q. P. *Histol. Histopathol.* **2008**, *23*, 101.

10 Hambley, T. *Dalton Trans.* **2007**, 4929.

11 Lee, D. H.; Goldberg, A. L. *Trend. Cell Biol.* **1998**, *8*, 397.

12 Hershko, A.; Ciechanover, A.; Heller, H.; Haas, A. L.; Rose, I. A. *Proc. Natl. Acad. Sci.* **1980**, *77*, 1783.

13 Hershko, A.; Ciechanover, A. *Annu. Rev. Biochem.* **1982**, *51*, 335.

14 Mani, A.; Gelman, E. P. *J. Clin. Onc.* **2005**, *23*, 4776.

15 Haas, A. L.; Warms, J. V.; Hershko, A.; Rose, I. A. *J. Biol. Chem.* **1982**, *257*, 2543.

16 Rajkumar, S. V.; Richardson, P. G.; Hideshima, T.; Anderson, K. C. *J. Clin. Onc.* **2005**, *23*, 630.

17 Hochstrasser, M. *Curr. Opin. Cell. Biol.* **1995**, *7*, 215.

18 Borissenko, L.; Groll, M. *Chem. Rev.* **2007**, *107*, 687.

19 Meiners, S.; Ludwig, A.; Stangl, V.; Stangl, K. *Med. Res. Rev.* **2008**, *28*, 309.

20 Glickman, M. H.; Rubi, D. M.; Coux, O.; Wefes, I.; Pfeifer, G.; Cjeka, Z.; Baumeister, W.; Fried, V. A.; Finley, D. *Cell* **1998**, *94*, 615.

21 Yao, T.; Cohen, R. E. *Nature* **2002**, *419*, 403.

22 Zwickl, P.; Baumeister, W. *Nat. Cell Biol.* **1999**, *1*, E97.

23 Ciechanover, A. *EMBO J.* **1998**, *17*, 7151.

24 Orlowski, R. Z.; Kuhn, D. J. *Clin. Cancer Res.* **2008**, *14*, 1649.

25 Adams, J.; Palombella, V. J.; Sausville, E. A.; Johnson, J.; Destree, A.; Lazarus, D. D.; Maas, J.; Pien, C. S.; Prakash, S.; Elliott, P. J. *Cancer Res.* **1999**, *59*, 2615.

26 Andela, V. B.; Gordon, A. H.; Zotalis, G.; Rosier, R. N.; Goater, J.; Lewis, G. D.; Schwartz, E. M.; Puzas, J. E.; O'Keefe, R. J. *J. Clin. Orthop. Relat. R.* **2003**, *415*, 85.

27 Lee, D. H.; Goldberg, A. L. *J. Biol. Chem.* **1996**, *271*, 27280.

28 Marques, A. J.; Palanimurugan, R.; Matias, A. C.; Ramos, P. C.; Dohmen, R. J. *Chem. Rev.* **2009**, *109*, 1509.

29 Bogyo, M.; McMaster, J. S.; Gaczynska, M.; Tortorella, D.; Goldberg, A. L.; Ploegh, H. *Proc. Nat. Aca. Sci.* **1996**, 6629.

30 Armstrong, A.; Scutt, J. N. *Org. Lett.* **2003**, *5*, 2331.

31. Adams, J.; Kauffman, M. *Cancer Invest.* **2004**, *22*, 304.

32 Richardson, P. G.; Mitsiades, C.; Hideshima, T.; Anderson, K. C. *Annu. Rev. Med.* **2006**, *57*, 33.

33. Kisselev, A. F.; Goldberg, A. L. *Chem. Biol.* **2001**, *8*, 739.

34 Adams, J. *Curr. Opin. Chem. Biol.* **2002**, *6*, 493.

35 Fisher, R. I.; Bernstein, S. H.; Kahl, B.; Djulbegovic, B.; Robertson, M. J.; de Vos Sven, K.; Epner, E.; Krishnan, A.; Leonard, J. P.; Lonial, S.; Stadtmauer, E. A.; O'Connor, O. A.; Shi, H.; Boral, A. L.; Goy, A. J. *J. Clin. Oncol.* 2006, 24, 4867.

36 Shah, J. J.; Orlowski, R. Z. *Leukemia*, **2009**, *23*, 1979.

37 Chen, D.; Cui, Q. C.; Yang, H.; Dou, Q. P. *Cancer Res.* **2006**, *66*, 10425.

38 Chen, D.; Cui, Q. C.; Yang, H.; Barrea, R. A.; Sarkar, F. H.; Sheng, S. *Cancer Res.* **2007**, *67*, 1636.

39 Cvek, B.; Milacic, V.; Taraba, J.; Dou, Q. P. *J. Med. Chem.* **2008**, *51*, 6256.

40 Daniel, K. G.; Gupta, P.; Harbach, R. H.; Guida, W. C.; Dou, Q. P. *Biochem. Pharmacol.* **2004**, *67*, 1139.

41 Frezza, M.; Hindo, S.; Chen, D.; Davenport, A.; Schmitt, S.; Tomco, D.; Dou, Q. P. *Curr Pharm Des.* **2010**, *16*, 1813.

42 Verani, C. N. *J. Inorg. Biochem.* **2012**, *106*, 59.

43 Shakya, R.; Peng, F.; Liu, J.; Heeg, M. J.; Verani, C. N. *Inorg. Chem.* **2006**, *45*, 6263.

44 Chen, D.; Frezza, M.; Shakya, R.; Cui, C. Q.; Milacic, V.; Verani, C. N.; Dou, Q. P. *Cancer Res.* **2007**, *67*, 9258.

45 Hindo, S.; Frezza, M.; Tomco, D.; Heeg, M. J.; Hryhorczuk, L.; McGarvey, B. R.; Dou, Q. P.; Verani, C. N. *Eur. J. Med. Chem.* **2009**, *44*, 4353.

46 Frezza, M.; Hindo, S. S.; Tomco, D.; Allard, M.; Cui, Q. C.; Heeg, M. J.; Chen, D.; Dou, Q. P.; Verani, C. V. *Inorg. Chem.* **2009**, *48*, 5928.

47 Li, B.; Dou, Q. P. *Proc. Natl. Acad. Sci.* **2000**, *97*, 3850.

48 Golovine, K.; Makhov, P.; Uzzo, R. G.; Kutikov, A.; Kaplan, D. J.; Fox, E.; Kolenko, V. M. *Mol. Cancer*, **2010**, *9*, 183.

49 Siu, E. R.; Mruk, D. D.; Porto, C. S.; Cheng, C. Y. *Toxicol. Appl. Pharmacol.* **2009**, *238*, 240.

50 Bulato, C.; Bosello, V.; Ursini, F.; Maiorino, M. *Free Radic. Biol. Med.* **2007**, *42*, 118.

51 Padya, C.; Gupta, S.; Pillai, P.; Bhandarkar, A.; Khan, A.; Prajapati, A.; Gupta, S. *Biol. Trace Elem. Res.* **2013**.

CHAPTER 2

MATERIALS, METHODS, AND CHARACTERIZATION TECHNIQUES

2.1. General

Reagents and solvents used in **Chapters 3 – 6** were obtained from commercial sources and handled without further purification. Infrared spectra were measured from 4000 to 400 cm^{-1} on a Tensor 27 FTIR spectrophotometer as KBr pellets. Electrospray ionization mass spectra were measured in the positive mode (ESI positive) using Micromass Quattro LC triple quadrupole mass spectrometer. Nuclear Magnetic Resonance (NMR) experiments including ^{1}H- and ^{13}C-NMR were measured using a Varian Mercury-400 and VNMRS-500 MHz spectrometers in $CDCl_3$, DMSO-d_6, and DMF-d_7 at 298 K. Specific experimental conditions including 2D-NMR are described in **Chapter 3**. Elemental analyses were performed by Midwest Microlab, Indianapolis, using V_2O_5 for complete combustion Indiana. Diffraction data were measured on a Bruker *X8 APEX-II* kappa geometry diffractometer with Mo radiation and a graphite monochromator. UV–visible spectroscopy from 1.0×10^{-4} M N,N-dimethylformamide (DMF) solutions and 9.0×10^{-5} M DMF/H_2O (90:10%, v/v) were run using a Cary 50 spectrophotometer in the range of 250–1100 nm. Cyclic voltammetry (CV) experiments were performed at room temperature under anaerobic conditions using argon gas in HPLC grade N,N-dimethylformamide at concentration of 1.0×10^{-3} and 9.0×10^{-4} M DMF/H_2O (90:10%, v/v) solutions. The experiments were carried out using a standard three-electrode cell with an Ag/AgCl as the reference electrode, a glassy-carbon working electrode, a Pt-wire as the auxillary electrode, and. Voltammograms were recorded using a BAS 50 W voltammetric analyzer at a scan rate of 100 mV s^{-1}. The supporting electrolyte of tetra-n-butylammonium hexafluorophosphate ($TBAPF_6$) was used 0.1 M concentration. The reversibility of the redox

processes for the cobalt ion was determined by the peak to peak separation ($\Delta Ep = |Ep_c - Ep_a|$) values and $|ip_c/ip_a|$ ratio.

The fluorogenic peptide substrate SucLLVY-AMC for the proteasomal chymotrypsin-like activity measurements was purchased from Calbiochem, Inc. (San Diego, CA). Trypan blue exclusion dye was purchased from Sigma Aldrich (St. Louis, MO). Mouse monoclonal antibody against human poly (ADP-ribose) polymerase (PARP) was purchased from BIOMOL International LP (Plymouth Meeting, PA). RPMI 1640, penicillin, and streptomycin were purchased from Invitrogen (Carlsbad, CA), whereas fetal bovine serum was purchased from Aleken Biologicals (Nash, TX). Antibodies against ubiquitin (P4D1), actin (C-11), and secondary antibodies were purchased from Santa Cruz Biotechnology (Santa Cruz, CA). Biological assays and cellular culture techniques included in **Chapters 3**, **5**, and **6**, were performed by Sara Schmitt in the Dou Lab at Barbara Ann Karmanos Cancer Institute.

Computational calculations for **Chapter 4** were performed by Dr. Marco M. Allard, a former student in the Verani Lab, using Gaussian 09 suite of programs[1] with density functional theory (DFT). These calculations were carried out with the B3PW91[2] functional basis set.

2.2. Cyclic Voltammetry

Cyclic voltammetry is an electroanalytical technique that measures the electron transfer (current) of a complex solution upon an applied potential.[3] It best describes oxidation-reduction reactions and the flow of electronic charge in solution. The system consists of a standard three-electrode cell connected to a potentiostat. The three electrodes, namely working, reference, and auxiliary are employed in the electrochemical cell containing the complex solution of interest and supporting electrolyte. The electrolyte used for our experiments is tetra-n-butylammonium hexafluorophosphate ($TBAPF_6$) at 0.1 M. A typical cyclic voltammogram[3] for a reversible one

electron process is shown in **Figure 2.2**. At point E, only the oxidized form of the redox couple is present in solution. As the forward negative scan of the potential progresses towards point F, the oxidized species start to convert to its reduced form. Once the net cathodic current (i_{pc}) is reached, any of the oxidized species will be quickly reduced on the surface of the electrode. At point G, only the reduced form of the initial species is present in solution on the electrode surface. When the scan is reversed towards point H, the reduced species starts to convert back to its oxidized form, while a net anodic current (i_{pa}) is reached at point H. As the anodic current approaches zero, only the oxidized species is present in solution (point E). The equilibrium concentration between the oxidized and reduced species is expressed using the Nernst equation.[4] For a reversible one electron process the current ratio $| i_{pc}/i_{pa} |$ has to equal 1.0.

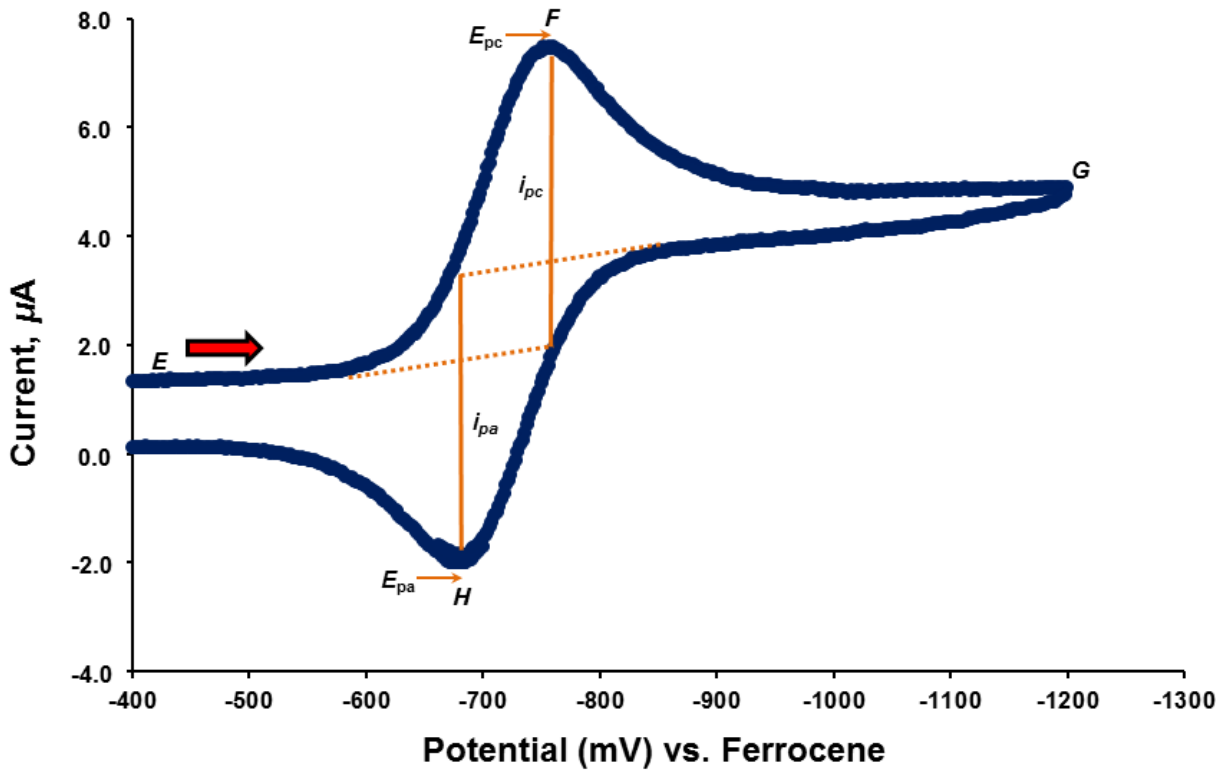

Figure 2.2. Cyclic voltammogram for one electron process (adapted from ref. 3).

2.3. Spectroelectrochemistry

The experimental setup of spectroelectrochemistry involves the concerted use of electrochemical and UV-visible techniques. This technique was employed to measure the reduction of a cobalt complex in solution by monitoring the disappearance of the ligand to metal charge transfer band (LMCT) upon an applied fixed potential. Spectroelectrochemical experiments were performed at room temperature by employing an optically transparent thin-layer cell (ca. 0.1 mm) inside of which a U-shaped flat platinum wire acting as the working electrode was placed between two glassy slides and was extended outside of the slides for electrical contact. The inner parts of these slides were coated with indium-tin oxide (ITO) (8-2 Ω/sq). A second platinum wire was used as the counter electrode and the Ag/AgCl wire was the reference electrode. The cobalt complex was dissolved in DMF and the solution was purged with argon before it was introduced into the cell through a capillary. The electrochemical potential applied to the cell was higher (−1200 mV versus Fc/Fc^{+}) than the cathodic potential for the cobalt(III)/(II) couple. This potential was achieved using a BAS 50 W potentiostat and the spectra were collected using a Varian Cary 50 apparatus within a time interval of 30 s frames following the disappearance of the phenolate to cobalt(III) charge transfer (LMCT).

2.4. Chemical Reduction

Chemical reduction experiments were performed by UV-visible spectroscopy to observe the disappearance of the LMCT band of the cobalt complex in presence of ascorbic acid reductant to mimic the reductive intracellular environment. The chemical reduction experiments were carried out at room temperature in a freshly prepared DMF/H_2O (90:10%, v/v). Each spectrum was recorded within an interval of 30 min in the range of 300–900 nm following the decrease of the ligand to metal charge transfer (LMCT) band over a time period of 18 h. The

experimental setup employed a 4 mL quartz cuvette (1 cm optical path) where 2700 μL of the cobalt complex was dissolved in DMF under anaerobic conditions ([complex 1] = 1.0×10^{-4} M) and then mixed with 300 μL of an aqueous oxygen-free ascorbic acid solution ([AA] = 1.0×10^{-2} M) stabilized with nitric acid. The final concentration of the complex solution inside the cell was ($[\text{complex 1 + AA}]_{\text{final}} = 9.0 \times 10^{-5}$ M), under apparent pH 3. The control samples were prepared under the same conditions without the addition of the reductant (AA) ($[\text{complex 1}]_{\text{final}} = 9.0 \times 10^{-5}$ M) and DMF/H_2O (90:10%, v/v) solution) under pH 3 and pH 1, respectively. Data was treated as a pseudo-first order reaction, where the excess AA is maintained near constant through time. The concentration of the cobalt(III) complex is monitored as a function of time and fitted as a pseudo-first order exponential decaying equation, [C]t = [C]o × e*k*t. In order to evaluate the rate constant, the natural log of the decay data is plotted versus time and fitted with the following equation: ln[C]t = −*k*t + ln[C]o where [C]o, is the initial concentration (mol L^{-1}), [C]t is the concentration at a given time, *k* is the first order rate constant (s^{-1}), and t is time in seconds. The half-life of the cobalt(III) complex upon reduction was calculated using the $t_{1/2} = \ln 2/k_{obs}$ equation.

2.5. Western Blot Analysis

Western blotting was used to isolate and identify proteins of interest based on the principle of antibody-antigen binding. It was first discovered in 1979 by the scientist Harry Towbin.[5] In this chapter Western blotting technique is described based on the experiments performed to identify levels of ubiquinated proteins and the enzyme poly ADP ribose polymerase (PARP) which are extracted from treated prostate cancer cells with various concentrations of metal-based compounds synthesized in the Verani Lab. This section includes a

description of how cells were prepared for the Western blot analysis, and how this technique was used to identify the proteins of interest.

Preparation of Cell Extracts

Prostate cancer cells (PC-3) were grown in a RPMI 1640 cell culture (100*20 mm) tissue culture dish containing sterile media treated with 10% fetal bovine serum, 100 µg/mL of streptomycin, and 100 units/mL of penicillin incubated overnight with 5% CO_2 at 37^o C. After they reached 80% confluence, PC-3 cells were treated with increasing concentrations of the metal complexes and incubated for 18-24 hours. The cells were detached from the culture plates and spun at 1500 rpm for 3 min in order to separate the cell media; e.g., serum. Collected cell pellets were washed three times with phosphorus buffer saline (PBS) solution and then were centrifuged at 5000 rpm for 3 min. Cells were lysed with Tris-HCl lysis buffer in order to break the cellular wall of the phospholipid bilayer and vortexed for 20 min at 4^o C followed by centrifugation for 12 min at 1200 rpm. This process separates proteins from the genetic material. The proteins of interest were collected from the supernatant (cell lysates).

Gel Electrophoresis

Separation of proteins based on their charge and molecular size was performed by gel electrophoresis.[6] Cell lysates were treated with a loading buffer which was used to denature the proteins. This enables the cell lysates to travel easily through the 10% polyacrylamide gel under the applied voltage. Bromophenol blue dye was added to the cell lysates to track how far the proteins have migrated through the gel. Cell lysates (40 µg of proteins) were separated by sodium dodecyl sulfate polyacrylamide gel electrophoresis (SDS-PAGE) under 26-35 Volts. The SDS detergent was used due to its anionic nature, thus giving the proteins an overall negative

charge. Therefore, protein migration through the gel upon an applied voltage was solely based on their molecular size. The smaller weight proteins will travel farthest down the gel.

Once the proteins were separated *via* gel electrophoresis, they were transferred to a nitrocellulose membrane to isolate the proteins of interest including ubiquinated proteins and PARP. The protein transfer process (blotting) was performed by placing the nitrocellulose membrane between the gel and the positive electrode where upon an applied electric field the negatively charged proteins migrated towards the membrane.[7] The nitrocellulose membrane was incubated overnight at 4^{o} C with the primary mouse monoclonal antibody against ubiquitin (P4D1). Following the next day, the membrane was washed three times with Tris buffer saline solution to eliminate any unbound proteins, and then incubated overnight at 4^{o} C with the secondary antibody which specifically binds to the primary antibody, as shown in **Figure 2.5**. The nitrocellulose membrane was washed three times with Tris buffer saline solution followed by the addition of enhanced chemiluminescence (ECL) substrate which was cleaved by the enzyme horseradish peroxidase, thus emitting light.[8,7] The same procedure is applied for isolation of PARP by using mouse monoclonal antibody against human PARP.

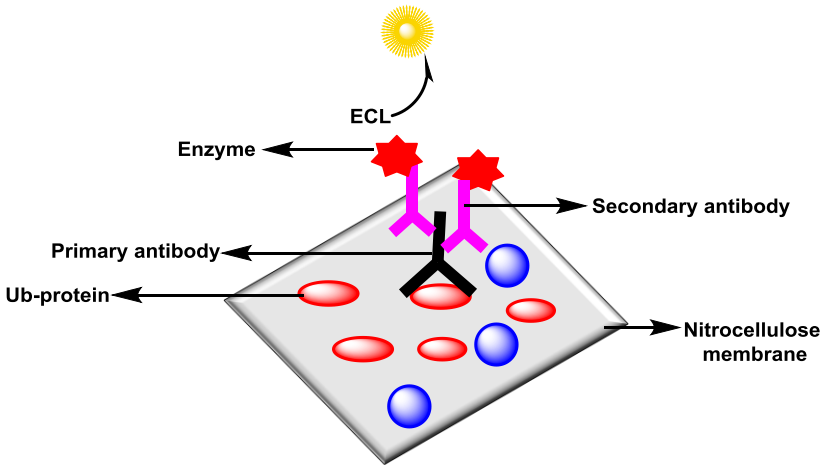

Figure 2.5. Isolation of Ub-proteins by Western blot analysis (adapted from ref. 8).

2.6. References

1 Frisch, M. J.; Trucks, G. W.; Schlegel, H. B.; Scuseria, G. E.; Robb, M. A.; Cheeseman, J. R.; Scalmani, G.; Barone, V.; Mennucci, B.; Petersson, G. A.; Nakatsuji, H.; Caricato, M.; Li, L.; Hratchian, H. P.; Izmaylov, A.F.; Bloino, J.; Zheng, G.; Sonnenberg, J. L.; Hada, M.; Ehara, M.; Toyota, K.; Fukuda, R.; Hasegawa, J.; Ishida, M.; Nakajima, T.; Honda, Y.; Kitao, O.; Nakai, H.; Vreven, T.; Montgomery, J. A.; Peralta, J. E.; Ogliaro, F.; Bearpark, M.; Heyd, J.; Brothers, J. E.; Kudin, K. N.; Staroverov, V. N.; Kobayashi, R.; Normand, J.; Raghavachari, A.; Rendell, A.; Burant, J. C.; Iyengar, S. S.; Tomasi, J.; Cossi, M.; Rega, N.; Millam, J. M.; Klene, M.; Knox, J. E.; Cross, J. B.; Bakken, V.; Adamo, C.; Jaramillo, J.; Gomperts, R.; Stratmann, R. E.; Yazyev, O.; Austin, A. J.; Cammi, R.; Pomelli, C.; Ochterski, J. W.; Martin, R.L.; Morokuma, K.; Zakrzewski, V.G.; Voth, G.A.; Salvador, P.; Dannenberg, J.J.; Dapprich, S.; Parandekar, P.V.; Mayhall, N.J.; Daniels, A.D.; Farkas, O.; Foresman, J.B.; Ortiz, J. V.; Cioslowski, J.; Fox, D. J. *Gaussian G09 Wallingford CT*, **2009**.

2 Krishnan, R; Binkley, J. S.; Seeger, R.; Pople, J. A. *J. Chem. Phys.* **1980**, *72*, 650.

3 Wang, J. *Analytical Electrochemistry; Chapter 2, Wiley & Sons, Inc.* New York, **2000**.

4 Chang, R.; Goldsby, K.; *Chemistry, 11th edition, Chapter 18, Electrochemistry, The McGraw-Hill Companies, Inc., New York, NY 10020*, **2013**, pp. 830.

5 Towbin, H.; Staehelin, T.; Gordon, J. *Proc. Natl. Acad.Sci.* **1979**, *76*, 4350.

6 Kryndushkin, D. S.; Alexandrov, I. M.; Ter-Avanesyan, M. D.; Kushnirov, V. V. *J. Biol. Chem.* **2003**, *278*, 49636.

7 Mahmood, T.; Yang, P.-C. N. *Am. J. Med. Sci.* **2012**, *4*, 429.

8 http://www.piercenet.com/method/overview-western-blotting#introduction

CHAPTER 3

EFFECTS OF TETHERED LIGAND AND OF METAL OXIDATION STATE ON THE INTERACTION OF COBALT COMPLEXES WITH THE 26S PROTEASOME

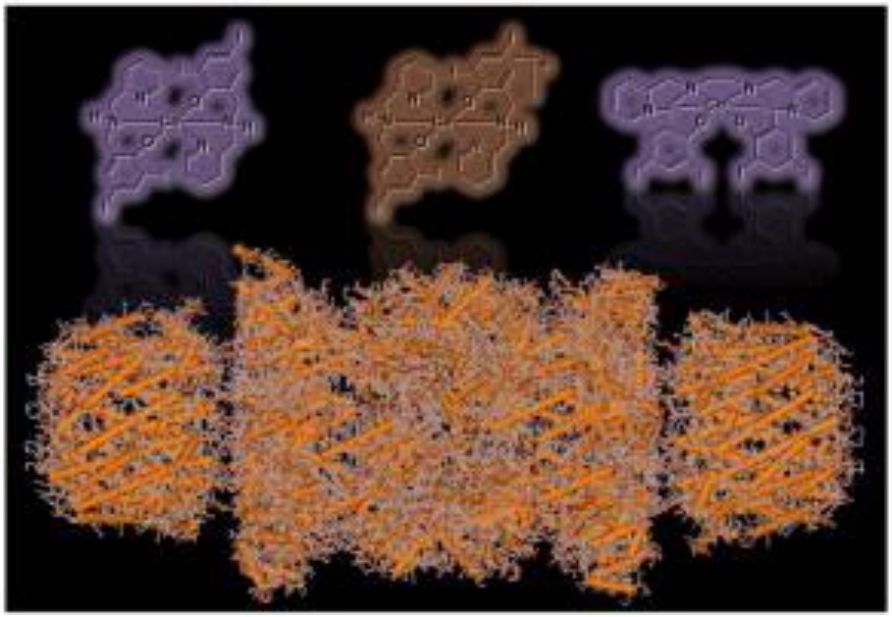

CHAPTER 3

EFFECTS OF TETHERED LIGAND AND OF METAL OXIDATION STATE ON THE INTERACTION OF COBALT COMPLEXES WITH THE 26S PROTEASOME

Published with minor changes as Tomco, D.; Schmitt, S,; Ksebati, B.; Heeg, M. J.; Dou, Q. P.; Verani, C. N.* *J. Inorg. Biochem*, **2011**, *105*, 1759.

3.1. Introduction

Our groups have been interested in the development of coordination complexes capable of inhibiting the activity of the 26S proteasome in tumorous prostate cells. The 26S proteasome is a large protein complex responsible for the destruction of faulty proteins and enzymes.[1,2] In tumor cells the activity of the 26S proteasome goes in overdrive fostering the proteolysis of inhibition factors such as IκB releasing NFκB nuclear factor that support the development of blood vessels and promote tumor cell growth.[3,4] Inhibition of this activity leads to cellular apoptosis, or programmed cell death.

We have demonstrated recently that a series of gallium complexes $[Ga(L^{NN'O})_2]$ with the substituted ligand 2,4-di-X-6-((pyridine-2-ylmethylamino)methyl)phenol (where X = bromo or iodo)[5,6] were active against the proteasome, as measured by the inhibition of its chymotrypsin-like activity (CT) and resulting accumulation of ubiquitinated proteins. This activity triggered cell death both *in vitro* and *in vivo*. Thus, we proposed that in order to inhibit the proteasome activity, this species would likely bind to available amino acids along the α channels of the proteasome, or to the terminal threonines of the β active sites in a similar way as reported to the antineoplastic agent bortezomib (valcade).[7] The $[ML_2]^+$ species would need to be converted into a $[ML]^+$ species, in order to establish a metal/amino acid chemical bond. Evidence for such mechanism was gathered when 2:1 and 1:1 copper(II) complexes showed comparable CT

inhibition activities in purified 20S and 26S proteasomes, in C4-2B and PC-3 cell extracts, as well as in intact cells.[8] Consistently we have also observed that [ML_2] complexes with labile zinc(II) ions show considerable activity, whereas more inert and redox-inactive metal ions such as nickel(II) show negligible results.[9]

In this chapter, we further this investigation by comparing the inhibition activity of three cobalt complexes described as **[$Co^{II}(L^1)_2$] (1)**, **[$Co^{II}(L^2)$] (2)**, and **[$Co^{III}(L^1)_2ClO_4$] (3)** (**Scheme 3.1**). We are interested in the comparison of **1** and **2** that allows further analysis for the need of ligand dissociation, where the newly designed ligand used in **2** hinders such dissociation. Similarly we want to compare **1** and **3** to examine the role of the oxidation states and the potential of redox changes in proteasome inhibition. The antitumor activity of cobalt species is fairly understudied,[10] but activity against prostate cancer has been recently demonstrated by McNeil et al. for bivalent cobalt.[11] On the other hand, Teicher, Ware, Hambley,[12] and more recently Donelly[13] have taken advantage of bioreductive activation of its trivalent counterpart for the treatment of hypoxic tumors. In this case, intracellular redox conversion of Co(III) into Co(II) releases alkylating mustards.

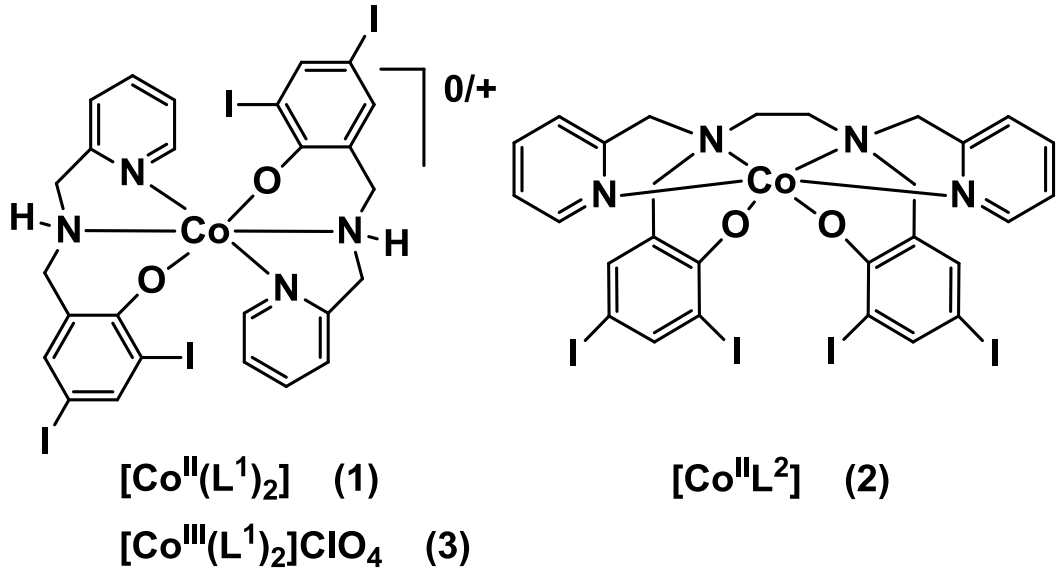

Scheme 3.1. Cobalt complexes.

3.2. Results and Discussion

3.2.1. Synthesis and Characterization

Both ligands **HL^1** and **H$_2$L^2** were synthesized in moderate yields following procedures available in the literature.[14,15] The condensation reaction of picolinaldehyde with ethane-1,2-diamine produced the corresponding Schiff base ligand. This was followed by reduction with sodium borohydride to generate the intended *N*^{1},*N*^{2}-bis(pyridin-2-ylmethyl)ethane-1,2-diamine precursor. Formation of the new **H$_2$L^2** ligand, as shown in **Scheme 3.2.1**, was obtained by reaction of this amino-pyridine precursor with 2-(chloromethyl)-4,6-diiodophenol in the presence of base. The ^{1}H-NMR spectra of the ligands were measured and will be relevant for future comparisons. The spectrum for **HL^1** was recorded in DMSO-d_6 in order to compare with the ^{1}H NMR of **3**. A complete characterization of HL^1 ligand including the ^{1}H-NMR spectra and ^{1}H-^{1}H COSY is given in **Figures A.3.2.1.1**, **A.3.2.1.2**, and **A.3.2.1.3**. From the ^{1}H-NMR spectra, the two methylene protons from both the pyridine rings (H5, H5$^{'}$) and phenol (H6, H6$^{'}$) appear as two distinct singlet resonances centered at 3.83 ppm and 3.87 ppm, respectively, whereas the aromatic protons lie between the 7.28-8.60 ppm region. The exchangeable protons from the aliphatic nitrogen atom (H9) and the phenol group (H10) are observed as a broad resonance between 6.60-7.10 ppm. The (H1) proton from the pyridine ring resonates as a doublet at 8.54 ppm.

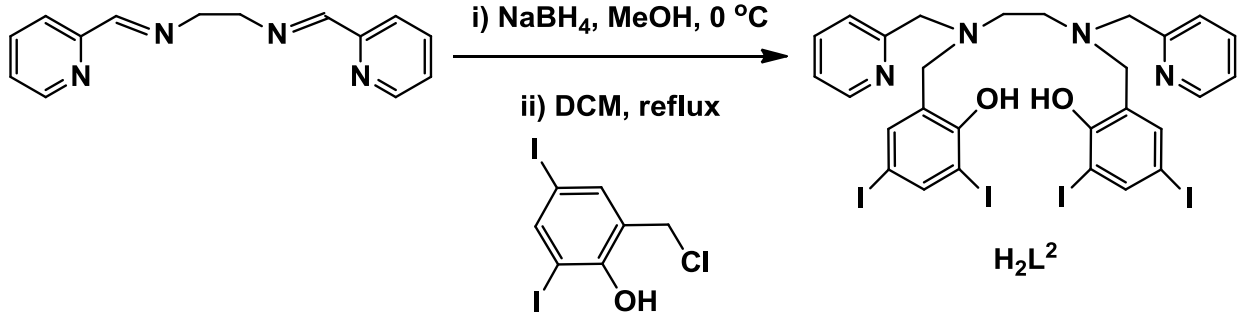

Scheme 3.2.1. Synthesis of the **H$_2$L^{2}** ligand.

The spectrum for $\mathbf{H_2L^2}$ recorded in $CDCl_3$, provides evidence for a symmetric ligand in the solution, as Orvig *et al*[16] and Neves *et al*[17] have similarly observed with other related H_2bbpen ligands. Therefore, three sharp singlet resonances are shown at 2.67 ppm, 3.61 ppm, and 3.72 ppm representing the four protons from ethane-1,2-diamine, phenolic-methyl, and pyridyl-methyl groups, respectively; whereas the aromatic protons are displayed between the region of 7.11-8.60 ppm. Complexes **1-3** were synthesized by the reaction of the metal salt with the appropriate ligand in methanol or dichloromethane in the presence of triethylamine base. Characterization of all of the metal complexes includes spectroscopic and spectrometric techniques consisting of IR, NMR, ESI-MS, and elemental analyses. Infrared analysis confirms that both C=N and $C=C_{Ar}$ stretching modes shift *ca.* 40-60 cm^{-1} to lower frequencies due to metal coordination. Characteristic for the infrared spectrum of the $\mathbf{[Co^{III}(L^1)_2]ClO_4}$ **(3)** complex is the presence of a strong broad band at 1098 cm^{-1}, corresponding to the perchlorate counterion. Spectrometric analysis for complexes **1-3** was performed by ESI-MS in the positive mode and in methanol solutions. The results showed excellent agreement between the experimental and the simulated data as presented in **Figure 3.2.1**. As previously published,[14] complex **1** shows the presence of the molecular ion peak observed at m/z^+ = 989.9 (100%) which corresponds to the $\{[Co(L^1)_2] + H^+\}^+$ species. Alternatively, for complex **3** the main peak is detected at m/z^+ = 988.9 (100%) and assigned to the $[Co(L^1)_2]^+$ species providing strong evidence for the coordination of the cobalt(III) ion. ESI-MS for complex **2** shows the parent peak for $\{[Co(L^2)] + H^+\}^+$ species at m/z^+ = 1015.7 (100%). The isotopic distribution for both complexes **2** and **3** are shown in **Figure 3.2.1.** All of the above data confirm the expected configurations of 1:2 and 1:1 metal-to-ligand species containing six-coordinate cobalt ions bound to $\mathbf{HL^1}$ or $\mathbf{H_2L^2}$, respectively.

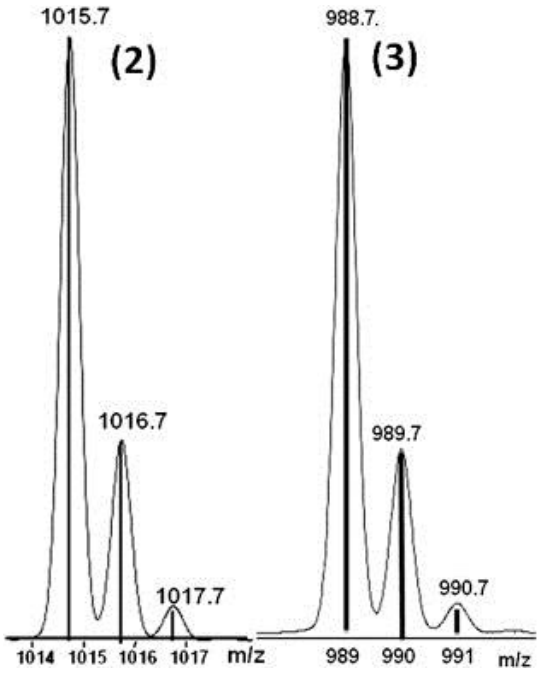

Figure 3.2.1. Isotopic distribution for complex **2** (left) and **3** (right). The bars indicate the experimental results and the continuous spectra indicate the simulated results.

3.2.2 Molecular Structural Characterization of $[Co^{II}L^{2}]$ (2)

X-ray diffraction was used to determine the molecular structure of single crystals of compound **2** isolated from slow solvent evaporation of a 1:1 mixture of dichloromethane and methanol. **Figure 3.2.2** displays the ORTEP diagram for complex **2** with selected bond lengths and angles. Compound **2** consists of a neutral cobalt(II) species with coordination environment arranged about a fully deprotonated hexadentate ligand $(L^{2})^{2-}$, containing two [NN′O] donor sets. The pseudo-octahedral cobalt(II) center is oriented in a two-fold rotation axis with each half of the ligand in a facial arrangement. We have previously reported on similar coordination spheres for cobalt(II) complexes containing two independent [NN′O] ligands, in which all equivalent donors are positioned *trans* to each other.[14,18] In contrast, complex **2** displays an arrangement of *cis* phenolates, *trans* pyridines, and *cis* nitrogen atoms, rather observed for iron(III) and

manganese(III) complexes with similar hexadentate ligand.[19,20,21] The short cobalt-donor bonds, along with the absence of counterions support the bivalent nature of the metal ion. The observed Co-$O_{phenolate}$ distance is 2.00 Å, whereas Co-$N_{pyridine}$ is 2.14 Å, and Co-N_{amine} is 2.23 Å. These values are in good agreement with the literature.[14]

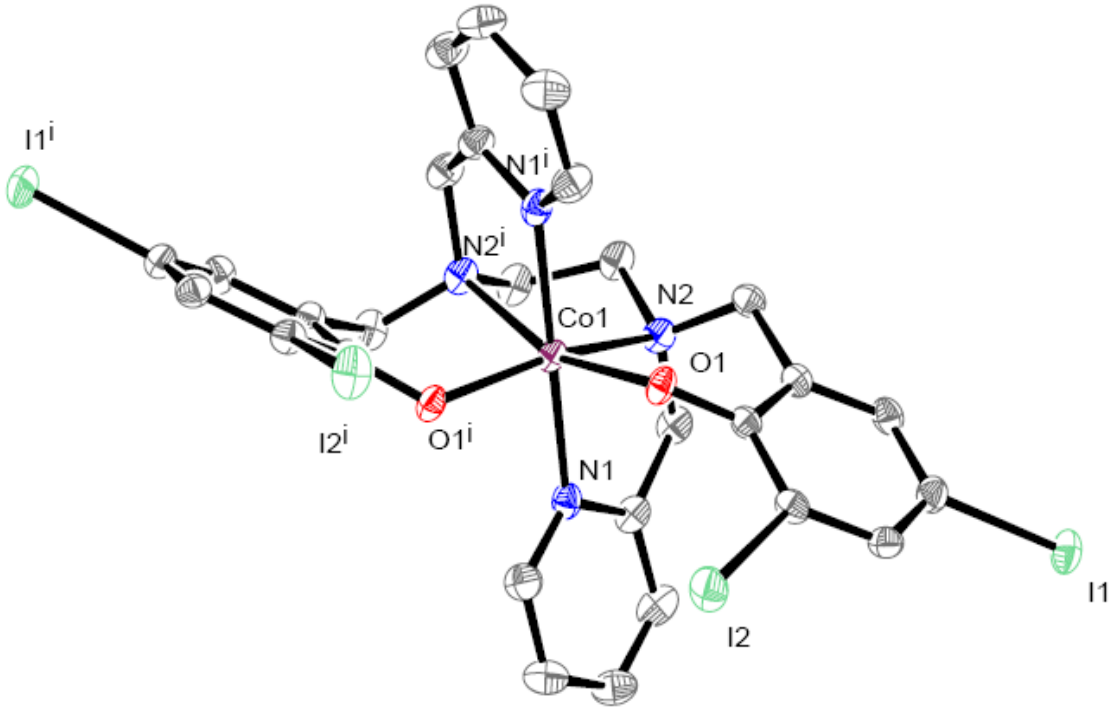

Figure 3.2.2. ORTEP diagram at 50% probability level for **2**. Selected bond lengths include Co(1)-O(1) = 2.003(3), Co(1)-N(1) = 2.139(3), Co(1)-N(2) = 2.234(3) Å. Selected angles include N(1)-Co(1)-N(2) = 76.57(12), O(1)-Co(1)-N(1) = 90.32(12), O(1)-Co(1)-N(2) = 89.65(11). Goodness of fit is given by $R(F)$ (%) = 3.13.

3.2.3. NMR Spectroscopic Studies

The ^{1}H-NMR spectra for compound **3** were taken in DMSO-*d6* at 298 K, and are shown in **Figure 3.2.3**. A comparison of the proton chemical shifts of **HL^{1}** and **3** is given in **Table 3.2.3** and (**Table A.3.2.3**).

The ^{1}H-NMR spectrum of **3** showed eleven distinctive resonances between 3.41 and 9.00 ppm, indicating that the compound has a diamagnetic $3d^{6}_{\text{low-spin}}$ electronic configuration. The ^{13}C-NMR spectrum of complex **3** confirmed the presence of thirteen different carbon chemical peaks corresponding with half the number of carbons present in the molecule, suggesting that this complex is symmetric in solution. A combination of DEPT, COSY (**Figures A.3.2.3.1** and **A.3.2.3.2**), and HMQC experiments were used to establish proton and carbon connectivity in the isolated spin systems for **3**, whereas NOE was employed to confirm the proposed structure. DEPT analysis revealed two signals corresponding to two methylene groups, and six distinct CH peaks giving a total of ten protons, whereas ^{13}C-NMR/DEPT studies confirmed the presence of five fully-substituted aromatic carbons.

Characteristic for the ^{1}H NMR spectra for complex **3** is the observation of the chemical shifts and splittings of the proton resonances attributed to metal coordination for the two methylene protons **Figure 3.2.3 (a)**. The original singlet peak observed at 3.83 ppm (H5) in the non-metallated ligand now appears as the two doublets observed at 4.39 and 5.58 ppm for the complex, possibly due to the coupling with the aliphatic amine proton (H9). The same phenomenon was observed for the initial singlet peak at 3.87 ppm (H6), which transforms into two distinct resonances appearing as doublets at 3.48 and 3.66 ppm for **3.**

The connectivity of the protons to the carbons for complex **3** was supported by the HMQC experiment, as shown in (**Figure 3.2.3 (b)** and **Figure A.3.2.3.3**; where the identity of

the exchangeable proton attached to the aliphatic nitrogen atom (H9) was revealed. In this spectrum, one resonance corresponding to the proton on the aliphatic amine (H9) appears as a broad singlet and is shifted downfield to 8.33 ppm. Also, in comparison to the ^{1}H NMR spectra of the ligand HL[1], where the exchangeable proton of the phenol group is centered between 6.60 and 7.10 ppm, complex **3** has no such peak present which indicates ligand deprotonation.

The aromatic proton found on the 1-position of the pyridine ring (H1) shifts downfield to 8.99 ppm and appears as a doublet of a doublet due to metal coordination. Only slight changes of the proton chemical shifts were observed for all aromatic protons as shown in **Table 3.2.3**, and no broadening of the signal indicative of dynamic equilibria[22] were observed.

To confirm the thermodynamic stability of **3** in solution, variable-temperature ^{1}H-NMR experiments were performed in DMSO-*d6* (25 to 80 $^{\circ}$ C, not shown), as well as in DMF-*d7* (25 to -40 $^{\circ}$ C, **Figure A.3.2.3.4**). No significant changes were observed, thus supporting the idea that the $3d^{6}_{\text{low spin}}$ assignment for **3** is the stable conformation in the timeframe of these experiments.

Proton H	HL^1 (ppm)	$[Co^{III}(L^1)_2ClO_4]$ (ppm)
H1	8.54 (d)	8.99 (dd)
H2	7.29 (dd)	7.46 (t)
H3	7.8 br (dt)	7.95 (t)
H4	7.37 (d)	7.57 (d)
H5 H5'	3.83 (s)	4.39(d) 5.58 (dd)
H6 H6'	3.87 (s)	3.48(dd) 3.66 (d)
H7	7.33 (d)	7.39 (s)
H8	7.78 (d)	7.34 (s)
H9	6.60-7.10 br (s)	8.33 (s)
H10	6.60-7.10 br (s)	no peak

Table 3.2.3. ^{1}H NMR assignment for **HL^1** and **$[Co(L^1)_2]ClO_4$ (3)** in DMSO-*d6*.

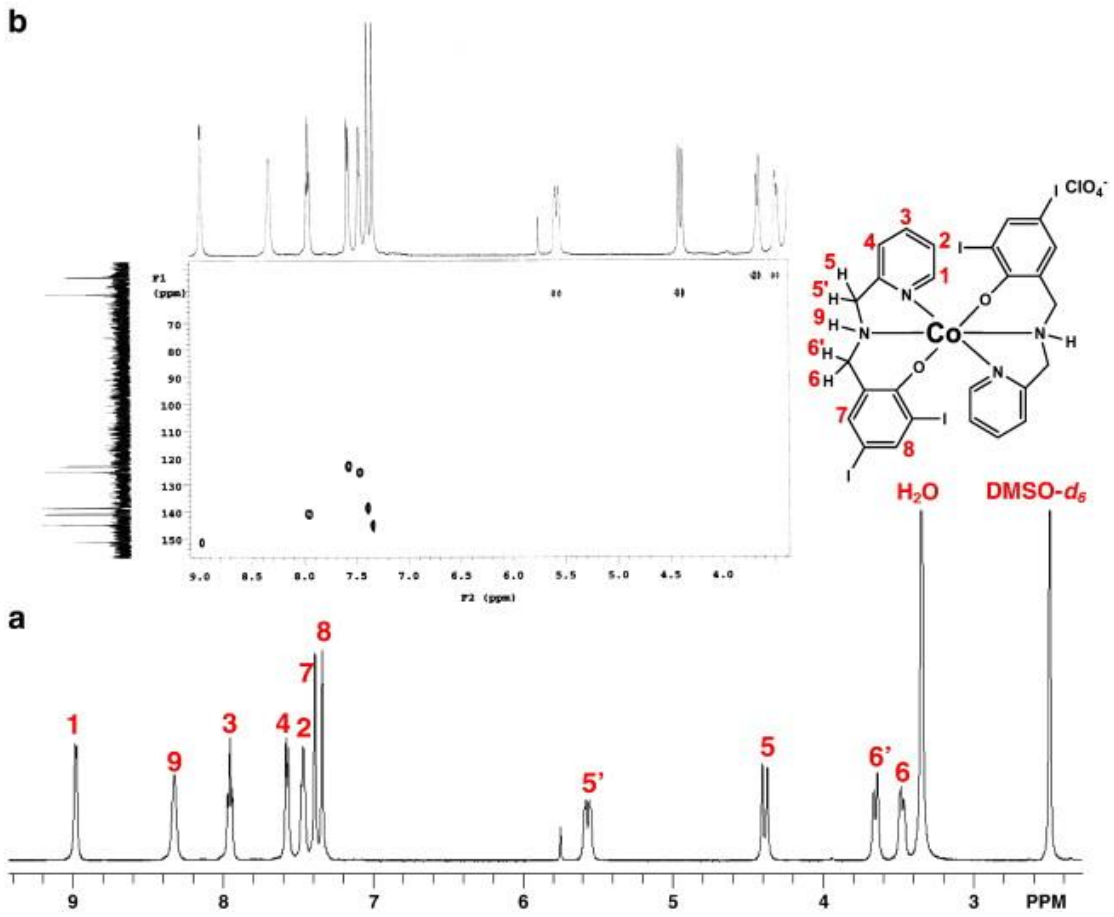

Figure 3.2.3. NMR spectroscopic measurements for complex **3**; (a) ^{1}H-NMR spectrum and (b) HMQC spectra.

3.2.4. UV-visible Spectroscopy

The UV–visible spectra of complexes **1**–**3** were taken in 1.0×10^{-4} M DMF solutions to assure consistency of solubility properties (**Figure 3.2.4**). The noticeable absence[18] of a ligand-to-metal charge transfer band at about 450 nm is diagnostic of the $3d^7_{\text{high spin}}$ cobalt(II) center in complexes **1** and **2**. This very characteristic process is observed for complex **3** at 441 nm corresponding to a $p\pi_{\text{phenolate}} - d\sigma^*_{\text{cobalt (III)}}$ charge transfer. Another band at 630 nm usually attributed to d-d transitions is also present, confirming the trivalent character of the $3d^6_{\text{low spin}}$ cobalt(III) species. Other observed features include the intense $\pi - \pi^*$ intraligand bands at about 320 nm for all species. These results are in good agreement with the previously published data on cobalt complexes containing [NN′O] donor ligands[10,23].

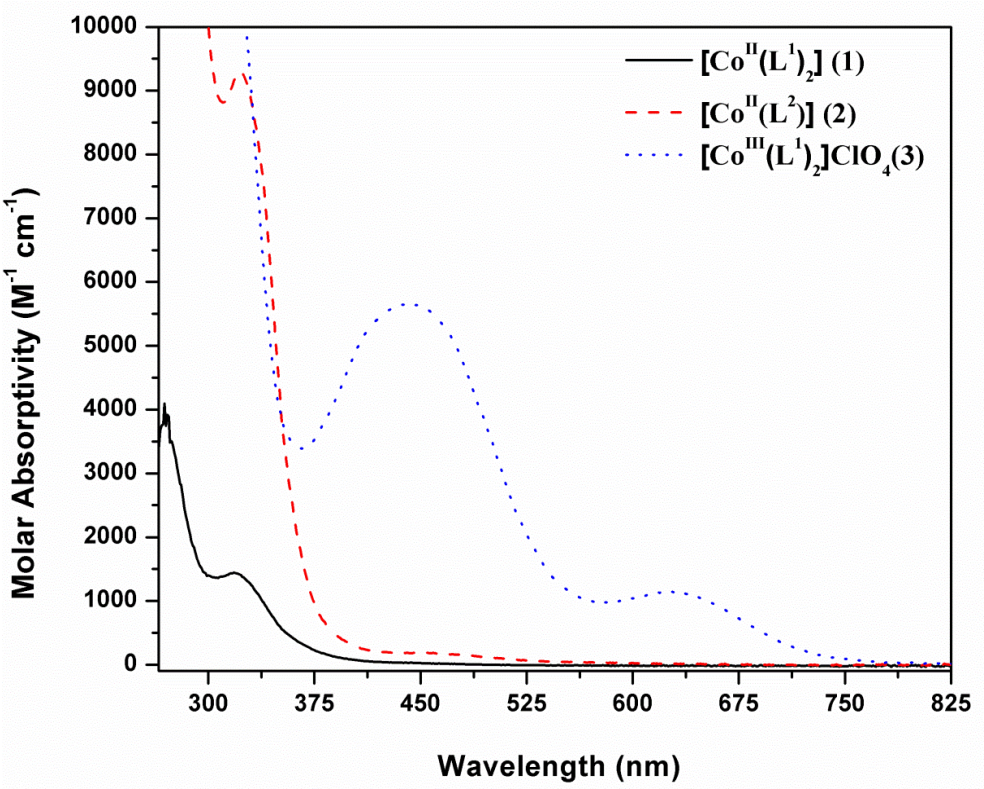

Figure 3.2.4. UV–visible spectra of complexes **1**–**3** in N,N-dimethylformamide, 1.0×10^{-4} M.

3.2.5. Biological Results

Biological data were gathered regarding the inhibition activity of species **1**–**3** toward cell proliferation, the purified 20S proteasome, and intact PC-3 prostate cancer cells. Inhibition of cell proliferation in human PC3 cells was successful with species **3**. Cell proliferation was decreased by 40% upon treatment with 20 μM, and reached nearly 100% inhibition at a concentration of 30 μM. A less remarkable activity was observed for **1**, where noticeable inhibition required considerably higher concentrations, e.g. ~ 30% inhibition at 50 μM (**Figure 3.2.5.1**). Initially, this observation seems to contradict the proposed ligand exchange mechanism observed for similar copper, nickel and zinc complexes with similar ligand.[8,9]

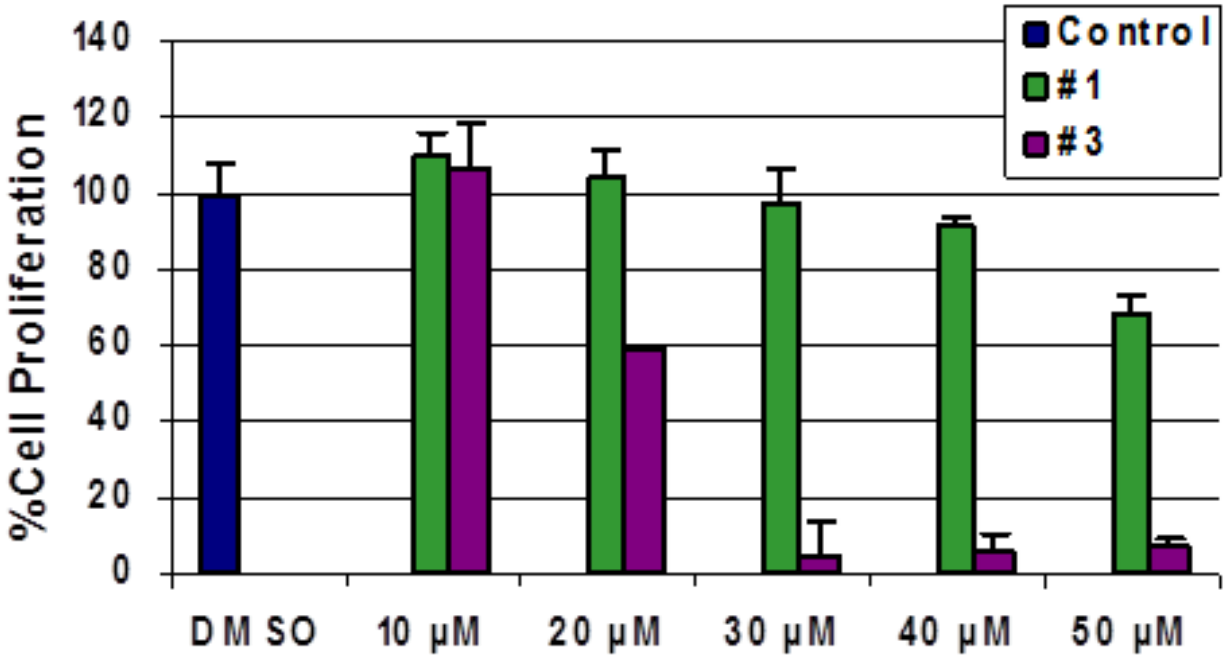

Figure 3.2.5.1. MTT, PC-3 cells after 18 h treatment. Control is DMSO, for each concentration from 10 to 50 μM, compound **1** is indicated in the left column and **3** is indicated in the right column.

To test the *in vitro* 20S proteasome inhibition ability of these species, a comparison of the inhibitory activity of **1**, **2** and **3** to the 20S proteasomal activity was performed under cell-free conditions. Human purified 20S proteasome was incubated with the $Co(ClO_4)_2 \cdot 6H_2O$ salt as control, as well as with **1**, **2,** and **3** at different concentrations, followed by measurement of CT-like activity. This activity was marginally inhibited by the ligands and was inhibited by the highest concentration (50 μM) of cobalt salt at a 50% level. This result confirms that in 20S proteasome – where the regulatory 19S caps have been removed – metal ions will show some inhibitory effect, as previously observed for gallium salts.[24] In spite of modest activities, comparison between complexes **1** and **2**, displayed in **Figure 3.2.5.2 (top)** shows the highest inhibition for **1** (40% at 10 μM), where two independent ligands are present. This result reinforces the notion that facilitated ligand exchange will foster inhibition. No activity is observed for **2** even at 50 μM. The activities of **1** and **3** were also compared, as shown in **Figure 3.2.5.2 (bottom)**. These species show constant 1:2 metal-to-ligand ratio but allow for the respective comparison between a labile 3 d^7 and an inert 3 d^6 metal center. The latter is expected to display little or no inhibitory effects, as observed for the equally inert nickel(II) ion.[9] Unexpectedly, species **3** displays remarkably better CT-like activity inhibition of the 20S core than its labile counterpart.

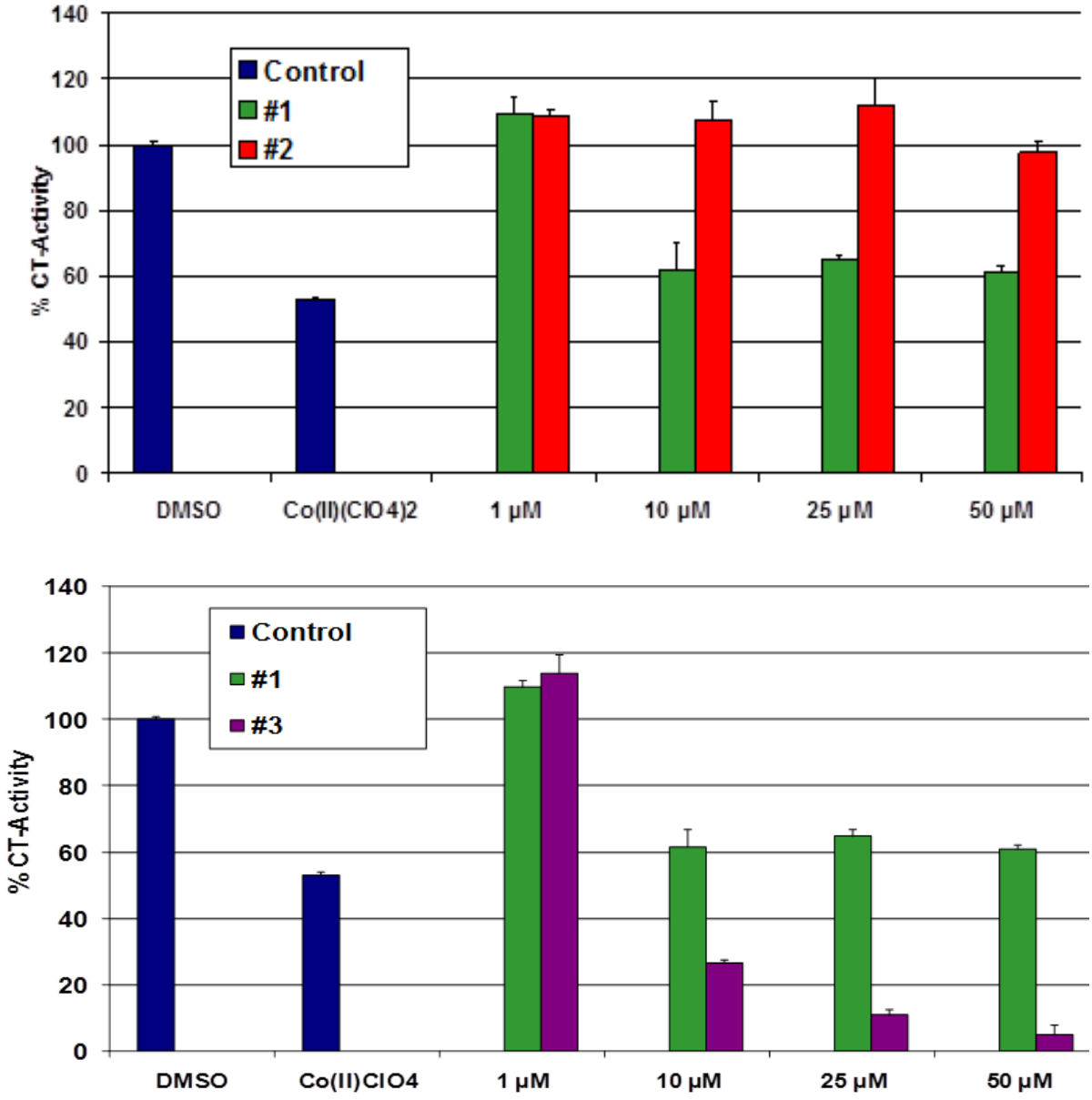

Figure 3.2.5.2. Chymotrypsin-activity inhibition in human purified 20S proteasome; DMSO and $Co^{II}(ClO_4)_2$ are controls. Top: comparison between **1** (left column) and **2** (right column); bottom comparison between **1** (left column) and **3** (right column).

Intrigued by the previous results, proteasome inhibition and apoptosis induction were tested in intact PC-3 human prostate cancer cells to confirm the potential activity of **3**. Cells were first treated with different concentrations (up to 50 μM) of **1** and **3** for 18 h, followed by measurement of proteasome inhibition. PC-3 cells treated with **3** showed a dose-dependent inhibition of the proteasomal activity by ~ 35% at 30 μM and ~ 95% at 50 μM (**Figure 3.2.5.3**). Consistently, levels of ubiquitinated proteins were increased in a dose-dependent manner in PC-3 cells for **3**, whereas **1** showed negligible inhibition.

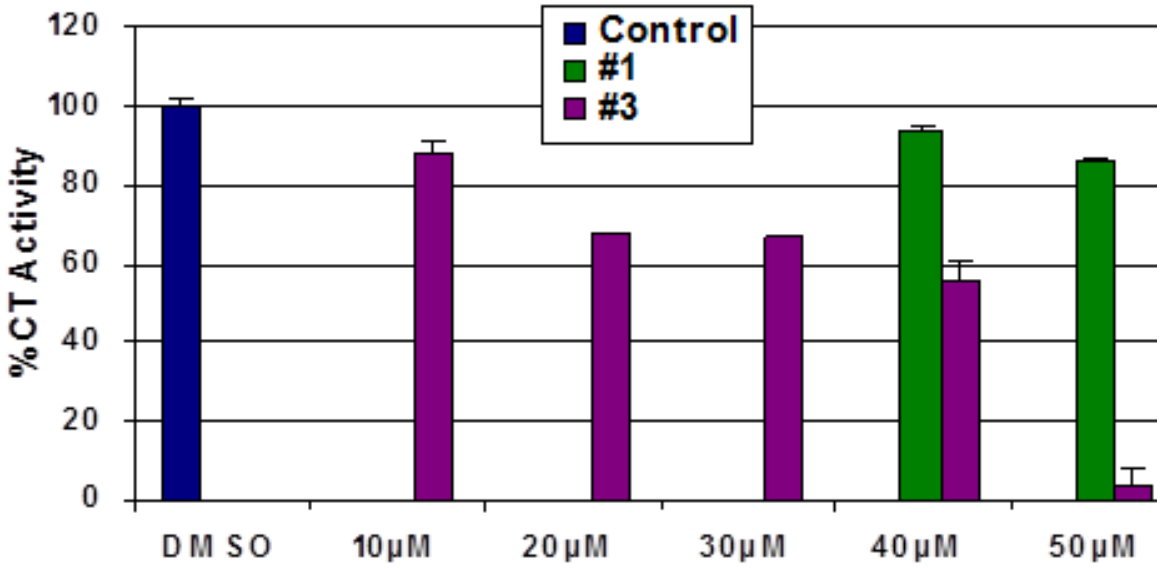

Figure 3.2.5.3. Chymotrypsin-activity inhibition in PC-3 cell lysates after 18 h treatment. Compound **1** was measured at 40 and 50 μM and is shown in the left column. Compound **3** is shown as a single column for 1–30 μM and in the right column for 40 and 50 μM. DMSO is the control.

Previous reports have indicated that inhibition of proteasomal chymotrypsin-like activity in tumor cells may result in the induction of apoptosis.[25] To investigate whether proteasome inhibition is associated with apoptotic cell death, apoptotic-specific caspase-3 induction (**Figure 3.2.5.4**) and related PARP disappearance (**Figure 3.2.5.5**) were measured spectrophotometrically and by Western blotting, respectively. Dramatic induction of caspase-3 was observed in cells

treated with **3** at 40 μM. As expected, abrogation of full length PARP only occurred in cells treated with 30–50 μM of **3**, whereas cells treated with **1** at the highest concentration tested had little visible effect. These results show that induction of apoptosis by **3** in PC-3 cells is associated with inhibition of proteasomal chymotrypsin-like activity.

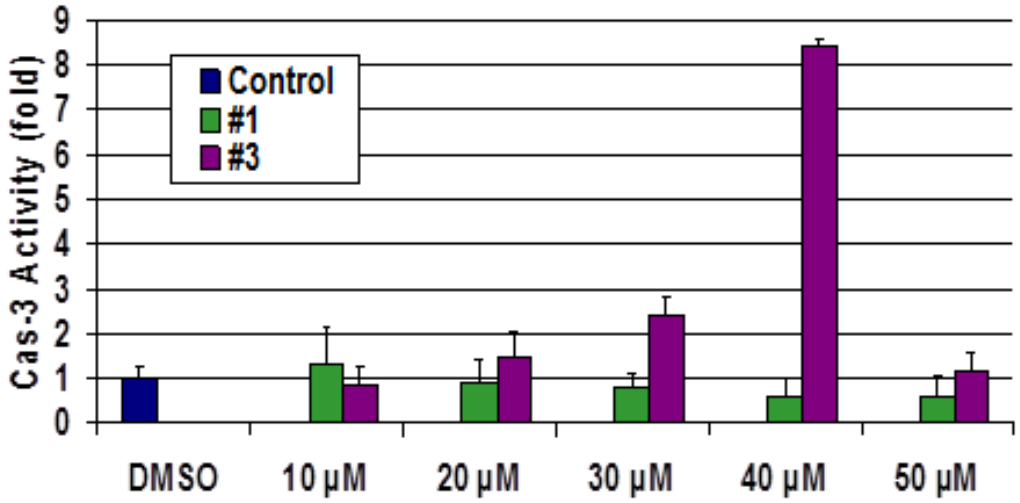

Figure 3.2.5.4. Comparison between **1** (left column) and **3** (right column) for Caspase-3 (apoptosis) Induction in PC-3 cell lysates after 18 h treatment. DMSO is the control.

These results confirm the need for ligand dissociation, as shown by comparison between the activities of **1** and **2**, both with a labile 3 d^7 configuration. However, it is puzzling that compound **1** has proven to be less active than the inert 3 d^6 metal-containing complex **3**. Unlike the previously studied inert 3 d^8 nickel(II) ion, cobalt(III) is a redox-active species capable of being reduced to cobalt(II) within the reducing cellular environment by available reductants. This reduction has been demonstrated individually by several groups[12,13] and utilized for release of alkylating agents such as nitrogen mustards. The redox potential for the cytosolic environment is reported to be around − 0.3 V vs. NHE by Østegaard.[26] A preliminary cyclic voltammogram for **3** in DMSO/$TBAPF_6$ suggests the Co(III)/Co(II) couple at around − 0.5 V vs. NHE. Although

more negative, the result suggests bioreductive activation as a valid working hypothesis in need of further exploration.

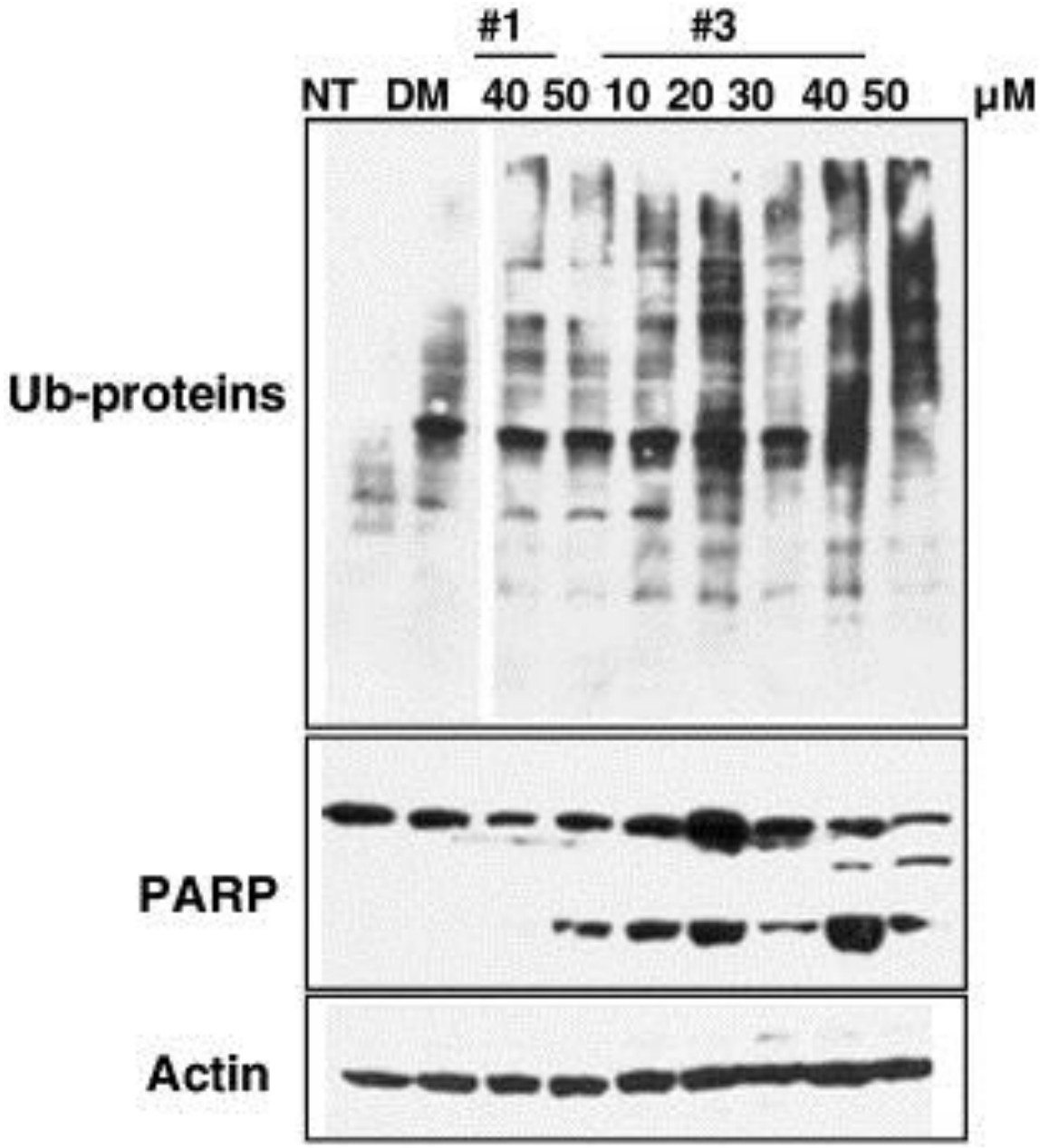

Figure 3.2.5.5. Western blot for PC-3 cell lysates after 18 h treatment.

3.3. Conclusions

In this paper we have investigated the interaction of cobalt complexes with the 26S proteasome. We have compared the behavior of 1:2 and 1:1 metal-to-ligand six-coordinate cobalt species toward cell proliferation, the purified 20S proteasome, and intact PC-3 prostate cancer cells. The 1:2 species described as **1** and **3** are formed respectively between cobalt(II) or cobalt(III) ions and two deprotonated [NN′O] ligands $(L^1)^-$, whereas the 1:1 species **2** is based on a cobalt(II) ion and the new $[N_2N'_2O_2]$ ligand $\mathbf{H_2L^2}$ in its deprotonated form. Detailed characterization along with a crystal structure allows for unquestionable identification of **2**, whereas meticulous NMR spectroscopic evaluation indicated configurational stability of **3** from 80 to −40 °C. The CT-like activity inhibition is severely hampered for the 1:1 species **2**, reinforcing the current hypothesis of ligand dissociation as a requirement for proteasome inhibition. Surprisingly, the kinetically inert **3** showed remarkable proteasome inhibition, far superior to that observed for the labile **1**. We hypothesize that this difference is due to the fact that cobalt is redox-active and species **3** is likely to be reduced intracellularly. In this process a labile cobalt(II) species would be generated, favoring ligand dissociation and interaction with the proteasome. We also hypothesize that species **1**, already containing a labile cobalt(II) species will not remain intact intracellularly in order to reach the targeted proteasome. The possibility of using redox-active metals that can be intracellularly bioreduced opens a stimulating window of opportunity to explore proteasome inhibition, both by metal activation as demonstrated here and as suggested by Scarpellini[10] as well as by using metal ions as carriers for drug delivery.[12] Such studies are currently under investigation in our group.

3.4. Experimental

3.4.1. Materials and Methods

Chemical solvents and reagents were used as described in Chapter 2.

3.4.2. X-ray Structural Determination of [$Co^{II}L^2$] (2)

Diffraction data were measured on a Bruker *X8 APEX-II* kappa geometry diffractometer with Mo radiation and a graphite monochromator. Frames were collected at 100 K with the detector at 40 mm and 0.3° between each frame and were recorded for 10 s. *APEX-II*[27] and *SHELX*[28] software were used in the collection and refinement of the model. Crystals of **[$Co^{II}L^2$] (2)** appeared as amber plates. A total of 23770 reflections were measured, yielding 3750 unique data (Rint = 0.049). Hydrogen atoms were placed in calculated positions. The asymmetric unit contains one neutral complex without solvate. The complex crystallized in 1:1 ratio of dichloromethane and methanol solution **Table 3.4.2**.

3.4.3 NMR Spectroscopic Measurements

NMR spectra were measured using a Varian Mercury-400 and VNMRS-500 MHz spectrometers. Proton, carbon-13, distortionless enhancement by polarization transfer (DEPT), homonuclear correlation spectroscopy (COSY), and heteronuclear multiple quantum coherence (HMQC), and nuclear Overhauser effect (NOE) spectroscopy experiments were acquired in $CDCl_3$, DMSO-d_6 at 298 K and DMF-d_7 between 233 and 273 K.

	[$Co^{II}(L^2)$] (2)
Formula	$C_{28}H_{24}CoI_4N_4O_2$
M	1015.04
Space group	C2/c
a / Å	13.8089(4)
b/ Å	9.9958(4)
c/ Å	22.0818(9)
α/ °	
β/ °	96.013(2)
γ/ °	
V/ $Å^3$	3031.20(19)
Z	4
T/ K	100(2)
λ/ Å	0.71073
D_{calc}/ g cm^{-3}	2.224
μ/ mm^{-1}	4.673
R(*F*) (%)	3.13
Rw(*F*) (%)	6.82

[a] $R(F) = \sum \| F_o | - | F_c \| / \sum | F_o |$ for $I > 2s(I)$; $Rw(F) = [\sum w(F_o^2 - F_c^2)^2 / \sum w(F_o^2)^2]^{1/2}$ for $I > 2s(I)$.

Table 3.4.2. Crystal data and structure refinement results for **[$Co^{II}L^2$] (2)**.

3.4.4. Biological Assays

3.4.4.1 Proteasomal activity in purified 20S proteasome

Purified human 20S proteasome (35 ng) was incubated with 10 μM of CT substrate, SucLLVYAMC, in 100 μL of assay buffer [20 mM Tris-HCl (pH 7.5)] in the presence of complexes 1-3 at various concentrations, as well as the salt $[Co(H_2O)_6](ClO_4)_2$ and DMSO solvent as control experiments. After 2 h of incubation at 37 $^\circ$ C, the production of hydrolyzed AMC groups was measured using a Wallac Victor3 multilabel counter with an excitation filter of 365 nm and an emission filter of 460 nm.[29]

3.4.4.2 Cell cultures and whole cell extract preparation

PC-3 human prostate cancer cells were grown in RPMI1640 supplemented with 10% fetal bovine serum and maintained at 37 °C and 5% CO

$_2$. A whole cell lysate was prepared as previously described.[30]

3.4.4.3 Cell proliferation assay

Cells were seeded in quadruplicate in a 96 well plate and grown to 70−80% confluence, followed by treatment with the indicated agents for 18 h followed by measurement of cell proliferation by the 3(4,5dimethylthiazol-2-yl)2,5diphenyltetrazolium bromide (MTT) assay as described previously.[31]

3.4.4.4 Proteasome CT-like activity in cells

Proteins extracted from cells after each treatment were incubated for 2 h at 37 $^\circ$ C in 100 μL of assay buffer (50 mM Tris-HCl, pH 7.5) with 10 μM of fluorogenic CT substrate SucLLVYAMC, as described previously.[31]

3.4.4.5 Western blot analysis

Cell extracts were separated by SDS-PAGE and transferred to a nitrocellulose membrane. A western blot analysis was performed using specific antibodies to PARP or ubiquitin, followed by visualization using the HyGLO reagent (Denville Scientific, Metuchin, NJ).

3.4.5. Syntheses

3.4.5.1. Ligand syntheses

The iodo-substituted ligand **HL**[1] was synthesized as previously described[14,32] by the treatment of 2-hydroxy-3,5-diiodobenzaldehyde with pyridin-2-ylmethanamine in methanol followed by reduction with sodium borohydride.

The organic precursor 2,4-di-iodo-6-(chloromethyl)phenol was synthesized as previously reported [21]. Yield: 90%. IR (KBr, cm^{-1}, s = strong) 1450(s) (C = C_{ar}); 1265 (s) (C − O); ^{1}H − NMR [δ, ppm; s = singlet, 400 MHz, $CDCl_3$, 300 K] = 4.60, [2x s 2x 1H (CH_2)]; 7.60 [s, 1 H (aryl)]; 7.93 [s, 1 H (aryl)].

The new tethered ligand 6,6′-((ethane-1,2-diylbis((pyridin-2-ylmethyl)azanediyl)) bis(methylene))bis(2,4-diiodophenol) **H_2L^2** was synthesized by adapting available procedures for similar species [22]. The precursor *N1*,*N2*-bis(pyridin-2-ylmethyl)ethane-1,2-diamine was obtained when a 40 mL methanolic solution (0.9 g, 15 mmol) of ethane-1,2-diamine, was treated with two equivalents of picolinaldehyde (3.21 g, 30 mmol) and refluxed for 2 hours. The resulting yellow Schiff base was reduced by addition of sodium borohydride (1.4 g, 37 mmol) at 0 °C. The solvent was rotoevaporated and the crude product was dissolved in 100 mL of brine. Extraction with 4 × 25 mL of dichloromethane followed, and the combined extracts were dried over $MgSO_4$. The solution was rotoevaporated and the product was obtained as a viscous oil.

The precursor N^1,N^2-bis(pyridin-2-ylmethyl)ethane-1,2-diamine (0.31 g, 1.3 mmol) was dissolved in 40 mL dichloromethane, when triethylamine base (0.6 g, 6.4 mmol) was added dropwise and followed by the addition of 2-(chloromethyl)-4,6-diiodophenol (1.0 g, 2.5 mmol). The solution was refluxed for 48 h. The product was extracted with 3 × 25 mL of dichloromethane to remove the triethylammonium chloride salt. The organic layer was dried over $MgSO_4$ and rotoevaporated to give a yellow amorphous foamy solid which was then recrystallized in methanol to yield a microcrystalline solid. Yield: 75%. Mp 158–160 °C; IR (KBr, cm^{-1}, s = strong, m = medium) 2818(s) (C-H), 1596(s), 1540(s) (C = N_{Py}, C = C_{Ar}); 1363(m) (C-O); 1250 (s), (C-N); ^{1}H NMR [δ, ppm; s = singlet, d = doublet, dd = doublet of doublet, 400 MHz, $CDCl_3$, 300 K] 2.67, [4x s, 4x 1H (2 CH_2) -N-CH_2-CH_2-N-]; 3.61, [4x s, 4x 1H (2 CH_2) –N-CH_2-phenol]; 3.72, [4x s, 4x 1H (2 CH_2) –N-CH_2-pyridyl]; 7.11-7.13, [4x 4x 1H (phenol)]; 7.20-7.23, [2x dd, 2x 1H (py-2)]; 7.66-7.70, [2x dd, 2x 1H (py-3)]; 7.91, [2x d, 2x 1H (py-4)]; 8.59, [2x d, 2x 1H (py-1)]; ESI^+ in MeOH: *m/z* (100%) = 959.1 for $[H_2L^2 + H^+]^+$.

3.4.5.2. Complex syntheses

$[Co^{II}(L^1)_2]$ (1). Synthesis of this complex followed the previously described procedure.[14]

Yield: 85%; IR data: (KBr, cm^{-1}, s = strong, m = medium) 1603(m), 1560(s), 1446(s) (C = N_{Py}, C = C_{Ar}); 1328(m) (C-O); ESI^+ in MeOH: *m/z* (100%) = 990.1 for $[Co^{II}(L^1)_2 + H^+]^+$; Anal. Calc. (%) for **$1 \cdot H_2O$** (%, $C_{26}H_{24}CoI_4N_4O_3$, FW = 1007.04 $g.mol^{-1}$) C, 31.01; H, 2.40; N, 5.56. Found (%): C, 31.14; H, 2.16; N, 5.39.

$[Co^{II}L^2]$ (2). $[Co(H_2O)_6](ClO_4)_2$ (0.12 g, 0.31 mmol) was dissolved in 5 mL of methanol and was added dropwise under anaerobic conditions to a 10 mL dichloromethane solution containing (0.3 g, 0.31 mmol) of the **H_2L^2** ligand and Et_3N (0.079 g; 79.2 mmol). The solution was stirred at room temperature for 3 h, when a color change was observed from yellow to brown. No

precipitate was formed observed. The solution gave orange colored crystals after 48 h. Yield: 65%; IR data: (KBr, cm^{-1}, s = strong, m = medium) 2839(m) (C-H), 1558(s), 1483(s) (C = N_{Py}, C = C_{Ar}); 1363(m) (C-O); ESI^+ in MeOH: *m/z* (100%) = 1015.7 for $[Co^{II}L^2]^+$; Anal. Calc. for **2** (%, $C_{28}H_{24}CoI_4N_4O_2$, FW = 1014.74 $g.mol^{-1}$); C, 33.13; H, 2.38; N, 5.52. Found (%): C, 33.25; H, 2.44; N, 5.44.

$[Co^{III}(L^1)_2]ClO_4$(3). The $[Co(H_2O)_6](ClO_4)_2$ salt (0.37 g, 1.0 mmol) was dissolved in 5 mL of methanol and added to a 30 mL dichloromethane solution containing the ligand **HL^1** (0.98 g, 2.0 mmol) and Et_3N (0.28 mL; 2.0 mmol) under aerobic condition. The solution was refluxed for 4 h, when a brownish product was vacuum filtered and washed with cold methanol and ether. Yield: 70%; IR data (KBr, cm^{-1}, s = strong, m = medium): 1603(m), 1560(s), 1446(s) (C = N_{Py}, C = C_{Ar}); 1099(s) cm^{-1} (ClO_4^-) 1328(m) (C-O); ESI^+ in MeOH: *m/z* (100%) = 989 for $[Co^{III}(L^1)_2]^+$; Anal. Calc. for **3** (%,$C_{26}H_{22}CoI_4N_4O_6Cl$, FW = 1088.48 $g.mol^{-1}$) C, 28.69; H, 2.04; N, 5.15. Found (%): C, 28.72; H, 2.17; N, 5.05.

3.5 References

1 Kaiser, P.; Huang, L. *Genome Biol.* **2005**, *6*, 233.

2 Hochstrasser, M. *Curr. Opin. Cell. Biol.* **1995**, *7*, 215.

3 Meiners, S.; Ludwig, A.; Stangl, V.; Stangl, K. *Med. Res. Rev.* **2008**, *28*, 309.

4 Borissenko, L.; Groll, M. *Chem. Rev.* **2007**, *107*, 687.

5 Shakya, R.; Peng, F.; Liu, J.; Heeg, M. J.; Verani, C. N. *Inorg. Chem.* **2006**, *45*, 6263.

6 Frezza, M.; Verani, C. N.; Chen, D.; Dou, Q. P. *Lett. Drug Des. Discov.* **2007**, *4*, 311.

7 Kisselev, A. F.; Goldberg, A. L. *Chem. Biol.* **2001**, *8*, 739.

8 Hindo, S.; Frezza, M.; Tomco, D.; Heeg, M. J.; Hryhorczuk, L.; McGarvey, B. R.; Dou, Q. P.; Verani, C. N. *Eur. J. Med. Chem.* **2009**, *44*, 4353.

9 Frezza, M.; Hindo, S. S.; Tomco, D.; Allard, M.; Cui, Q. C.; Heeg, M. J.; Chen, D.; Dou, Q. P.; Verani, C. V. *Inorg. Chem.* **2009**, *48*, 5928.

10 Souza, E.T.; Castro, L.C.; Castro, F.A.V.; do Canto Visentin, L.; Pinheiro, C.B.; Pereira, M.D.; de Paula Machado, S.; Scarpellini, M. *J. Inorg. Biochem.* **2009**, *103*, 1355.

11 Gurley, L.; Beloukhina, N.; Boudreau, K.; Klegeris, A.; McNeil, W. S. *J. Inorg. Biochem.* **2011**, *105*, 858.

12 Hall, M. D.; Failes, T. W.; Yamamoto, N.; Hambley, T. W. *Dalton Trans.* **2007**, 3983.

13 Schieber, C.; Howitt, J.; Putz, U.; White, J. M.; Parish, C. L.; Donnelly, P. S.; Tan, S.-S. *J. Biol. Chem.* **2011**, *286*, 8555.

14 Shakya, R.; Hindo, S. S.; Wu, L.; Allard, M.; Heeg, M. J.; Hratchian, H. P.; McGarvey, B. R.; da Rocha, S.; Verani, C. N. *Inorg. Chem.* **2007**, *46*, 9808.

15 dos Anjos, A.; Bortoluzzi, A. J.; Szpoganicz, B.; Caro, M. S. B.; Friedermann, G. R.; Mangrich, A. S.; Neves, A. *Inorg. Chim. Acta* **2005**, *358*, 3106.

16 Wong, E.; Liu, S.; Rettig, S. J.; Orvig, C. *Inorg. Chem.* **1995**, *34*, 3057.

17 Neves, A.; Erthal, S. M. D.; Vencato, I.; Ceccato, A. S.; Mascarenhas, Y. P.; Nascimento, O. R.; Hörner, M.; Batista, A. A. *Inorg. Chem.* **1992**, *31*, 4749.

18 Kepert, D. L.; *Inorganic Stereochemistry*, *Springer-Verlag*, New York, **1982**, p. 114.

19 Setyawati, I. A.; Rettig, S. J.; Orvig, C. *Can. J. Chem.* **1999**, *77*, 2033.

20 Lanznaster, M.; Neves, A.; Bortoluzzi, A. J.; Assumpção, A. M. C.; Vencato, I.; Machado, S. P.; Drechsel, S. M. *Inorg. Chem.* **2006**, *45*, 1005.

21 Neves, A.; Vencato, I.; Erthal, S. M. D. *Inorg. Chim. Acta* **1997**, *262*, 77.

22 Silva, F.; Marques, F.; Santos, I. C.; Paulo, A.; Rodrigues, A. S.; Rueff, J.; Santos, I. *J. Inorg. Biochem.* **2010**, *104*, 523.

23 Shakya, R.; Imbert, C.; Hratchian, H. P.; Lanznaster, M.; Heeg, M. J.; McGarvey, B. R.; Allard, M. M.; Schlegel, H. B.; Verani, C. N. *Dalton Trans.* **2006**, 2517.

24 Chen, D.; Frezza, M.; Shakya, R.; Cui, C. Q.; Milacic, V.; Verani, C. N.; Dou, Q. P. *Cancer Res.* **2007**, *67*, 9258.

25 An, B.; Goldfarb, R. H.; Siman, R.; Dou, Q. P. *Cell Death Diff.* **1998**, *5*, 1062.

26 Østergaard, H.; Tachibana, C.; Winther, J. R. *J. Cell Biol.* **2004**, *166*, 337.

27 APEX II collection and processing programs are distributed by the manufacturer, Bruker AXS Inc, Madison WI, USA, **2009**.

28 Sheldrick, G. M. *Acta Crystallograhica*, **2008**, *A64*, 112.

29 Daniel, K. G.; Gupta, P.; Harbach, R. H.; Guida, W. C.; Dou, Q. P. *Biochem. Pharmacol.* **2004**, *67*, 1139.

30 Chen, D.; Cui, Q. C.; Yang, H.; Dou, Q. P. *Cancer Res.* **2006**, *66*, 10425.

31 Daniel, K. G.; Chen, D.; Orlu, S.; Cui, Q. C.; Miller, F. R.; Dou, Q. P. *Breast Cancer*

Res. **2005**, *7*, R897.

32 Imbert, C.; Hratchian, H. P.; Lanznaster, M.; Heeg, M. J.; Hryhorczuk, L. M.; McGarvey, B. R.; Schlegel, H. B.; Verani, C. N. *Inorg. Chem.* **2005**, *44*, 7414.

CHAPTER 4

PROBING CHEMICAL REDUCTION IN A COBALT(III) COMPLEX AS A VIABLE ROUTE FOR THE INHIBITION OF THE 20S PROTEASOME

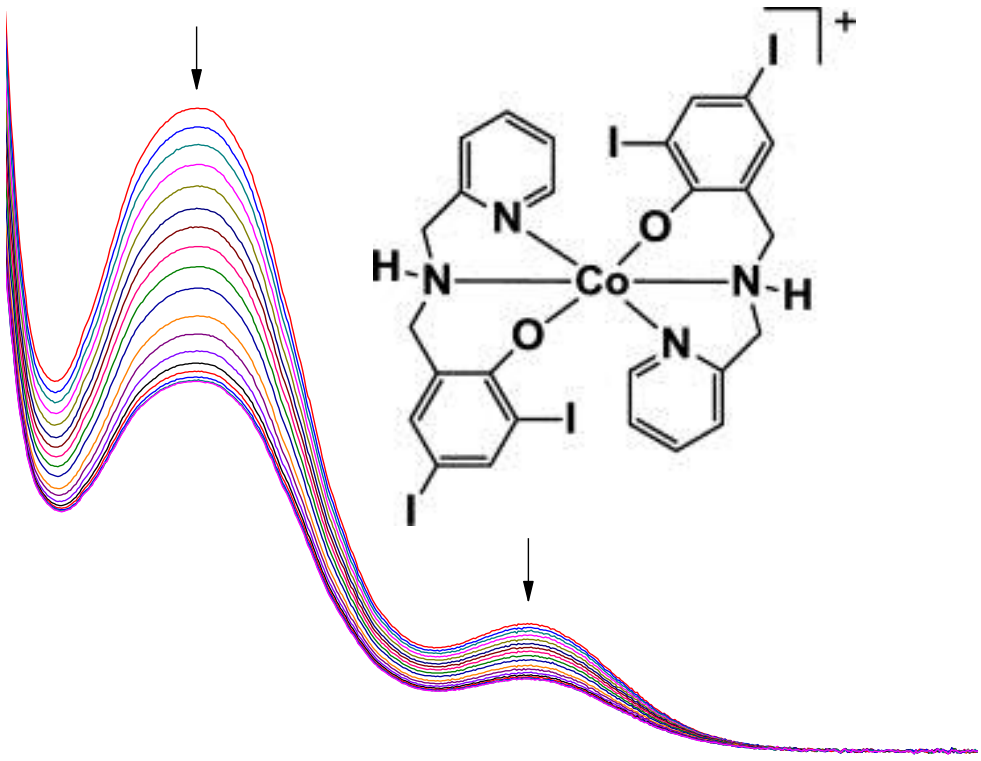

CHAPTER 4

PROBING CHEMICAL REDUCTION IN A COBALT(III) COMPLEX AS A VIABLE ROUTE FOR THE INHIBITION OF THE 20S PROTEASOME

Published with minor changes as Tomco, D.; Xavier, F.; Allard, M. M.; Verani, C. N.* *Inorg. Chim. Acta*, **2012**, *393*, 269.

4.1. Introduction

In the previous chapter, we compared the inhibition activity of the complex **$[Co^{II}(L^1)_2]$** and its counterpart **$[Co^{III}(L^1)_2ClO_4]$**[1] (**Scheme 4.1**). The former species contains a relatively labile bivalent high-spin cobalt ion,[2] whereas the latter contains an inert trivalent low-spin cobalt ion that has shown unexpectedly better CT inhibition in cells. Considering the evidence for a relationship between cytotoxic activity and metal ion lability observed for **$[Ni^{II}(L^1)_2]$**,[3] the biological accessibility of different oxidation states in the abovementioned cobalt complexes is the most relevant mechanism to allow for the switching between an inert d^6 low-spin and a labile d^7 high-spin character. In spite of the rich cobalamin chemistry[4,5] the use of cobalt species for antitumor applications remains underdeveloped.[6,7]

Evidence for cobalt(III) complexes used as chaperones to carry specific matrix metalloproteinases including marimastat[8] drug have been reported by Hambley[9] and co-workers,[10,11,12] where enhanced antitumor activity was observed once marimastat was chelated to a Co^{III}-tris(methylpyridyl)amine complex. The inert character of the cobalt(III) ion increases the intracellular transportation of the complex, and depending on the redox potential of Co(III)/Co(II) couple bioreductive activation allows for conversion to a more labile Co(II) species, hence release of the drug. In this chapter, we evaluate the chemical and electrochemical reduction of the cobalt complex **$[Co^{III}(L^1)_2]ClO_4$** (**1**) and the viability of ligand dissociation in

order to form an active pharmacophore $[ML]^+$. We aim to (i) evaluate the redox potentials for the Co(II)/Co(III) couple, (ii) observe the spectroelectrochemical and chemical reduction behavior at controlled pH via monitoring of the phenolate-to-cobalt LMCT band observed at 440 ± 5 nm in the UV‑Vis spectrum, and (iii) assess resulting products of reduction by HR-ESI^+ mass spectrometry. These results will be presented and discussed in detail.

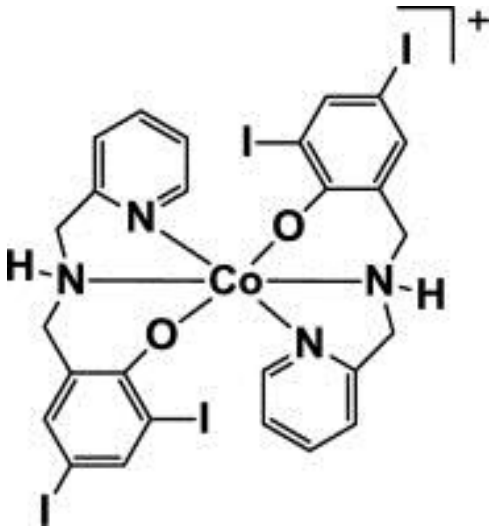

Scheme 4.1. Structure of complex **$[Co^{III}(L^1)_2]ClO_4$ (1)**.

4.2. Results and Discussion

Complex **1** was synthesized according to a previously published procedure in our group.[1] UV–Vis spectroscopy in DMF confirms the presence of $p\pi_{phenolate} \rightarrow d\sigma^*_{cobalt(III)}$ charge transfer band at 440 nm. The CT-like activity inhibition of **1** was measured in purified 20S proteasome showing over than 90% inhibition at a concentration of 25 μM. Cell proliferation inhibition tests resulting with $IC_{50} \leqslant 25$ μM were obtained in PC-3 cells once treated with **1**.

4.2.1 Cyclic Voltammetry

The redox properties of complex **1** were recorded in two solvent systems namely DMF and DMF/H_2O (90:10% v/v) under argon, where $TBAPF_6$ was used as a supporting electrolyte.

The potential values are measured *versus* Ag/AgCl and reported against the Fc/Fc^+ redox couple as an internal standard.[13] This data is summarized in **Table 4.2.1**. For the DMF solution, complex **1** demonstrates a quasi-reversible metal-centered Co^{III}/Co^{II} couple (**Figures B.4.2.1.1** and **B.4.2.1.2**) at $E_{½} = -705$ mV versus Fc/Fc^+ ($\Delta E_p = 105$ mV; $|i_{pc}/i_{pa}| = 1.12$). This redox potential changes slightly for the DMF/H_2O (90:10% v/v) solvent system (**Figure 4.2.1** and **Figure B.4.2.1.3)**, where $E_{½} = -668$ mV versus Fc/Fc^+ ($\Delta E_p = 120$ mV; $|i_{pc}/i_{pa}| = 0.90$). The reversibility of the Co^{III}/Co^{II} couple given by the $|i_{pc}/i_{pa}|$ is nearly equivalent between the two solvent systems. It has been observed that the Co^{III}/Co^{II} reduction potential is highly effected by the substituents (electron withdrawing/donating) present on the ligand.[14] Previously published cobalt(III) complexes[15] with similar ligands containing *t*-butyl groups decreased the redox potential on the cobalt ion, whereas the chloro-substituents increased such potential.[16,17]

The redox potential for bioactivated cobalt(III) complexes is found between −600 and −800 mV versus Fc/Fc^+ (−200 to −400 mV versus NHE).[18] Therefore, the observed potential for **1** is well within this range and the complex is a viable candidate for intracellular reduction.

	DMF, mV	DMF:H_2O, mV
E_{pc}	-757	-728
E_{pa}	-652	-608
$E_{1/2}$ (ΔE) *vs.* Fc/Fc^+	-705 (105)	-668 (120)

Table 4.2.1. Electrochemical values for complex **1** in DMF and DMF/H2O (90:10% v/v) solvents. Potentials are measured for Co(III)/Co(II) couple vs. Ag/AgCl and plotted vs. Fc/Fc^+ reference standards in mV.

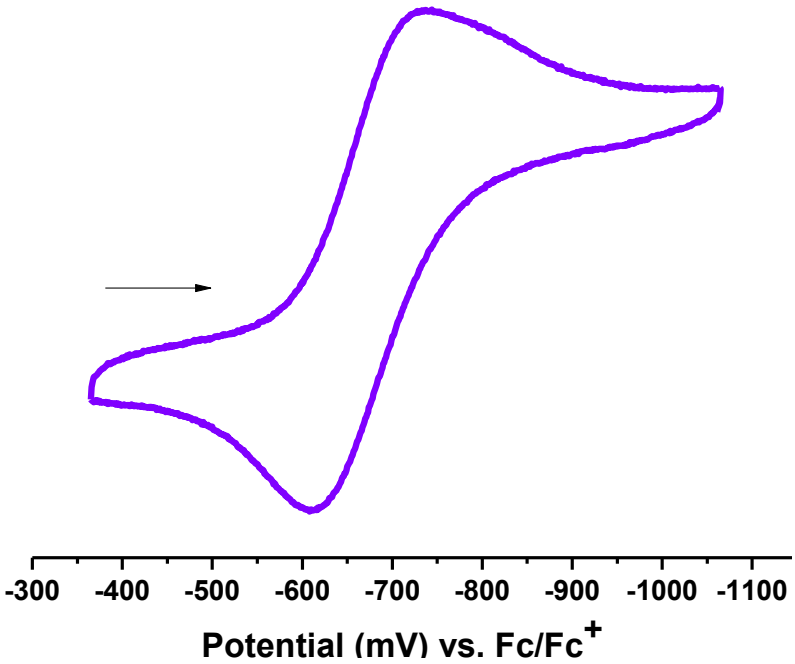

Figure 4.2.1. Cyclic voltammograms of complex (**1**) in DMF/H_2O 90:10% v/v solvent system with concentration of 9.0×10^{-4} M. $TBAPF_6$ was used as supporting electrolyte. The redox potential for Co(III)/(II) couple is measured vs. Ag/AgCl and plotted using Fc/Fc^+ as an internal reference at room temperature.

4.2.2. Computational Studies

Polyphenolate complexes with metal centers are long known to be difficult for differentiating and identifying their formal redox centers.[19,20] We have previously[21] used computational methods for this purpose, and reported on the electronic structure of similar cobalt,[15,22] zinc,[3] and iron(III) complexes. In this report, we are interested in the redox properties relating to the reduction of these complexes. Calculations were performed on the $[Co(L^1)_2]^+$ ($S = 0$) and high-spin $[Co(L^1)_2]^0$ ($S = 3/2$) to assess information on bonding interactions and identify the frontier orbitals involved in both the electrochemistry and electronic spectroscopy. It is clearly indicated in **Figure 4.2.2** that the initial Co(III) complex is consistent with a low-spin Co d^6 with no unpaired electron (left). Upon reduction, the resulting

complex is consistent with a Co(II) d^7 high-spin complex with three unpaired electrons, as can be shown in the spin density plot (right). The Co(III) shows that the first two empty unoccupied orbitals, namely LUMO and LUMO+1 are cobalt-based, consistent with empty anti-bonding d orbitals expected for a low-spin d^6 metal complex. The first two occupied orbitals (HOMO, and HOMO−1) are phenolato-based, consistent with our previously shown assessments.[15,22,23]

It is interesting to note that unlike our previous electronic structure on –H substituted [35] phenolate groups, it seems the –iodo groups are heavily involved in some of the frontier orbitals in HOMO−2, −3, −4, and −5. As expected, the remaining three d metal cobalt orbitals are low in energy. Upon addition of an electron to reduce $[Co^{III}(L^1)_2]^+$, one would expect the population of the LUMO, which is cobalt centered, and upon oxidation we would expect to form a phenoxyl radical as per the nature of the HOMO. Indeed, for the reduced species, namely $[Co^{II}(L^1)_2]^0$, we observed a Co(II) d^7 high-spin complex with the three magnetically relevant orbitals shown in **Figure 4.2.2** on the right (**Table B.4.2.2**), consistent with our cyclic voltammetry assignment.

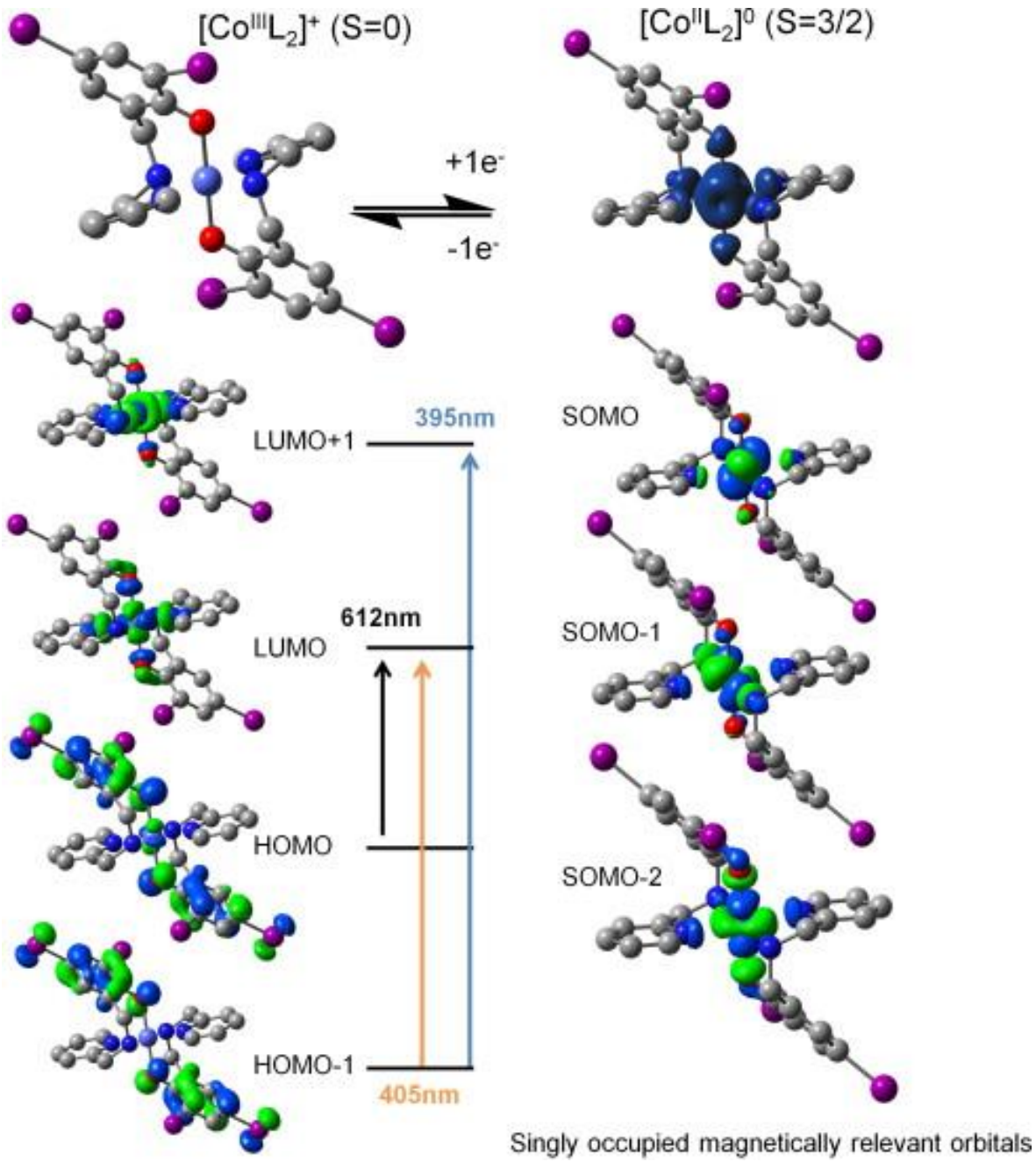

Figure 4.2.2. Relevant frontier orbitals for $[Co^{III}(L^1)_2]^+$ (left) and $[Co^{II}(L^1)_2]^0$ (right) including their spin density (top). TD-DFT electronic transitions for $[Co(L^1)_2]^+$ are shown in the middle.

4.2.3. Electronic Spectroscopy

According to time-dependent density functional theory (TD-DFT) the spectra of the cobalt(III) complexes are dominated by three low energy charge transfer bands. The HOMO → LUMO transition at 612 nm is identified as a phenolate → cobalt LMCT, and the two bands close in energy are associated with HOMO−1 → LUMO and HOMO−1 → LUMO+1 at 405 and 395 nm, respectively (see inset **Figure 4.2.2**). These prominent bands are the result of phenolato-to-cobalt charge transfer bands, and are consistent with the frontier orbitals discussed in the previous section. This behavior is expected for Co(III) complexes with electroactive ligands, in which charge transfer from fully occupied ligand orbitals to low energy Co(III) empty d orbitals can be expected to dominate the low energy end of the spectra (>350 nm). The higher energy (<350 nm) is dominated by intra-ligand $\pi \rightarrow \pi^*$ inter-valence charge transfers (IVCT). Thus upon reduction of these complexes, the change from a singlet d^6 metal complex to a quartet high-spin d^7 complex spectra should result in a complex with very low energy (>1000 nm) d-d charge transfer bands (mostly absent in the Co(III) spectra), and similar intra-ligand charge transfers, but the LMCT charge transfer bands should either be absent or have very small molar absorptivity. Our modeling indicates the near absence of bands with wavelengths above 500 nm and IVCT bands centering around 375-400 nm; all related to various $\pi \rightarrow \pi^*$ transitions within the ligand. Therefore according to these calculations, we conclude that the bands at 440 and 625 nm can be assigned to phenolato-to-cobalt charge transfers (LMCT) and both are expected to disappear upon reduction.

In order to investigate the spectroscopic properties of the reduced complex **1**, reductive room temperature spectroelectrochemical spectra were obtained under argon using $TBAPF_6$ in DMF. Upon an applied fixed potential of −1200 mV versus Fc/Fc^+, a marked decrease of the

LMCT bands was observed over time **Figure 4.2.3**. The calculated spectra are shown in (**Figure B.4.2.3**).

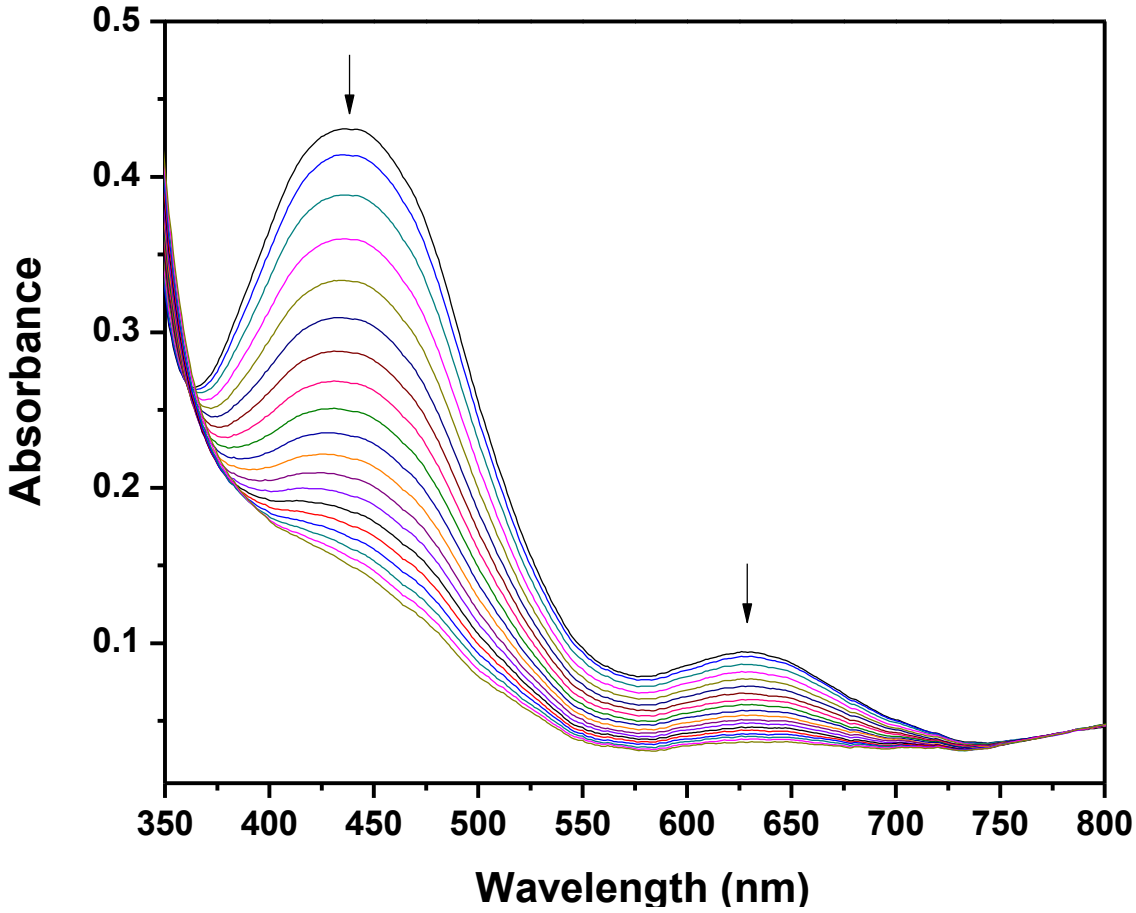

Figure 4.2.3. Spectroelectrochemical spectra for complex **1** in DMF in the presence of $TBAPF_6$ as supporting electrolyte. The decrease of the phenolate to Co(III) charge transfer band at 440 nm was followed over time upon the applied fixed potential of −1200 mV vs. Fc/Fc^+.

4.2.4. Chemical Reduction

Chemical reduction using ascorbic acid (AA) was performed in order to evaluate whether biological agents can carry on the Co(III)/Co(II) reduction and to assess the timeframe required for such process. We conducted these experiments at room temperature under inert conditions using a large excess of AA as to mimic a pseudo-first order reaction mechanism. The results

allow us to estimate an approximate reduction rate constant and to analyze the resulting products of this chemical reduction. The experiment was performed in a freshly prepared DMF/H_2O (90:10% v/v) solution and followed spectrophotometrically at the maxima (λ_{max} = 440 nm) by the decrease of the phenolate to cobalt(III) charge transfer band over time, as well as the decrease of the second LMCT band at 625 nm shown in **Figure 4.2.4.1**.

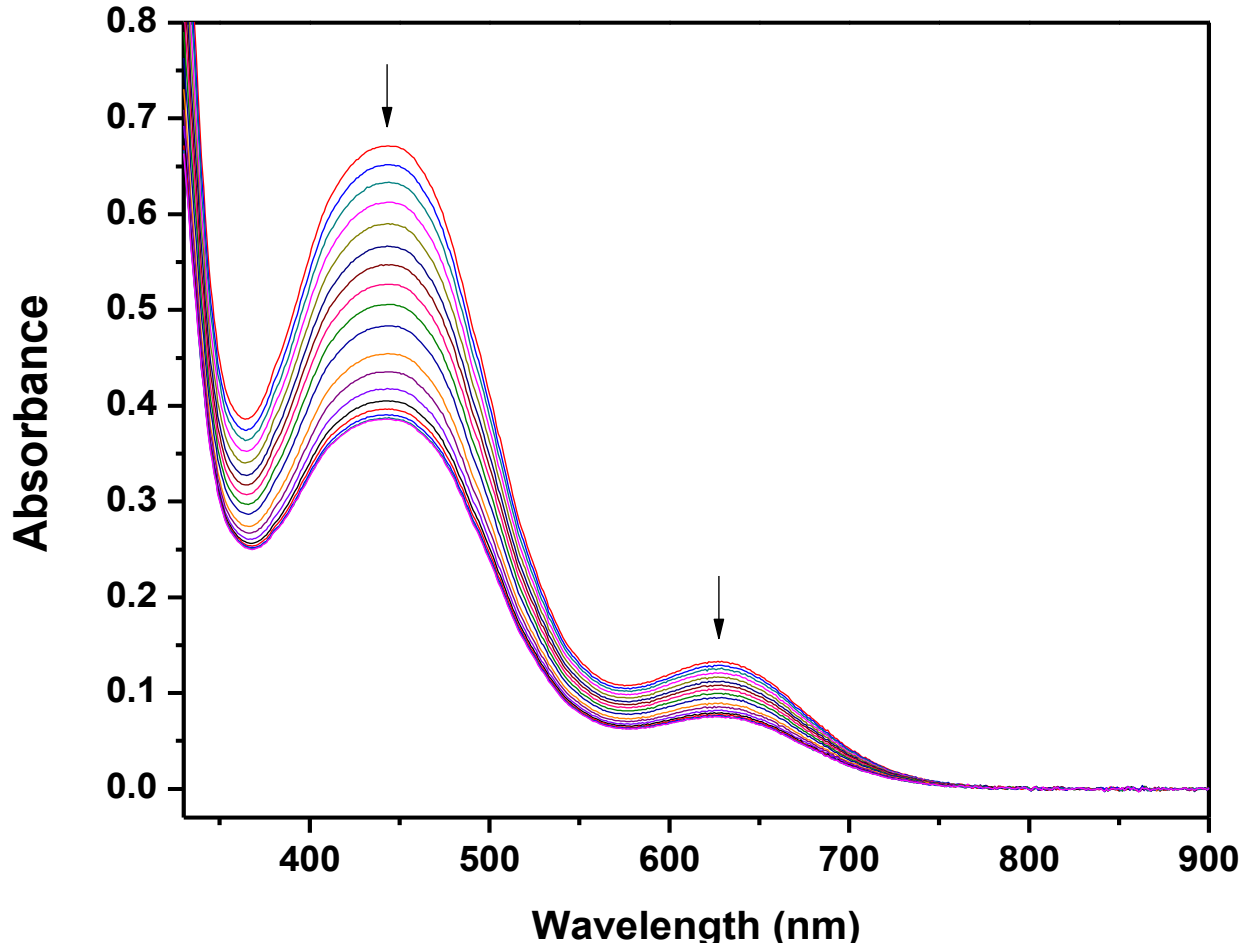

Figure 4.2.4.1. Chemical reduction experiment of complex **1** with ascorbic acid in DMF/H_2O (90:10% v/v) with final concentration of 9.0 $\times$ 10^{-5} M. Each spectrum is recorded every 30 min and the decrease of $p\pi_{\text{phenolate}} \rightarrow d\sigma^{*}_{\text{cobalt(III)}}$ charge transfer band at 440 nm over time was observed for a time period of 18 h.

Each spectrum was recorded periodically every 30 min for 18 h until the equilibrium between the oxidized/reduced species was reached. A control sample was prepared under the same conditions without the presence of the reductant AA (**Figure B.4.2.4.1**). Two other control experiments were performed without AA, but the solutions were adjusted to an apparent pH 3 and pH 1, (**Figures B.4.2.4.2** and **B.4.2.4.3**), respectively. The phenolate-to-cobalt(III) charge transfer band was monitored spectrophotometrically overnight. These data showed no change in the absorbance, position, or shape of the LMCT band thus indicating that the stability of 1 is maintained in both of the acidic solutions. This observation implies that even under these conditions the phenolato groups from the ligand are not being protonated. Both experiments strengthen the conclusion that AA is reducing the metal center rather than promoting the protonation of the ligand. The concentration dependence of complex **1** *versus* time was measured following the decrease of the LMCT band and the data was fitted using a pseudo-first order approach and treated using a first order rate equation (**Figure 4.2.4.2**). The approximate rate constant (k_{obs}) value was obtained from the linearized data (curve slope) and half-life ($t_{½}$) was calculated. The values for $k_{obs} = 2.03 \pm 0.04 \times 10{-}5\ s^{-1}$ and $t_{½} \sim 9.5$ h which indicates that the reduction of the cobalt center is occurring at a considerably slow pace. This time window falls well within the observed time frame for biological experiments.[1]

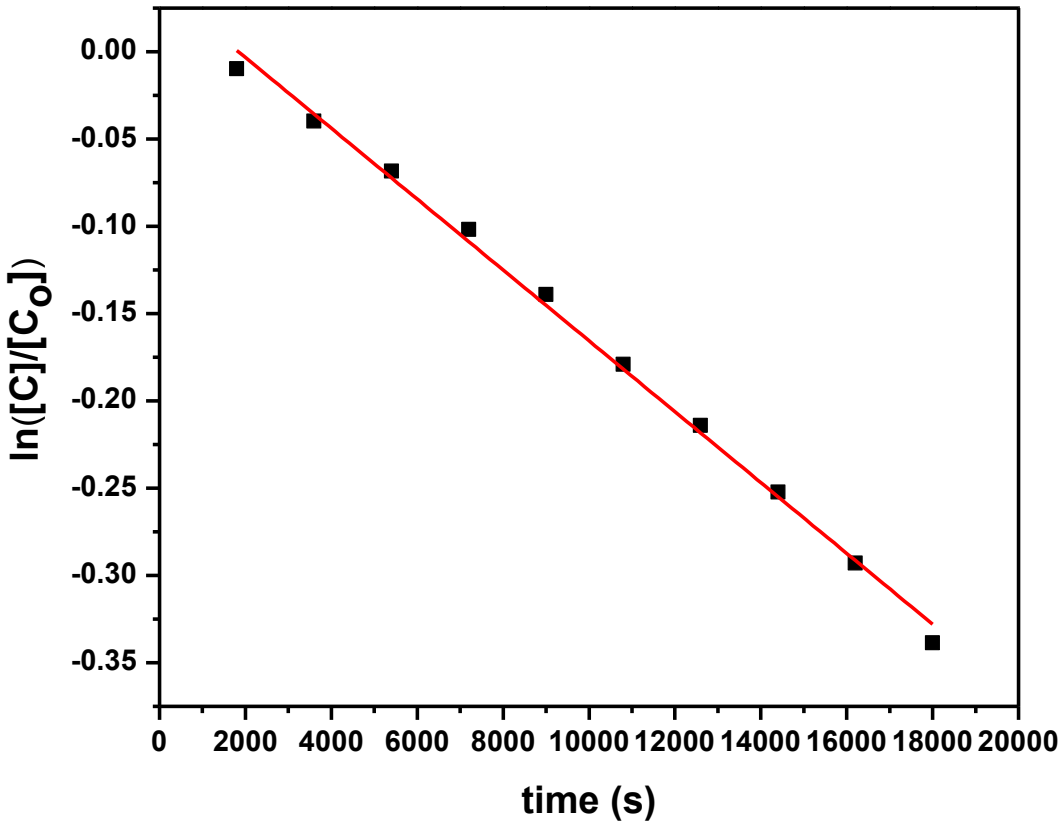

Figure 4.2.4.2. Linearized plot of the pseudo-first order rate law.

4.2.5. Product Analysis via HR-ESI$^+$-MS After Chemical Reduction

High resolution mass spectrometry, HR-(+)-ESI-MS, was used in fresh solutions of **1** in order to evaluate the products of chemical reduction and possibly detect ligand dissociation. All the experimental *m*/*z* results were in good agreement with calculated *m*/*z* values and with the expected isotopic distributions for the species of interest (**Figure 4.2.5.1**).

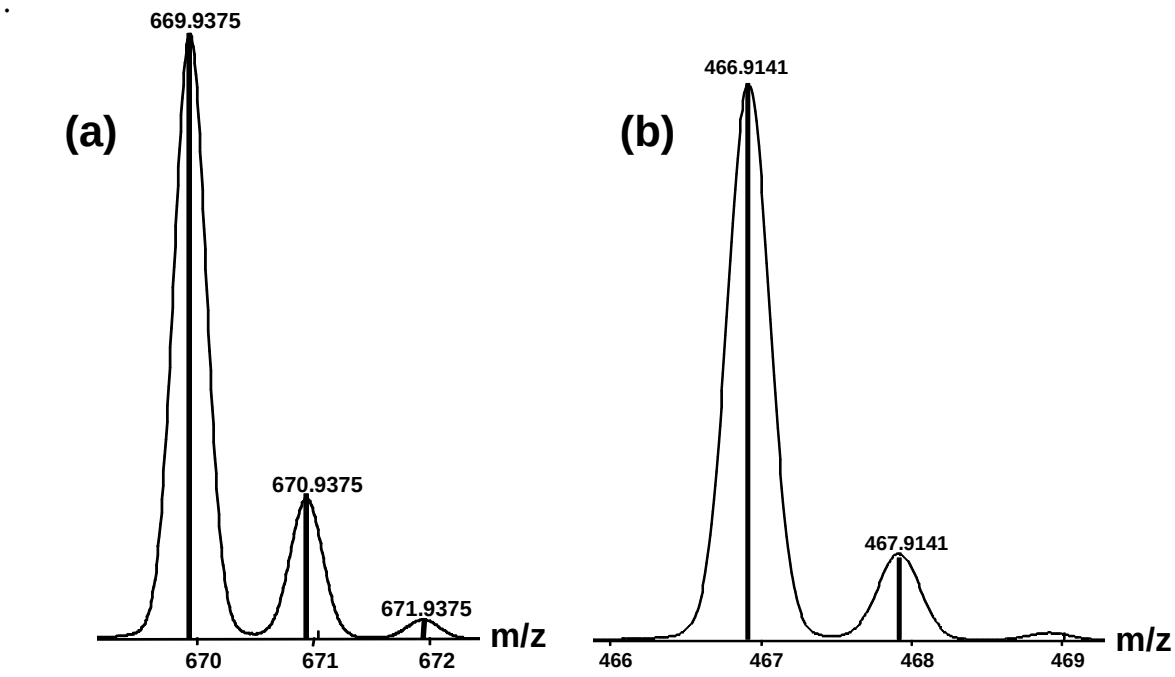

Figure 4.2.5.1. Mass spectrometry results for **1** after treatment with AA; peak position and isotopic distribution for (a) $[Co^{II}(L^1)+2DMF]^+$ and (b) $[HL^1+H^+]^+$. The bars represent the experimental data, whereas the continuous spectra show the simulated data.

Immediately after the completion of the chemical reduction, an aliquot of the reaction was diluted in methanol and injected in the mass spectrometer and relevant peak clusters were detected. The molecular ion peak observed at $m/z = 988.72$ (100%) corresponds to the $[Co^{III}(L^1)_2]^+$ complex (**Figure B.4.2.5.1**). We were unable to detect the reduced **$[Co^{II}(L^1)_2]$** species by mass spectrometry, both due to its neutral charge as well as to *in situ* oxidation. In fact, the mass spectrometry data for the isolated and previously published **$[Co^{II}(L^1)_2]$** complex showed the presence of $[Co^{III}(L^1)_2]^+$ at $m/z = 988.64$ rather than the peak at 989.64 attributed to $[Co^{II}(L^1)_2+H^+]^+$ even a lower cone voltages (**Figure B.4.2.5.2**).[22] These results strongly suggest that the **$[Co^{II}(L^1)_2]$** complex obtained by chemical reduction would be easily reoxidized in the

mass spectrometer. Thus, the observed peak at m/z = 988.72 is associated with the $[Co^{III}(L^1)_2]^+$ species from non-reduced **1** as well as from reoxidation of **$[Co^{II}(L^1)_2]$**. Therefore, we looked for other species in which the cobalt(II) ion can be detected; we observed a peak at m/z = 669.98 (Fig. 6a, S8) attributed to $[Co^{II}(L^1)+2DMF]^+$ species. The presence of DMF solvent in the peak confirms that this species is formed in the original solution. This peak has not been detected in the control solution (**Figure B.4.2.5.3**) and reinforces the idea of ligand dissociation due to metal reduction. The ligand itself is observed exclusively in the chemically reduced sample as the $[HL^1+H^+]^+$ species at m/z = 466.91 (**Figure 4.2.5.1 (b)** and **Figure B.4.2.5.1**). The presence of these peaks suggests that ascorbic acid has indeed reduced the inert cobalt(III) ion to the more labile cobalt(II) ion, thus increasing the probability of the loss of one ligand in the solution generating the biologically active pharmacophore species. Based on the available spectroelectrochemical, chemical reduction, and product analysis evidence, a plausible scheme for these transformations is offered in **Figure 4.2.5.2.**

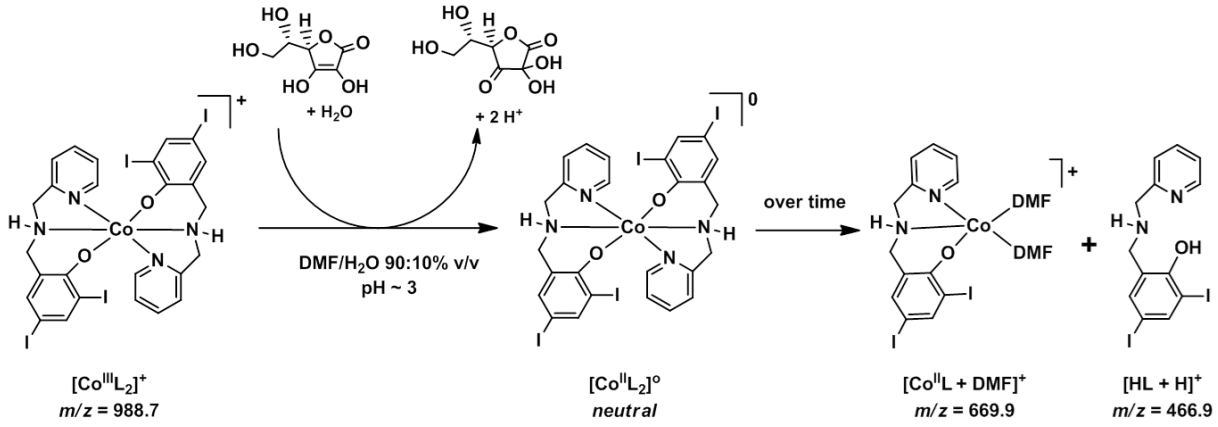

Figure 4.2.5.2. Proposed mechanism for the ligand release upon chemical reduction in the presence of ascorbic acid.

4.3. Conclusions

In this chapter we have investigated a possible way on how complex **1**, containing an inert cobalt(III) ion, can be reduced into a more labile Co(II) species, as well as the viability of ligand dissociation from this labile species in order to form a pharmacophore able to inhibit the 20S proteasome such as the $[Co^{II}L(DMF)_2]^+$ species. We evaluated the redox potentials for the Co(III)/Co(II) couple in DMF and DMF/H_2O and found them to be compatible with the range for bioactivation and spectroelectrochemical results support this assessment with a decrease of the phenolate-to-cobalt MLCT band. The experimental results were corroborated by DFT calculations. Chemical reduction with ascorbic acid also indicated a decrease of the LMCT band and MS data confirmed the presence of $[Co^{II}L(DMF)_2]^+$ along with the dissociated ligand. These species were not observed in control samples lacking the reducing agent even if at considerably acidic conditions. These results point out to biological reduction as a viable way to promote ligand dissociation and, therefore, pharmacophore formation in cobalt(III) prodrugs.

4.4. Experimental Section

Materials and methods were used as described in Chapter 2. Electronic structure calculations were carried out with the GAUSSIAN 09 suite of programs[24] using density functional theory (DFT) calculations with the B3PW9[25,26] and SDDAll basis set.[27,28,29] The closed shell cobalt(III) ($S = 0$) complexes are calculated as singlets, using spin restricted wavefunctions, whereas the cobalt(II) ($S = 3/2$) complexes were calculated as quartets using open-shell unrestricted wavefunctions. The geometries were fully optimized and vibrational frequencies were computed to confirm that the structures were energy minima.[30,31] Solvent effects in DMF were estimated using the IEF-PCM polarizable continuum model.[32] Vertical electronic excitation energies and intensities were calculated by time-dependent density functional theory (TD-

DFT).[33,34] Molecular orbitals were plotted with GaussView.[35] All geometries match well with previously reported[15,22] crystallographic data.

5.5. References

1 Tomco, D.; Schmitt, S.; Ksebati, B.; Heeg, M. J.; Dou, Q. P.; Verani, C. N. *J. Inorg. Biochem.* **2011**, *105*, 1759.

2 Shakya, R.; Hindo, S.; Wu, L.; Ni, S.; Allard, M.; Heeg, M.; da Rocha, S.; Yee, G.; Hratchian, H.; Verani, C. *Chem. Eur. J.* **2007**, *13*, 9948.

3 Frezza, M.; Hindo, S. S.; Tomco, D.; Allard, M.; Cui, Q. C.; Heeg, M. J.; Chen, D.; Dou, Q. P.; Verani, C. V. *Inorg. Chem.* **2009**, *48*, 5928.

4 Bertini, I.; Gray, H. B.; Stiefel, E. I.; Valentine, J. S. *Biological Inorganic Chemistry: Structure and Reactivity* University Science Books, Sausalito, California, **2007**, p. 562-574.

5 Kaim, W.; Schwederski, B. *Bioinorganic Chemistry: Inorganic Elements in the Chemistry of Life* Wiley, New York, **1994**, p. 39-55.

6 Dabrowiak, J. C. *Metals in Medicine* Wiley, New York, **2009**.

7 Alessio, E. *(Ed.) Bioinorganic Medicinal Chemistry*, Wiley-VCH, **2011**.

8 Dickens, J. P.; Crimmin, M. J.; Beckett, R. P. British Bio-Technology Limited UK, PCT Int. Appl. WO 9005719, **1994**.

9 Failes, T. W.; Cullinane, C.; Diakos, C. I.; Yamamoto, N.; Lyons, J. G.; Hambley, T. W. *Chem. Eur. J.* **2007**, *13*, 2974.

10 Denny, W. A. *Eur. J. Med. Chem.* **2001**, *36*, 577.

11 Ware, D. C.; Palmer, H. R.; Brujin, F. B.; Anderson, R. F.; Brothers, P. J.; Danny, W. A.; Wilson, W. R. *Anti-Cancer Drug Des.* **1998**, *13*, 81.

12 Schieber, C.; Howitt, J.; Putz, U.; White, J. M.; Parish, C. L.; Donnelly, P. S.; Tan, S.-S. *J. Biol. Chem.* **2011**, *286*, 8555.

13 Gagne, R.; Koval, C.; Licenski, G. *Inorg. Chem.* **1980**, *19*.

14 Souza, E. T.; Maia, P. J. S.; Azevedo, É. M.; Kaiser, C. R.; Resende, J. A. L. C.; Pinheiro, C. B.; Heinrich, T. A.; da Silva, R. S.; Scarpellini, M. *J. Inorg. Biochem.* **2011**, *105*, 1767.

15 Shakya, R.; Imbert, C.; Hratchian, H. P.; Lanznaster, M.; Heeg, M. J.; McGarvey, B. R.; Allard, M. M.; Schlegel, H. B.; Verani, C. N. *Dalton Trans.* **2006**, 2517.

16 Fritz, H. P.; Vitè, L. W. G. *Z. Anorg. Allg. Chem.* **1972**, *392*, 271.

17 Pui, A.; Berdan, I.; Morgenstern-Badarau, I.; Gref, A.; Perrée-Fauvet, M. *Inorg. Chim. Acta* **2001**, *320*, 167.

18 Ware, D. C.; Palmer, B. D.; Willson, W. R.; Danny, W. A. *J. Med. Chem.***1993**, *36*, 1846.

19 Kaim, W. *Eur. J. Inorg. Chem.* **2012**, 343.

20 Kaim, W.; Schwederski, B. *Coord. Chem. Rev.* **2010**, *254*, 1580.

21 Allard, M. M.; Sonk, J. A.; Heeg, M. J.; McGarvey, B. R.; Schlegel, H. B.; Verani, C. N. *Angew. Chem. Int. Ed. Engl.* **2012**, *51*, 3178.

22 Shakya, R.; Hindo, S. S.; Wu, L.; Allard, M.; Heeg, M. J.; Hratchian, H. P.; McGarvey, B. R.; da Rocha, S.; Verani, C. N. *Inorg. Chem.* **2007**, *46*, 9808.

23 Shakya, R.; Allard, M. M.; Johann, M.; Heeg, M. J.; Rentschler, E.; Shearer, J. M.; McGarvey, B.; Verani, C. N. *Inorg. Chem.* **2011**, *50*, 8356.

24 Frisch, M. J.; Trucks, G. W.; Schlegel, H. B.; Scuseria, G. E.; Robb, M. A.; Cheeseman, J. R.; Scalmani, G.; Barone, V.; Mennucci, B.; Petersson, G. A.; Nakatsuji, H.; Caricato, M.; Li, L.; Hratchian, H. P.; Izmaylov, A.F.; Bloino, J.; Zheng, G.; Sonnenberg, J. L.; Hada, M.; Ehara, M.; Toyota, K.; Fukuda, R.; Hasegawa, J.; Ishida, M.; Nakajima, T.; Honda, Y.; Kitao, O.; Nakai, H.; Vreven, T.; Montgomery, J. A.; Peralta, J. E.; Ogliaro,

F.; Bearpark, M.; Heyd, J.; Brothers, J. E.; Kudin, K. N.; Staroverov, V. N.; Kobayashi, R.; Normand, J.; Raghavachari, A.; Rendell, A.; Burant, J. C.; Iyengar, S. S.; Tomasi, J.; Cossi, M.; Rega, N.; Millam, J. M.; Klene, M.; Knox, J. E.; Cross, J. B.; Bakken, V.; Adamo, C.; Jaramillo, J.; Gomperts, R.; Stratmann, R. E.; Yazyev, O.; Austin, A. J.; Cammi, R.; Pomelli, C.; Ochterski, J. W.; Martin, R.L.; Morokuma, K.; Zakrzewski, V.G.; Voth, G.A.; Salvador, P.; Dannenberg, J.J.; Dapprich, S.; Parandekar, P.V.; Mayhall, N.J.; Daniels, A.D.; Farkas, O.; Foresman, J.B.; Ortiz, J. V.; Cioslowski, J.; Fox, D. J. *Gaussian G09 Wallingford CT*, **2009**.

25 Krishnan, R.; Binkley, J. S.; Seeger, R.; Pople, J. A. *J. Chem. Phys.* **1980**, *72*, 650.

26 Perdew, J. P. *Phys. Rev. B.* **1986**, *33*, 8822.

27 Dunning Jr., T. H.; Hay, P. J.; SDALL, in: Schaefer, H. F. III *(Ed.) Modern theoretical Chemistry*, Plenum, New York, **1976**, pp. 1.

28 Fuentealba, P.; Stoll, H.; Szentpaly, L. V.;Schwerdtfeger, P.; Preuss, H. *J. Phys. B: At Mol. Phys.* **1983**, *11*, L323.

29 Leininger, T.; Nicklass, A.; Stoll, H.; Dolg, M.; Schwerdtfeger, P. *J. Chem. Phys.* **1996**, *105*,1052.

30 Schlegel, H. B. *J. Comput. Chem.* **1982**, *3*, 214.

31 Hratchian, H. P.; Schlegel, H. B. *Theory and Applications of Computational Chemistry: The First Forty Years*, *Elsevier*, Amsterdam, **2005**.

32 Miertuš, S.; E. Scrocco, J. Tomasi, *Chem. Phys.* **1981**, *55*, 117.

33 Vlcek, A.; Zális, S. Jr. *Coord. Chem. Rev.* **2007**, *251*, 258.

34 Grimme, S. *Calculation of the Electronic Spectra of Large Molecules, in: R.L.T.R.C. Kenny B. Lipkowitz (Ed.), Reviews in Computational Chemistry*, **2004**, pp. 153.

35 An, B. G.; Siman, R.; Dou, Q.P. *Cell Death Differ*. **1998**, *5*, 1062.

CHAPTER 5

IN VITRO STUDIES OF GALLIUM(III) AND ZINC(II) SPECIES ON THE INHIBITION ACTIVITY OF THE 26S PROTEASOME

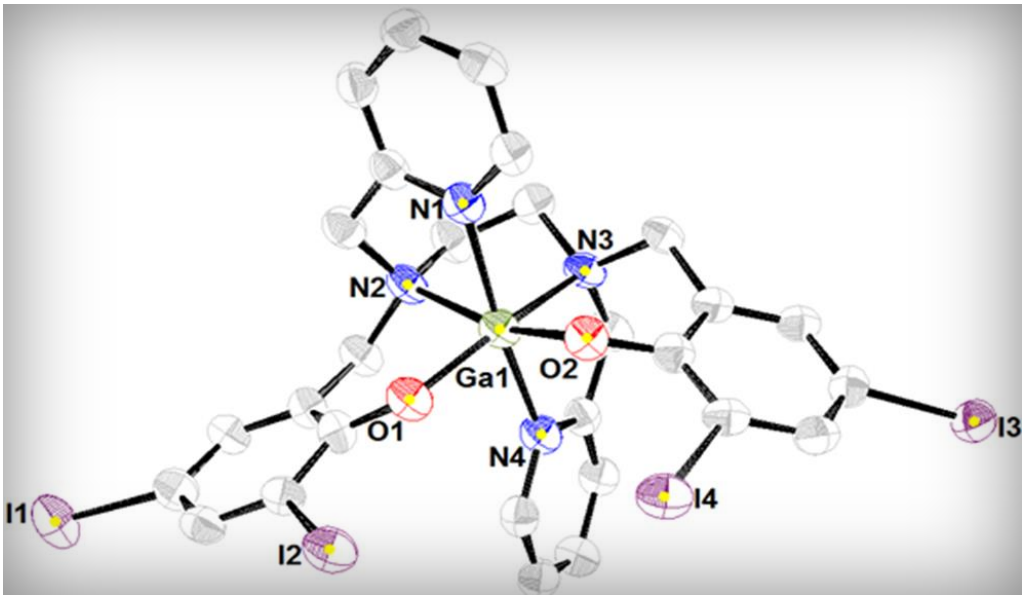

CHAPTER 5

IN VITRO STUDIES OF GALLIUM(III) AND ZINC(II) SPECIES ON THE INHIBITION ACTIVITY OF THE 26S PROTEASOME

Tomco, D.; Schmitt, S.; Heeg, M. J.; Dou, Q. P.; Verani, C. N.*

5.1. Introduction

In Chapters **3** and **4**, we concluded that the inhibition activity of the 20S proteasome is highly dependent on the redox properties of the metal ion of choice and the ligand design. The hexadentate H_2L^2 ligand coordinated to a cobalt(II) metal ion showed no inhibition properties towards purified 20S and 26S proteasome. Because the increased chelation effect of the H_2L^2 ligand prevented the inhibition of the chymotrypsin-like (CT) activity of the proteasome, the question remains whether this ligand will possess the same properties if it is coordinated to a more labile metal ion with higher oxidation state. To address this issue, we synthesized and characterized two complexes coordinated to the H_2L^2 ligand, namely **$[Ga^{III}(L^2)]ClO_4$** (**1**) and **$[Zn^{II}(L^2)]$** (**2**), (**Scheme 5.1**), and investigated the inhibition properties towards purified human proteasome and proteasome in prostate cancer cells. The selection of gallium(III) and zinc(II) ions[1] is related not only by their wide therapeutic properties towards of various diseases,[2] but also by their redox inertness.

A gallium nitrate salt has been used in treatment of hypercalcemia, a metabolic disorder related to increased concentration of the calcium ions in blood. Gallium nitrate inhibits calcium resorption from bones and stimulates bone formation.[3] To date, the coordination compound gallium maltolate has completed phase I clinical trials in treatment of renal cancer.[4] One of the possible mechanisms of action for gallium maltolate is generation of reactive oxygen speciesin mitochondria.[5]

As a trace element zinc is associated with various metabolic processes in cells including structural stabilization of various proteins such as zinc fingers, signal transduction, and regulation of cellular apoptosis.[6] The ability of both gallium- and zinc-containing complexes as proteasome inhibitors has been successfully demonstrated by the Verani and Dou labs,[7,8,9] and the following study will investigate the effect that redox-inactive metal ions have on the CT-inhibition activity of the proteasome in PC-3 cells.

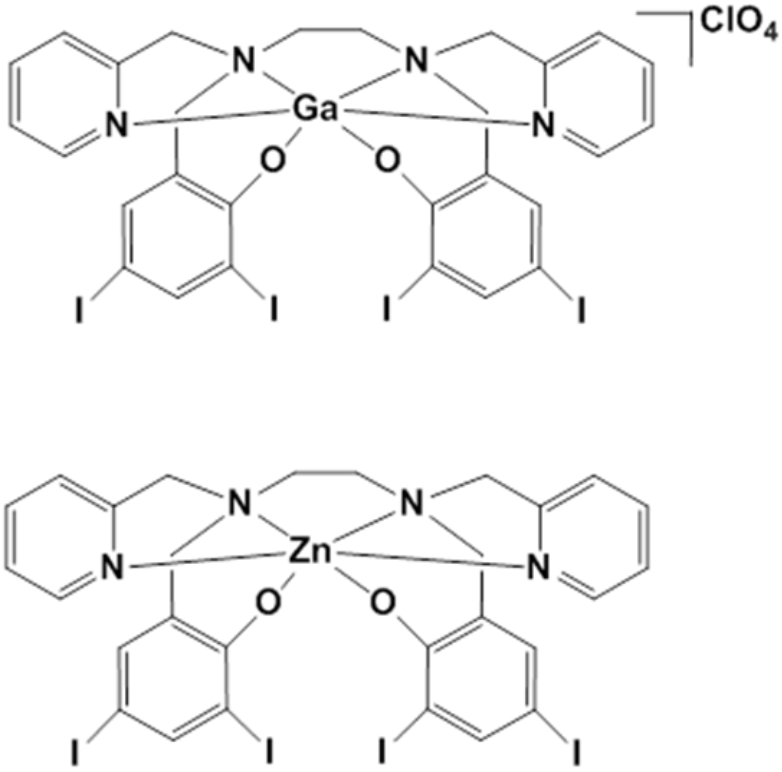

Scheme 5.1. Chemical structures of **[Ga^{III}(L^{2})]ClO$_4$** (**1**) and **[Zn^{II}(L^{2})]** (**2**) complexes.

5.2. Results and Discussion

5.2.1. Synthesis and Characterization

The H_2L^2 ligand was synthesized and characterized using methods from previously reported procedures.[10] Synthesis of the complexes was accomplished following procedures as shown in **Scheme 5.2.** Complex **1** was synthesized using Schlenk technique under nitrogen gas by dissolving the ligand H_2L^2 (0.3 g, 0.31mmol) in 15 mL methanol while stirring and heating the solution followed by addition of triethylamine base (0.063 g, 0.62 mmol). A methanolic solution of $GaCl_3$ salt (0.06 g, 0.34 mmol) was added to the ligand dropwise under anaerobic conditions and the reaction was refluxed for three hours. Concentrated sodium perchlorate solution was then added to the reaction mixture for counterion exchange which resulted in formation of a white precipitate. The solution was concentrated until most of the methanol solvent was removed and the crude product was filtered and washed with cold methanol and distilled water. The collected precipitate was dissolved in methanol and set for crystallization under room temperature for 48 hours. This resulted in formation of rod-shaped crystals.

Complex **2** was synthesized by dissolving the H_2L^2 ligand (0.2 g, 0.21 mmol) and triethylamine base (0.043 g, 0.42 mmol) in 15 mL methanol while heating and stirring (**Scheme 5.2.1**). $ZnCl_2$ salt (0.032 g, 0.23 mmol) was dissolved in 3 mL methanol and then added slowly to the deprotonated ligand. The solution was refluxed under aerobic conditions for 3 hours and then concentrated under vacuum. No precipitate was obtained, so the solution was set for crystallization at room temperature. Rod shaped crystals were collected within 72 hours and characterized by X-ray crystallography.

Chemical characterization of complexes **1** and **2** was performed by spectroscopic and spectrometric techniques to confirm the composition and purity of both complexes. Infrared

analysis shows strong bands at 1602-1611, 1560-1569, and 1433-1444 cm^{-1} attributed to $C{=}N_{pyridine}$ and $C{=}C_{Aromatic}$ stretches. The perchlorate counterion shift at 1088 cm^{-1} is present as a broad band for complex **1.** Elemental analysis for complexes **1** and **2** were found to be in good agreement between the theoretical and the experimental values. Characterization of both complexes by mass spectrometry in the positive mode resulted in excellent agreement between the experimental and simulated data. The molecular ion peak for complex **1** is detected at m/z^+ = 1024.76 (100%) and attributed to the $[Ga^{III}(L^2)]^+$ species without the perchlorate ion. For complex **2**, the molecular ion peak associated with $\{[Zn^{II}(L^2)] + H^+\}^+$ species is found at m/z^+ = 1020.85 (100%) and confirms the bivalent nature of the zinc ion. The above spectrometric data support the assignment of 1:1 metal ion to ligand ratio for both complexes **1** and **2**.

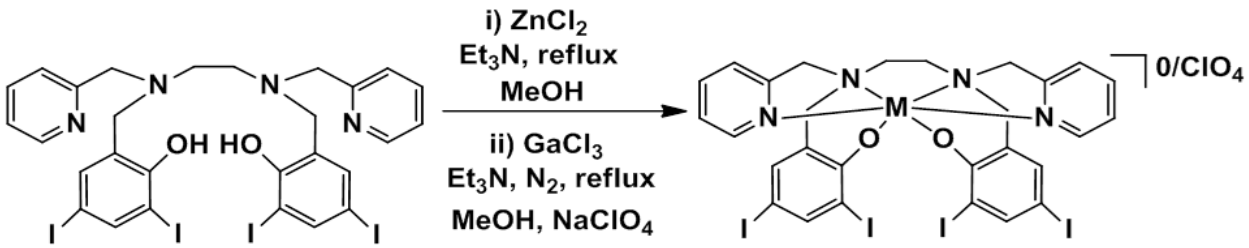

Scheme 5.2. Synthetic routes for complexes **1** and **2**.

5.2.2. Crystal Structure Characterization for $[Ga^{III}(L^2)]ClO_4$ (1) and $[Zn^{III}(L^2)]$ (2)

X-ray diffraction analysis was used to determine the chemical structures of complexes **1** and **2** which are displayed in **Figures 5.2.2.1** and **5.2.2.2**, respectively. Both structures reveal the presence of the deprotonated hexadentate $(L^2)^{2-}$ ligand chelating the gallium(III) and zinc(II) ions in a pseudo-octahedral geometry. The arrangement of the donor sets around the both metal ions can be described as *cis* phenolates, *cis* aliphatic amines, and *trans* pyridines which is in agreement with the previously reported $[Co^{II}(L^2)]$ complex[10] and other complexes from the literature.[11,12] The presence of the perchlorate counterion in complex **1** neutralizes the 3+ charge

of the gallium ion (**Figure 5.2.2.1**) and confirms the fully deprotonated form of the ligand. In contrast to complex **1**, no counterions are observed for complex **2** (**Figure 5.2.2.2**). Average bond lengths between the gallium ion and the donor sets are as follows: Ga-$O_{phenolate}$ as 1.890 Å, Ga-$N_{aliphatic}$ as 2.138 Å, and Ga-$N_{pyridine}$ as 2.102 Å. These values are slightly shorter compared to the zinc analog with bond distances of 1.992 Å for Zn-$O_{phenolate}$, 2.259 Å for Zn-$N_{aliphatic}$, and 2.169 Å for Zn-$N_{pyridine}$. These corresponding bond distances are similar to those found in the $[Co^{II}(L^2)]$ complex[10] and other reported zinc-containing complexes.[9] Such shortening of bond distances in the $[Ga^{III}(L^2)]ClO_4$ complex could be explained due to the higher charge of the metal ion. Selected bond lengths and angles are presented in the figures below.

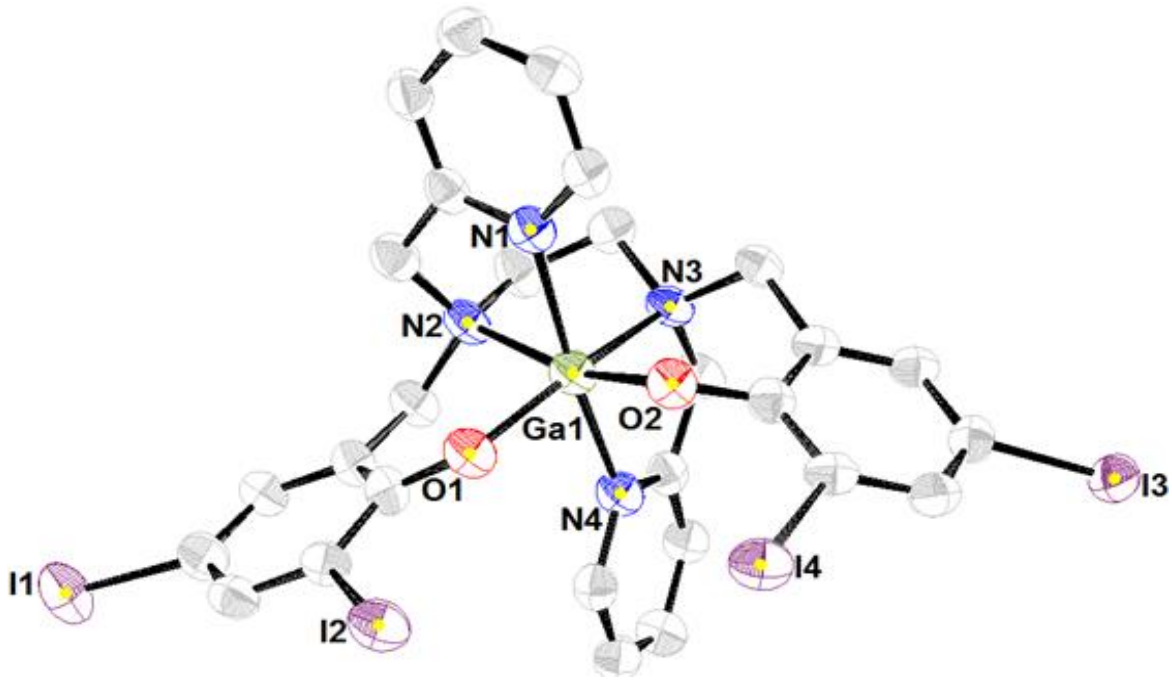

Figure 5.2.2.1. Crystal structure for Ga complex (**1**). ORTEP diagram reported at 50% probability level. Selected bond lengths include: Ga(1)-O(2) = 1.880(3), Ga(1)-O(1) = 1.900(3), Ga(1)-N(4) = 2.091(5), Ga(1)-N(1) = 2.113(5), Ga(1)-N(2) = 2.127(4), Ga(1)-N(3) = 2.149(4) Å. Selected angles include: O(2)-Ga(1)-O(1) = 95.65(15), N(4)-Ga(1)-N(1) = 170.69(16), N(2)-Ga(1)-N(3) = 82.66(16), O(1)-Ga(1)-N(4) = 90.62(16), O(2)-Ga(1)-N(1) = 87.07(16). Goodness of fit is given by R(F) (%) = 4.20.

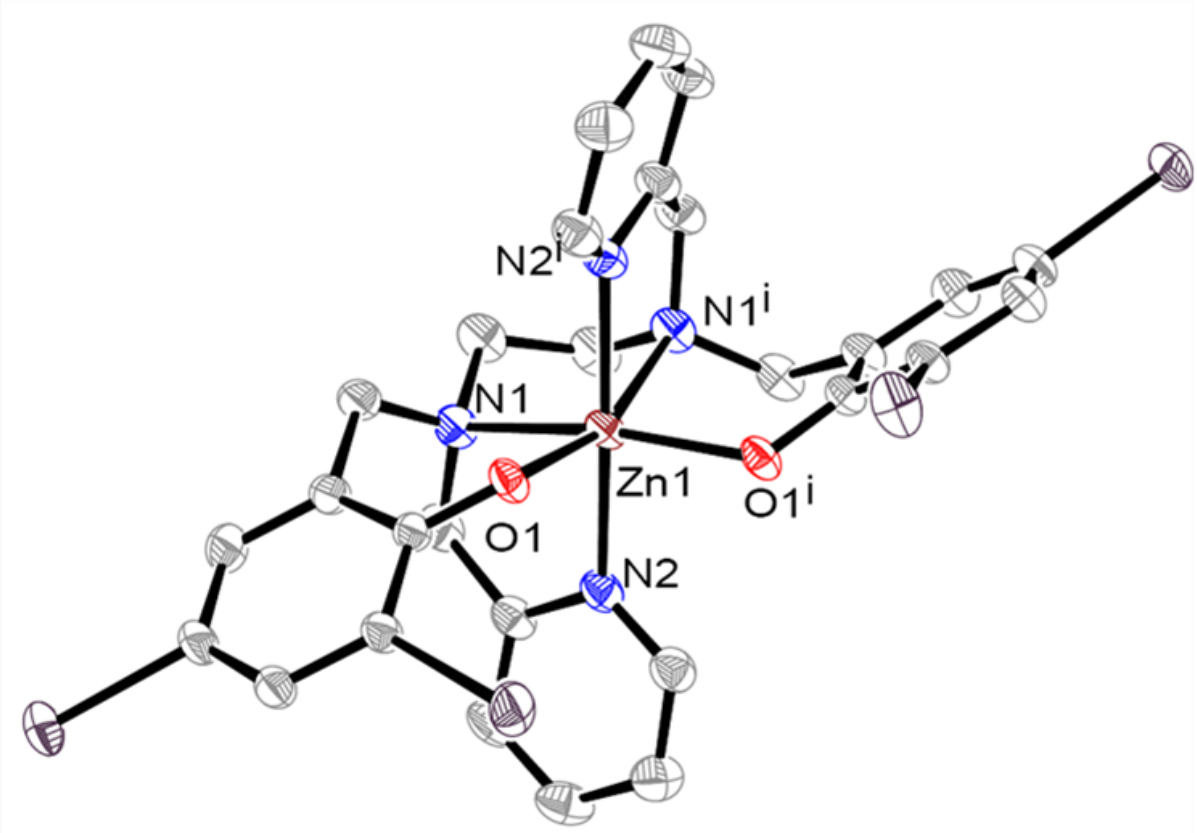

Figure 5.2.2.2. Crystal structure for Zn complex (**2**). ORTEP diagram reported at 50% probability level. Selected bond lengths include: Zn(1)-O(1) = 1.992(2), Zn(1)-N(2) = 2.169(3), Zn(1)-N(1) = 2.259(3) Å. Selected angles include: O(1)-Zn(1)-N(2) = 90.38(11), N(2)-Zn(1)-N(1) = 75.88(11), O(1)-Zn(1)-N(1) = 89.99(10). Goodness of fit is given by R(F) (%) = 3.95.

5.2.3. Biological Results

The biological activity of both complexes against the 20S purified proteasome and 26S proteasome from both PC-3 and non-cancerous CRL2221 cells were measured and the results are discussed. The anti-proliferative effect of the gallium- and zinc-containing complexes on prostate cancer cells were evaluated by MTT assay treating PC-3 cells with **1** and **2** (**Figure 5.2.3.1**). The results reveal a distinct difference in the percent cell proliferation remaining after treatment with both complexes. Complex **1** is highly potent against the growth of these cells even at lower concentrations (20 µM and 30 µM with 15% and 8.0% respectively of cellular proliferation left after treatment). Almost no cell growth is observed after treatment with the highest concentration of 50 µM. On the contrary, complex **5** shows insignificant anti-proliferative effects at lower concentrations and ~85% cell growth remaining at the highest concentration of 50 µM (**Figure 5.2.3.1**). These results suggest that the gallium-containing complex suppresses the proliferation of the prostate cancer cells very effectively even at lower concentrations.

The inhibitory properties of complexes **1** and **2** against the chymotrypsin-like activity have been investigated (**Figure 5.2.3.2**). Treatment of human purified proteasome with both complexes at concentrations from 5-50 µM resulted in unexpected findings. Complex **1** demonstrates excellent CT-like activity inhibition in a concentration dependent manner with 97% at 10 µM, 99% at 25 µM, and ~100% at 50 µM, and overall $IC_{50} \approx 0.6$ µM. Complex **2** shows much less inhibitory effect against purified proteasome with the following values: 23%, 31%, and 50% at 10, 25, and 50 µM concentrations, respectively, and $IC_{50} \approx 50$ µM.

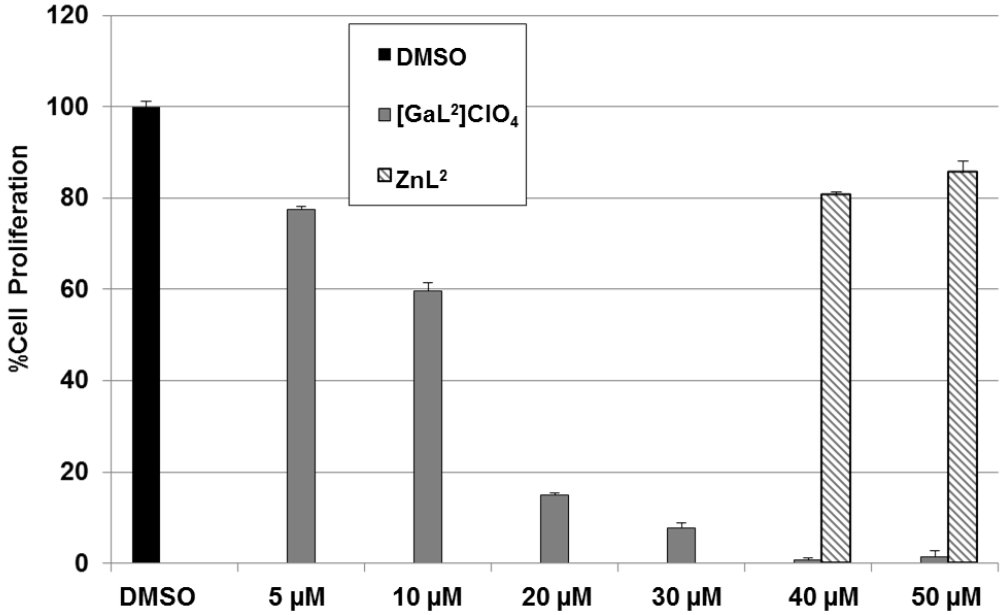

Figure 5.2.3.1. Anti-proliferative effects of complexes **1** and **2** in prostate cancer PC-3 cells.

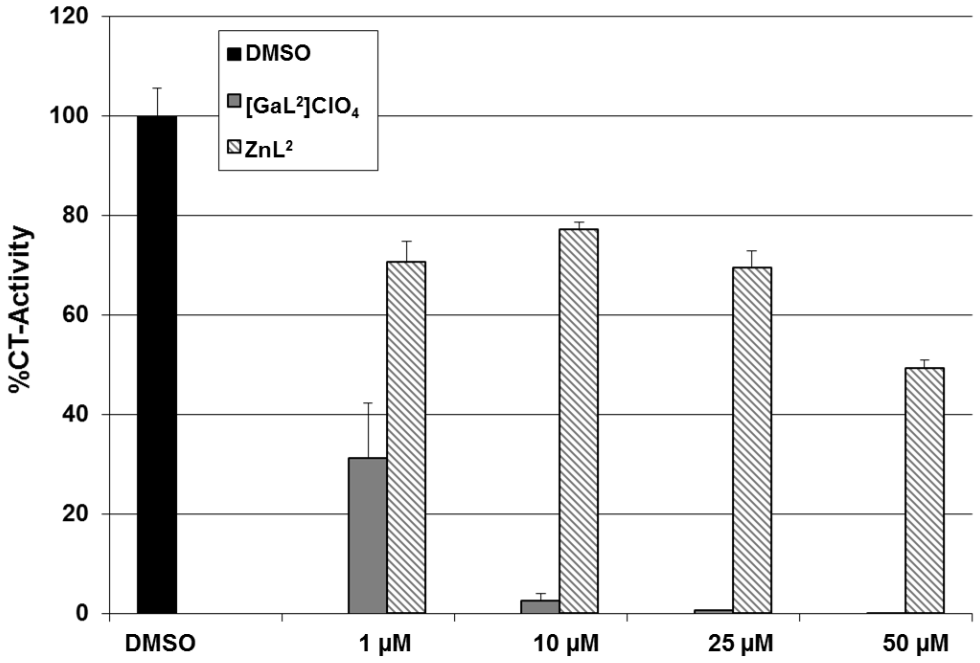

Figure 5.2.3.2. Chymotrypsin-like activity inhibition of purified 20S proteasome after treatment with complexes **1** and **2**.

The ability of complexes **1** and **2** to inhibit chymotrypsin-like activity of cellular proteasome was measured by treatment of PC-3 cells with different concentrations of both complexes following 24 hours incubation. Consistent with the purified proteasome results, complex **1** showed excellent inhibitory effects against chymotrypsin-like activity of the proteasome in PC-3 cells, as shown in **Figure 5.2.3.3**. These results indicate a direct relationship of CT-inhibition activity and the increase in concentration of complex **1** pro-drug. Complex **1** showed $IC_{50} \approx 22$ μM comparable to the values of the $[Co^{III}(L^1)_2]ClO_4$ complex[10] with $IC_{50} \approx 23$ μM. On the other hand, complex **2** did not show any chymotrypsin-like activity inhibition even at high concentrations. These findings correspond with the previously published results of the $[Co^{II}(L^2)]$ complex which showed no inhibition properties against CT-like activity of the proteasomes in PC-3 cells. Based on these results, we suggest that the higher oxidation state metal ions present higher inhibition levels of chymotrypsin-like activity of the proteasome.

To determine whether proteasome inhibition induces cancer cell apoptosis, PC-3 cells were treated with both complexes **1** and **2** at various concentrations. Upon cell lysis, Western blot analysis was performed to detect increased levels of ubiquitianted (Ub) proteins and PARP cleavage or disappearance. As observed in **Figure 5.2.3.4**, increased levels of Ub-proteins are present for complex **1** specifically at 30-50 μM concentrations indicated by the appearance of darker bands in the gel. These results strongly support that complex **1** does indeed inhibit the proteasome activity in the PC-3 cells. Surprisingly, complex **2** shows increased levels of ubiquitinated proteins at 40 and 50 μM concentrations. These are unexpected results because complex **2** does not inhibit the chymotrypsin-like activity of the proteasome in PC-3 cells, yet the proteasome is not active since Ub-proteins are present. These findings suggest that complex **2** could possibly inhibit the activity of the proteasome by interacting with other proteolytic sites

including caspase- and trypsin-like activities. Another possible target could be the 19S regulatory subunit particularly, the JAMM domain.[13,14] Further studies have to be performed in the future in order to investigate whether the Zn-containing complex **2** could inhibit the activity of such catalytic or regulatory sites of the 26S proteasome.

To prove that proteasome inhibition activity leads to prostate cancer cell apoptosis, poly ADP ribose polymerase (PARP) cleavage was measured (**Figure 5.2.3.4.**). The data confirms that at 30 µM and 50 µM concentrations, complex **1** shows PARP cleavage (reduced band) and disappearance, respectively. No such results were obtained for complex **2**.

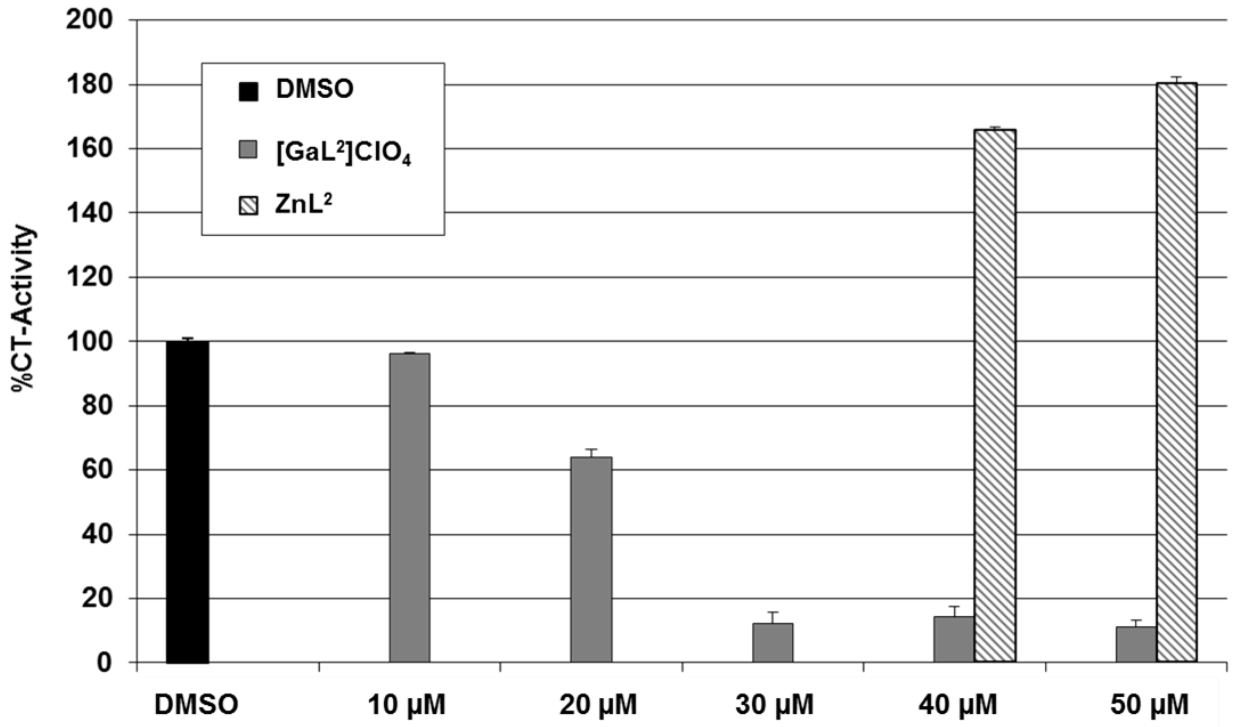

Figure 5.2.3.3. Comparison of the chymotrypsin-like activity levels of the proteasome in PC-3 cells after treatment with complexes **1** and **2** at different concentrations.

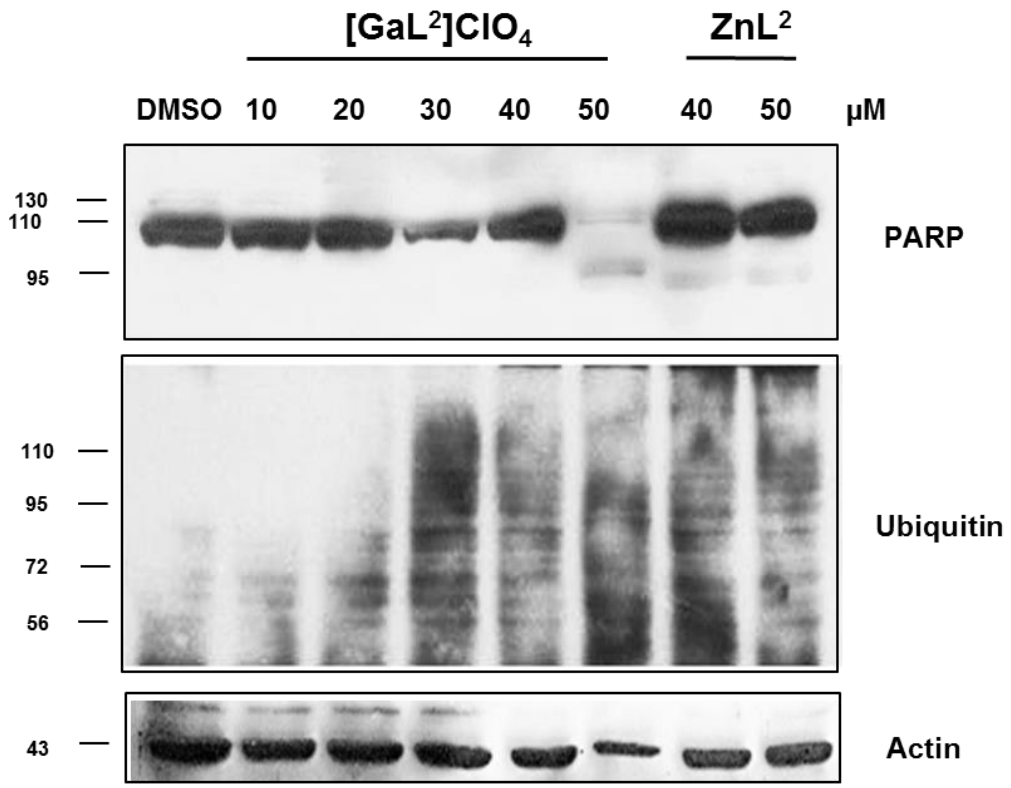

Figure 5.2.3.4. Comparison of Western blot analysis for complexes **1** and **2**. Increased levels of Ub-proteins are shown for complex **1** at 30-50 μM. PARP cleavage is observed for complex **1**.

Confirmation of cellular apoptosis was demonstrated by monitoring the prostate cancer cellular morphological changes upon treatment with complexes **1** and **2**. As expected, the gallium-containing species caused apoptotic bleeding of the PC-3 cells at increasing concentrations; whereas, the zinc-containing analog showed no such effects (**Figure 5.2.3.5**). Thus, we conclude, that prostate cancer cells undergo apoptosis through the inhibition activity of the chymotrypsin-like activity of the proteasome due to treatment with complex **1**.

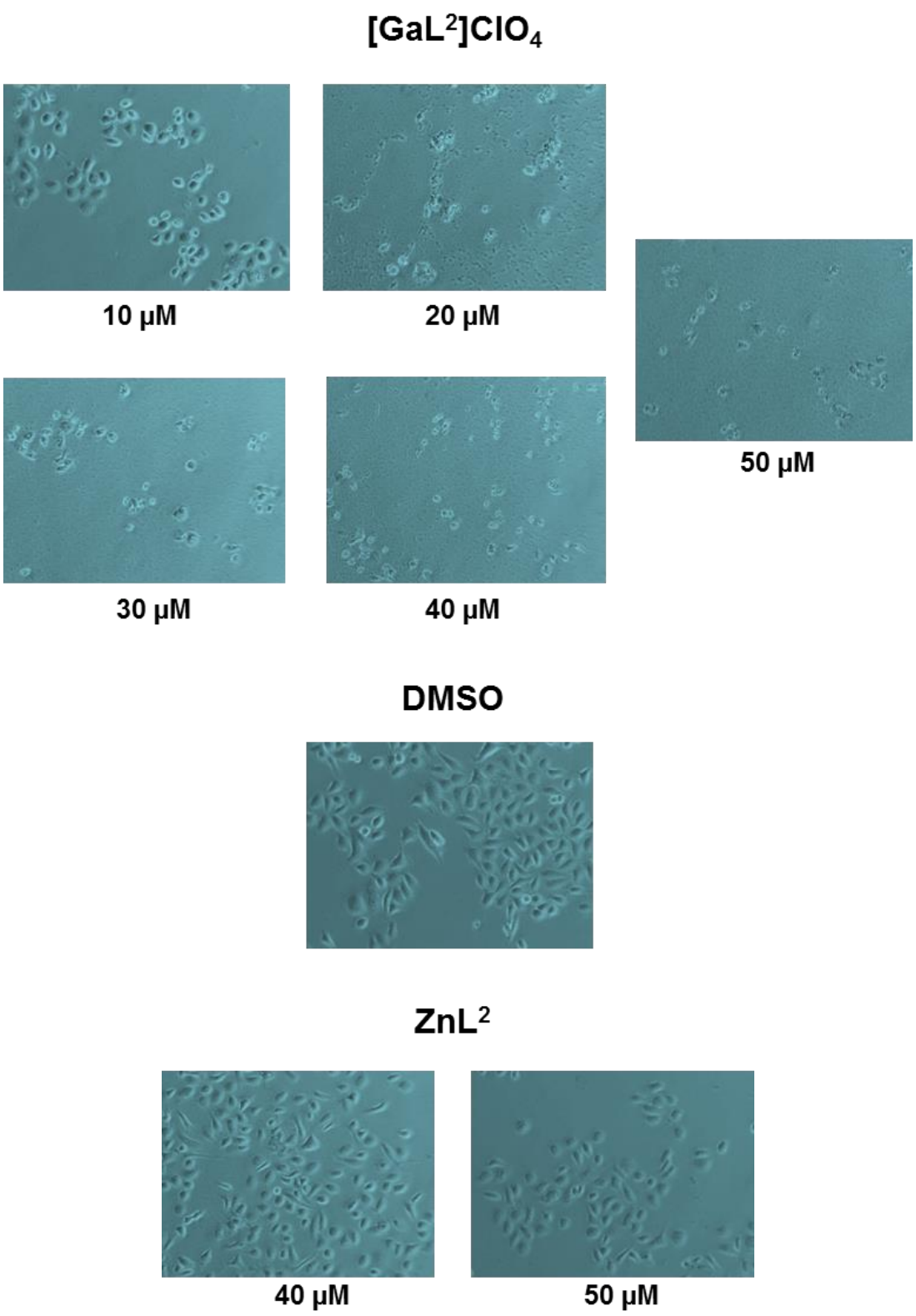

Figure 5.2.3.5. Morphological changes of PC-3 cells upon treatment with **1** and **2**. Rounded detached cells have undergone apoptosis.

Toxicity of **$[Ga^{III}(L^2)]ClO_4$** and **$[Zn^{II}(L^2)]$** complexes was tested against non-cancerous immortalized human epithelial prostate cell extracts upon treatment with different concentrations of both compounds. Inhibition of the chymotrypsin-like activity was measured and the results are included in **Figure 5.2.3.6**. Neither of the complexes shows inhibition activity at lower concentrations and the Ga-containing compound shows only 20% inhibition at the highest concentration of 50 μM. These findings are significant because they confirm selectivity of complex **1** towards cancer cells.

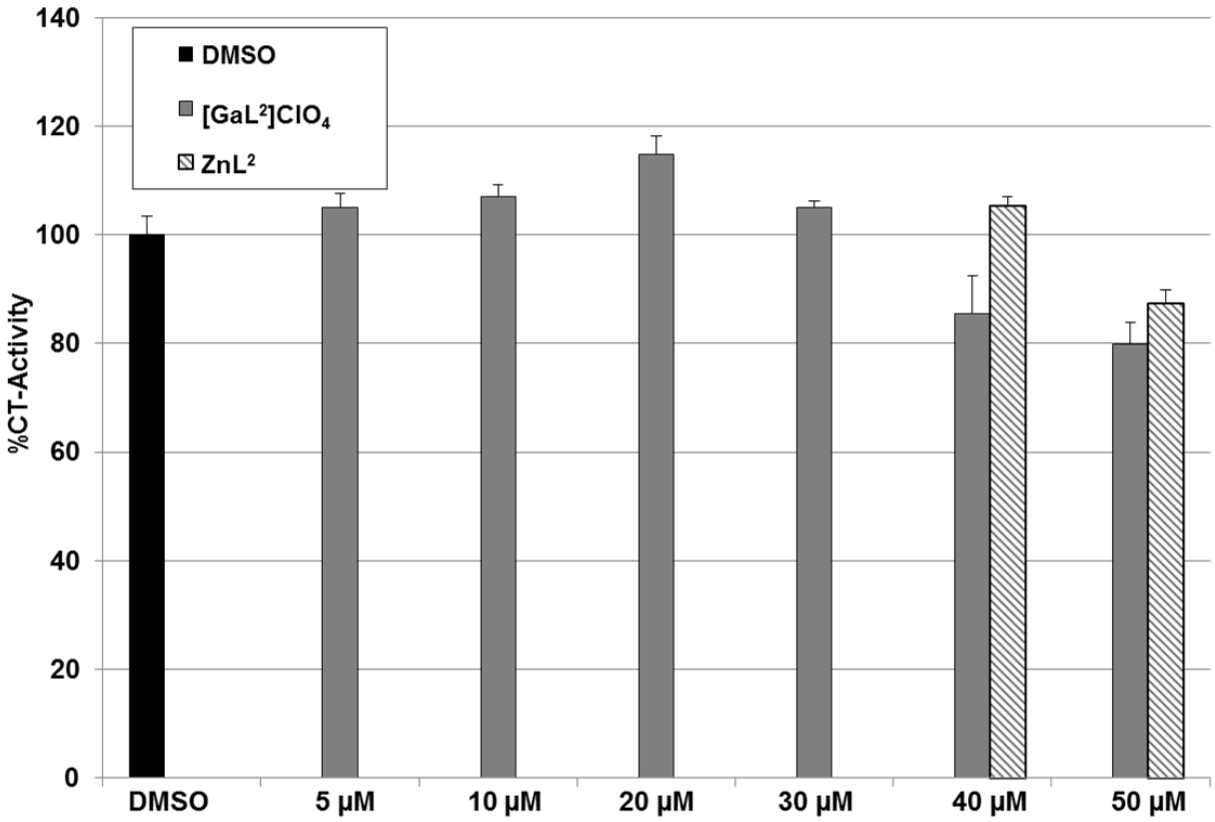

Figure 5.2.3.6. Selectivity of complexes **1** and **2** towards non-cancerous CRL2221 cells.

5.3. Conclusions

In this chapter, we evaluated the inhibitory effects of two complexes **$[Ga^{III}(L^2)]ClO_4$** and **$[Zn^{II}(L^2)]$** against proteasome activity. The chemical structures of both complexes were confirmed by X-ray crystallography. From these studies we concluded that the Ga-containing complex is considerably more potent towards inhibition of the CT-like activity compared to the zinc analog in both purified and cellular proteasome. Complex **1** induces prostate cancer cellular apoptosis as supported by PARP cleavage resulting from the inhibition activity of the proteasome. On the contrary, the Zn-containing complex **2** showed insignificant CT-like activity inhibition in prostate cancer PC-3 cells, but increased levels of the ubiquinated proteins. This suggests that other proteolytic sites could be the targets of action. Cytotoxic properties of both complexes were tested in non-cancerous CRL2221 cells showing minimal CT-like activity inhibition even at the highest concentration of 50 μM. Based on these findings, we conclude that the complex containing the higher oxidation state metal ion gallium(III) induces inhibition of CT-like activity at higher levels compared to metal ions with lower oxidation states; such as the zinc counterpart.

Compared to the other metal-based proteasome inhibitors reported by the Verani and Dou groups, complex **1** is the most effective CT-inhibitor in purified proteasome with IC_{50} values of 0.6 μM which makes this pro-drug an excellent candidate for *in vivo* studies.

5.4. Experimental Procedures

Chemical characterization of both complexes was performed using the techniques described in **Chapter 2**. The biological assays were run under the same conditions as described in **Chapter 3**, **Section 3.4.4**.

5.4.1. Crystal Structure Analysis of $[Ga^{III}(L^2)]ClO_4$ and $[Zn^{II}(L^2)]$ Complexes

	(1)	(2)
Formula	$C_{30.75}H_{32.25}ClGaI_4N_4O_{7.38}$	$C_{28}H_{24}I_4N_4O_2Zn$
M	1188.63	1021.48
Space group	Monoclinic, P21/c	Monoclinic, C2/c
a / Å	16.8166 (9)	13.8723 (4)
b/ Å	26.2253 (14)	9.9255 (4)
c/ Å	19.3957 (10)	21.9417 (7)
α/ °	90	90
β/ °	113.43 (2)	95.772 (2)
γ/ °	90	90
V/ $Å^3$	7848.9 (7)	3005.8 (18)
Z	8	4
T/ K	100 (2)	100 (2)
λ/ Å	0.71073	0.71073
D_{calc}/ g cm^{-3}	2.012	2.257
μ/ mm^{-1}	3.964	4.958
R(*F*) (%)	4.20	3.95
Rw(*F*) (%)	8.98	8.76

[a] $R(F) = \sum \| F_o \| - | F_c \| / \sum | F_o |$ for $I > 2s(I)$; $Rw(F) = [\sum w(F_o^2 - F_c^2)^2 / \sum w(F_o^2)^2]^{1/2}$ for $I > 2s(I)$.

Table 5.4.1. Crystal data and structure refinement results for complexes **1** and **2**.

5.4.2. Characterization of $[Ga^{III}(L^2)]ClO_4$ and $[Zn^{II}(L^2)]$ Complexes

$[Ga^{III}(L^2)]ClO_4$ (1). Yield: 90%; IR data: (KBr, cm^{-1}) 1611, 1569, 1433, ($C{=}N_{Pyridine}$ $C{=}C_{Aromatic}$); 1302, (C-O); ESI^+ in MeOH: *m/z* (100%) = 1024.73 for to $[Ga^{III}(L^2)]^+$; Anal. Calc. (%) for ($[Ga^{III}(L^2)]ClO_4$, $C_{28}H_{24}ClGaI_4N_4O_6$) C, 29.89; H, 2.15; N, 4.98 Found (%): C, 29.60; H, 2.21; N, 4.78.

$[Zn^{II}(L^2)]$ (2). Yield: 80%; IR data: (KBr, cm^{-1}) 1602, 1560, 1444, ($C{=}N_{Pyridine}$ $C{=}C_{Aromatic}$); 1328, (C-O); ESI^+ in MeOH: *m/z* (100%) = 1020.85 for $\{[Zn^{II}(L^2)] + H^+\}^+$; Anal. Calc. (%) for ($[Zn^{II}(L^2)]\cdot H_2O$, $C_{28}H_{26}ZnI_4N_4O_3$) C, 32.35; H, 2.52; N, 5.39 Found (%): C, 32.29; H, 2.52; N, 4.81.

5.5. References

1 Liguori, P. F.; Valentini, A.; Palma, M.; Bellusci, A.; Bernardini, S.; Ghedini, M.; Panno, M. L.; Pettinari, C.; Marchetti, F.; Crispini, A.; Pucci, D. *Dalton Trans.* **2010**, *39*, 4205.

2 Jakupec, M. A.; Keppler, B. K. *Curr. Top. Med. Chem.* **2004**, *4*, 1575.

3 Body, J. J.; Louviaux, I.; Dumon, J. C. *Supp. Care Can.* **2000**, *8*, 398.

4 Jakupec, M. A.; Keppler, B. K. *Met. Ions Biol. Syst.* **2004**, *42*, 425.

5 Chitambar, C. R.; Purpi, D. P.; Woodliff, J.; Yang, M.; Wereley, J. P. *JPET* **2007**, *322*, 1228.

6 Franklin, R. B.; Costello, L. C. *J. Cell Biochem.* **2009**, *106*, 750.

7 Shakya, R.; Peng, F.; Liu, J.; Heeg, M. J.; Verani, C. N. *Inorg. Chem.* **2006**, *45*, 6263.

8 Chen, D; Frezza, M.; Shakya, R.; Cui, C. Q.; Milacic, V.; Verani, C. N.; Dou, Q. P. *Cancer Res.* **2007**, *67*, 9258.

9 Frezza, M.; Hindo, S. S.; Tomco, D.; Allard, M.; Cui, Q. C.; Heeg, M. J.; Chen, D.; Dou, Q. P.; Verani, C. N. *Inorg. Chem.* **2009**, *48*, 5928.

10 Tomco, D.; Schmitt, S,; Ksebati, B.; Heeg, M. J.; Dou, Q. P.; Verani, C. N. *J. Inorg. Biochem.* **2011**, *105*, 1759.

11 Wong, E.; Liu, S.; Rettig, S. J.; Orvig, C. *Inorg. Chem.* **1995**, *34*, 3057.

12 Setyawati, I. A.; Rettig, S. J.; Orvig, C. *Can. J. Chem.* **1999**, *77*, 2033.

13 Milacic, V.; Chen, D.; Giovagnini, L.; Diez, A.; Fregona, D.; Dou,Q. P. *Toxicol. Appl. Pharmacol.* **2008**, *231*, 24.

14 Cvek, B.; Milacic, V.; Taraba, J.; Dou, Q. P. *J. Med. Chem.* **2008**, *51*, 6256.

CHAPTER 6

INHIBITION OF THE 26S PROTEASOME AS A POSSIBLE MECHANISM FOR TOXICITY OF HEAVY METAL SPECIES

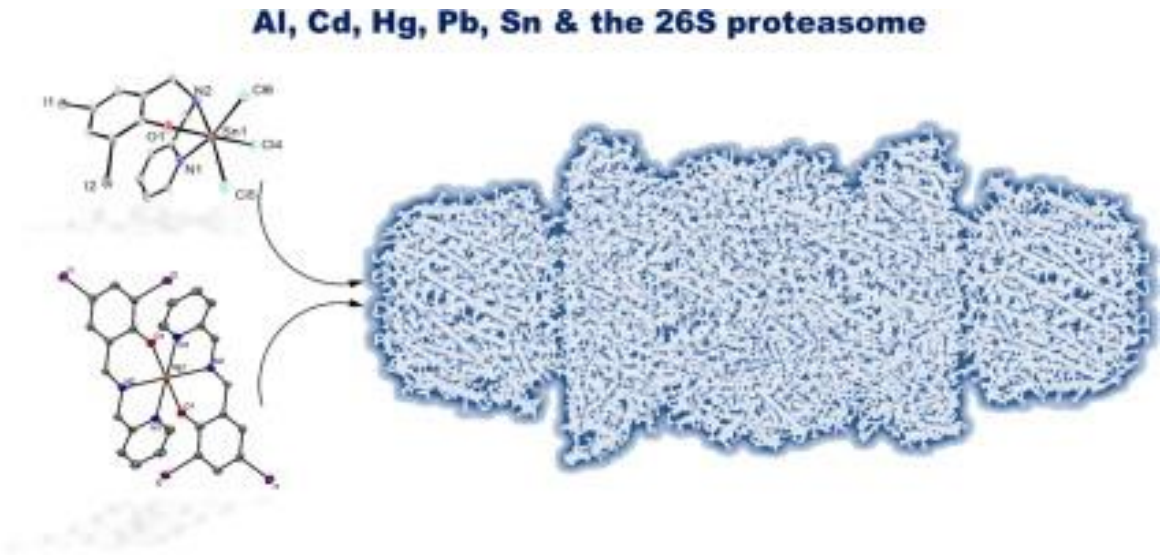

CHAPTER 6

INHIBITION OF THE 26S PROTEASOME AS A POSSIBLE MECHANISM FOR TOXICITY OF HEAVY METAL SPECIES

Published with minor changes as Tomco, D.; Schmitt, S.; Heeg, M. J.; Dou, Q. P.; Verani, C. N.* *J. Inorg. Biochem.* **2014**, *132*, 96.

6.1. Introduction

In this chapter, we hypothesize that heavy metal ions associated to the toxic organoaluminum, organocadmium, organomercury, organolead and organotin species might inhibit the proteasome as a secondary mechanism for toxicity in non-cancerous cells. These species are associated with a number of conditions that affect normal cell function. It is well established that organoaluminum species are linked to bone and central nervous system accumulation by interaction with erythrocytes and desferrioxamine, as well as to mitochondrial functions accompanying globular astrocyte generation.[1,2] Cadmium poisoning[3] is related to lack of specificity towards cell organelles, interactions with the DNA, and increased oxidative stress.[4,5] Organomercury species can accumulate in the mitochondria and irreversibly inhibit selenoenzymes[6], leading to the damage of the nervous system.[7,8] Organolead species substitute divalent metal ions and disrupt homeostasis, thus affecting the central nervous system as a substitute for calcium in ATPase pumps.[9] Finally, organotin[10] species are related to the incorporation of cationic tin to the Golgi apparatus, as well as in the coordination to intracellular phospholipids.[11] Although considerable knowledge on the primary toxicity mechanisms for such species has been established, some evidence is available linking proteasome inhibition to cadmium and lead in erythrocytes[12] and with organometallic polyphenyl and polybutyl tin species,[13] and it is likely that other cellular secondary targets are involved.

In order to verify our hypothesis we have generated five new coordination complexes containing aluminum, cadmium, mercury, lead and tin with the proteasome-innocuous ligand HL^{iodo}. We report on the new species $[Al^{III}(L^{iodo})_2]ClO_4$ **(1)**, $[Cd^{II}(L^{iodo})Cl]\bullet H_2O$ **(2)**, $[Hg^{II}(L^{iodo})_2]\bullet 4DMSO$ **(3)**, $[Pb^{II}(L^{iodo})NO_3]$ **(4)**, and $[Sn^{IV}(L^{iodo})Cl_3]$ **(5)**, **Scheme 6.1**, thoroughly characterized by spectrometric, spectroscopic, and structural methods, and their action on CRL2221 transformed human prostate epithelial cells. These cells mimic the behavior of normal non-cancerous prostate cells. We conclude discussing the validity of the potential role of such heavy metal species on proteasome inhibition.

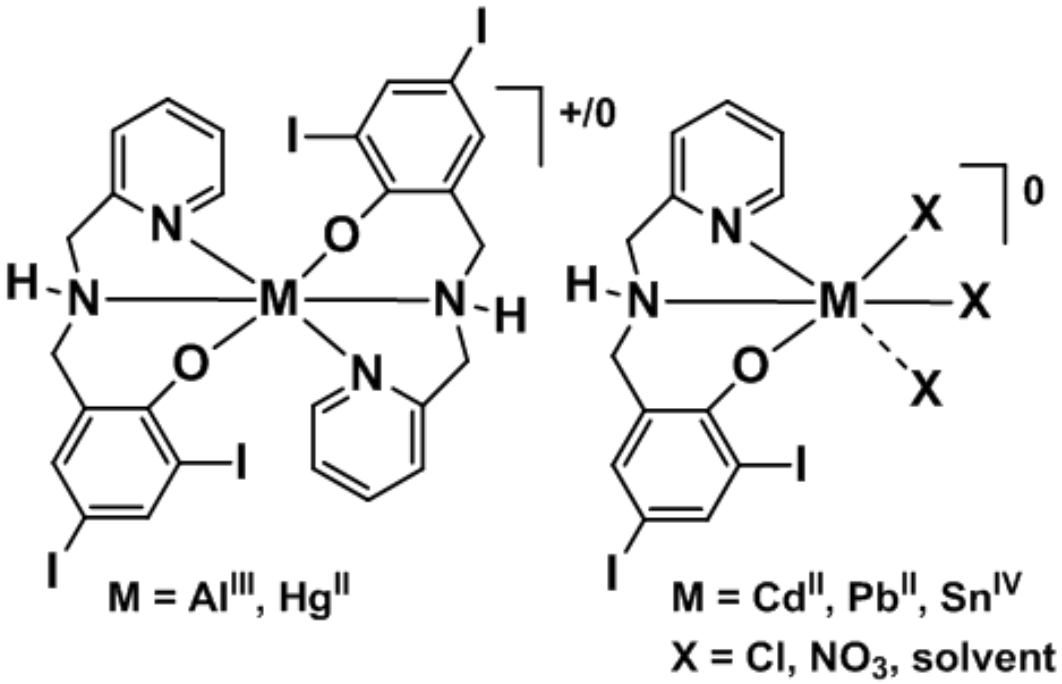

Scheme 6.1. Metal complexes.

6.2. Chemical Results and Discussion

6.2.1. Synthesis and Characterization

Complexes 1-5 were synthesized by adding the appropriate metal salt to a methanol or ethanol solution of the [NN'O] ligand HL^{iodo} previously treated with triethylamine. The purity of the complexes was confirmed by standard characterization techniques including IR, ESI-MS, and elemental analyses. Species **3** and **5** had their structures solved by X-ray crystallography. Infrared spectroscopy indicates that strong ligand bands at 1593, 1570, 1428 cm^{-1} associated with $C{=}N_{py}$ and $C{=}C_{Ar}$ vibrations, show characteristic shifting upon coordination with the metal ions. A strong broad band at 1095 cm^{-1} observed for the aluminum-containing **1** is assigned to the perchlorate counterion. All species were analyzed by room temperature ^{1}H- and ^{13}C-NMR spectroscopy and show the expected ligand peaks shifted by metal coordination. Details, including the stability of the compounds in solution, are discussed in **Section 6.2.3**. Good agreement was found between elemental analyses and the proposed compositions for **1-5**. ESI-MS results were taken in the positive mode and show good agreement with the expected fragmentation and isotopic distribution for complexes **1-5**. Complex **1** shows the presence of the cationic species $[Al^{III}(L^{iodo})_2]^+$observed at m/z^+ = 956.8 (100 %), whereas complex **3** shows the molecular ion peak assigned to the $[Hg^{II}(L^{iodo})_2 + H^+]^+$ at m/z^+ = 1132.77 (100 %). ESI-MS for complex **4** reveals the main peaks present at *m/z* (100 %) = 672.8 for $[Pb^{II}(L^{iodo})]^+$. Simulation assignments for the peak to peak position between the experimental and calculated values for complexes **3** and **4** are included in the supplementary material (**Figure D.6.2.1**). Complex **5** shows some variance in its fragmentation patterns, indicating that solvent molecules can replace one of the chlorido coligands, as seen for species $[Sn^{IV}(L^{iodo})Cl_2(CH_3OH)]^+$ detected at *m/z* (100 %) = 686.8. Equally distinctive, the isotopic distributions for complexes **1** and **3-5** are a

reflection of their compositions. As such the $[Al^{III}(L^{iodo})_2]^+$ fragment displays a simpler profile than that of $[Hg^{II}(L^{iodo})_2 + H^+]^+$. Whereas the former has three main peaks associated with the contributions of 100 % ^{27}Al and the ligand, the latter displays seven peaks associated with the contributions of mercury (^{196}Hg, 0.5 %; ^{198}Hg, 34.1 %; ^{199}Hg, 57.3 %; ^{200}Hg, 77.9 %; ^{201}Hg, 44.5 %; ^{202}Hg, 100 %; ^{204}Hg, 22.9 %) and the ligand. Similar results are found for $[Pb^{II}(L^{iodo})]^+$ and $[Sn^{IV}(L^{iodo})Cl_2(CH_3OH)]^+$.

6.2.2 Solid State Structural Information

The structures of **3** and **5** were determined using X-ray crystallography.Their ORTEP diagrams along with selected bond lengths and angles are shown in **Figures 6.2.2.1** and **6.2.2.2**, respectively. Complex **3** crystallized as single colorless crystals under slow solvent evaporation from a concentrated dimethylsulfoxide solution at room temperature. The X-ray data reveals a single mercury(II) ion coordinated to two deprotonated HL^{iodo} ligands in a *pseudo*-octahedral geometry. Each ligand displays a facial arrangement around the Hg(II) ion, as previously described for other metal ions[11,14] with the same HL^{iodo} ligand. The equivalent $[N_{pyrdine}N_{amine}O_{phenolate}]$ donor sets from each ligand are *trans*-oriented to each other, and the Hg^{II}–$N_{pyridine}$ and Hg^{II}–N_{amine} bond distances reach 2.50 and 2.22 Å. The Hg^{II}–$O_{phenolate}$ bond lengths are 2.51 Å, thus in good agreement with other available mercury(II) species in the literature.[15,16] Due to an inversion center, all angles comprised of equivalent *trans* donors are 180° from each other. Complex **5** was isolated as colorless crystals from an ethanolic solution. The tin ion is chelated to one deprotonated HL^{iodo} ligand and three anionic chlorido ligands complete the octahedron occupying the fourth, fifth and sixth position. Considering the overall charges, as well as the lack of counterions, this arrangement confirms the tetravalent character of the metal center. The bond lengths of Sn^{IV}–$N_{pyridine}$, Sn^{IV}–N_{amine}, and Sn^{IV}–$O_{phenolate}$ are 2.21,

2.24, and 2.06 Å respectively; whereas Sn^{IV}–Cl bond distances average to 2.38 Å. These values are comparable to those found in the literature.[17,18] As expected, the ligand is facially coordinated to the tin(IV) cation, which is favored over the *meridional* arrangement due to the structural flexibility of the [NN'O] ligand.[19,20]

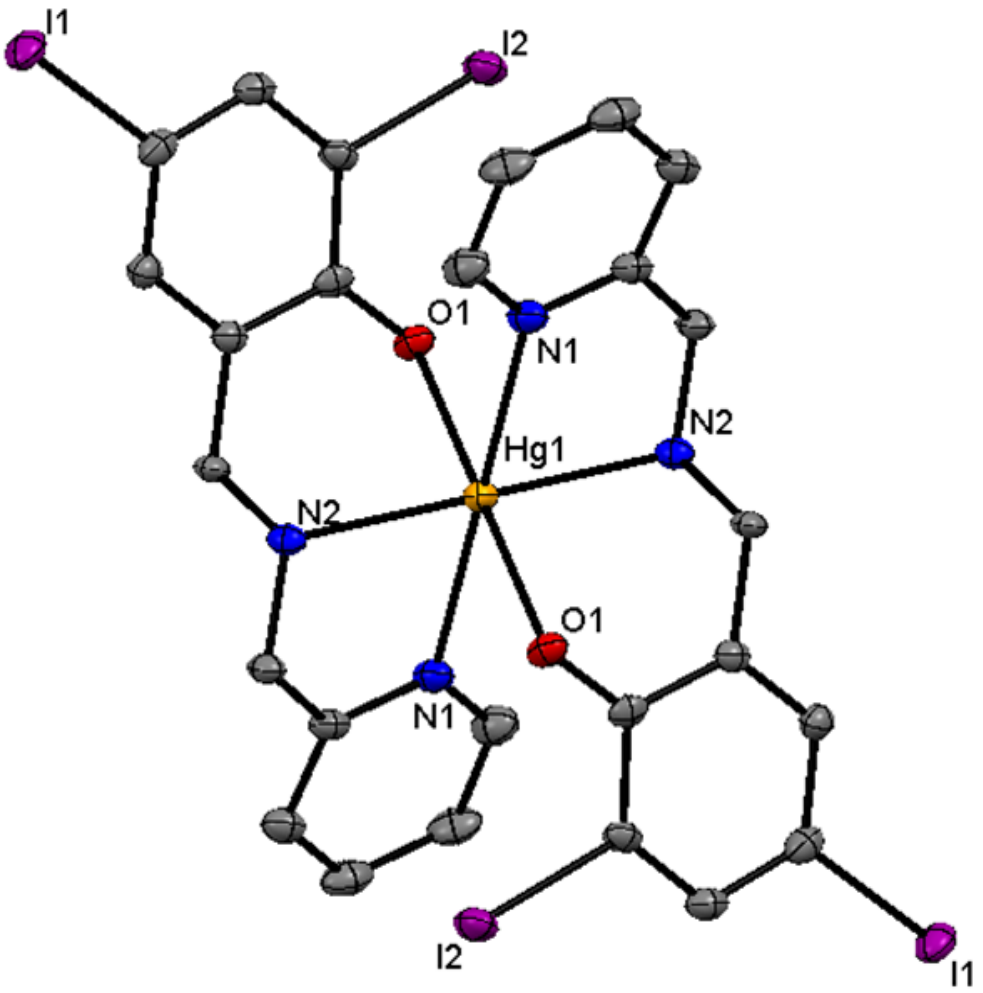

Figure 6.2.2.1. ORTEP diagram for complex **3**. Selected bond lengths: Hg(1)-O(1) = 2.506(19), Hg(1)-N(1) = 2.505(2), Hg(1)-N(2) = 2.225(2) Å. Selected angles: N(1)-Hg(1)-O(1) = 96.51(7), N(2)-Hg(1)-N(1) = 72.42(8), N(2)-Hg(1)-O(1) = 87.14(8). Hydrogen atoms have been omitted.

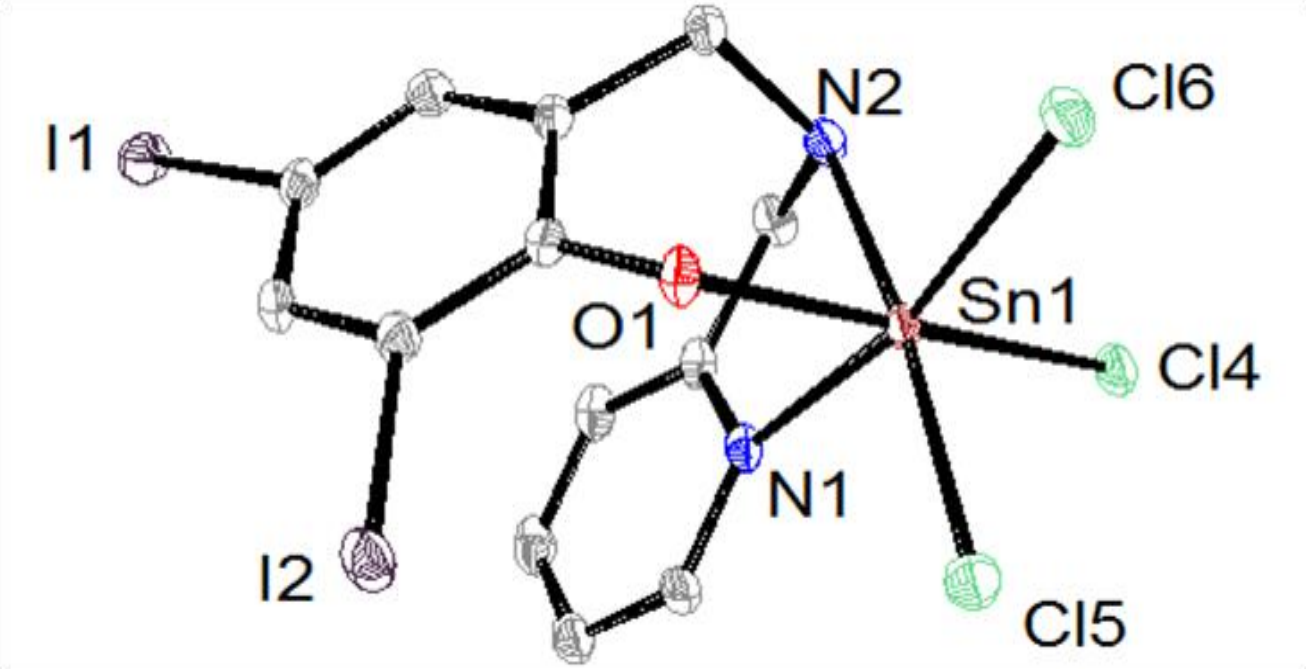

Figure 6.2.2.2. ORTEP diagram for complex 5. Selected bond lengths: Sn(1)-O(1) = 2.056(18), Sn(1)-N(1) = 2.215(2), Sn(1)-N(2) = 2.243(2), Sn(1)-Cl(4) = 2.423(7), Sn(1)-Cl(5) = 2.348(7), Sn(1)-Cl(6) = 2.356(7) Å. Selected angles: O(1)-Sn(1)-N(1) = 83.87(8), N(1)-Sn(1)-N(2) = 76.41(9), O(1)-Sn(1)-N(2) = 87.27(8), Cl(5)-Sn(1)-Cl(4) = 92.70(3), Cl(5)-Sn(1)-Cl(6) = 97.99(3), Cl(6)-Sn(1)-Cl(4) = 93.34(2). Hydrogen atoms have been omitted.

6.2.3. Structural Information in Solution

Proton and carbon NMR spectra for complexes **1-5** were recorded in DMSO-d_6 at ambient temperature. In addition, time-dependent NMR spectra were measured over a period of 48 hours to determine the stability of the complexes in solution. Both ^{1}H- and ^{13}C-NMR spectra showed peak signals associated with the ligand between 3.00 to 9.90 and 45.0 to 170 ppm, respectively. These spectra were compared to the chemical shifts of the ligand **HL^{iodo}** in DMSO-d_6, as previously reported [15]. Selected NMR data for the complexes are included in **Appendix D** where the recorded spectra showed considerable peak shift when compared to the unmetallated and protonated ligand due to metal coordination. The data is summarized in **Table 6.2.3**.

	H1 (ppm)	H2 (ppm)	H3 (ppm)	H4 (ppm)	H5,5'/H6,6' (ppm)	H7 (ppm)	H8 (ppm)	H9 (ppm)
HL^{iodo}	d (8.54)	dd (7.29)	br. dt (7.80)	d (7.37)	s (3.83) s (3.87)	d (7.33)	d (7.78)	s br. 6.60 – 7.10
1	d (9.68)	(7.26 – 8.13)			(3.60 – 4.79)	(7.26 – 8.13)		
2	d br. (8.58)	m br. (7.34-7.41)	t br. (7.87)	m br. (7.34-7.41)	d br. (3.75 &3.61) s br. (4.16) s br. (3.98)	s br. (7.12)	s br. (7.54)	s br. (8.28)
3	(7.25 – 8.75)				(3.55 – 4.51)	(7.25 – 8.75)		
4	d (8.66)	m (7.31-7.34)	dt (7.79)	m (7.31-7.34)	d (4.54) s br. (4.07)	s (7.23)	s (7.55)	Ex. proton
5	d (8.87)	t (7.69)	dt (8.09)	d (7.40)	dd (4.53) d (4.42) d (4.36) dd (3.85)	s (7.44)	s (7.53)	s br. (7.77)

Table 6.2.3. ^{1}H-NMR spectra assignments for complexes **1-5** compared to the **HL^{iodo}** ligand in DMSO-d_6 at room temperature. Table legend: br. = broad; d = doublet; dd = doublet of doublet; dt = doublet of triplet; m = multiplet; s = singlet; Ex. = exchangable.

The ^{1}H- and ^{13}C- NMR spectra for the aluminum-containing complex **1** show twice the number of signals related to the ligand, as in the previously reported $[Zn^{II}(L^{iodo})_2]$ complex [13]. This behavior is suggestive of lack of symmetry about the aluminum(III) ion indicating the presence of non-equivalent ligands with different geometries in solution. The ^{1}H-NMR spectrum is shown in **Figure D.6.2.3.1** In the case of $[Zn^{II}(L^{iodo})_2]$, an available X-ray crystallographic structure allowed us to confirm the *cis* geometry among the phenolates. In absence of structural information for **1** in the solid state, confirmation of geometry is challenging. Nonetheless, a similar spectrum is observed after 48 hours, as shown in **Figure D.6.2.3.2**, and we tentatively attribute this behavior to the orientation of the phenolates and nitrogen donor sets.

For both the cadmium(II)- and lead(II)-based complexes **2** and **4** the methylene protons display peak broadening upon metal coordination (**Figure D.6.2.3.3**). For the tin-complex **5** the coordinated $\mathbf{L^{iodo}}$ yields a well-behaved spectrum comparable to that of the unmetallated ligand. The methylene protons appear as multiplets between 3.8 and 4.5 ppm, suggesting ligand rearrangement (**Figure D.6.2.3.4**). Since there is only one ligand present, the generation of different isomeric species in solution cannot be ruled out, as expected for a main group ion. The solid state structure of the mercury-containing complex **3** shows two equivalent ligands positioned around the Hg(II) ion, where the phenolates and nitrogen donor sets are *trans*-oriented to each other. This geometry relates to the described geometry for the counterpart $[Co^{III}(L^{iodo})_2]ClO_4$ as measured by heteronuclear multiple quantum coherence (HMQC) in DMSO-d_6 and also in agreement with the X-ray structure for other $[Co^{III}(L^{tBu})_2]ClO_4$ species reported by our group.[21] In spite of the general agreement on the positions of bonds, species **3** shows considerably broad signals indicative of a non-rigid structure in solution.[22] Nonetheless

time-dependent NMR data confirms the stability of **3** at ambient conditions, as these peaks persist over a 48 hour period, indicating that no major decomposition takes place in DMSO-d_6, as shown in **Figure 6.2.3**. The stability of all complexes was also verified over a 48 hour period, where the position and intensity of the proton peaks remained unchanged.

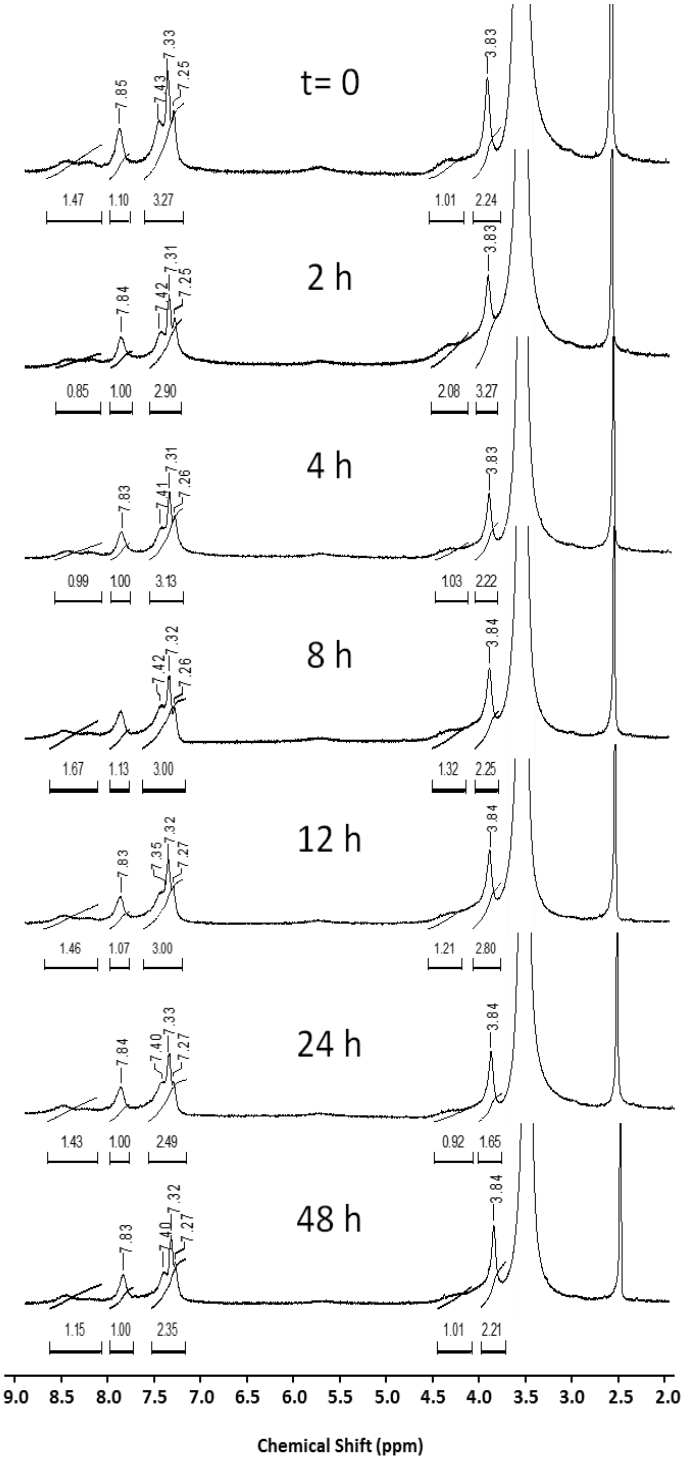

Figure 6.2.3. Time dependent ^{1}H-NMR spectra for complex **3** in DMSO-d_6 at room temperature. Each spectrum was taken under the highlighted time over a period of 48 h.

6.3. Biological Results

6.3.1. Cell Viability

In order to evaluate the effect of the heavy metal complexes on cell proliferation, CRL2221 transformed human prostate epithelial cells were treated with various concentrations of **1-5** and DMSO as a control for 72 h followed by measurement by MTT assays, as shown in **Figure 6.3.1**. The complexes show a dose-dependent decrease in cell proliferation. The IC_{50} values for complexes **1-5** are 2 µmol/L, 4 µmol/L, 6 µmol/L, 3 µmol/L, and 4 µmol/L respectively. At lower concentrations the aluminum-containing **1** and the lead-containing **4** show the highest inhibition of cell proliferation (89 and 95% and 84 and 86%, at 5 and 10 µmol/L, respectively), followed by complex **2** (99% at 10 µmol/L). Treatment with **2**, **3**, and **4** resulted in even higher inhibition of cellular proliferation (97-99%) at 25 and 50 µmol/L. Complex **5** shows a dose-dependent decrease of cell proliferation with the highest inhibition of 95% at 50 µmol/L. The above results allow us to draw some conclusions about the action of complexes **1-5** on toxicity in epithelial CRL2221 prostate cells. These MTT results suggest that all species are toxic towards intact cells and lead to cell death. The aluminum-containing **1** is rather toxic at all tested concentrations, while the cadmium-containing **2** and the lead-containing **4** show similar profiles where toxicity is marked at concentrations of 10, 25, 50 µmol/L. The mercury- and tin-containing species **3** and **5** exhibit pronounced toxicity at higher concentrations. These results indicate cell toxicity, although *per se*, they cannot be directly linked to proteasome activity.

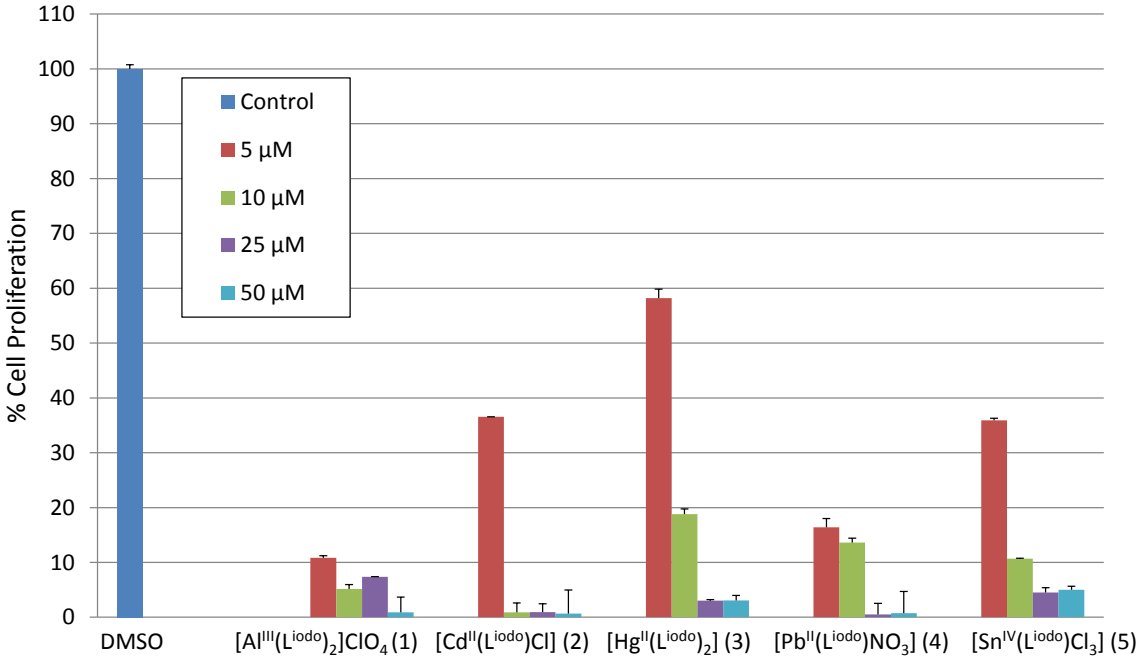

Figure 6.3.1. Percent cell proliferation in CRL2221 cells. Cells were treated with complexes **1-5** for 72 h at the given concentrations of 5-50 µmol/L incubated under 37 ˚C. DMSO is used as a control.

6.3.2. Inhibition of the Chymotrypsin-like Activity in Purified 20S Proteasome

To confirm the ability of these complexes to inhibit chymotrypsin-like activity of the proteasome, species **1-5** were incubated with purified human 20S proteasome under cell-free conditions and the CT fluorogenic substrate N-Succinyl-Leucine-Leucine-Valine-Tyrosine-(7-amino-4-methyl-coumarin) (SucLLVYAMC) followed by measurement of the hydrolyzed 7-amino-4-methylcoumarin groups. **Figure 6.3.2** summarizes the data. At lower concentrations of 1 and 5 µmol/L the mercury-containing complex **3** shows the highest CT-like activity inhibition of 88 % and 98 % respectively, followed by the cadmium-containing **2** with 70 % and 84 % for the same concentrations. Both complexes **1** and **4** show dose-dependent decreases of 84% and 83%, respectively, in CT-like activity in purified proteasome at the highest concentration of 25

μmol/L, whereas **5** showed only 30-40% inhibition regardless of the concentration. Complexes **1-5** show toxicity towards 20S proteasome, whereas previously reported results indicated that the ligand **HL^{iodo}** had negligible effect on the CT-like activity of the 20S proteasome even at higher concentrations.[14] By monitoring the inhibition of CT-like activity in purified 20S proteasome, a better correlation between the toxicity of species **1-5** and the proteasome can be observed. It becomes evident that high concentrations of **1, 4**, and **5** are needed for inhibition of the purified 20S proteasome, and while **2** shows increased potency, **3** is extremely potent from 10 to 50 μmol/L, thus suggesting a potential link between proteasome inhibition and cell toxicity.

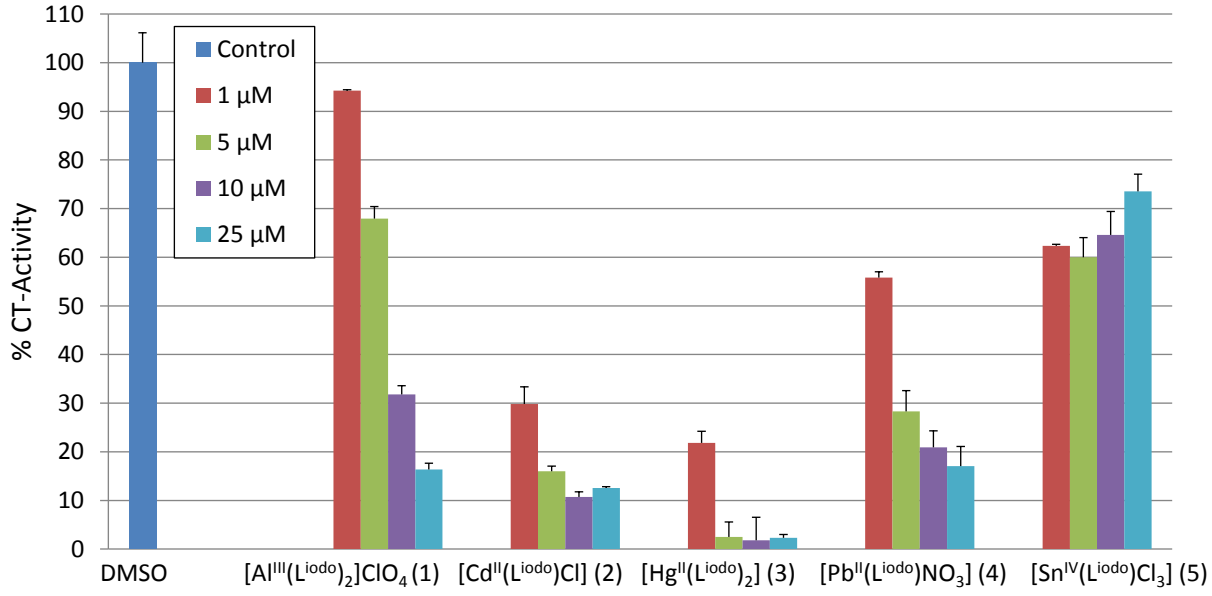

Figure 6.3.2. Measurement of chymotrypsin-like activity inhibition in human purified 20S proteasome upon treatment with complexes **1-5** at concentrations 1-25 μmol/L.

6.3.3. Inhibition of Proteasomal Chymotrypsin-like Activity in Intact CRL2221 Cells

To verify the ability of **2-5** to inhibit proteasome activity, intact transformed human prostate epithelial cells CRL2221 were treated with different concentrations (up to 25 μmol/L) of complex for 48 h, followed by measurement of proteasome inhibition, as shown in **Figure 6.3.3**. CRL2221 cells treated with the lead-containing **4** showed dose-dependent inhibition of proteasomal CT-like activity by 41 % at 5 μmol/L, 46 % at 10 μmol/L, and 73 % at 25 μmol/L. Consistently, levels of proteasomal CT-like activity were decreased after treatment with the cadmium- and mercury-species **2** and **3** at 10 μmol/L by 52 % and 43 %, respectively. On the other hand, cells treated with the tin-containing **5** showed negligible proteasome inhibition at lower concentrations, and only at 25 μmol/L was about 50% inhibition of CT-like activity observed. The results with intact cells suggest that higher concentrations of **2-5** are necessary for CT-inhibition of the proteasome, implying that some of these toxic species might be prevented from crossing the cell membrane or be deterred by other intracellular targets before reaching the proteasome. Nonetheless, at 5 and 10 μmol/L , the cadmium- , mercury-, and lead-containing species **2**, **3**, and **4** show inhibition of about 40-60 %, whereas **4** shows a noticeable 70 % inhibition at higher concentrations.

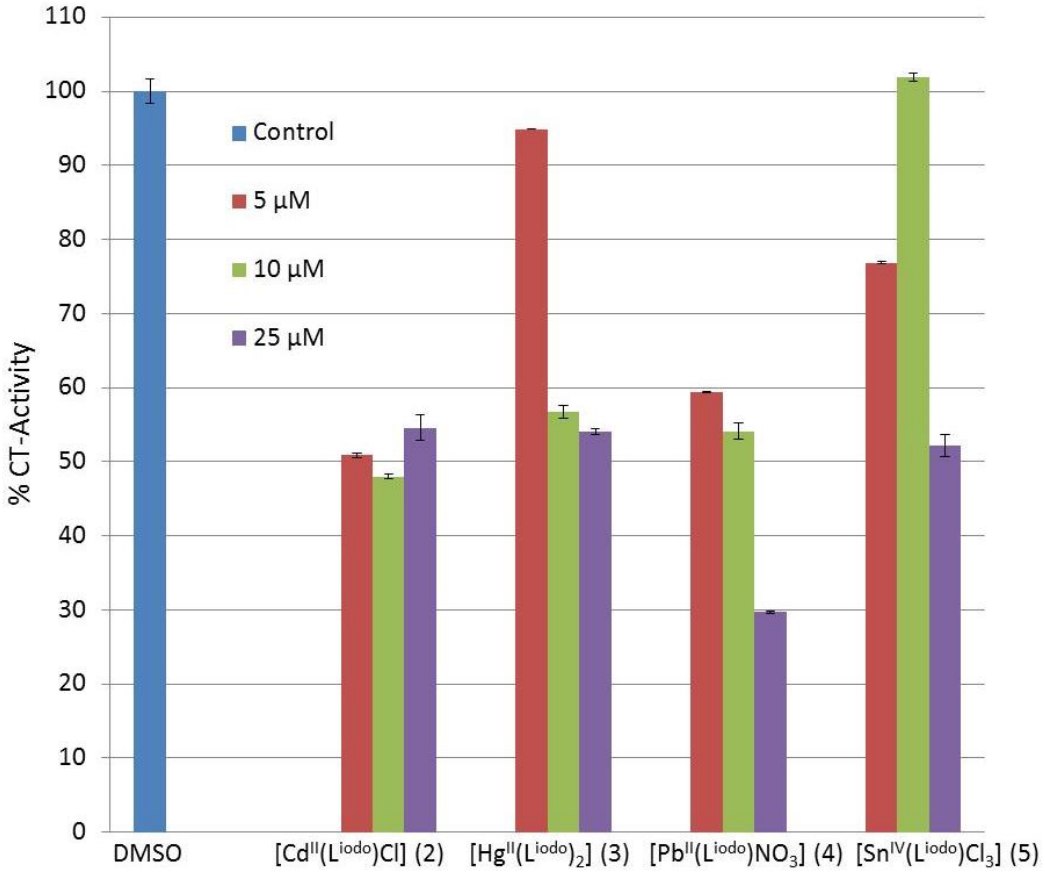

Figure 6.3.3. Chymotrypsin-like activity inhibition in intact CRL2221 cells. Proteins extracted from the CRL2221 cells after 48 h treatment with complexes **2-5** at concentrations 5-10 µmol/L were incubated at 37 ˚C with the chymotrypsin substrate for 4 h. DMSO is used as control.

6.3.4. Inhibition of Proteasomal Chymotrypsin-like Activity Cell Extracts

Inhibition of proteasomal CT-like activity was also measured in CRL2221 cell extracts after 24 h treatment with complexes **1-5**, as shown in **Figure 6.3.4**. Data indicate that the mercury-containing complex **3** showed the highest CT-like inhibition values in a dose-dependent manner reaching 99% inhibition at 25 µmol/L. On the contrary, complex **1** demonstrated no proteasome inhibitory effect even at the highest concentration of 25 µmol/L. We found that when these CRL2221 cell extracts were treated with **4** and **5** only about 30 % of the CT-like activity

was inhibited at 25 µmol/L. Our data suggest that **3** is the most potent proteasome inhibitor in cell extracts, further supporting the hypothesis that toxicity towards epithelial prostate cells might be associated with proteasome inhibition.

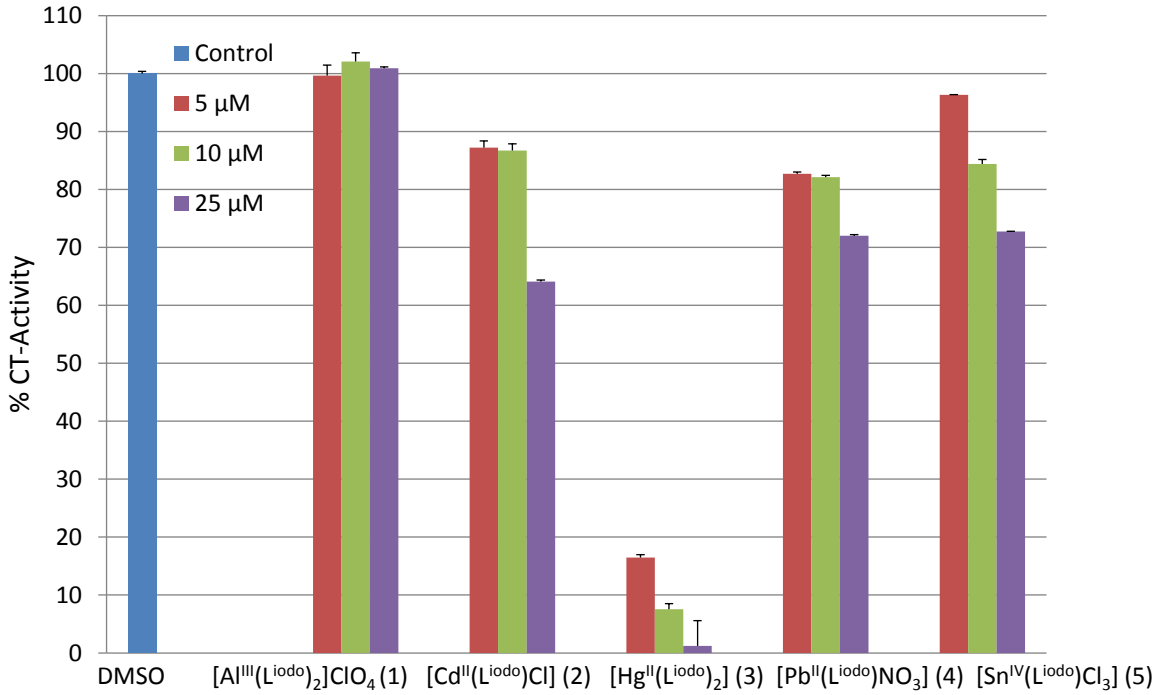

Figure 6.3.4. Chymotrypsin-like activity inhibition in CRL2221 cell extracts. CRL2221 protein extract was treated with complexes **1-5** at various concentrations 5-10 µmol/L. DMSO as a control.

6.4. Overview and Conclusions

The toxicity of five metal complexes was investigated towards transformed human prostate epithelial CRL2221 cells at various concentrations. The percent cell proliferation after treatment with complexes **1-5** was measured and all five species demonstrated high levels of inhibition of cell growth in a concentration-dependent manner. Particularly, aluminum-containing species **1** seemed to be the most toxic against cell viability even at lower concentrations, whereas the tin-containing complex **5** showed toxicity only at very high concentrations. The ability of species **1-5** to inhibit the proteasomal activity was tested and the results indicate that the cadmium, mercury and lead species **2**, **3**, and **4** have the highest inhibitory ability against the chymotrypsin-like activity of purified 20S, as well as in intact CRL2221 cells. In cell extracts, the mercury species **3** proved to be the most potent against CT-like activity, with **2** and **4** as distant next candidates.

Considering the above results, the toxicity of the aluminum species, albeit high, cannot be directly associated to the proteasome. A similar conclusion can be drawn regarding the tin-containing complex. On the other hand, the toxicity of other species such as cadmium and lead are potentially associated with proteasome inhibition, although CT-activity inhibition in cell extracts makes it difficult to be categorically affirmative. The mercury species, particularly at higher concentrations, has shown cell toxicity and CT-like inhibition in purified proteasome, cell extracts and intact cells, and its relationship towards the proteasome is strongly suggested. Therefore, in spite of the known prevalent mechanisms of cellular toxicity for mercury species, in particular the inhibition of selenoenzymes, proteasome inhibition is a viable secondary route for toxicity. Further studies will be necessary to elucidate the nature of the final agent of inhibition, either as a complex or ionic entity.

6.5. Experimental

6.5.1. Materials and Methods

Reagents and solvents were purchased from commercial sources. Time-dependent NMR experiments were recorded over 48 hours at room temperature. Other characterization methods were used as described in Chapter 2.

6.5.2. X-ray Structural Determination of $[Hg^{II}(L^{iodo})_2]$•4DMSO (3) and $[Sn^{IV}(L^{iodo})Cl_3]$ (5)

Diffraction data were measured on a Bruker APEX-II kappa geometry diffractometer[23] with Mo radiation and a graphite monochromator at 100 K. Frames were collected as a series of sweeps with the detector at 40 mm and 0.3 degrees between each frame. All structures were refined using Sheldrick's *SHELX-97* software.[24] A summary of the crystal structure parameters is contained in **Table 6.5.2**. The species **$[Hg^{II}(L^{iodo})_2]$•4DMSO (3)** was crystallized as tiny colorless rods. A sample 0.17 x 0.08 x 0.07 mm^3 was used for data collection. A total of 3759 frames was collected at 10 s/frame, yielding 19903 reflections, of which 5455 were independent. Hydrogen atoms were placed at calculated positions. The asymmetric unit contains one half complex with Hg occupying an inversion center plus two DMSO solvates. **$[Sn^{IV}(L^{iodo})Cl_3]$ (5)** crystallized as colorless rod fragments. A sample 0.20 x 0.16 x 0.10 mm^3 was used for data collection. A total of 3445 frames was collected at 10 s/frame, yielding 14665 reflections, of which 4368 were independent. Hydrogen positions were calculated. The asymmetric unit consists of 1 neutral molecule without ions or solvates.

	(3)	(5)
Formula	$C_{34}H_{46}HgI_4N_4O_6S_4$	$C_{13}H_{11}SnI_4N_4OCl_3$
M	1443.18	690.08
Space group	Triclinic, P-1	Triclinic, P-1
a / Å	10.3784 (4)	7.8380 (5)
b/ Å	10.7497 (4)	10.1607 (6)
c/ Å	11.0349 (4)	11.8911 (7)
α/ ^{o}	77.982 (2)	101.008 (2)
β/ ^{o}	89.147 (2)	103.100 (2)
γ/ ^{o}	71.429 (2)	97.885 (2)
V/ Å^3	1139.67 (7)	889.11 (9)
Z	1	2
T/ K	100 (2)	100 (2)
λ/ Å	0.71073	0.71073
D_{calc}/ g cm^{-3}	2.103	2.578
μ/ mm^{-1}	6.312	5.361
R(*F*) (%)	2.26	2.07
Rw(*F*) (%)	4.48	4.98

[a] $R(F) = \sum \| F_o \| - | F_c \| / \sum | F_o |$ for $I > 2s(I)$; $Rw(F) = [\sum w(F_o^2 - F_c^2)^2 / \sum w(F_o^2)^2]^{1/2}$ for $I > 2s(I)$.

Table 6.5.2. Crystal data and structure refinements for **[Hg^{II}(L^{iodo})$_2$] •4DMSO (3)** and **[Sn^{IV}(L^{iodo})Cl$_3$] (5)**

6.5.3. Syntheses

6.5.3.1. Ligand syntheses

The **HL^{iodo}** ligand has been previously synthesized according to well established procedures in our lab.[21,25]

6.5.3.2. Complex syntheses

$[Al^{III}(L^{iodo})_2]ClO_4$ (1). The HL^{iodo} ligand (0.50 g, 1.1 mmol) was dissolved in 30 mL of methanol followed by the dropwise addition of Et_3N (0.16 g, 1.6 mmol). Anhydrous $AlCl_3$ salt (0.072 g, 0.54 mmol) dissolved in minimum amount of methanol was added slowly to the ligand solution while stirring under heating. The reaction mixture was refluxed for 2 h under aerobic conditions then cooled to room temperature. Counterion exchange was followed by addition of a methanolic solution containing $NaClO_4$ to the reaction mixture. A yellow precipitate formed immediately, which was isolated and washed with cold methanol and water to eliminate the excess salts. After washing with ether, the product was vacuum dried and characterized. Yield: 93%; IR data: (KBr, cm^{-1}) 1616, 1574, 1451, ($C{=}N_{Py}$, $C{=}C_{Ar}$); 1319, (C-O); 1095, (Cl-O, perchlorate); ^{1}H-NMR (MR-400, DMSO, 298 K) δ 9.68 (d, 1H, J = 5.40 Hz), δ 8.05-8.13 (m, 2H), δ 7.86-7.92 (m, 1H), δ 7.68 (t, 1H, J = 6.16 Hz), δ 7.53 (d, 2H, J = 2.35 Hz), δ 7.47 (s, 1H), δ 7.42 (d, 1H, J = 7.33 Hz), δ 7.35-7.41 (m, 2H), δ 7.27 (d, 2H, J = 3.81 Hz), δ 6.59 (d, 1H, J = 6.56), δ 5.75 (s, 1H), δ 4.78 (dd, 1H, J = 10.72, 5.46 Hz, $–CH_2$), δ 4.54 (d, 1H, J = 11.79 Hz, $–CH_2$), δ 4.44 (d, 1H, J = 13.40 Hz, $–CH_2$), δ 3.87-4.02 (m, 4H, $–CH_2$), δ 3.81 (d, 1H, J = 11.25 Hz, $–CH_2$), δ 3.58 (d, 1H, J = 13.40 Hz, $–CH_2$), ESI$^+$ in MeOH: *m/z* (100%) = 956.8 for $[Al^{III}(L^{iodo})_2]^+$; Anal. Calc. for **2** (%, $C_{26}H_{22}AlI_4N_4ClO_6$, FW = 1056.53 $g.mol^{-1}$); C, 29.56; H, 2.10; N, 5.30. Found (%): C, 29.51; H, 2.02; N, 5.20.

$[Cd^{II}(L^{iodo})Cl]\cdot H_2O$ (2). The metal salt $CdCl_2$ (87 mg, 0.48 mmol) was dissolved in 5 mL of ethanol and slowly added to a 30 mL ethanol solution containing the ligand HL^{iodo} (0.20 g, 0.43 mmol) and Et_3N (0.07 g; 0.69 mmol). The solution was refluxed for 24 h under aerobic conditions, when a light yellow precipitate was formed and then filtered and washed with cold ether. Yield: 70%; IR data (KBr, cm^{-1}): 1601, 1564, 1422, ($C{=}N_{Py}$, $C{=}C_{Ar}$); 1303, (C-O); ^{1}H-NMR (MR-400, DMSO, 298 K) δ 8.58 (d br., 1H, *J* = 2.74 Hz), δ 7.87 (t br., 1H, *J* = 7.33, 7.10 Hz), δ 7.54 (s br., 1H), δ 7.34-7.41 (m br., 3H), δ 7.12 (s br., 1H), δ 4.16 (s br., 1H, $–CH_2$), δ 3.98 (s br., 1H, $–CH_2$), δ 3.75-3.61(d br., 5H, $–CH_2$), Anal. Calc. (%) for (%,$C_{13}H_{13}CdI_2N_2O_2Cl$, FW = 630.93 $g.mol^{-1}$) C, 24.75; H, 2.08; N, 4.44. Found (%): C, 25.09; H, 1.95; N, 4.36.

$[Hg^{II}(L^{iodo})_2]\cdot 4DMSO$ (3). To a methanolic solution containing HL^{iodo} ligand (0.31 g, 0.66 mmol) and Et_3N (0.10 g, 0.99 mmol), $Hg(NO_3)_2\cdot H_2O$ salt (0.11 g, 0.31 mmol) was added and the reaction was stirred for 2 h under 30 °C. The solvent was rotoevaporated until half of the solvent was removed, and the resulting yellow precipitate was filtered and washed with cold methanol. The product was dissolved in a minimum amount of dimethylsulfoxide, and colorless crystals were obtained after 48 h under slow solvent evaporation. Yield: 70%; IR data: (KBr, cm^{-1}) 1599, 1559, 1421, ($C{=}N_{Py}$ $C{=}C_{Ar}$); 1318, (C-O); ESI^+ in MeOH: *m/z* (100%) = 1132.8 for $[Hg^{II}(L^{iodo})_2 + H^+]^+$; Anal. Calc. (%) for $[Hg^{II}(L^{iodo})_2]\cdot 2DMSO$ (ground, vacuum dried sample**:** %, $C_{30}H_{34}HgI_4N_4O_4S_2$, FW = 1286.95 $g.mol^{-1}$) C, 28.00; H, 2.66; N, 4.35. Found (%): C, 28.06; H, 2.21; N, 4.57.

$[Pb^{II}(L^{iodo})NO_3]$ (4). The $Pb(NO_3)_2$ salt (0.40 g, 1.2 mmol) was dissolved in 5 mL ethanol and added to a 30 mL ethanolic solution containing the ligand HL^{iodo} (0.50 g, 1.1 mmol) and Et_3N (0.17 g; 1.7 mmol) under aerobic condition. The solution was refluxed for 24 h, when a white product was vacuum filtered and washed with cold ethanol and ether. Yield: 86%; IR data

(KBr, cm^{-1}): 1602, 1562, 1421, ($C=N_{Py}$, $C=C_{Ar}$); 1301, (C-O); ^{1}H-NMR (MR-400, DMSO, 298 K) δ 8.66 (d, 1H, *J* = 5.18 Hz), δ 7.79 (dt, 1H, *J* = 7.12 Hz), δ 7.55 (s, 1H), δ 7.31-7.34 (m, 2H), δ 7.23 (s, 1H), δ 4.54 (d br., 3H, $–CH_2$), δ 4.07 (s br., 1H, $–CH_2$); ESI^+ in MeOH: *m/z* (100%) = 672.8 for $[Pb^{II}(L^{iodo})]^+$; Anal. Calc. for **3** (%,$C_{13}H_{11}PbI_4N_3O_4$, FW = $g.mol^{-1}$) C, 21.27; H, 1.51; N, 5.72. Found (%): C, 21.30; H, 1.50; N, 5.55.

$[Sn^{IV}(L^{iodo})Cl_3]$ (5). The HL^{iodo} ligand (0.50 g, 1.1 mmol) was dissolved in 30 mL of ethanol and Et_3N (0.14 g, 1.3 mmol) was added dropwise. $SnCl_2·2H_2O$ (0.24 g, 1.1 mmol) was dissolved in minimum amount of ethanol and added slowly to the ligand solution while stirring. The reaction mixture was then refluxed for 48 h under aerobic conditions. No precipitate was observed; hence the solution was concentrated by rotoevaporation and set for crystallization. Colorless crystals were afforded after 72 h under room temperature by slow solvent evaporation. Yield: 88%; IR data: data (KBr, cm^{-1}): 1609 1568, 1432 ($C=N_{Py}$, $C=C_{Ar}$); 1294 (C-O); ^{1}H-NMR (MR-400, DMSO, 298 K) δ 8.87 (d, 1H, *J* = 6.46 Hz), δ 8.09 (dt, 1H, *J* = 7.81, 1.70 Hz), δ 7.77 (s br., 1H), δ 7.69 (t, 1H, *J* = 7.03 Hz), δ 7.53 (s, 1H), δ 7.44 (s, 1H), δ 7.40 (d, 1H, *J* = 8.09 Hz), δ 4.53 (dd, 1H, *J* = 16.73, 6.23 Hz, $–CH_2$), δ 4.42 (d, 1H, *J* = 12.84 Hz, $–CH_2$), δ 4.32 (d, 1H, *J* = 17.51 Hz, $–CH_2$), δ 3.85 (dd, 1H, *J* = 13.23, 1.95 Hz, $–CH_2$), ESI^+ in MeOH: *m/z* (100%) = 686.8 for $[Sn^{IV}(L^{iodo})Cl_2CH_3OH]^+$; Anal. Calc. for **2** (%, $C_{13}H_{11}SnI_2N_2OCl_3$, FW = 690.12 $g.mol^{-1}$); C, 22.63; H, 1.61; N, 4.06. Found (%): C, 22.85; H, 1.78; N, 3.92.

6.5.4. Biological Assays

6.5.4.1. Inhibition of Proteasomal Activity in Purified 20S Proteasome

Purified human 20S proteasome (35 ng; Boston Biochem; Cambridge, MA) was incubated with 10 μM of CT substrate, SucLLVYAMC (AnaSpec; Fremont, CA) , in 100 μL of assay buffer [20 mM Tris-HCl (pH 7.5)] in the presence of complexes **1-5** at various

concentrations, with DMSO as the solvent control. After 2 h incubation at 37 °C, the production of hydrolyzed AMC groups was measured using a Wallac Victor3 multilabel counter (PerkinElmer; Waltham, MA) with an excitation filter of 365 nm and an emission filter of 460 nm.[25]

6.5.4.2. Cell Cultures and Whole Cell Extract Preparation

CRL2221 transformed human prostate epithelial cells were grown in RPMI1640 supplemented with 10% fetal bovine serum, 100 units/ml penicillin and 100 µg/ml streptomycin and maintained at 37 °C with 5% CO_2. Whole cell lysates were prepared as previously described.[26]

6.5.4.3. Cell Proliferation Assay

Cells were seeded in quadruplicate in a 96-well plate and grown to 70−80% confluence, followed by treatment with the indicated agents for 72 h followed by measurement of cell proliferation by the 3(4,5dimethylthiazol-2-yl)2,5diphenyltetrazolium bromide (MTT) assay as described previously.[27]

6.5.4.4. Proteasome CT-like Activity in Intact CRL2221 Cells

Proteins extracted from cells after each treatment were incubated at 37 °C for 2-4 h in 100 µL of assay buffer (50 mM Tris-HCl, pH 7.5) with 10 µM of fluorogenic CT substrate SucLLVYAMC, and production of hydrolyzed AMC groups was measured using a Wallac Victor3 multilabel counter with an excitation filter of 365 nm and an emission filter of 460 nm, as described previously.[27]

6.5.4.5. Proteasome CT-like Activity in Cell Extracts

CRL2221 protein extract (10 µg) was treated with complexes **1-5** at various concentrations (or DMSO as solvent control) for 24h at 37 °C with 10 µM of CT substrate in 100

μL assay buffer [20 mM Tris-HCl (pH 7.5)]. After incubation, the production of hydrolyzed AMC groups was measured using a Wallac Victor3 multilabel counter (PerkinElmer; Waltham, MA) with an excitation filter of 365 nm and an emission filter of 460 nm.

6.6. References

1 Jeffery, E. H. *Biochemical mechanisms of aluminum toxicity, Toxicology of Metals in Handbook of Experimental Pharmacology*, **1995**, *115*, 139-161.

2 Lemire, J.; Appanna, V. D. *J. Inorg. Biochem.* **2011**, *105*, 1513.

3 Wolfgang, M.; Jean-Marc, M. *The Bioinorganic Chemistry of Cadmium in the Context of its Toxicity, Cadmium: From Toxicology to Essentiality Metal Ions in Life Sciences, Springer*, **2013**, *11*, pp. 1-30.

4 Larregle, E. V.; Ferranola, M. L. *Molecular mechanisms of cadmium toxicity in mammals in Metals in Biological Systems, Gimenez Maria Sofia ED.* **2010**, pp.163-185.

5 Moulis, J.-M. *Bio. Metals* **2010**, *23*, 877.

6 Yang, D.-Y.; Chen, Y.-W.; Gunn, J.M.; Belzile, N. *Environ. Rev.* **2008**, *16*, 71.

7 Neustadt, J.; Pieczenik, S. *Integ. Medic.* **2007**, *6*, 26.

8 Guzzi, G.; La Porta, C. A. M. *Toxicology* **2008**, *244*, 1.

9 Yasuhiro, S.; Toshiyuki, K. *Biol. Pharm. Bull.* **2012**, *35*, 1885.

10 Blunden, S.; Wallace, T. *Food Chem. Toxicol.* **2003**, *41*, 651.

11 Arakawa, Y. Biomed. *Res. Trace Elements* **2000**, *11*, 259.

12 Neslund-Dudas, C.; Mitra, B.; Kandegedara, A.; Chen, D.; Schmitt, S.; Shen, M.; Cui, Q.; Rybicki, B. A.; Dou, Q. P. *Biol. Trace Elem. Res.* **2012**, *149*, 5.

13 Shi, G.; Chen, D.; Zhai, G.; Chen, M. S.; Cui, Q. C.; Zhou, Q.; He, B.; Dou, Q. P.; Jiang, G. *Environ. Health Perspect.* **2009**, *117*, 379.

14 Shakya, R.; Hindo, S. S.; Wu, L.; Allard, M.; Heeg, M. J.; Hratchian, H. P.; McGarvey, B. R.; da Rocha, S.; Verani, C. N. *Inorg. Chem.* **2007**, *46*, 9808.

15 Xavier, F. R.; Peralta, R. A.; Bortoluzzi, A. J.; Drago, V.; Castellano, E. E.; Haase, W.; Tomkowicz, Z.; Neves, A. *J. Inorg. Biochem.* **2011**, *105*, 1740.

16 Biswas, S.; Saha, R.; Ghosh, A. *Organometallics* **2012**, *31*, 3844.

17 Chen, Z.-F.; Peng, Y.; Gu, Y.-Q.; Liu, Y.-C.; Liu, M.; Huang, K.-B.; Hu, K.; Liang, H. *Eur. J. Med. Chem.* **2013**, *62*, 51.

18 Momeni, B. Z.; Kia, R.; Ghanbarzadeh, S. *Monatsh. Chem. Springer* **2012**, *143*, 1479.

19 Shakya, R.; Peng, F.; Liu, J.; Heeg, M. J.; Verani, C. N. *Inorg. Chem.* **2006**, *45*, 6263.

20 Lesh, F. D.; Hindo, S. S.; Heeg, M. J.; Allard, M. M.; Jain, P.; Peng, B.; Hryhorczuk, L.; Verani, C. N. *Eur. J. Inorg. Chem.* **2009**, 345.

21 Shakya, R.; Imbert, C.; Hratchian, H. P.; Lanznaster, M.; Heeg, M. J.; McGarvey, B. R.; Allard, M. M.; Schlegel, H. B.; Verani, C. N. *Dalton Trans.* **2006**, 2517.

22 Mugesh, G.; Singh, H. B.; Butcher, R. J. *Eur. J. Inorg. Chem.* **2001**, 669.

23 *APEX II* collection and processing programs are distributed by the manufacturer. Bruker AXS Inc., Madison WI, USA, **2009**.

24 Sheldrick, G. M. *Acta Cryst.* **2008**, *A64*, 112.

25 Daniel, K. G.; Gupta, P.; Harbach, R. H.; Guida, W. C.; Dou, Q. P. *Biochem. Pharmacol.* **2004**, *67*, 1139.

26 Chen, D.; Cui, Q. C.; Yang, H.; Dou, Q. P. *Cancer Res.* **2006**, *66*, 10425.

27 Daniel, K. G.; Chen, D.; Orlu, S.; Cui, Q. C.; Miller, F. R.; Dou, Q. P. *Breast Cancer Res.* **2005**, *7*, R897.

CHAPTER 7

CONCLUSIONS AND FUTURE DIRECTIONS

CHAPTER 7

CONCLUSIONS AND FUTURE DIRECTIONS

7.1. Conclusions

My contributions through this research have furthered our understanding of the metal-based behavior proteasome inhibitors. We have successfully demonstrated the appropriate selection of the metal ions based on their oxidation state, redox properties, coordination numbers, and chemical properties including the inertness and lability of these metal ions. We have also showed that tuning the properties of the ligand can dramatically change the effects of these complexes against the inhibition of the 26S proteasome activity.

In **Chapter 3**, the first Research Objective of *interrogating the mechanism of inhibition of the 26S proteasome using inert/labile metal ions coordinated to tri/hexadentate ligands* has been accomplished by the synthesis and characterization of three cobalt complexes described as $[Co^{II}(L^1)_2]$, $[Co^{II}(L^2)]$, and $[Co^{III}(L^1)_2]ClO_4$. These complexes contain the deprotonated forms of the [NN′O] tridentate ligand HL^1 and its newly synthesized $[N_2N'_2O_2]$ hexadentate counterpart H_2L^2, namely, 2,4-diiodo-6-((pyridine-2-ylmethylamino)methyl)phenol and 6,6′-((ethane-1,2-diylbis((pyridin-2-ylmethyl)azanediyl))bis(methylene))bis(2,4-diiodophenol). Characterizations of these three complexes included electrospray ionization (ESI) spectrometry, infrared and UV-visible spectroscopies, and elemental analyses. A detailed ^{1}H-NMR study was conducted for $[Co^{III}(L^1)_2]ClO_4$ and X-ray structural data was obtained for $[Co^{II}(L^2)]$ complex. The viability of this series as potential agents for proteasome inhibition and cell apoptotic induction involving PC-3 cancer cells is presented comparing the behavior of the

untethered $[NN'O]_2$ six-coordinate $[Co^{II}(L^1)_2]$ and $[Co^{III}(L^1)_2]ClO_4$ and the tethered counterpart $[Co^{II}(L^2)]$ with a 1:1 metal-to-ligand ratio. It is observed that the tethering in $[Co^{II}(L^2)]$ decreases inhibition activity. When $[Co^{II}(L^1)_2]$ and $[Co^{III}(L^1)_2]ClO_4$ were compared, the most inert, but redox-active, cobalt(III) species showed the highest chymotrypsin-like activity inhibition on purified proteasome and PC-3 cancer cells.

In the second Research Objective, described in **Chapter 4**, we have *evaluated the chemical reduction as a viable mechanism for the inhibition of the 20S proteasome.* The viability of ligand dissociation in the cobalt complex $[Co^{III}(L^1)_2]ClO_4$ following biological reduction has been established. We performed detailed electrochemical characterization of $[Co^{III}(L^1)_2]ClO_4$ in several solvents, along with spectroelectrochemical and chemical reduction to monitor the phenolate-to-cobalt(III) LMCT band observed at 440 nm in the UV–Vis region in presence and absence of a sacrificial reductant. DFT calculations were performed to confirm the nature of this band. Species $[Co^{III}(L^1)_2]ClO_4$ displays no signs of ligand protonation at pH 3 over a period of 24 h while probing its stability in solution. Spectrophotometric monitoring at pH 3 in presence of ascorbic acid shows clearly a decrease of the LMCT band, implying that reduction of the metal center has taken place.

The products of chemical reduction were analyzed by high resolution ESI^+ mass spectrometry and support a mechanism in which biological reduction leads to ligand dissociation. This mechanism explains why the substitutionally inert cobalt (III) complex $[Co^{III}(L^1)_2]ClO_4$ revealed high levels of proteasomal inhibition via deactivation of chymotrypsin-like activity; hence, induction of cellular apoptosis in PC-3 cells compared to the more labile Co(II) containing species $[Co^{II}(L^1)_2]$. These promising results support

our hypothesis that loss of one ligand from 2:1 ligand to metal ratio is required for the pharmacophore species $[ML]^+$ to be formed. Such pharmacophore species provides the available open coordination sites for the appropriate amino acid chains such as threonine, tyrosine, and histidine containing hydroxyl or imidazole functional groups in the chymotrypsin pocket to coordinate to the metal ion center.

Chapter 5 covers the third Research Objective of *comparing the effect of the ion charge towards the inhibition activity of the 26S proteasome.* Two new complexes containing a higher oxidation state gallium(III) metal ion $[Ga^{III}(L^2)]ClO_4$ and a lower oxidation state zinc(II) ion $[Zn^{II}(L^2)]$ with the deprotonated form of H_2L^2 ligand 6,6′-((ethane-1,2-diylbis((pyridin-2-ylmethyl)azanediyl))bis(methylene))bis(2,4-diiodophenol) were successfully synthesized and characterized. The structural information of the deprotonated hexadentate ligand coordinated to the Ga and Zn ions was confirmed by X-ray crystallography where both complexes are arranged in a 1:1 metal to ligand ratio. Their biological effect against the proliferation of prostate cancer PC-3 cells *via* proteasome inhibition activity was measured. From the biological results it is concluded that the Ga-containing complex is highly potent towards the inhibition activity of the purified 20S proteasome (IC_{50} = 0.6 μM) and 26S proteasome as well as apoptosis induction in PC-3 cells, compared to the zinc-containing analog. Western blotting analysis reveals that both complexes inhibit the 26S proteasome activity by the increased levels of the ubiquitinated proteins. Thus, we can hypothesize that the $[Zn^{II}(L^2)]$ complex possibly inhibits the activity of the proteasome not by the inhibition of chymotrypsin-like activity, but by other proteolytic sites such as trypsin- or caspase-like. Further studies have to be completed in order to fully support such a hypothesis.

Chapter 6, which includes the fourth Research Objective, addresses *the effect of aluminum and heavy metal ions on inhibition activity of the 20S and 26S proteasome in non-cancerous prostate cells*. In this chapter, we report on the synthesis of five metal complexes coordinated to the [NN′O] ligand HL^{iodo} (2,4-diiodo-6-((pyridine-2-ylmethylamino)methyl)phenol), namely $[Al^{III}(L^{iodo})_2]ClO_4$, $[Cd^{II}(L^{iodo})Cl]\cdot H_2O$, $[Hg^{II}(L^{iodo})_2]\cdot 4DMSO$, $[Pb^{II}(L^{iodo})NO_3]$, and $[Sn^{IV}(L^{iodo})Cl_3]$. These species are thoroughly characterized by spectroscopic and spectrometric methods, as well as by elemental analysis. X-ray crystallographic results for complex $[Hg^{II}(L^{iodo})_2]\cdot 4DMSO$ indicate the presence of Hg(II) ion hexacoordinated to two facially oriented [NN′O] ligands, whereas for complex $[Sn^{IV}(L^{iodo})Cl_3]$ an Sn(IV) ion chelates to one deprotonated ligand and three chlorido coligands. The toxicity of these complexes is tested against transformed human prostate epithelial cells CRL2221 and we observed that the five complexes demonstrate high levels of cell growth inhibition in a dose-dependent manner. In order to evaluate the relationship between these species and the proteasome, we test them against purified 20S, CRL2221 cell extracts, and intact cells, followed by the measurement of the percent chymotrypsin-like activity inhibition levels. Results suggest a good correlation between the toxicity of $[Hg^{II}(L^{iodo})_2]\cdot 4DMSO$ and proteasome inhibition.

7.2. Future Directions

Innovative ideas in development of the next generation metal-based proteasome inhibitors are focused on the challenges of increasing drug selectivity and introducing low levels of intracellular toxicity. These challenges will be addressed by designing and synthesizing 26S proteasome inhibitors incorporating new ligand scaffolds. Since the

ligand HL^{iodo} (2,4-diiodo-6-((pyridine-2-ylmethylamino)methyl)phenol) has been proven to successfully carry various metal ions intracellulary, it is wise to link this ligand with the peptide unit of bortezomib and MG132 aldehyde inhibitor. The secondary amine group found in the HL^{iodo} ligand will serve as the attachment site of these peptide-based fragments. Therefore, we should develop these new ligands Pyz-Phe-Leu-$L^{iodo}H$, (Pyz = pyrazinoic acid), and Z-Leu-Leu-Leu-$L^{iodo}H$, (Z = benzyloxycarbonyl) by incorporating amino acid sequences of Pyz-Phe-Leu- and Z-Leu-Leu-Leu- found in highly selective proteasome inhibitors such as bortezomib and the aldehyde MG132[1,2] (**Figure 7.2.**). Synthesis of the Pyz-Phe-Leu-$L^{iodo}H$ ligand series can be obtained by Suzuki[3] or Stille[4] coupling, whereas the Z-Leu-Leu-Leu-$L^{iodo}H$ series can be synthesized by Schiff condensation/alkylation. Such amino acid chains are accepted to form hydrogen bonding with the chymotrypsin-like pocket of the 20S proteasome, therefore increasing drug selectivity for such site.

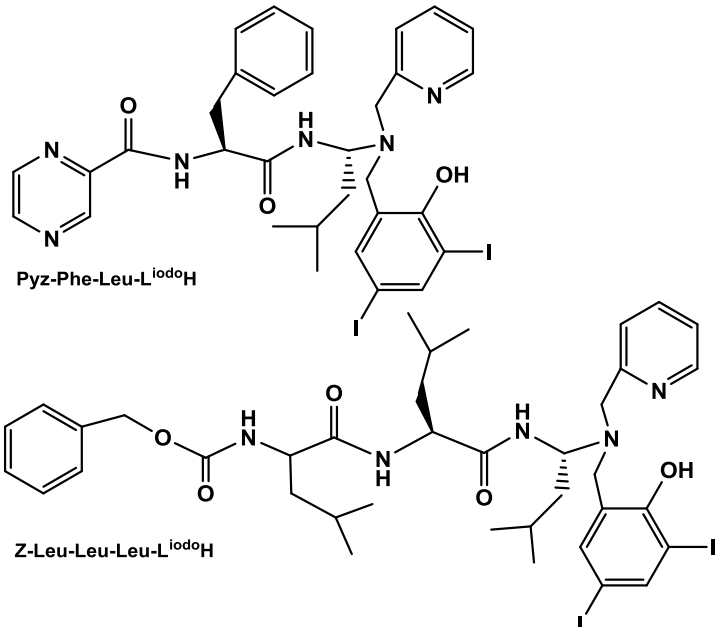

Figure 7.2. New ligands containing bortezomib (top) and MG132 (bottom) derivatives.

Also, the interesting results obtained in **Chapter 5** where the zinc-containing complex $[Zn^{II}(L^2)]$ did not show inhibition activity of chymotrypsin in purified 20S and cellular 26S proteasome, but demonstrated increased levels of ubiquitinated proteins from PC-3 cell extracts, should be further investigated for proteasome inhibition activity. The next step is to validate $[Zn^{II}(L^2)]$ complex against other proteolytic sites of the proteasome including trypsin-, and caspase-like activity as well as the JAMM domain of the 19S particle of the proteasome.[5]

The Verani group also needs to address the proteasome inhibition activity *in vivo*. Considering our best proteasome inhibitor pro-drugs $[Ga^{III}(L^2)]ClO_4$ and $[Co^{III}(L^1)_2]ClO_4$ *in vitro*, we will continue these studies following the protocols established in the Dou Lab for *in vivo* measurements.[6,7,8]

7.3. References

1 Banerjee, D.; Liefshitz, A. *Antican. Res.* **2001**, *21*, 3941.

2 Tsubuki, S.; Saito, Y.; Tomioka, M.; Ito, H.; Kawashima, S. *J. Biochem.* **1996**, *119*, 572.

3 Kirchhoff, J. H.; Netherton, M. R.; Hills, I. D.; Fu, G. C. *J. Am. Chem. Soc.* **2002**, *124*, 13662.

4 Li, J-H.; Liang, Y.; Wang, D-P.; Liu, W-J.; Xie, Y-X.; Yin, D-L. *J. Org. Chem.* **2005**, *70*, 2832.

5 Cvek, B.; Milacic, V.; Taraba, J.; Dou, Q. P. *J. Med. Chem.* **2008**, *51*, 6256.

6 Chen, D.; Frezza, M.; Shakya, R.; Cui, C. Q.; Milacic, V.; Verani, C. N.; Dou, Q. P. *Cancer Res.* **2007**, *67*, 9258.

7 Yang, H.; Chen, D.; Cui, Q. C.; Yuan, X.; Dou, Q. P. *Cancer Res.* **2006**, *66*, 4758.

8 Chen, D.; Cui, Q. C.; Yang, H.; Dou, Q. P. *Cancer Res.* **2006**, *66*, 10425.

APPENDIX A

Supplementary Material for Chapter 3

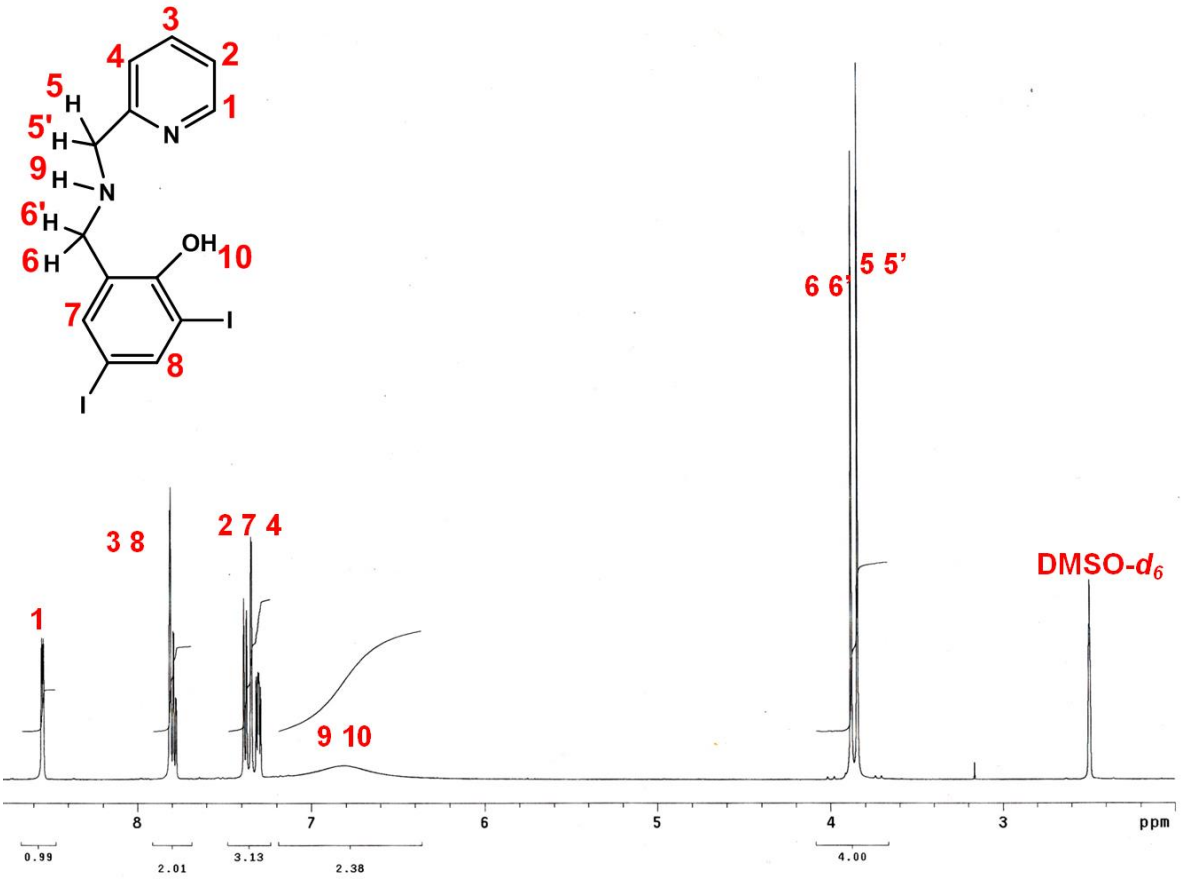

Figure A.3.2.2.1 ^{1}H-NMR of HL^{1} ligand.

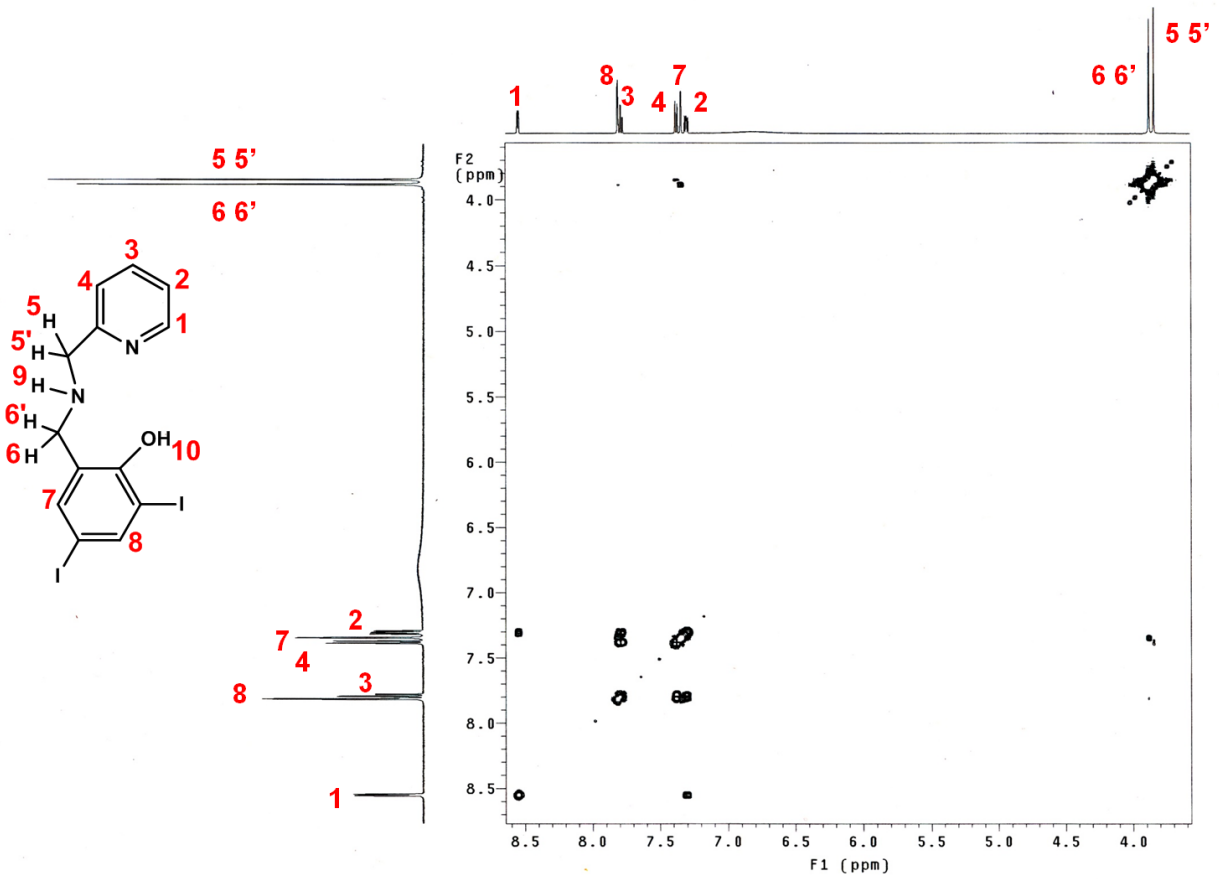

Figure A.3.2.1.2. ^{1}H-^{1}H COSY for HL^{1} ligand.

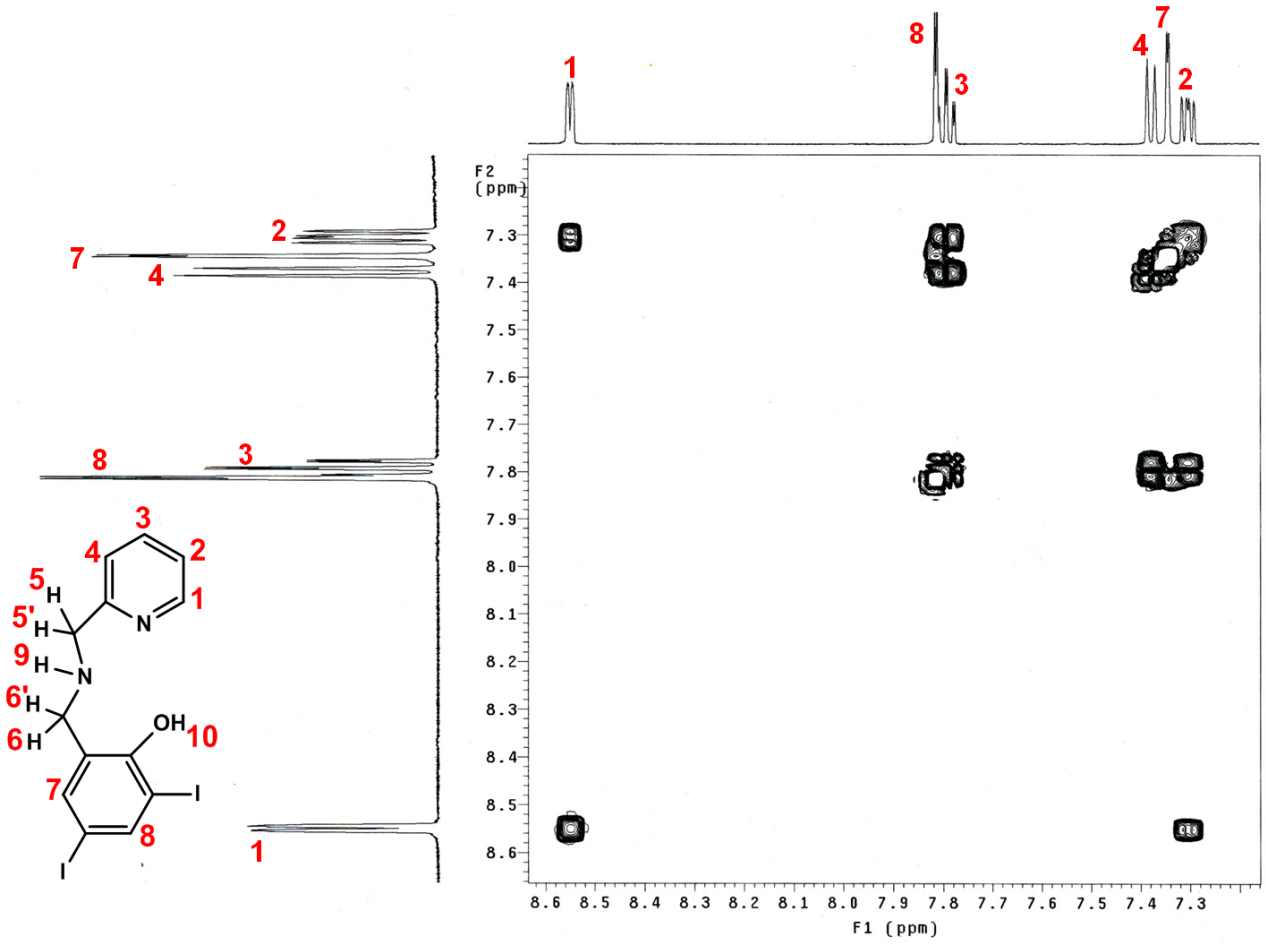

Figure A.3.2.1.3. Expanded picture of the aromatic region of ^{1}H-^{1}H COSY for HL^{1} ligand.

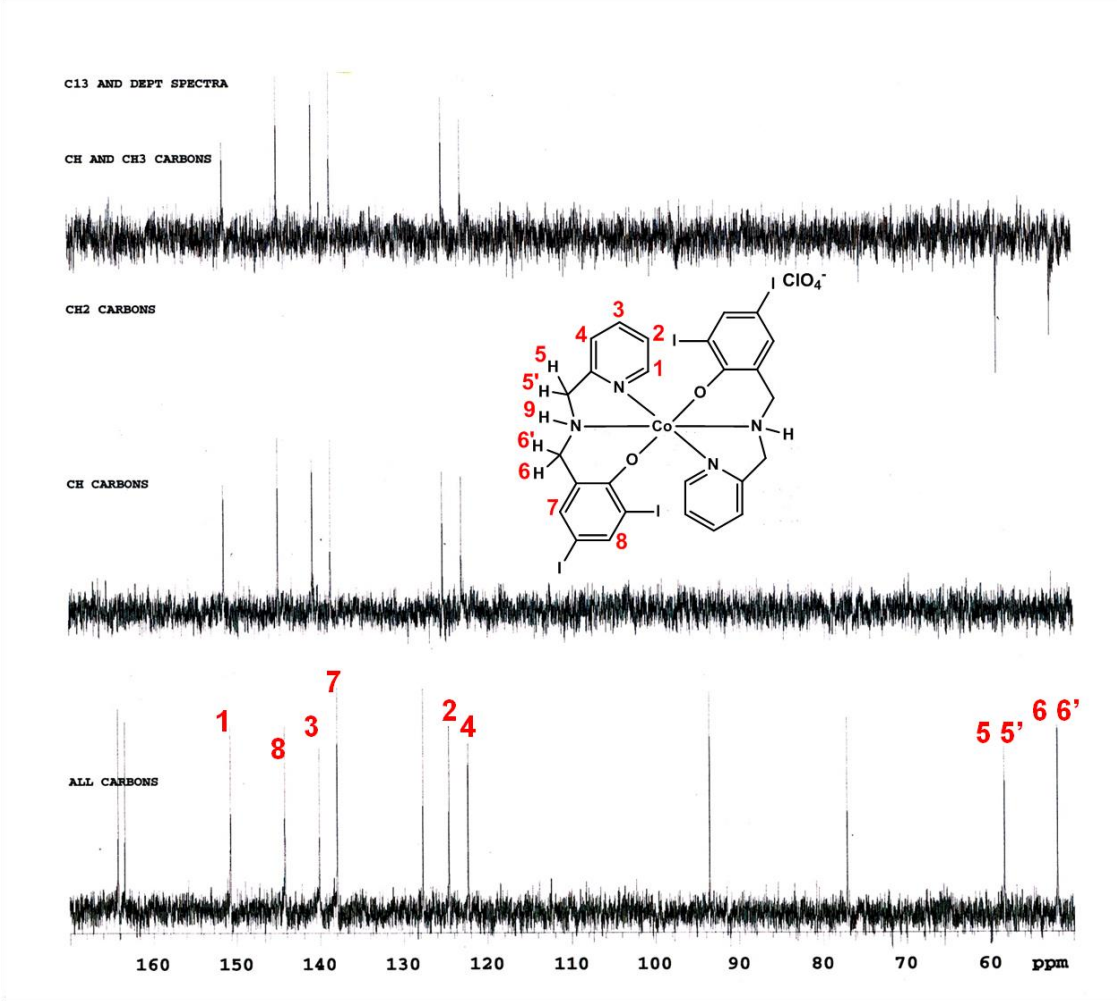

Figure A.3.2.3.1. ^{13}C NMR / DEPT for complex **3**.

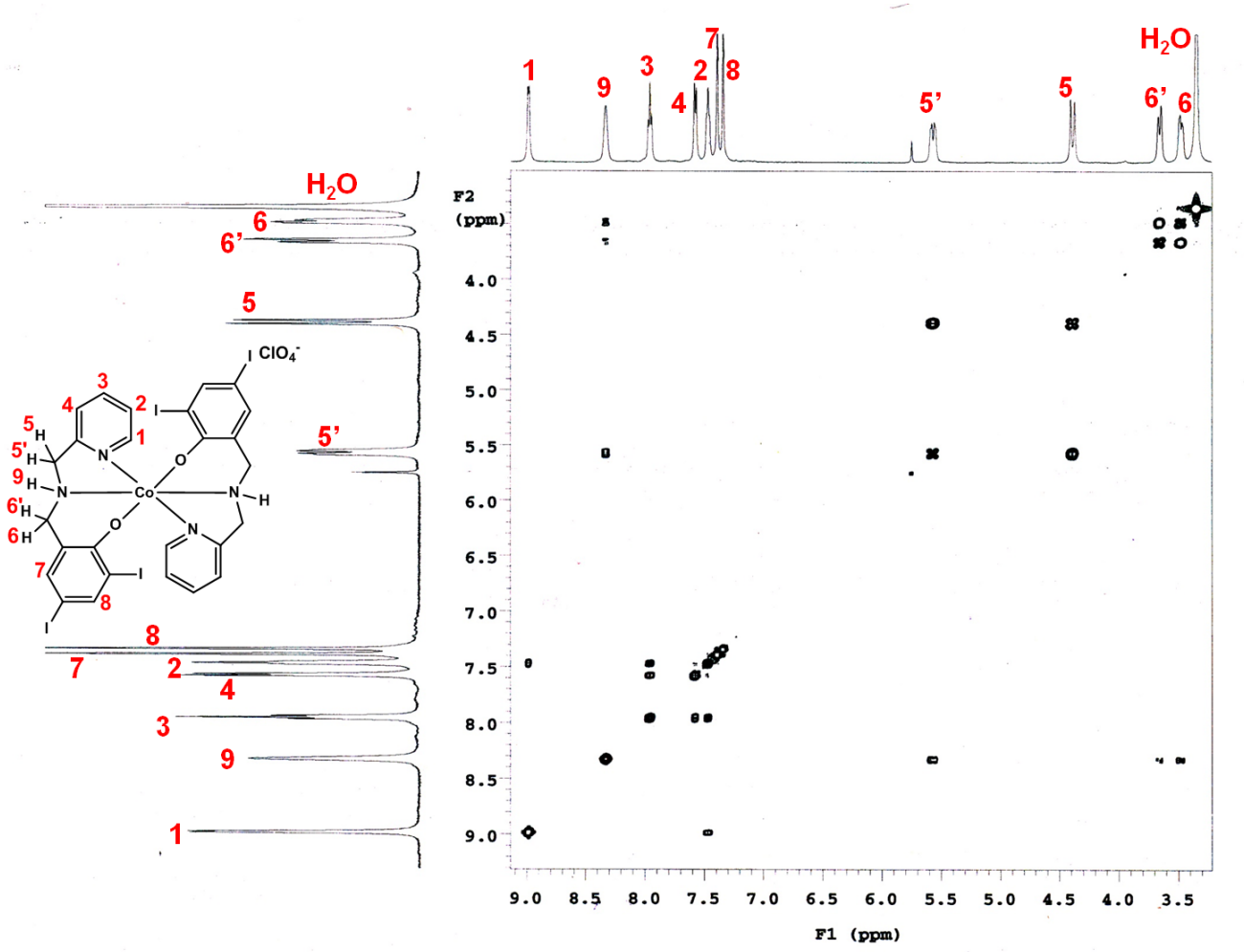

Figure A.3.2.3.2. ^{1}H-^{1}H COSY for complex **3**.

Proton H	HL^1 (ppm) *J*-coupling (Hz)	$[Co^{III}(L^1)_2ClO_4]$ (ppm) *J*-coupling (Hz)
H1	8.54 d (J_{1-2} = 4.8)	8.99 dd (J_{1-2} = 5.5)
H2	7.29 dd (J_{2-3} = 7.7) (J_{2-4} = 4.8)	7.46 t (J_{2-3} = 6)
H3	7.8 br dt (J_{3-2} = 7.7) (J_{3-1} = 1.8)	7.95 t (J_{3-4} = 7.7)
H4	7.37 d (J_{4-3} = 7.7)	7.57 d (J_{4-3} = 7.7)
H5 H5'	3.83 (s)	4.39 d (J = 16.6) 5.58 dd (J = 16.6, 5.5)
H6 H6'	3.87 (s)	3.48 dd (J = 16.6, 4.1) 3.66 br d (J = 11.6)
H7	7.33 d (J_{7-8} = 2.1)	7.39 (s)
H8	7.78 d (J_{8-7} = 2.1)	7.34 (s)
H9	6.60-7.10 br (s)	8.33 (s)
H10	6.60-7.10 br (s)	no peak

Table A.3.2.3 ^{1}H NMR assignment including *J*-coupling values for **HL^1** and **$[Co(L^1)_2]ClO_4$ (3)** in DMSO-d_6.

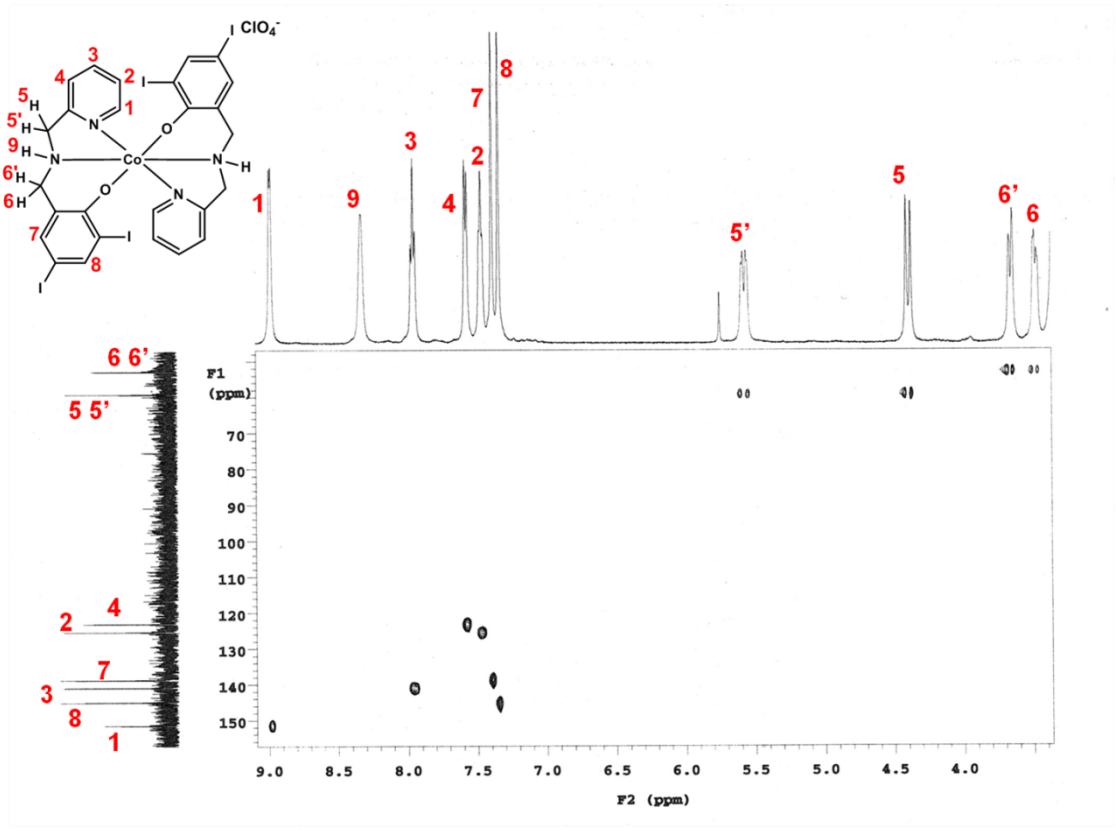

Figure A.3.2.3.3 HMQC for complex **3**.

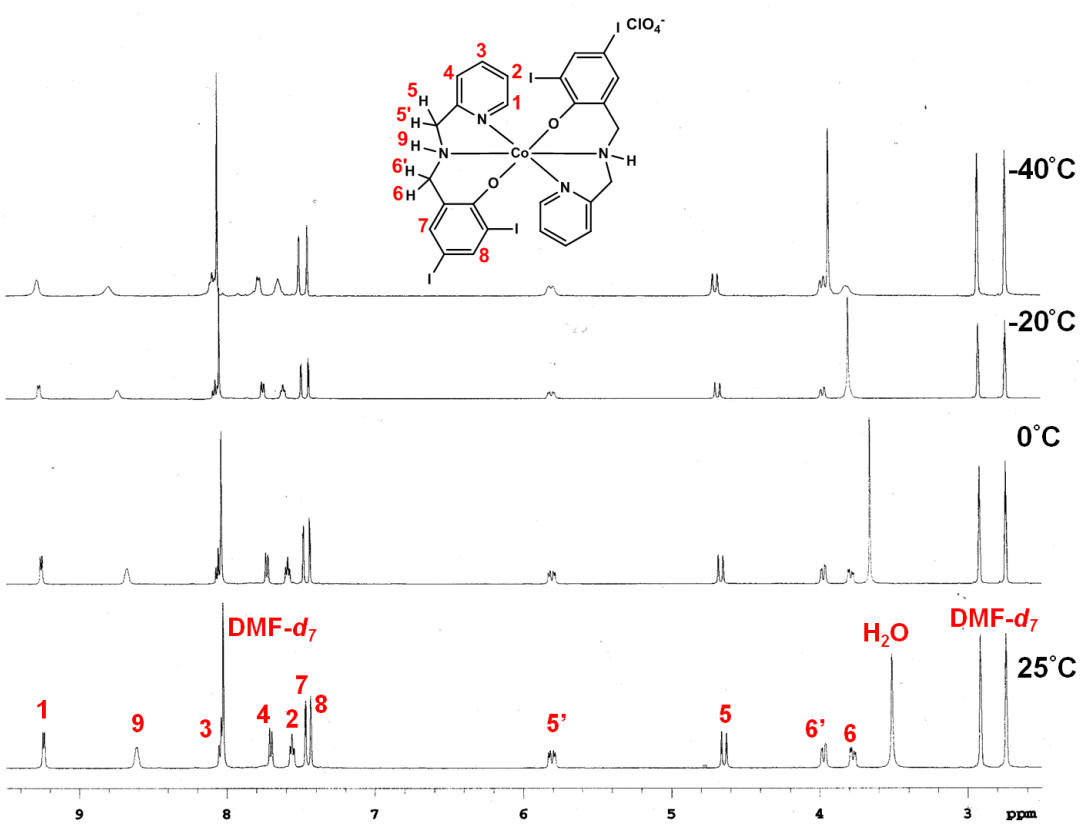

Figure A.3.2.3.4. Low Temperature ^{1}H NMR for complex **3**.

Table S2. Atomic coordinates (x 10^4) and equivalent isotropic displacement parameters (A^2 x 10^3) for **2**. U(eq) is defined as one third of the trace of the orthogonalized Uij tensor.

	x	y	z	U(eq)
I(1)	8862(1)	5403(1)	311(1)	29(1)
I(2)	6038(1)	2026(1)	1522(1)	30(1)
Co(1)	5000	5900(1)	2500	17(1)
N(1)	4436(2)	5877(3)	1560(2)	21(1)
C(1)	3841(3)	4895(4)	1330(2)	27(1)
C(2)	3621(4)	4700(4)	711(2)	31(1)
C(3)	4019(3)	5558(5)	314(2)	33(1)
C(4)	4633(3)	6562(4)	545(2)	30(1)
C(5)	4825(3)	6698(4)	1172(2)	23(1)
C(6)	5459(3)	7808(4)	1449(2)	25(1)
N(2)	5784(2)	7586(3)	2101(2)	21(1)
C(7)	5548(3)	8754(4)	2467(2)	26(1)
C(8)	6838(3)	7256(4)	2193(2)	24(1)
C(9)	7087(3)	6086(4)	1808(2)	21(1)
C(10)	7733(3)	6238(4)	1367(2)	23(1)
C(11)	7932(3)	5164(4)	1001(2)	24(1)
C(12)	7476(3)	3941(4)	1053(2)	21(1)
C(13)	6831(3)	3802(4)	1490(2)	20(1)
C(14)	6634(3)	4831(4)	1893(2)	18(1)
O(1)	6071(2)	4654(2)	2324(1)	20(1)

Table S3. Bond lengths [A] and angles [deg] for **2**.

I(1)-C(11)	2.106(4)
I(2)-C(13)	2.091(4)
Co(1)-O(1)	2.003(3)
Co(1)-O(1)#1	2.003(3)
Co(1)-N(1)#1	2.139(3)
Co(1)-N(1)	2.139(3)
Co(1)-N(2)#1	2.234(3)
Co(1)-N(2)	2.234(3)
N(1)-C(5)	1.339(5)
N(1)-C(1)	1.346(5)
C(1)-C(2)	1.382(6)
C(2)-C(3)	1.381(6)
C(3)-C(4)	1.376(7)
C(4)-C(5)	1.389(6)
C(5)-C(6)	1.503(6)
C(6)-N(2)	1.480(5)
N(2)-C(7)	1.476(5)
N(2)-C(8)	1.485(5)
C(7)-C(7)#1	1.535(8)
C(8)-C(9)	1.506(5)
C(9)-C(10)	1.396(5)
C(9)-C(14)	1.424(5)
C(10)-C(11)	1.389(6)
C(11)-C(12)	1.385(6)
C(12)-C(13)	1.388(5)
C(13)-C(14)	1.405(5)
C(14)-O(1)	1.302(4)
O(1)-Co(1)-O(1)#1	103.12(15)
O(1)-Co(1)-N(1)#1	88.91(11)
O(1)#1-Co(1)-N(1)#1	90.32(12)
O(1)-Co(1)-N(1)	90.32(12)
O(1)#1-Co(1)-N(1)	88.91(12)
N(1)#1-Co(1)-N(1)	178.76(18)
O(1)-Co(1)-N(2)#1	160.79(12)
O(1)#1-Co(1)-N(2)#1	89.65(11)
N(1)#1-Co(1)-N(2)#1	76.57(12)
N(1)-Co(1)-N(2)#1	104.40(12)
O(1)-Co(1)-N(2)	89.65(11)
O(1)#1-Co(1)-N(2)	160.79(12)
N(1)#1-Co(1)-N(2)	104.40(12)
N(1)-Co(1)-N(2)	76.57(12)
N(2)#1-Co(1)-N(2)	82.03(16)
C(5)-N(1)-C(1)	118.4(4)
C(5)-N(1)-Co(1)	119.0(3)
C(1)-N(1)-Co(1)	121.4(3)
N(1)-C(1)-C(2)	122.6(4)
C(3)-C(2)-C(1)	118.6(4)
C(4)-C(3)-C(2)	119.3(4)
C(3)-C(4)-C(5)	119.1(4)
N(1)-C(5)-C(4)	122.0(4)
N(1)-C(5)-C(6)	116.6(4)
C(4)-C(5)-C(6)	121.3(4)
N(2)-C(6)-C(5)	112.9(3)
C(7)-N(2)-C(6)	110.6(3)
C(7)-N(2)-C(8)	111.7(3)
C(6)-N(2)-C(8)	111.1(3)
C(7)-N(2)-Co(1)	103.7(2)
C(6)-N(2)-Co(1)	112.8(2)

C(8)-N(2)-Co(1)	106.7(2)
N(2)-C(7)-C(7)#1	109.2(3)
N(2)-C(8)-C(9)	111.9(3)
C(10)-C(9)-C(14)	120.6(4)
C(10)-C(9)-C(8)	120.6(3)
C(14)-C(9)-C(8)	118.8(3)
C(11)-C(10)-C(9)	120.1(4)
C(12)-C(11)-C(10)	121.0(3)
C(12)-C(11)-I(1)	118.5(3)
C(10)-C(11)-I(1)	120.4(3)
C(11)-C(12)-C(13)	118.4(4)
C(12)-C(13)-C(14)	123.3(3)
C(12)-C(13)-I(2)	119.0(3)
C(14)-C(13)-I(2)	117.6(3)
O(1)-C(14)-C(13)	122.2(3)
O(1)-C(14)-C(9)	121.3(3)
C(13)-C(14)-C(9)	116.5(3)
C(14)-O(1)-Co(1)	124.6(2)

Symmetry transformations used to generate equivalent atoms:
#1 -x+1,y,-z+1/2

Table A.3.4.2.1. Anisotropic displacement parameters (A^2 x 10^3) for **2**.
The anisotropic displacement factor exponent takes the form:
-2 pi^2 [h^2 a*^2 U11 + ... + 2 h k a* b* U12]

	U11	U22	U33	U23	U13	U12
I(1)	25(1)	34(1)	28(1)	4(1)	12(1)	-1(1)
I(2)	31(1)	19(1)	41(1)	-5(1)	12(1)	-8(1)
Co(1)	21(1)	13(1)	18(1)	0	6(1)	0
N(1)	21(2)	18(2)	24(2)	1(1)	7(1)	-1(1)
C(1)	32(2)	23(2)	25(2)	2(2)	5(2)	-6(2)
C(2)	39(3)	26(2)	27(2)	-4(2)	-4(2)	-2(2)
C(3)	43(3)	35(3)	18(2)	2(2)	-3(2)	1(2)
C(4)	43(3)	24(2)	24(2)	5(2)	8(2)	8(2)
C(5)	30(2)	17(2)	22(2)	4(2)	6(2)	4(2)
C(6)	33(2)	16(2)	25(2)	4(2)	8(2)	-3(2)
N(2)	27(2)	14(2)	24(2)	-1(1)	7(2)	-3(1)
C(7)	33(2)	13(2)	32(2)	-4(2)	11(2)	-2(2)
C(8)	24(2)	21(2)	27(2)	-6(2)	4(2)	-8(2)
C(9)	20(2)	21(2)	23(2)	-1(2)	3(2)	-4(2)
C(10)	20(2)	20(2)	28(2)	1(2)	4(2)	-5(2)
C(11)	21(2)	31(2)	20(2)	3(2)	4(2)	-1(2)
C(12)	23(2)	23(2)	18(2)	-2(2)	0(2)	-1(2)
C(13)	21(2)	15(2)	23(2)	2(2)	1(2)	-5(2)
C(14)	18(2)	17(2)	20(2)	1(2)	1(2)	-2(2)
O(1)	24(1)	16(1)	21(1)	2(1)	10(1)	0(1)

Table A.3.4.2.1 Hydrogen coordinates (x 10^4) and isotropic displacement parameters (A^2 x 10^3) for **2**.

	x	y	z	U(eq)
H(1)	3560	4312	1603	32
H(2)	3204	3991	562	38
H(3)	3872	5456	-113	39
H(4)	4920	7155	279	36
H(6A)	6038	7895	1222	29
H(6B)	5093	8660	1404	29
H(7A)	5728	9589	2265	31
H(7B)	5922	8712	2874	31
H(8A)	7023	7043	2628	29
H(8B)	7220	8046	2089	29
H(10)	8037	7078	1318	27
H(12)	7602	3214	795	26

Table A.3.4.2.3 Torsion angles [deg] for **2**.

O(1)-Co(1)-N(1)-C(5)	-83.4(3)
O(1)#1-Co(1)-N(1)-C(5)	173.5(3)
N(1)#1-Co(1)-N(1)-C(5)	-135.0(3)
N(2)#1-Co(1)-N(1)-C(5)	84.1(3)
N(2)-Co(1)-N(1)-C(5)	6.1(3)
O(1)-Co(1)-N(1)-C(1)	83.6(3)
O(1)#1-Co(1)-N(1)-C(1)	-19.5(3)
N(1)#1-Co(1)-N(1)-C(1)	32.0(3)
N(2)#1-Co(1)-N(1)-C(1)	-108.9(3)
N(2)-Co(1)-N(1)-C(1)	173.2(3)
C(5)-N(1)-C(1)-C(2)	0.3(6)
Co(1)-N(1)-C(1)-C(2)	-166.8(3)
N(1)-C(1)-C(2)-C(3)	-0.8(7)
C(1)-C(2)-C(3)-C(4)	1.0(7)
C(2)-C(3)-C(4)-C(5)	-0.8(7)
C(1)-N(1)-C(5)-C(4)	-0.1(6)
Co(1)-N(1)-C(5)-C(4)	167.3(3)
C(1)-N(1)-C(5)-C(6)	178.0(4)
Co(1)-N(1)-C(5)-C(6)	-14.6(5)
C(3)-C(4)-C(5)-N(1)	0.3(6)
C(3)-C(4)-C(5)-C(6)	-177.6(4)
N(1)-C(5)-C(6)-N(2)	16.9(5)
C(4)-C(5)-C(6)-N(2)	-165.0(4)
C(5)-C(6)-N(2)-C(7)	-126.9(3)
C(5)-C(6)-N(2)-C(8)	108.5(4)
C(5)-C(6)-N(2)-Co(1)	-11.3(4)
O(1)-Co(1)-N(2)-C(7)	-146.5(3)
O(1)#1-Co(1)-N(2)-C(7)	81.3(4)
N(1)#1-Co(1)-N(2)-C(7)	-57.7(3)
N(1)-Co(1)-N(2)-C(7)	123.1(3)
N(2)#1-Co(1)-N(2)-C(7)	16.1(2)
O(1)-Co(1)-N(2)-C(6)	93.8(3)
O(1)#1-Co(1)-N(2)-C(6)	-38.4(5)
N(1)#1-Co(1)-N(2)-C(6)	-177.4(2)
N(1)-Co(1)-N(2)-C(6)	3.4(2)
N(2)#1-Co(1)-N(2)-C(6)	-103.5(3)
O(1)-Co(1)-N(2)-C(8)	-28.4(2)
O(1)#1-Co(1)-N(2)-C(8)	-160.6(3)
N(1)#1-Co(1)-N(2)-C(8)	60.4(2)
N(1)-Co(1)-N(2)-C(8)	-118.8(2)
N(2)#1-Co(1)-N(2)-C(8)	134.2(3)
C(6)-N(2)-C(7)-C(7)#1	75.2(4)
C(8)-N(2)-C(7)-C(7)#1	-160.5(4)
Co(1)-N(2)-C(7)-C(7)#1	-45.9(4)
C(7)-N(2)-C(8)-C(9)	-178.5(3)
C(6)-N(2)-C(8)-C(9)	-54.5(4)
Co(1)-N(2)-C(8)-C(9)	68.8(3)
N(2)-C(8)-C(9)-C(10)	118.3(4)
N(2)-C(8)-C(9)-C(14)	-60.2(5)
C(14)-C(9)-C(10)-C(11)	0.7(6)
C(8)-C(9)-C(10)-C(11)	-177.8(4)
C(9)-C(10)-C(11)-C(12)	1.8(6)
C(9)-C(10)-C(11)-I(1)	177.6(3)
C(10)-C(11)-C(12)-C(13)	-1.5(6)
I(1)-C(11)-C(12)-C(13)	-177.3(3)
C(11)-C(12)-C(13)-C(14)	-1.5(6)
C(11)-C(12)-C(13)-I(2)	174.2(3)
C(12)-C(13)-C(14)-O(1)	-175.8(4)
I(2)-C(13)-C(14)-O(1)	8.4(5)

C(12)-C(13)-C(14)-C(9)	3.8(6)
I(2)-C(13)-C(14)-C(9)	-171.9(3)
C(10)-C(9)-C(14)-O(1)	176.2(4)
C(8)-C(9)-C(14)-O(1)	-5.2(6)
C(10)-C(9)-C(14)-C(13)	-3.4(6)
C(8)-C(9)-C(14)-C(13)	175.1(4)
C(13)-C(14)-O(1)-Co(1)	-132.7(3)
C(9)-C(14)-O(1)-Co(1)	47.7(5)
O(1)#1-Co(1)-O(1)-C(14)	139.2(3)
N(1)#1-Co(1)-O(1)-C(14)	-130.7(3)
N(1)-Co(1)-O(1)-C(14)	50.3(3)
N(2)#1-Co(1)-O(1)-C(14)	-90.3(4)
N(2)-Co(1)-O(1)-C(14)	-26.3(3)

Symmetry transformations used to generate equivalent atoms:
#1 -x+1,y,-z+1/2

Least-squares planes (x,y,z in crystal coordinates) and deviations from them
(* indicates atom used to define plane)

10.9112 (0.0152) x - 6.1256 (0.0142) y - 2.0561 (0.0377) z = 0.9207 (0.0149)

*	-0.0007 (0.0027)	N1
*	-0.0018 (0.0030)	C1
*	0.0044 (0.0032)	C2
*	-0.0046 (0.0032)	C3
*	0.0021 (0.0031)	C4
*	0.0005 (0.0028)	C5
	-0.0454 (0.0066)	C6
	0.4070 (0.0058)	Co1

Rms deviation of fitted atoms = 0.0029

9.5697 (0.0166) x - 2.8548 (0.0155) y + 12.9335 (0.0301) z = 7.3948 (0.0141)

Angle to previous plane (with approximate esd) = 44.30 (0.15)

*	-0.0115 (0.0029)	C9
*	-0.0071 (0.0030)	C10
*	0.0153 (0.0030)	C11
*	-0.0038 (0.0029)	C12
*	-0.0152 (0.0029)	C13
*	0.0223 (0.0028)	C14
	0.0918 (0.0056)	O1
	-0.0858 (0.0067)	C8
	-1.0609 (0.0070)	Co1

Rms deviation of fitted atoms = 0.0139

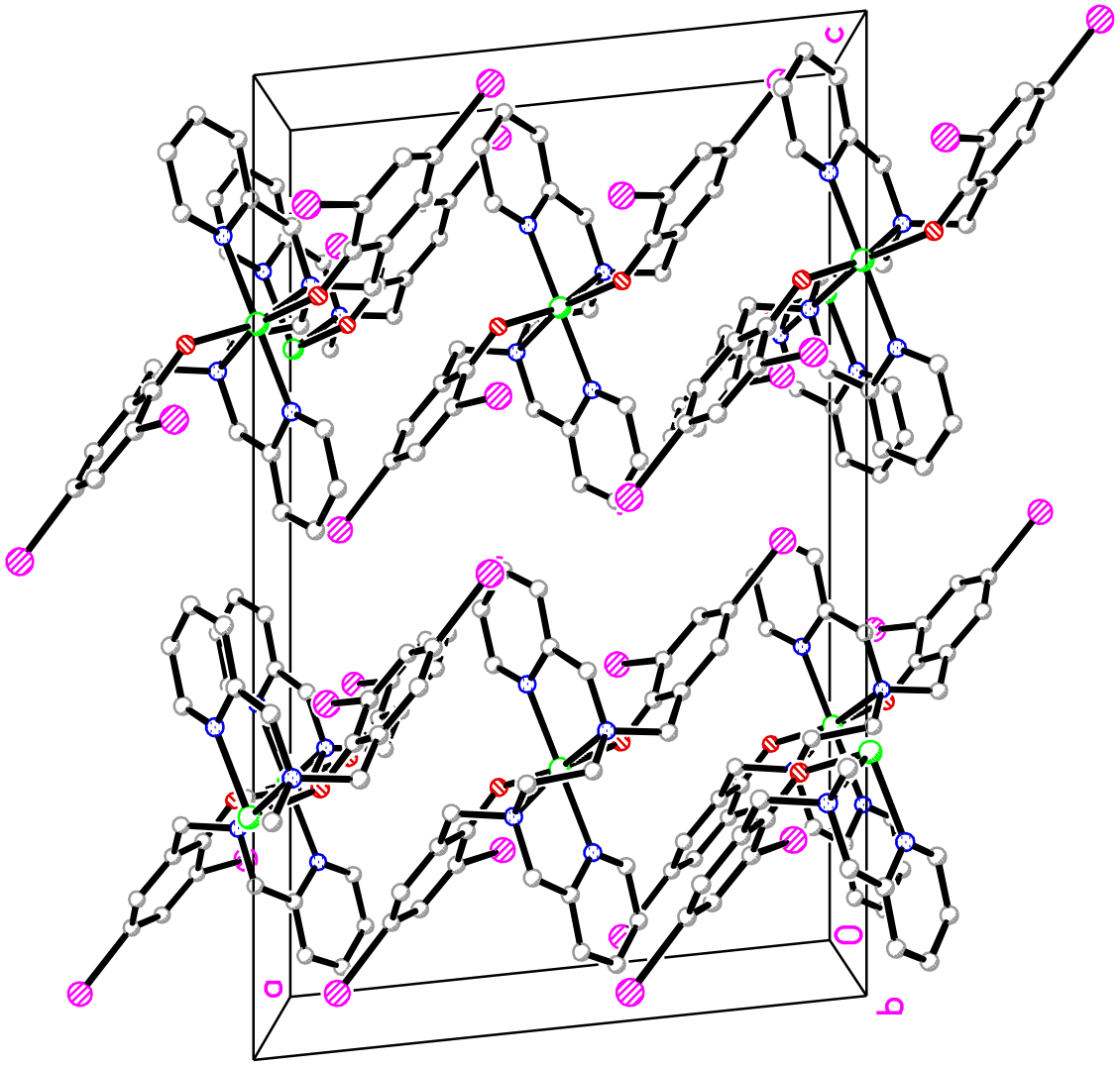

Figure A.3.4.2.1 Unit cell structure for complex **2**.

APPENDIX B

Supplementary Material for Chapter 4

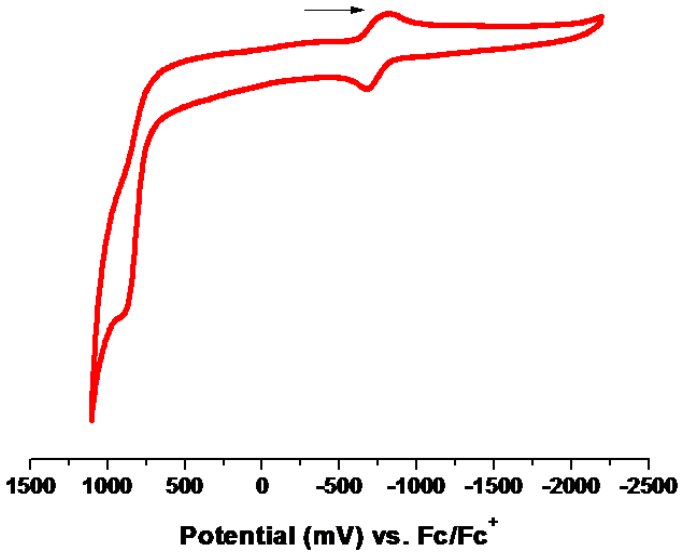

Figure B.4.2.1.1 Cyclic voltammograms of complex **1** in DMF with concentration [C] = 9.0 x 10^{-4} M. $TBAPF_6$ was used as supporting electrolyte. The redox potential for Co(III)/(II) couple is measured *vs.* Ag/AgCl and plotted *vs*. Fc/Fc^+ at room temperature. Potential parameters for the cobalt processes are: E_{pc} = -826 mV; E_{pa} = -679 mV; $E_{½}$ = -753 mV; ΔE_p = 147 mV; *vs.* Fc/Fc^+.

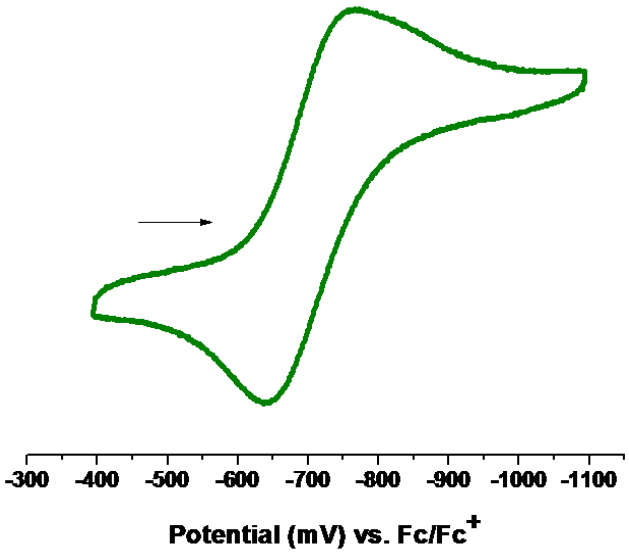

Figure B.4.2.1.2 Cyclic voltammogram of complex **1** in DMF with concentration [C] = 9.0 x 10^{-4} M. $TBAPF_6$ was used as supporting electrolyte. The redox potential for Co(III)/(II) couple is measured *vs.* Ag/AgCl and plotted *vs*. Fc/Fc^+ at room temperature and the data are shown in Table 1 in the text.

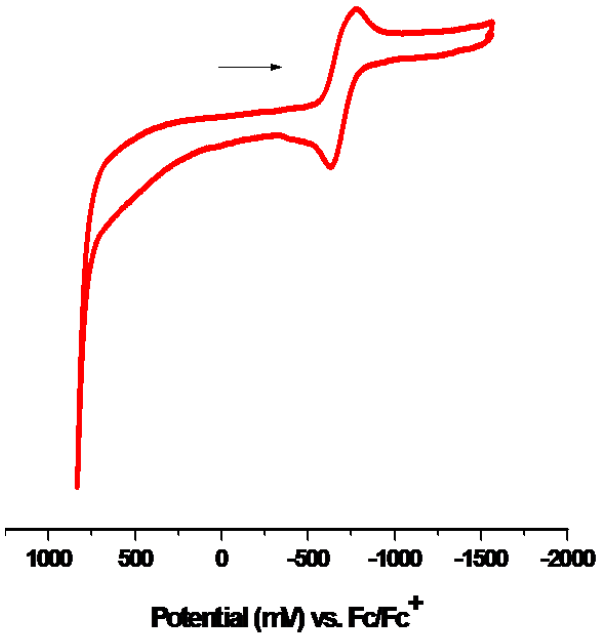

Figure B.4.2.1.3 Cyclic voltammogram of complex **1** in DMF/H_2O 90:10% v/v. solvent system with concentration [C] = 0.9 x 10^{-3} M. $TBAPF_6$ was used as supporting electrolyte. The redox potential for Co(III)/(II) couple is measured *versus* Ag/AgCl and plotted *vs*. Fc/Fc^+ at room temperature. Potential parameters for the cobalt processes are: E_{pc} = -777 mV; E_{pa} = -629 mV; $E_{½}$ = -703 mV; ΔE_p = 148 mV; *vs*. Fc/Fc^+.

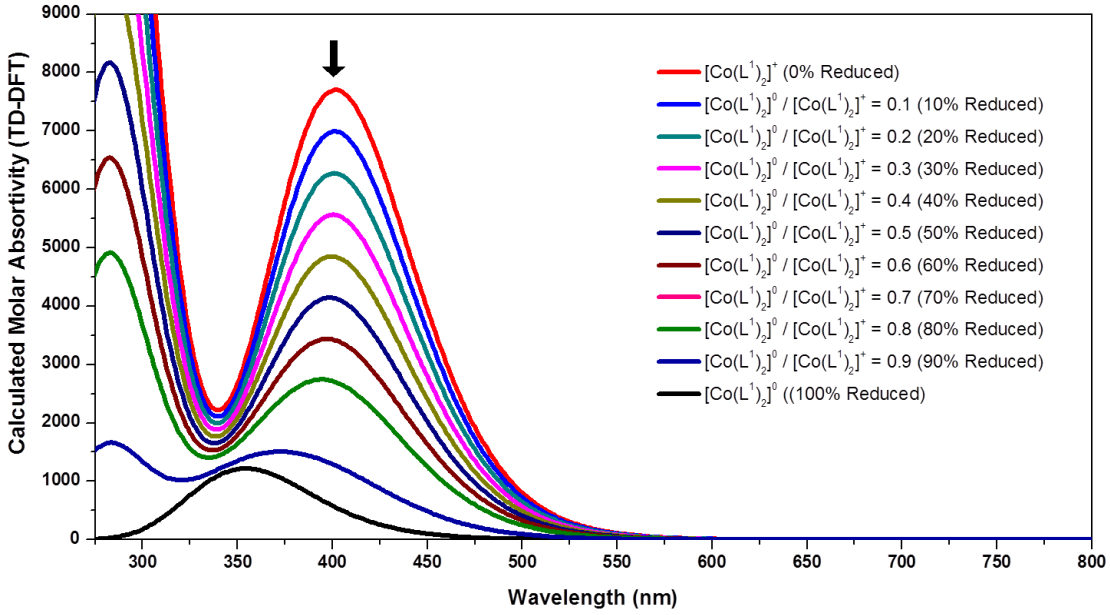

Figure B.4.2.3 TD-DFT calculated spectroelectrochemistry.

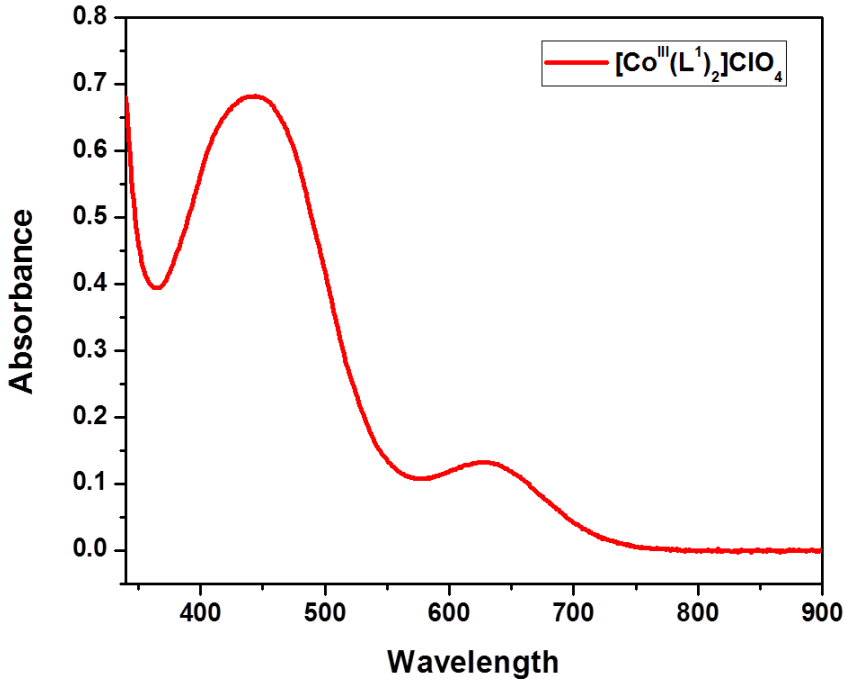

Figure B.4.2.4.1 UV-visible spectroscopy for complex **1** in DMF/H_2O (90:10% v/v.) with final concentration of 9.0 x 10^{-5} M. The presence of $p\pi_{phenolate} \rightarrow d\sigma^*_{cobalt(III)}$ charge transfer band at was observed at 440 nm.

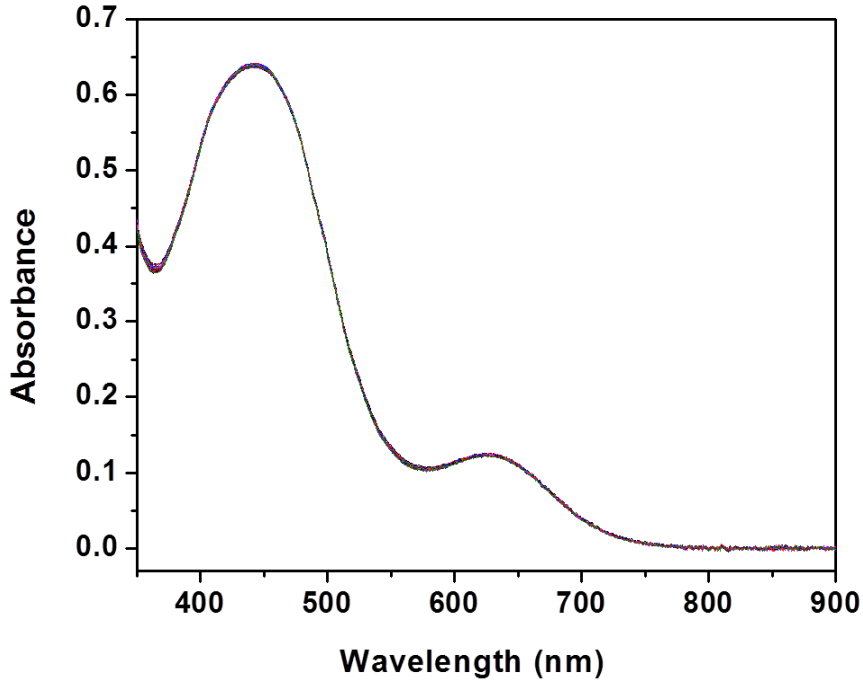

Figure B.4.2.4.2 Chemical stability of complex **1** in DMF/H_2O (90:10% v/v.). with final concentration of 9.0 x 10^{-5} M without ascorbic acid at pH 3. Each spectrum is recorded every 30 min over a time period of 24 h. No decrease of $p\pi_{phenolate} \rightarrow d\sigma^*_{cobalt(III)}$ charge transfer band at 440 nm was observed over time.

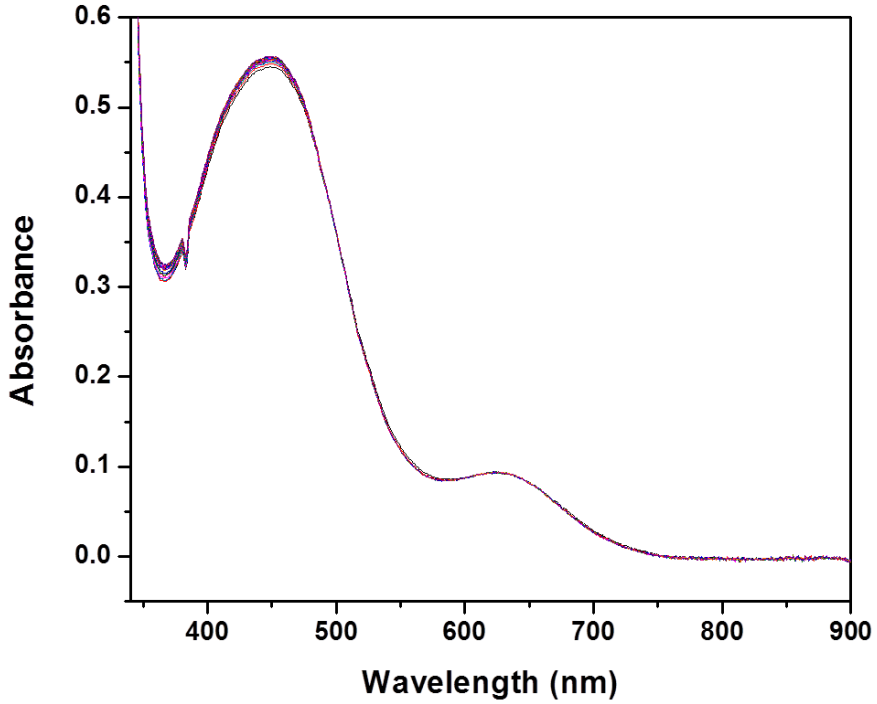

Figure B.4.2.4.3 Chemical stability of complex 1 in DMF/H_2O (90:10% v/v.) with final concentration of 9.0 x 10^{-5} M without ascorbic acid at pH 1.0 adjusted with nitric acid. Each spectrum is recorded every 30 min over a time period of 24 h. No decrease of $p\pi_{phenolate} \rightarrow d\sigma^*_{cobalt(III)}$ charge transfer band at 440 nm was observed over time.

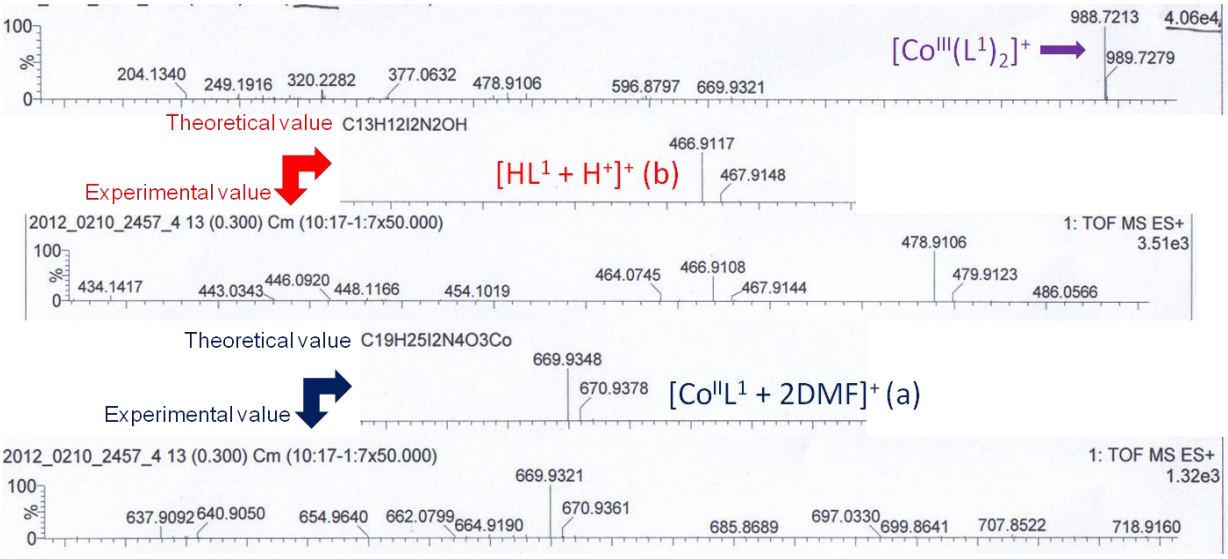

Figure 4.2.5.1 High resolution ESI^+ mass spectrometry results for complex 1 after the completion of the chemical reduction experiment. Theoretical and experimental data are given for species (a) and (b) as indicated, being in good agreement.

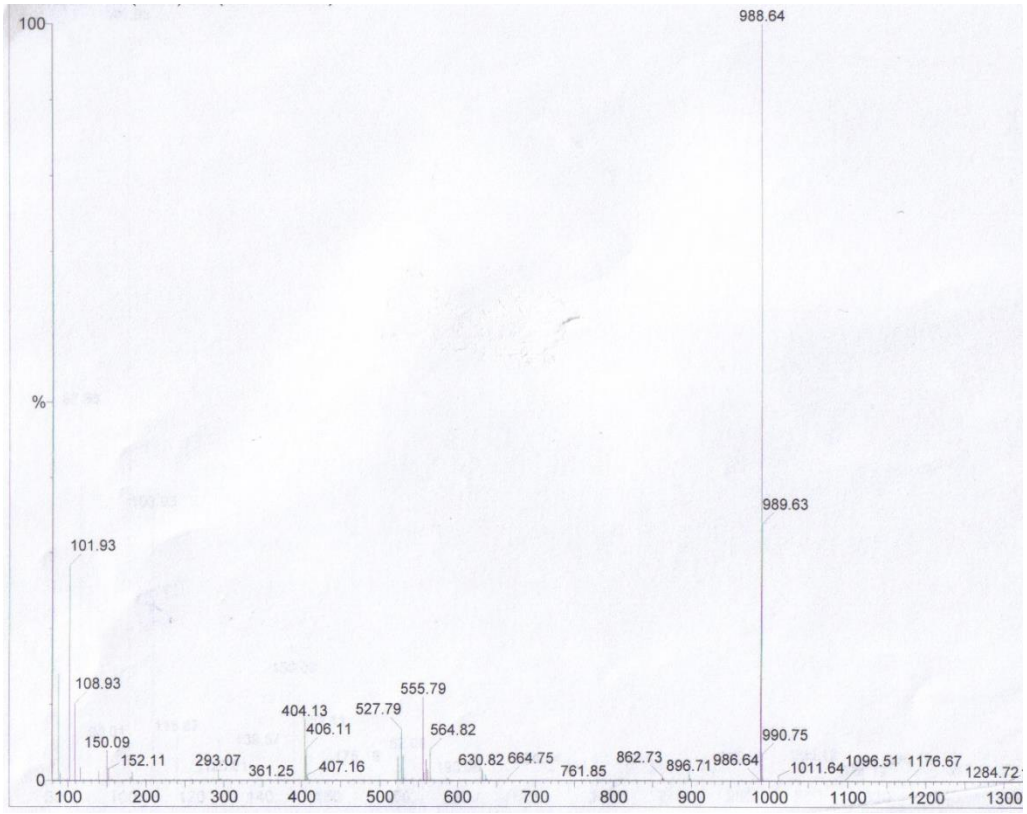

Figure 4.2.5.2 ESI^+-MS spectrum for the previously synthesized $[Co(L^1)_2]$ complex. The charge on cobalt is (II), therefore the compound is neutral. We expected to observe a peak for $[Co(L^1)_2 + H^+]^+$ species *m/z* = 989.64 at 100%; instead we found the 100% peak at *m/z* = 988.64 which corresponds with the $[Co(L^1)_2]^+$ species. Therefore, in the mass spectrometry instrument, oxidation of cobalt(II) has occurred.

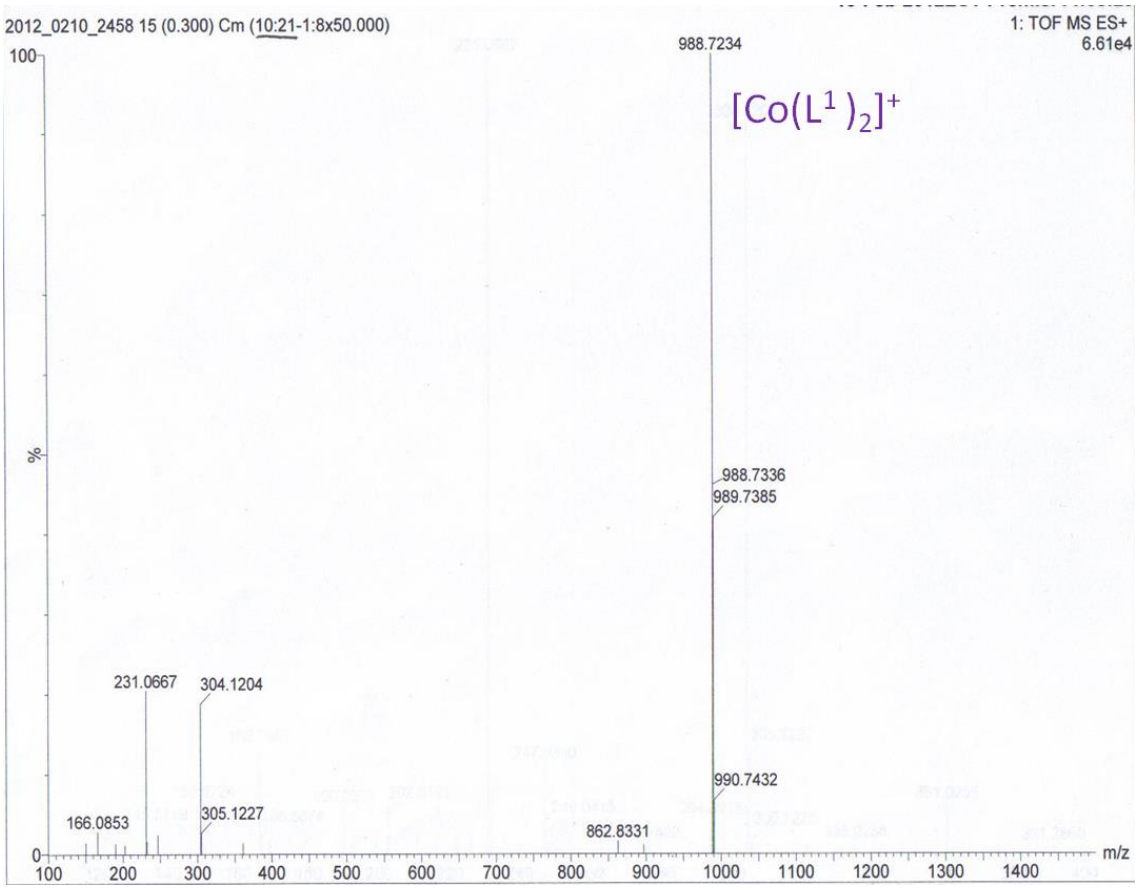

Figure 4.2.5.3 High resolution ESI^+ mass spectrometry results for 1, the control sample no ascorbic acid added. As shown from the spectrum, there is no indication of the molecular ions peaks related to species (a) and (b).

Table B.4.2.2 Cartesian Coordinates for $[Co(L^1)_2]^+$ and $[Co(L^1)_2]^0$ species.

$[Co(L^1)_2]^+$

H	4.50227200	2.43264400	-1.04177000
H	2.37303800	2.94403900	3.17284500
H	1.73950400	3.27808800	0.68982200
C	4.31970000	1.38768100	-0.82001600
H	2.22686100	2.76630400	-1.56259200
C	5.37016000	0.53746600	-0.47619700
C	2.06112400	1.91505500	3.04613000
H	2.89723200	1.21697100	4.90454300
C	0.97335300	2.51240500	0.83436500
H	0.04173700	3.00977900	1.11393600
C	1.88650900	1.74161200	-1.38562000
C	3.01852500	0.88625700	-0.89895300
C	2.35451400	0.95029600	4.00632700
C	1.35994300	1.54526300	1.89937500
H	-0.06040200	2.24785600	-0.89422800
H	1.50201900	1.34455000	-2.33020000
C	5.14361000	-0.81405300	-0.21025600
N	0.71973700	1.77421400	-0.44052500
H	5.95999600	-1.47475400	0.05006100
C	2.75034000	-0.47358200	-0.61156000
C	1.95041500	-0.36767500	3.78472500
C	3.83829900	-1.30035400	-0.27442900
N	0.95592200	0.26611200	1.69598100
H	-0.96489600	1.69333600	-2.42655300
H	2.16888100	-1.15259400	4.49632700
C	1.26098100	-0.67436000	2.61937400
O	-1.49721600	0.96137500	0.68274700
Co	-0.00001300	-0.00003600	0.00005500
O	1.49720100	-0.96145100	-0.68263000
C	-1.26114900	0.67432900	-2.61918200
H	-2.16912500	1.15257800	-4.49609500
C	-3.83829200	1.30037100	0.27451100
C	-1.95054000	0.36763500	-3.78455700
H	0.96457200	-1.69333800	2.42683700
N	-0.95594800	-0.26617500	-1.69587000
C	-2.75036400	0.47353800	0.61159500
H	-5.95997000	1.47485600	-0.05005500
C	-5.14361000	0.81410700	0.21022400
N	-0.71974900	-1.77430500	0.44057900
H	0.06034600	-2.24792200	0.89438400
C	-2.35444100	-0.95038000	-4.00626500
H	-1.50226300	-1.34480600	2.33019300
C	-1.35980800	-1.54536300	-1.89934800
C	-3.01859200	-0.88632500	0.89883400
H	-2.89711300	-1.21706400	-4.90450600
H	-0.04142300	-3.00970000	-1.11386700
C	-1.88664300	-1.74175900	1.38552100

C	-0.97314700	-2.51249700	-0.83435700
C	-2.06092800	-1.91517000	-3.04613500
C	-5.37020100	-0.53743800	0.47600000
C	-4.31977600	-1.38771200	0.81977700
H	-2.22704700	-2.76645800	1.56234900
H	-1.73918800	-3.27830700	-0.68990100
H	-2.37270700	-2.94418500	-3.17292200
H	-4.50238100	-2.43269400	1.04141200
I	-7.36804900	-1.31723700	0.35074800
I	-3.45939500	3.36611100	-0.13642800
I	7.36799900	1.31732000	-0.35114000
I	3.45946200	-3.36605300	0.13676500

$[Co(L^1)_2]^0$

H	-4.63187300	2.32272700	1.24551900
H	-2.90913600	3.27263400	-2.68486900
H	-2.02709200	3.40515100	-0.36372200
C	-4.45161500	1.29217400	0.95975300
H	-2.46288600	2.61116200	1.89131200
C	-5.50552500	0.47776400	0.54555500
C	-2.50410800	2.26916000	-2.74577400
H	-3.45038700	1.79235700	-4.62272900
C	-1.24908100	2.66137800	-0.57641200
H	-0.34650600	3.20813600	-0.86738900
C	-2.04435900	1.64697900	1.57329000
C	-3.15090400	0.78687400	1.02346900
C	-2.80639700	1.44038800	-3.82537700
C	-1.66934100	1.79257700	-1.73015000
H	-0.15331200	2.33557800	1.11873200
H	-1.61156900	1.16428200	2.45647400
C	-5.28229600	-0.85414400	0.19669800
N	-0.91354200	1.87067700	0.62668400
H	-6.09687700	-1.49334700	-0.11843800
C	-2.86851600	-0.56586900	0.65682100
C	-2.27423900	0.14841400	-3.85985000
C	-3.98055200	-1.34849900	0.25812600
N	-1.15720700	0.54231200	-1.76842800
H	1.04100300	1.26034700	2.78913500
H	-2.48904600	-0.52767500	-4.67774000
C	-1.46020100	-0.26331600	-2.80911400
O	1.63163500	1.04734800	-0.70120800
Co	0.00000100	0.00000900	0.00000200
O	-1.63163400	-1.04735000	0.70120200
C	1.46021500	0.26334800	2.80912200
H	2.48907600	0.52771300	4.67773800
C	3.98055500	1.34849200	-0.25813600
C	2.27425700	-0.14838100	3.85985500
H	-1.04098000	-1.26031200	-2.78913200
N	1.15720800	-0.54228500	1.76844400

C	2.86851600	0.56586300	-0.65682400
H	6.09688100	1.49333700	0.11842200
C	5.28229700	0.85413300	-0.19670500
N	0.91353000	-1.87066900	-0.62666100
H	0.15329300	-2.33556400	-1.11870300
C	2.80640400	-1.44036000	3.82538900
H	1.61156600	-1.16430700	-2.45646100
C	1.66933100	-1.79255600	1.73017200
C	3.15089800	-0.78688500	-1.02345600
H	3.45039600	-1.79232800	4.62274000
H	0.34647200	-3.20809900	0.86742800
C	2.04434900	-1.64699300	-1.57326700
C	1.24905600	-2.66136100	0.57644400
C	2.50410100	-2.26913700	2.74579500
C	5.50552200	-0.47777800	-0.54555200
C	4.45160700	-1.29219000	-0.95973600
H	2.46287300	-2.61118300	-1.89127200
H	2.02705500	-3.40515100	0.36376100
H	2.90911900	-3.27261600	2.68489500
H	4.63186100	-2.32274600	-1.24549300
I	7.50088700	-1.28117800	-0.44655700
I	3.63690100	3.40194800	0.27111800
I	-7.50089400	1.28115900	0.44656300
I	-3.63689000	-3.40194800	-0.27114900

APPENDIX C

Supplementary Material for Chapter 5

Crystal Structure Data for Complex 1

Table C.1. Atomic coordinates (x 10^4) and equivalent isotropic displacement parameters (A^2 x 10^3) for 1. U(eq) is defined as one third of the trace of the orthogonalized Uij tensor.

	x	y	z	U(eq)
Cl(1)	-3808(1)	1956(1)	-797(1)	60(1)
O(5)	-3988(3)	2455(2)	-1104(3)	88(2)
O(6)	-3053(3)	1759(2)	-874(3)	92(2)
O(7)	-4531(3)	1633(2)	-1184(3)	78(2)
O(8)	-3676(3)	1978(2)	-27(3)	95(2)
Cl(2)	4821(1)	1369(1)	1954(1)	71(1)
O(9)	5437(3)	1270(2)	2679(2)	111(2)
O(10)	3968(2)	1426(2)	1893(3)	95(2)
O(11)	5043(4)	1830(2)	1708(4)	150(3)
O(12)	4886(5)	1039(3)	1413(3)	151(3)
Ga(1)	-1336(1)	1575(1)	3077(1)	37(1)
N(1)	-875(3)	2331(2)	3328(2)	37(1)
C(1)	-311(3)	2558(2)	3093(3)	39(1)
C(2)	-51(3)	3057(2)	3272(3)	42(1)
C(3)	-416(4)	3330(2)	3676(3)	47(2)
C(4)	-989(4)	3099(2)	3928(3)	45(1)
C(5)	-1196(3)	2599(2)	3740(3)	38(1)
C(6)	-1807(4)	2314(2)	3997(3)	46(1)
N(2)	-2251(3)	1906(2)	3450(2)	39(1)
C(7)	-2577(3)	1519(2)	3836(3)	43(1)
C(8)	-1869(3)	1298(2)	4541(3)	37(1)
C(9)	-2066(4)	1216(2)	5162(3)	42(1)
C(10)	-1479(4)	984(2)	5800(3)	46(1)
C(11)	-703(4)	805(2)	5814(3)	41(1)
C(12)	-488(3)	901(2)	5216(3)	37(1)
C(13)	-1037(3)	1172(2)	4572(3)	37(1)
O(1)	-747(2)	1297(1)	4054(2)	40(1)
C(14)	-2987(4)	2105(2)	2788(3)	47(2)
C(15)	-2724(3)	2239(2)	2148(3)	42(1)
N(3)	-2280(3)	1793(2)	1992(2)	37(1)
C(16)	-2918(3)	1375(2)	1637(3)	42(1)
C(17)	-2711(3)	892(2)	2070(3)	37(1)
C(18)	-3236(4)	467(2)	1839(3)	42(1)
C(19)	-2975(4)	15(2)	2233(3)	52(2)
C(20)	-2194(4)	0(2)	2848(3)	46(1)
C(21)	-1716(3)	438(2)	3068(3)	38(1)
N(4)	-1969(3)	881(2)	2693(2)	39(1)
C(22)	-1814(3)	1926(2)	1495(3)	37(1)
C(23)	-1287(3)	1487(2)	1414(3)	35(1)
C(24)	-1453(3)	1282(2)	705(3)	37(1)
C(25)	-936(3)	899(2)	629(3)	38(1)
C(26)	-244(4)	712(2)	1241(3)	41(1)

C(27)	-91(3)	915(2)	1945(3)	36(1)
C(28)	-602(3)	1291(2)	2050(3)	37(1)
O(2)	-444(2)	1468(1)	2741(2)	40(1)
I(1)	-1787(1)	904(1)	6741(1)	63(1)
I(2)	710(1)	655(1)	5257(1)	47(1)
I(3)	-1232(1)	549(1)	-422(1)	49(1)
I(4)	940(1)	632(1)	2895(1)	47(1)
Ga(2)	2544(1)	2857(1)	3556(1)	35(1)
N(5)	2131(3)	2494(2)	4309(2)	37(1)
C(29)	1490(4)	2147(2)	4116(3)	44(1)
C(30)	1238(4)	1928(2)	4651(3)	47(2)
C(31)	1662(4)	2070(3)	5385(4)	53(2)
C(32)	2313(4)	2430(2)	5582(3)	50(2)
C(33)	2537(3)	2634(2)	5026(3)	38(1)
C(34)	3235(4)	3020(2)	5187(3)	45(1)
N(6)	3591(3)	3017(2)	4602(2)	41(1)
C(35)	3972(3)	3522(2)	4567(3)	45(2)
C(36)	3355(3)	3960(2)	4430(3)	41(1)
C(37)	3696(3)	4414(2)	4809(3)	41(1)
C(38)	3191(4)	4846(2)	4700(3)	41(1)
C(39)	2338(3)	4841(2)	4192(3)	35(1)
C(40)	2007(3)	4391(2)	3831(3)	32(1)
C(41)	2474(3)	3938(2)	3938(3)	34(1)
O(3)	2083(2)	3509(1)	3596(2)	36(1)
C(42)	4273(4)	2616(2)	4750(3)	50(2)
C(43)	3894(4)	2121(2)	4378(3)	46(2)
N(7)	3337(3)	2210(2)	3570(3)	40(1)
C(44)	3904(4)	2315(2)	3156(3)	47(2)
C(45)	3674(4)	2811(2)	2721(3)	43(1)
C(46)	4046(4)	2935(3)	2223(3)	52(2)
C(47)	3796(4)	3386(3)	1834(3)	57(2)
C(48)	3184(4)	3699(2)	1933(3)	51(2)
C(49)	2846(4)	3534(2)	2430(3)	47(2)
N(8)	3087(3)	3113(2)	2832(2)	39(1)
C(50)	2775(3)	1760(2)	3239(3)	40(1)
C(51)	2123(3)	1849(2)	2430(3)	37(1)
C(52)	2100(3)	1502(2)	1881(3)	40(1)
C(53)	1453(4)	1528(2)	1172(3)	39(1)
C(54)	835(3)	1903(2)	999(3)	37(1)
C(55)	885(3)	2264(2)	1539(3)	34(1)
C(56)	1534(3)	2253(2)	2263(3)	37(1)
O(4)	1549(2)	2602(1)	2761(2)	36(1)
I(5)	3746(1)	5520(1)	5285(1)	50(1)
I(6)	708(1)	4391(1)	3049(1)	37(1)
I(7)	1468(1)	1007(1)	360(1)	51(1)
I(8)	-28(1)	2857(1)	1252(1)	39(1)

Table C.2. Bond lengths [A] and angles [deg] for **1**

Cl(1)-O(5)	1.419(5)
Cl(1)-O(8)	1.422(6)
Cl(1)-O(7)	1.425(5)
Cl(1)-O(6)	1.432(5)
Cl(2)-O(12)	1.3984(10)
Cl(2)-O(10)	1.3994(10)
Cl(2)-O(9)	1.3997(10)
Cl(2)-O(11)	1.4019(10)
Ga(1)-O(2)	1.880(3)
Ga(1)-O(1)	1.900(3)
Ga(1)-N(4)	2.091(5)
Ga(1)-N(1)	2.113(5)
Ga(1)-N(2)	2.127(4)
Ga(1)-N(3)	2.149(4)
N(1)-C(5)	1.329(6)
N(1)-C(1)	1.344(6)
C(1)-C(2)	1.380(8)
C(2)-C(3)	1.373(7)
C(3)-C(4)	1.380(8)
C(4)-C(5)	1.368(8)
C(5)-C(6)	1.508(8)
C(6)-N(2)	1.484(7)
N(2)-C(14)	1.480(6)
N(2)-C(7)	1.489(6)
C(7)-C(8)	1.525(7)
C(8)-C(9)	1.387(7)
C(8)-C(13)	1.415(7)
C(9)-C(10)	1.380(7)
C(10)-C(11)	1.377(8)
C(10)-I(1)	2.097(6)
C(11)-C(12)	1.370(7)
C(12)-C(13)	1.414(7)
C(12)-I(2)	2.086(5)
C(13)-O(1)	1.321(6)
C(14)-C(15)	1.515(7)
C(15)-N(3)	1.482(6)
N(3)-C(16)	1.495(7)
N(3)-C(22)	1.505(6)
C(16)-C(17)	1.483(7)
C(17)-N(4)	1.348(6)
C(17)-C(18)	1.382(7)
C(18)-C(19)	1.382(8)
C(19)-C(20)	1.380(8)
C(20)-C(21)	1.368(8)
C(21)-N(4)	1.347(7)
C(22)-C(23)	1.498(7)
C(23)-C(24)	1.396(7)
C(23)-C(28)	1.409(7)
C(24)-C(25)	1.375(7)
C(25)-C(26)	1.380(7)
C(25)-I(3)	2.107(5)
C(26)-C(27)	1.391(7)
C(27)-C(28)	1.374(7)
C(27)-I(4)	2.100(5)
C(28)-O(2)	1.342(6)
Ga(2)-O(4)	1.890(3)
Ga(2)-O(3)	1.893(3)
Ga(2)-N(8)	2.066(4)
Ga(2)-N(5)	2.081(4)
Ga(2)-N(6)	2.134(4)

Ga(2)-N(7)	2.153(4)
N(5)-C(33)	1.334(6)
N(5)-C(29)	1.345(7)
C(29)-C(30)	1.390(8)
C(30)-C(31)	1.366(8)
C(31)-C(32)	1.380(8)
C(32)-C(33)	1.384(8)
C(33)-C(34)	1.486(8)
C(34)-N(6)	1.478(7)
N(6)-C(35)	1.486(7)
N(6)-C(42)	1.496(7)
C(35)-C(36)	1.498(7)
C(36)-C(37)	1.398(7)
C(36)-C(41)	1.410(7)
C(37)-C(38)	1.380(8)
C(38)-C(39)	1.381(7)
C(38)-I(5)	2.108(5)
C(39)-C(40)	1.372(7)
C(40)-C(41)	1.393(7)
C(40)-I(6)	2.106(5)
C(41)-O(3)	1.337(6)
C(42)-C(43)	1.500(8)
C(43)-N(7)	1.491(7)
N(7)-C(50)	1.487(7)
N(7)-C(44)	1.496(7)
C(44)-C(45)	1.514(8)
C(45)-N(8)	1.349(7)
C(45)-C(46)	1.381(8)
C(46)-C(47)	1.377(9)
C(47)-C(48)	1.389(8)
C(48)-C(49)	1.368(8)
C(49)-N(8)	1.320(7)
C(50)-C(51)	1.534(7)
C(51)-C(52)	1.388(7)
C(51)-C(56)	1.399(7)
C(52)-C(53)	1.376(7)
C(53)-C(54)	1.371(7)
C(53)-I(7)	2.094(5)
C(54)-C(55)	1.389(7)
C(55)-C(56)	1.394(7)
C(55)-I(8)	2.100(5)
C(56)-O(4)	1.324(6)

O(5)-Cl(1)-O(8)	108.7(4)
O(5)-Cl(1)-O(7)	109.4(3)
O(8)-Cl(1)-O(7)	108.7(3)
O(5)-Cl(1)-O(6)	109.7(3)
O(8)-Cl(1)-O(6)	110.5(3)
O(7)-Cl(1)-O(6)	109.7(3)
O(12)-Cl(2)-O(10)	112.7(4)
O(12)-Cl(2)-O(9)	113.0(4)
O(10)-Cl(2)-O(9)	115.4(4)
O(12)-Cl(2)-O(11)	99.6(5)
O(10)-Cl(2)-O(11)	106.4(4)
O(9)-Cl(2)-O(11)	108.1(4)
O(2)-Ga(1)-O(1)	96.65(15)
O(2)-Ga(1)-N(4)	96.31(16)
O(1)-Ga(1)-N(4)	90.62(16)
O(2)-Ga(1)-N(1)	87.07(16)
O(1)-Ga(1)-N(1)	97.62(16)
N(4)-Ga(1)-N(1)	170.69(16)
O(2)-Ga(1)-N(2)	164.47(17)
O(1)-Ga(1)-N(2)	88.83(15)

N(4)-Ga(1)-N(2)	98.15(17)
N(1)-Ga(1)-N(2)	77.78(17)
O(2)-Ga(1)-N(3)	94.62(15)
O(1)-Ga(1)-N(3)	165.44(16)
N(4)-Ga(1)-N(3)	78.99(17)
N(1)-Ga(1)-N(3)	92.13(16)
N(2)-Ga(1)-N(3)	82.66(16)
C(5)-N(1)-C(1)	118.5(5)
C(5)-N(1)-Ga(1)	115.8(4)
C(1)-N(1)-Ga(1)	125.6(4)
N(1)-C(1)-C(2)	122.1(5)
C(3)-C(2)-C(1)	117.9(5)
C(2)-C(3)-C(4)	120.5(6)
C(5)-C(4)-C(3)	117.7(5)
N(1)-C(5)-C(4)	123.2(5)
N(1)-C(5)-C(6)	115.4(5)
C(4)-C(5)-C(6)	121.4(5)
N(2)-C(6)-C(5)	109.7(5)
C(6)-N(2)-C(14)	112.0(4)
C(6)-N(2)-C(7)	108.3(4)
C(14)-N(2)-C(7)	109.2(4)
C(6)-N(2)-Ga(1)	108.1(3)
C(14)-N(2)-Ga(1)	108.6(3)
C(7)-N(2)-Ga(1)	110.7(3)
N(2)-C(7)-C(8)	113.4(4)
C(9)-C(8)-C(13)	120.0(5)
C(9)-C(8)-C(7)	117.8(5)
C(13)-C(8)-C(7)	122.2(5)
C(10)-C(9)-C(8)	121.0(5)
C(11)-C(10)-C(9)	120.1(5)
C(11)-C(10)-I(1)	120.6(4)
C(9)-C(10)-I(1)	119.3(4)
C(12)-C(11)-C(10)	119.2(5)
C(11)-C(12)-C(13)	122.7(5)
C(11)-C(12)-I(2)	119.2(4)
C(13)-C(12)-I(2)	118.1(4)
O(1)-C(13)-C(12)	119.1(5)
O(1)-C(13)-C(8)	124.6(5)
C(12)-C(13)-C(8)	116.3(5)
C(13)-O(1)-Ga(1)	130.5(3)
N(2)-C(14)-C(15)	112.1(4)
N(3)-C(15)-C(14)	108.7(4)
C(15)-N(3)-C(16)	110.2(4)
C(15)-N(3)-C(22)	112.4(4)
C(16)-N(3)-C(22)	109.7(4)
C(15)-N(3)-Ga(1)	104.2(3)
C(16)-N(3)-Ga(1)	111.8(3)
C(22)-N(3)-Ga(1)	108.6(3)
C(17)-C(16)-N(3)	113.6(4)
N(4)-C(17)-C(18)	121.1(5)
N(4)-C(17)-C(16)	116.9(5)
C(18)-C(17)-C(16)	122.0(5)
C(19)-C(18)-C(17)	119.3(5)
C(20)-C(19)-C(18)	119.2(6)
C(21)-C(20)-C(19)	118.9(6)
N(4)-C(21)-C(20)	122.4(5)
C(17)-N(4)-C(21)	118.9(5)
C(17)-N(4)-Ga(1)	117.3(4)
C(21)-N(4)-Ga(1)	123.5(4)
C(23)-C(22)-N(3)	111.7(4)
C(24)-C(23)-C(28)	119.7(5)
C(24)-C(23)-C(22)	120.3(5)
C(28)-C(23)-C(22)	120.0(5)

C(25)-C(24)-C(23)	119.9(5)
C(24)-C(25)-C(26)	121.4(5)
C(24)-C(25)-I(3)	120.4(4)
C(26)-C(25)-I(3)	118.1(4)
C(25)-C(26)-C(27)	118.1(5)
C(28)-C(27)-C(26)	122.5(5)
C(28)-C(27)-I(4)	118.0(4)
C(26)-C(27)-I(4)	119.5(4)
O(2)-C(28)-C(27)	120.6(5)
O(2)-C(28)-C(23)	121.1(5)
C(27)-C(28)-C(23)	118.3(5)
C(28)-O(2)-Ga(1)	122.0(3)
O(4)-Ga(2)-O(3)	96.24(14)
O(4)-Ga(2)-N(8)	92.72(16)
O(3)-Ga(2)-N(8)	91.87(16)
O(4)-Ga(2)-N(5)	88.66(16)
O(3)-Ga(2)-N(5)	97.40(16)
N(8)-Ga(2)-N(5)	170.43(17)
O(4)-Ga(2)-N(6)	166.78(17)
O(3)-Ga(2)-N(6)	88.86(15)
N(8)-Ga(2)-N(6)	99.32(18)
N(5)-Ga(2)-N(6)	78.57(17)
O(4)-Ga(2)-N(7)	94.27(16)
O(3)-Ga(2)-N(7)	166.99(16)
N(8)-Ga(2)-N(7)	79.98(18)
N(5)-Ga(2)-N(7)	90.47(17)
N(6)-Ga(2)-N(7)	82.55(17)
C(33)-N(5)-C(29)	119.9(5)
C(33)-N(5)-Ga(2)	115.5(4)
C(29)-N(5)-Ga(2)	124.7(4)
N(5)-C(29)-C(30)	121.3(5)
C(31)-C(30)-C(29)	118.6(6)
C(30)-C(31)-C(32)	120.2(6)
C(31)-C(32)-C(33)	118.8(6)
N(5)-C(33)-C(32)	121.4(5)
N(5)-C(33)-C(34)	116.1(5)
C(32)-C(33)-C(34)	122.5(5)
N(6)-C(34)-C(33)	111.2(4)
C(34)-N(6)-C(35)	110.1(4)
C(34)-N(6)-C(42)	111.7(4)
C(35)-N(6)-C(42)	108.9(4)
C(34)-N(6)-Ga(2)	107.3(3)
C(35)-N(6)-Ga(2)	109.9(3)
C(42)-N(6)-Ga(2)	108.9(3)
N(6)-C(35)-C(36)	114.2(4)
C(37)-C(36)-C(41)	119.4(5)
C(37)-C(36)-C(35)	116.8(5)
C(41)-C(36)-C(35)	123.8(5)
C(38)-C(37)-C(36)	121.4(5)
C(39)-C(38)-C(37)	120.2(5)
C(39)-C(38)-I(5)	120.3(4)
C(37)-C(38)-I(5)	119.5(4)
C(38)-C(39)-C(40)	117.9(5)
C(39)-C(40)-C(41)	124.5(5)
C(39)-C(40)-I(6)	117.4(4)
C(41)-C(40)-I(6)	118.0(4)
O(3)-C(41)-C(40)	120.4(4)
O(3)-C(41)-C(36)	123.1(5)
C(40)-C(41)-C(36)	116.4(5)
C(41)-O(3)-Ga(2)	130.7(3)
N(6)-C(42)-C(43)	111.6(4)
N(7)-C(43)-C(42)	109.9(5)
C(50)-N(7)-C(43)	110.8(4)

C(50)-N(7)-C(44)	110.3(4)
C(43)-N(7)-C(44)	109.0(4)
C(50)-N(7)-Ga(2)	109.6(3)
C(43)-N(7)-Ga(2)	105.2(3)
C(44)-N(7)-Ga(2)	111.8(3)
N(7)-C(44)-C(45)	112.4(5)
N(8)-C(45)-C(46)	122.5(6)
N(8)-C(45)-C(44)	117.2(5)
C(46)-C(45)-C(44)	120.3(5)
C(47)-C(46)-C(45)	117.5(6)
C(46)-C(47)-C(48)	120.9(6)
C(49)-C(48)-C(47)	116.7(6)
N(8)-C(49)-C(48)	124.4(6)
C(49)-N(8)-C(45)	118.0(5)
C(49)-N(8)-Ga(2)	124.0(4)
C(45)-N(8)-Ga(2)	117.8(4)
N(7)-C(50)-C(51)	113.2(4)
C(52)-C(51)-C(56)	121.2(5)
C(52)-C(51)-C(50)	118.4(5)
C(56)-C(51)-C(50)	120.3(5)
C(53)-C(52)-C(51)	120.2(5)
C(52)-C(53)-C(54)	120.1(5)
C(52)-C(53)-I(7)	118.6(4)
C(54)-C(53)-I(7)	121.3(4)
C(53)-C(54)-C(55)	119.4(5)
C(54)-C(55)-C(56)	122.2(5)
C(54)-C(55)-I(8)	119.1(4)
C(56)-C(55)-I(8)	118.6(4)
O(4)-C(56)-C(55)	120.1(5)
O(4)-C(56)-C(51)	123.3(5)
C(55)-C(56)-C(51)	116.6(5)
C(56)-O(4)-Ga(2)	126.5(3)

Symmetry transformations used to generate equivalent atoms.

Table C.3. Anisotropic displacement parameters (A^2 x 10^3) for **1**. The anisotropic displacement factor exponent takes the form: -2 pi^2 [h^2 a*^2 U11 + ... + 2 h k a* b* U12]

	U11	U22	U33	U23	U13	U12
Cl(1)	28(1)	72(1)	73(1)	38(1)	12(1)	8(1)
O(5)	54(3)	78(4)	137(5)	59(3)	42(3)	19(3)
O(6)	42(3)	81(4)	152(5)	47(4)	38(3)	15(3)
O(7)	41(3)	103(4)	82(3)	26(3)	17(2)	3(3)
O(8)	44(3)	140(5)	78(4)	4(3)	0(3)	2(3)
Cl(2)	33(1)	119(2)	50(1)	-16(1)	6(1)	11(1)
O(9)	83(4)	142(6)	63(3)	31(3)	-19(3)	-42(4)
O(10)	50(3)	147(5)	100(4)	-17(4)	43(3)	-2(3)
O(11)	56(4)	244(10)	113(5)	69(6)	-6(4)	-4(5)
O(12)	127(6)	194(8)	130(6)	-51(5)	50(5)	57(6)
Ga(1)	28(1)	41(1)	39(1)	7(1)	11(1)	6(1)
N(1)	30(2)	41(3)	37(3)	7(2)	10(2)	8(2)
C(1)	34(3)	44(4)	38(3)	5(3)	15(3)	6(3)
C(2)	35(3)	44(4)	47(3)	12(3)	15(3)	2(3)
C(3)	52(4)	38(3)	56(4)	-1(3)	27(3)	3(3)

C(4)	50(4)	49(4)	41(3)	4(3)	23(3)	6(3)
C(5)	36(3)	43(4)	35(3)	11(3)	14(3)	8(3)
C(6)	45(3)	48(4)	49(4)	11(3)	23(3)	9(3)
N(2)	30(2)	45(3)	42(3)	15(2)	16(2)	8(2)
C(7)	32(3)	50(4)	47(3)	14(3)	17(3)	8(3)
C(8)	28(3)	44(3)	36(3)	3(2)	10(2)	2(2)
C(9)	39(3)	43(3)	42(3)	8(3)	14(3)	-1(3)
C(10)	43(3)	47(4)	48(4)	5(3)	18(3)	0(3)
C(11)	38(3)	36(3)	40(3)	7(2)	7(3)	-2(3)
C(12)	31(3)	36(3)	41(3)	4(2)	11(2)	1(2)
C(13)	31(3)	45(3)	36(3)	2(2)	14(2)	-3(3)
O(1)	24(2)	48(2)	42(2)	8(2)	7(2)	7(2)
C(14)	39(3)	61(4)	44(3)	17(3)	18(3)	14(3)
C(15)	33(3)	44(3)	48(3)	5(3)	16(3)	14(3)
N(3)	30(2)	38(3)	42(3)	11(2)	13(2)	5(2)
C(16)	24(3)	50(4)	45(3)	14(3)	5(2)	4(3)
C(17)	33(3)	44(3)	38(3)	3(3)	17(3)	6(3)
C(18)	35(3)	45(4)	44(3)	2(3)	13(3)	3(3)
C(19)	52(4)	49(4)	53(4)	6(3)	19(3)	1(3)
C(20)	43(3)	48(4)	43(3)	5(3)	13(3)	16(3)
C(21)	31(3)	46(4)	34(3)	1(3)	9(2)	4(3)
N(4)	30(2)	43(3)	39(3)	7(2)	9(2)	6(2)
C(22)	32(3)	38(3)	38(3)	10(2)	11(2)	2(2)
C(23)	29(3)	32(3)	46(3)	6(2)	17(3)	2(2)
C(24)	30(3)	32(3)	48(3)	3(3)	15(3)	-1(2)
C(25)	36(3)	39(3)	39(3)	-5(2)	15(3)	-7(3)
C(26)	39(3)	33(3)	58(4)	2(3)	26(3)	1(3)
C(27)	26(3)	32(3)	51(3)	4(3)	15(3)	-3(2)
C(28)	33(3)	38(3)	45(3)	3(3)	20(3)	-1(3)
O(2)	28(2)	46(2)	43(2)	4(2)	13(2)	5(2)
I(1)	57(1)	85(1)	51(1)	20(1)	25(1)	14(1)
I(2)	34(1)	49(1)	52(1)	12(1)	10(1)	7(1)
I(3)	55(1)	41(1)	55(1)	-3(1)	26(1)	-2(1)
I(4)	32(1)	44(1)	59(1)	9(1)	12(1)	7(1)
Ga(2)	28(1)	36(1)	38(1)	-4(1)	9(1)	2(1)
N(5)	27(2)	37(3)	40(3)	0(2)	8(2)	4(2)
C(29)	35(3)	45(4)	47(3)	3(3)	9(3)	11(3)
C(30)	36(3)	47(4)	59(4)	5(3)	18(3)	2(3)
C(31)	45(4)	64(4)	58(4)	7(3)	30(3)	9(3)
C(32)	49(4)	48(4)	46(4)	0(3)	12(3)	15(3)
C(33)	39(3)	39(3)	33(3)	0(2)	11(3)	14(3)
C(34)	44(3)	49(4)	34(3)	-6(3)	6(3)	5(3)
N(6)	31(2)	36(3)	47(3)	-7(2)	4(2)	3(2)
C(35)	23(3)	56(4)	47(3)	-10(3)	5(3)	6(3)
C(36)	32(3)	47(4)	42(3)	-1(3)	14(3)	5(3)
C(37)	29(3)	47(4)	43(3)	-12(3)	11(2)	-7(3)
C(38)	38(3)	45(4)	43(3)	-10(3)	18(3)	-11(3)
C(39)	36(3)	31(3)	42(3)	2(2)	18(3)	-2(2)
C(40)	24(3)	41(3)	32(3)	-3(2)	11(2)	-1(2)
C(41)	23(3)	43(3)	33(3)	-6(2)	9(2)	-7(2)
O(3)	28(2)	38(2)	38(2)	-7(2)	8(2)	0(2)
C(42)	36(3)	46(4)	50(4)	-11(3)	-2(3)	12(3)
C(43)	35(3)	49(4)	47(3)	-2(3)	7(3)	11(3)
N(7)	28(2)	36(3)	51(3)	-5(2)	11(2)	4(2)
C(44)	33(3)	45(4)	62(4)	-11(3)	18(3)	-1(3)
C(45)	36(3)	41(3)	47(3)	-9(3)	13(3)	-3(3)
C(46)	39(3)	62(4)	52(4)	-9(3)	17(3)	2(3)
C(47)	57(4)	68(5)	48(4)	1(3)	22(3)	-8(4)
C(48)	52(4)	53(4)	47(4)	-1(3)	18(3)	8(3)
C(49)	45(3)	51(4)	47(3)	-2(3)	22(3)	5(3)
N(8)	32(2)	38(3)	46(3)	-2(2)	13(2)	2(2)
C(50)	31(3)	29(3)	54(3)	0(3)	11(3)	7(2)
C(51)	32(3)	38(3)	42(3)	-7(3)	16(3)	-9(3)

C(52)	35(3)	39(3)	47(3)	-3(3)	17(3)	-3(3)
C(53)	44(3)	34(3)	46(3)	-3(3)	26(3)	-7(3)
C(54)	41(3)	32(3)	40(3)	-1(2)	19(3)	1(3)
C(55)	29(3)	34(3)	37(3)	2(2)	10(2)	-5(2)
C(56)	32(3)	40(3)	42(3)	-5(3)	19(3)	-6(3)
O(4)	29(2)	36(2)	37(2)	-8(2)	7(2)	1(2)
I(5)	45(1)	44(1)	55(1)	-12(1)	15(1)	-9(1)
I(6)	31(1)	38(1)	39(1)	-1(1)	11(1)	1(1)
I(7)	58(1)	47(1)	56(1)	-16(1)	30(1)	-5(1)
I(8)	38(1)	44(1)	35(1)	1(1)	13(1)	5(1)

Table C.4. Hydrogen coordinates (x 10^4) and isotropic displacement parameters (A^2 x 10^3) for **1**.

	x	y	z	U(eq)
H(1)	-84	2369	2794	46
H(2)	368	3208	3120	51
H(3)	-273	3679	3784	57
H(4)	-1231	3281	4221	54
H(6A)	-1480	2163	4498	55
H(6B)	-2242	2553	4040	55
H(7A)	-2853	1237	3481	51
H(7B)	-3027	1677	3975	51
H(9)	-2614	1320	5147	50
H(11)	-322	617	6234	49
H(14A)	-3221	2413	2936	57
H(14B)	-3453	1846	2614	57
H(15A)	-3243	2327	1694	50
H(15B)	-2330	2536	2287	50
H(16A)	-3501	1491	1582	50
H(16B)	-2940	1309	1127	50
H(18)	-3772	484	1414	51
H(19)	-3328	-280	2082	62
H(20)	-1991	-310	3114	55
H(21)	-1187	429	3500	46
H(22A)	-2242	2026	993	44
H(22B)	-1427	2221	1712	44
H(24)	-1924	1407	276	45
H(26)	116	451	1183	50
H(29)	1204	2049	3604	53
H(30)	781	1686	4509	57
H(31)	1508	1920	5761	63
H(32)	2601	2536	6090	60
H(34A)	3000	3363	5210	54
H(34B)	3705	2948	5682	54
H(35A)	4187	3515	4160	54
H(35B)	4476	3581	5046	54
H(37)	4287	4427	5148	49
H(39)	1991	5139	4095	42
H(42A)	4572	2563	5299	60
H(42B)	4708	2735	4561	60
H(43A)	4365	1880	4423	56
H(43B)	3543	1967	4631	56
H(44A)	3849	2031	2803	56

H(44B)	4516	2329	3520	56
H(46)	4459	2717	2153	62
H(47)	4046	3485	1493	69
H(48)	3009	4013	1670	61
H(49)	2408	3736	2489	56
H(50A)	2454	1674	3555	48
H(50B)	3146	1465	3248	48
H(52)	2532	1245	1997	48
H(54)	377	1916	514	44

Table C.5. Torsion angles [deg] for **1**

O(2)-Ga(1)-N(1)-C(5)	-168.2(4)
O(1)-Ga(1)-N(1)-C(5)	-71.9(4)
N(4)-Ga(1)-N(1)-C(5)	80.2(11)
N(2)-Ga(1)-N(1)-C(5)	15.2(3)
N(3)-Ga(1)-N(1)-C(5)	97.3(4)
O(2)-Ga(1)-N(1)-C(1)	13.4(4)
O(1)-Ga(1)-N(1)-C(1)	109.7(4)
N(4)-Ga(1)-N(1)-C(1)	-98.2(11)
N(2)-Ga(1)-N(1)-C(1)	-163.1(4)
N(3)-Ga(1)-N(1)-C(1)	-81.1(4)
C(5)-N(1)-C(1)-C(2)	0.6(7)
Ga(1)-N(1)-C(1)-C(2)	179.0(4)
N(1)-C(1)-C(2)-C(3)	-2.8(8)
C(1)-C(2)-C(3)-C(4)	3.4(8)
C(2)-C(3)-C(4)-C(5)	-2.0(9)
C(1)-N(1)-C(5)-C(4)	1.0(8)
Ga(1)-N(1)-C(5)-C(4)	-177.5(4)
C(1)-N(1)-C(5)-C(6)	-178.6(5)
Ga(1)-N(1)-C(5)-C(6)	2.9(6)
C(3)-C(4)-C(5)-N(1)	-0.3(8)
C(3)-C(4)-C(5)-C(6)	179.2(5)
N(1)-C(5)-C(6)-N(2)	-28.5(6)
C(4)-C(5)-C(6)-N(2)	152.0(5)
C(5)-C(6)-N(2)-C(14)	-80.6(5)
C(5)-C(6)-N(2)-C(7)	159.0(4)
C(5)-C(6)-N(2)-Ga(1)	39.0(5)
O(2)-Ga(1)-N(2)-C(6)	-42.3(7)
O(1)-Ga(1)-N(2)-C(6)	68.8(3)
N(4)-Ga(1)-N(2)-C(6)	159.2(3)
N(1)-Ga(1)-N(2)-C(6)	-29.3(3)
N(3)-Ga(1)-N(2)-C(6)	-123.1(3)
O(2)-Ga(1)-N(2)-C(14)	79.4(7)
O(1)-Ga(1)-N(2)-C(14)	-169.5(4)
N(4)-Ga(1)-N(2)-C(14)	-79.1(4)
N(1)-Ga(1)-N(2)-C(14)	92.4(4)
N(3)-Ga(1)-N(2)-C(14)	-1.4(4)
O(2)-Ga(1)-N(2)-C(7)	-160.7(5)
O(1)-Ga(1)-N(2)-C(7)	-49.7(3)
N(4)-Ga(1)-N(2)-C(7)	40.8(4)
N(1)-Ga(1)-N(2)-C(7)	-147.7(4)
N(3)-Ga(1)-N(2)-C(7)	118.5(3)
C(6)-N(2)-C(7)-C(8)	-56.3(6)
C(14)-N(2)-C(7)-C(8)	-178.5(5)
Ga(1)-N(2)-C(7)-C(8)	62.0(5)
N(2)-C(7)-C(8)-C(9)	139.9(5)
N(2)-C(7)-C(8)-C(13)	-41.1(7)

C(13)-C(8)-C(9)-C(10)	-3.7(8)
C(7)-C(8)-C(9)-C(10)	175.4(5)
C(8)-C(9)-C(10)-C(11)	-3.7(9)
C(8)-C(9)-C(10)-I(1)	176.8(4)
C(9)-C(10)-C(11)-C(12)	6.0(9)
I(1)-C(10)-C(11)-C(12)	-174.5(4)
C(10)-C(11)-C(12)-C(13)	-1.1(9)
C(10)-C(11)-C(12)-I(2)	177.5(4)
C(11)-C(12)-C(13)-O(1)	172.8(5)
I(2)-C(12)-C(13)-O(1)	-5.8(7)
C(11)-C(12)-C(13)-C(8)	-6.0(8)
I(2)-C(12)-C(13)-C(8)	175.4(4)
C(9)-C(8)-C(13)-O(1)	-170.5(5)
C(7)-C(8)-C(13)-O(1)	10.4(9)
C(9)-C(8)-C(13)-C(12)	8.2(8)
C(7)-C(8)-C(13)-C(12)	-170.8(5)
C(12)-C(13)-O(1)-Ga(1)	170.9(4)
C(8)-C(13)-O(1)-Ga(1)	-10.4(8)
O(2)-Ga(1)-O(1)-C(13)	-167.9(5)
N(4)-Ga(1)-O(1)-C(13)	-71.5(5)
N(1)-Ga(1)-O(1)-C(13)	104.2(5)
N(2)-Ga(1)-O(1)-C(13)	26.6(5)
N(3)-Ga(1)-O(1)-C(13)	-27.4(9)
C(6)-N(2)-C(14)-C(15)	93.4(6)
C(7)-N(2)-C(14)-C(15)	-146.7(5)
Ga(1)-N(2)-C(14)-C(15)	-25.9(6)
N(2)-C(14)-C(15)-N(3)	52.2(6)
C(14)-C(15)-N(3)-C(16)	70.8(5)
C(14)-C(15)-N(3)-C(22)	-166.6(4)
C(14)-C(15)-N(3)-Ga(1)	-49.2(5)
O(2)-Ga(1)-N(3)-C(15)	-136.9(3)
O(1)-Ga(1)-N(3)-C(15)	82.5(7)
N(4)-Ga(1)-N(3)-C(15)	127.6(3)
N(1)-Ga(1)-N(3)-C(15)	-49.6(3)
N(2)-Ga(1)-N(3)-C(15)	27.8(3)
O(2)-Ga(1)-N(3)-C(16)	104.2(3)
O(1)-Ga(1)-N(3)-C(16)	-36.5(8)
N(4)-Ga(1)-N(3)-C(16)	8.7(3)
N(1)-Ga(1)-N(3)-C(16)	-168.6(3)
N(2)-Ga(1)-N(3)-C(16)	-91.2(3)
O(2)-Ga(1)-N(3)-C(22)	-16.9(3)
O(1)-Ga(1)-N(3)-C(22)	-157.6(6)
N(4)-Ga(1)-N(3)-C(22)	-112.5(3)
N(1)-Ga(1)-N(3)-C(22)	70.3(3)
N(2)-Ga(1)-N(3)-C(22)	147.7(3)
C(15)-N(3)-C(16)-C(17)	-121.1(5)
C(22)-N(3)-C(16)-C(17)	114.7(5)
Ga(1)-N(3)-C(16)-C(17)	-5.8(5)
N(3)-C(16)-C(17)-N(4)	-3.2(7)
N(3)-C(16)-C(17)-C(18)	178.5(5)
N(4)-C(17)-C(18)-C(19)	-3.3(8)
C(16)-C(17)-C(18)-C(19)	174.9(5)
C(17)-C(18)-C(19)-C(20)	-0.1(9)
C(18)-C(19)-C(20)-C(21)	2.5(9)
C(19)-C(20)-C(21)-N(4)	-1.9(8)
C(18)-C(17)-N(4)-C(21)	4.0(7)
C(16)-C(17)-N(4)-C(21)	-174.3(5)
C(18)-C(17)-N(4)-Ga(1)	-170.5(4)
C(16)-C(17)-N(4)-Ga(1)	11.3(6)
C(20)-C(21)-N(4)-C(17)	-1.4(8)
C(20)-C(21)-N(4)-Ga(1)	172.7(4)
O(2)-Ga(1)-N(4)-C(17)	-104.7(4)
O(1)-Ga(1)-N(4)-C(17)	158.6(4)

N(1)-Ga(1)-N(4)-C(17)	6.3(13)
N(2)-Ga(1)-N(4)-C(17)	69.7(4)
N(3)-Ga(1)-N(4)-C(17)	-11.2(4)
O(2)-Ga(1)-N(4)-C(21)	81.2(4)
O(1)-Ga(1)-N(4)-C(21)	-15.6(4)
N(1)-Ga(1)-N(4)-C(21)	-167.9(9)
N(2)-Ga(1)-N(4)-C(21)	-104.5(4)
N(3)-Ga(1)-N(4)-C(21)	174.7(4)
C(15)-N(3)-C(22)-C(23)	173.6(4)
C(16)-N(3)-C(22)-C(23)	-63.6(5)
Ga(1)-N(3)-C(22)-C(23)	58.9(5)
N(3)-C(22)-C(23)-C(24)	120.1(5)
N(3)-C(22)-C(23)-C(28)	-62.1(6)
C(28)-C(23)-C(24)-C(25)	-1.6(8)
C(22)-C(23)-C(24)-C(25)	176.2(5)
C(23)-C(24)-C(25)-C(26)	-0.4(8)
C(23)-C(24)-C(25)-I(3)	175.5(4)
C(24)-C(25)-C(26)-C(27)	1.0(8)
I(3)-C(25)-C(26)-C(27)	-175.0(4)
C(25)-C(26)-C(27)-C(28)	0.4(8)
C(25)-C(26)-C(27)-I(4)	178.9(4)
C(26)-C(27)-C(28)-O(2)	178.4(5)
I(4)-C(27)-C(28)-O(2)	-0.1(7)
C(26)-C(27)-C(28)-C(23)	-2.3(8)
I(4)-C(27)-C(28)-C(23)	179.2(4)
C(24)-C(23)-C(28)-O(2)	-177.8(5)
C(22)-C(23)-C(28)-O(2)	4.4(7)
C(24)-C(23)-C(28)-C(27)	2.9(7)
C(22)-C(23)-C(28)-C(27)	-174.9(5)
C(27)-C(28)-O(2)-Ga(1)	-135.6(4)
C(23)-C(28)-O(2)-Ga(1)	45.2(6)
O(1)-Ga(1)-O(2)-C(28)	137.2(4)
N(4)-Ga(1)-O(2)-C(28)	45.9(4)
N(1)-Ga(1)-O(2)-C(28)	-125.4(4)
N(2)-Ga(1)-O(2)-C(28)	-112.7(6)
N(3)-Ga(1)-O(2)-C(28)	-33.5(4)
O(4)-Ga(2)-N(5)-C(33)	-166.6(4)
O(3)-Ga(2)-N(5)-C(33)	-70.4(4)
N(8)-Ga(2)-N(5)-C(33)	95.0(11)
N(6)-Ga(2)-N(5)-C(33)	16.9(4)
N(7)-Ga(2)-N(5)-C(33)	99.2(4)
O(4)-Ga(2)-N(5)-C(29)	11.9(4)
O(3)-Ga(2)-N(5)-C(29)	108.1(4)
N(8)-Ga(2)-N(5)-C(29)	-86.5(11)
N(6)-Ga(2)-N(5)-C(29)	-164.6(4)
N(7)-Ga(2)-N(5)-C(29)	-82.3(4)
C(33)-N(5)-C(29)-C(30)	-0.1(8)
Ga(2)-N(5)-C(29)-C(30)	-178.6(4)
N(5)-C(29)-C(30)-C(31)	-0.5(8)
C(29)-C(30)-C(31)-C(32)	1.3(9)
C(30)-C(31)-C(32)-C(33)	-1.4(9)
C(29)-N(5)-C(33)-C(32)	0.0(8)
Ga(2)-N(5)-C(33)-C(32)	178.6(4)
C(29)-N(5)-C(33)-C(34)	-179.8(5)
Ga(2)-N(5)-C(33)-C(34)	-1.2(6)
C(31)-C(32)-C(33)-N(5)	0.7(8)
C(31)-C(32)-C(33)-C(34)	-179.4(5)
N(5)-C(33)-C(34)-N(6)	-23.8(7)
C(32)-C(33)-C(34)-N(6)	156.3(5)
C(33)-C(34)-N(6)-C(35)	154.9(4)
C(33)-C(34)-N(6)-C(42)	-84.0(5)
C(33)-C(34)-N(6)-Ga(2)	35.4(5)
O(4)-Ga(2)-N(6)-C(34)	-43.1(9)

O(3)-Ga(2)-N(6)-C(34)	69.9(3)
N(8)-Ga(2)-N(6)-C(34)	161.6(3)
N(5)-Ga(2)-N(6)-C(34)	-27.9(3)
N(7)-Ga(2)-N(6)-C(34)	-119.9(4)
O(4)-Ga(2)-N(6)-C(35)	-162.8(6)
O(3)-Ga(2)-N(6)-C(35)	-49.8(3)
N(8)-Ga(2)-N(6)-C(35)	41.9(4)
N(5)-Ga(2)-N(6)-C(35)	-147.6(4)
N(7)-Ga(2)-N(6)-C(35)	120.4(3)
O(4)-Ga(2)-N(6)-C(42)	78.0(8)
O(3)-Ga(2)-N(6)-C(42)	-169.0(4)
N(8)-Ga(2)-N(6)-C(42)	-77.3(4)
N(5)-Ga(2)-N(6)-C(42)	93.2(4)
N(7)-Ga(2)-N(6)-C(42)	1.2(4)
C(34)-N(6)-C(35)-C(36)	-56.4(6)
C(42)-N(6)-C(35)-C(36)	-179.2(5)
Ga(2)-N(6)-C(35)-C(36)	61.5(5)
N(6)-C(35)-C(36)-C(37)	142.6(5)
N(6)-C(35)-C(36)-C(41)	-38.9(8)
C(41)-C(36)-C(37)-C(38)	-1.2(8)
C(35)-C(36)-C(37)-C(38)	177.4(5)
C(36)-C(37)-C(38)-C(39)	-2.1(8)
C(36)-C(37)-C(38)-I(5)	-179.8(4)
C(37)-C(38)-C(39)-C(40)	2.9(8)
I(5)-C(38)-C(39)-C(40)	-179.4(4)
C(38)-C(39)-C(40)-C(41)	-0.5(8)
C(38)-C(39)-C(40)-I(6)	-179.4(4)
C(39)-C(40)-C(41)-O(3)	175.9(5)
I(6)-C(40)-C(41)-O(3)	-5.2(6)
C(39)-C(40)-C(41)-C(36)	-2.7(8)
I(6)-C(40)-C(41)-C(36)	176.2(4)
C(37)-C(36)-C(41)-O(3)	-175.1(5)
C(35)-C(36)-C(41)-O(3)	6.3(8)
C(37)-C(36)-C(41)-C(40)	3.4(8)
C(35)-C(36)-C(41)-C(40)	-175.1(5)
C(40)-C(41)-O(3)-Ga(2)	174.0(3)
C(36)-C(41)-O(3)-Ga(2)	-7.4(7)
O(4)-Ga(2)-O(3)-C(41)	-166.1(4)
N(8)-Ga(2)-O(3)-C(41)	-73.2(4)
N(5)-Ga(2)-O(3)-C(41)	104.4(4)
N(6)-Ga(2)-O(3)-C(41)	26.1(4)
N(7)-Ga(2)-O(3)-C(41)	-22.4(10)
C(34)-N(6)-C(42)-C(43)	90.9(6)
C(35)-N(6)-C(42)-C(43)	-147.3(5)
Ga(2)-N(6)-C(42)-C(43)	-27.5(6)
N(6)-C(42)-C(43)-N(7)	51.1(7)
C(42)-C(43)-N(7)-C(50)	-164.9(4)
C(42)-C(43)-N(7)-C(44)	73.5(6)
C(42)-C(43)-N(7)-Ga(2)	-46.6(5)
O(4)-Ga(2)-N(7)-C(50)	-23.5(4)
O(3)-Ga(2)-N(7)-C(50)	-167.4(6)
N(8)-Ga(2)-N(7)-C(50)	-115.5(4)
N(5)-Ga(2)-N(7)-C(50)	65.2(4)
N(6)-Ga(2)-N(7)-C(50)	143.6(4)
O(4)-Ga(2)-N(7)-C(43)	-142.7(3)
O(3)-Ga(2)-N(7)-C(43)	73.5(8)
N(8)-Ga(2)-N(7)-C(43)	125.3(4)
N(5)-Ga(2)-N(7)-C(43)	-54.0(3)
N(6)-Ga(2)-N(7)-C(43)	24.4(3)
O(4)-Ga(2)-N(7)-C(44)	99.1(3)
O(3)-Ga(2)-N(7)-C(44)	-44.8(9)
N(8)-Ga(2)-N(7)-C(44)	7.1(3)
N(5)-Ga(2)-N(7)-C(44)	-172.2(4)

N(6)-Ga(2)-N(7)-C(44)	-93.8(4)
C(50)-N(7)-C(44)-C(45)	112.4(5)
C(43)-N(7)-C(44)-C(45)	-125.7(5)
Ga(2)-N(7)-C(44)-C(45)	-9.8(6)
N(7)-C(44)-C(45)-N(8)	7.9(7)
N(7)-C(44)-C(45)-C(46)	-170.9(5)
N(8)-C(45)-C(46)-C(47)	0.0(9)
C(44)-C(45)-C(46)-C(47)	178.7(5)
C(45)-C(46)-C(47)-C(48)	-0.8(9)
C(46)-C(47)-C(48)-C(49)	-0.4(9)
C(47)-C(48)-C(49)-N(8)	2.6(9)
C(48)-C(49)-N(8)-C(45)	-3.5(9)
C(48)-C(49)-N(8)-Ga(2)	-178.1(4)
C(46)-C(45)-N(8)-C(49)	2.1(8)
C(44)-C(45)-N(8)-C(49)	-176.7(5)
C(46)-C(45)-N(8)-Ga(2)	177.0(4)
C(44)-C(45)-N(8)-Ga(2)	-1.7(6)
O(4)-Ga(2)-N(8)-C(49)	77.7(5)
O(3)-Ga(2)-N(8)-C(49)	-18.7(5)
N(5)-Ga(2)-N(8)-C(49)	175.7(9)
N(6)-Ga(2)-N(8)-C(49)	-107.8(5)
N(7)-Ga(2)-N(8)-C(49)	171.5(5)
O(4)-Ga(2)-N(8)-C(45)	-96.9(4)
O(3)-Ga(2)-N(8)-C(45)	166.7(4)
N(5)-Ga(2)-N(8)-C(45)	1.2(12)
N(6)-Ga(2)-N(8)-C(45)	77.6(4)
N(7)-Ga(2)-N(8)-C(45)	-3.1(4)
C(43)-N(7)-C(50)-C(51)	174.3(4)
C(44)-N(7)-C(50)-C(51)	-64.9(5)
Ga(2)-N(7)-C(50)-C(51)	58.6(5)
N(7)-C(50)-C(51)-C(52)	126.5(5)
N(7)-C(50)-C(51)-C(56)	-57.3(6)
C(56)-C(51)-C(52)-C(53)	-4.7(8)
C(50)-C(51)-C(52)-C(53)	171.5(5)
C(51)-C(52)-C(53)-C(54)	1.0(8)
C(51)-C(52)-C(53)-I(7)	178.5(4)
C(52)-C(53)-C(54)-C(55)	2.1(8)
I(7)-C(53)-C(54)-C(55)	-175.4(4)
C(53)-C(54)-C(55)-C(56)	-1.6(8)
C(53)-C(54)-C(55)-I(8)	177.0(4)
C(54)-C(55)-C(56)-O(4)	-179.3(5)
I(8)-C(55)-C(56)-O(4)	2.2(7)
C(54)-C(55)-C(56)-C(51)	-1.9(8)
I(8)-C(55)-C(56)-C(51)	179.5(4)
C(52)-C(51)-C(56)-O(4)	-177.7(5)
C(50)-C(51)-C(56)-O(4)	6.2(8)
C(52)-C(51)-C(56)-C(55)	5.0(7)
C(50)-C(51)-C(56)-C(55)	-171.1(5)
C(55)-C(56)-O(4)-Ga(2)	-149.7(4)
C(51)-C(56)-O(4)-Ga(2)	33.2(7)
O(3)-Ga(2)-O(4)-C(56)	151.2(4)
N(8)-Ga(2)-O(4)-C(56)	59.0(4)
N(5)-Ga(2)-O(4)-C(56)	-111.5(4)
N(6)-Ga(2)-O(4)-C(56)	-96.6(8)
N(7)-Ga(2)-O(4)-C(56)	-21.1(4)

Symmetry transformations used to generate equivalent atoms.

Crystal Structure Data for Complex 2

Table C.6. Atomic coordinates (x 10^4) and equivalent isotropic displacement parameters (A^2 x 10^3) for **2**. U(eq) is defined as one third of the trace of the orthogonalized Uij tensor.

	x	y	z	U(eq)
I(1)	6051(1)	8016(1)	6499(1)	36(1)
I(2)	8882(1)	4591(1)	5324(1)	34(1)
Zn(1)	5000	4147(1)	7500	23(1)
O(1)	6046(2)	5408(2)	7309(1)	25(1)
C(1)	6626(2)	5208(3)	6894(2)	22(1)
C(2)	6836(3)	6232(3)	6482(2)	24(1)
C(3)	7493(3)	6087(4)	6052(2)	27(1)
C(4)	7943(3)	4852(4)	6006(2)	28(1)
C(5)	7742(3)	3789(4)	6382(2)	31(1)
C(6)	7092(3)	3945(3)	6819(2)	26(1)
C(7)	6841(3)	2773(4)	7204(2)	30(1)
C(8)	5544(3)	1263(3)	7476(2)	35(1)
C(9)	5484(3)	2199(4)	6449(2)	32(1)
N(1)	5795(2)	2427(3)	7098(1)	28(1)
C(10)	4825(3)	3280(3)	6170(2)	28(1)
C(11)	4652(3)	3427(4)	5537(2)	35(1)
C(12)	4012(3)	4387(4)	5307(2)	40(1)
C(13)	3571(3)	5217(4)	5705(2)	39(1)
C(14)	3777(3)	5016(4)	6322(2)	32(1)
N(2)	4392(2)	4068(3)	6551(1)	27(1)

Table C.7. Bond lengths [A] and angles [deg] for **2**.

I(1)-C(2)	2.081(3)
I(2)-C(4)	2.095(3)
Zn(1)-O(1)	1.992(2)
Zn(1)-O(1)#1	1.992(2)
Zn(1)-N(2)#1	2.169(3)
Zn(1)-N(2)	2.169(3)
Zn(1)-N(1)#1	2.259(3)
Zn(1)-N(1)	2.259(3)
O(1)-C(1)	1.290(4)
C(1)-C(2)	1.410(5)
C(1)-C(6)	1.427(4)
C(2)-C(3)	1.383(5)
C(3)-C(4)	1.384(5)
C(4)-C(5)	1.384(5)
C(5)-C(6)	1.390(5)
C(6)-C(7)	1.499(5)
C(7)-N(1)	1.487(5)
C(8)-N(1)	1.484(5)
C(8)-C(8)#1	1.524(9)
C(9)-N(1)	1.464(5)
C(9)-C(10)	1.499(5)
C(10)-N(2)	1.332(4)
C(10)-C(11)	1.391(5)
C(11)-C(12)	1.364(6)
C(12)-C(13)	1.386(6)
C(13)-C(14)	1.372(6)
C(14)-N(2)	1.333(5)
O(1)-Zn(1)-O(1)#1	102.20(13)
O(1)-Zn(1)-N(2)#1	90.23(11)
O(1)#1-Zn(1)-N(2)#1	92.38(11)
O(1)-Zn(1)-N(2)	92.38(11)
O(1)#1-Zn(1)-N(2)	90.23(11)
N(2)#1-Zn(1)-N(2)	175.83(16)
O(1)-Zn(1)-N(1)#1	162.04(11)
O(1)#1-Zn(1)-N(1)#1	89.88(10)
N(2)#1-Zn(1)-N(1)#1	75.88(11)
N(2)-Zn(1)-N(1)#1	100.90(11)
O(1)-Zn(1)-N(1)	89.88(10)
O(1)#1-Zn(1)-N(1)	162.04(11)
N(2)#1-Zn(1)-N(1)	100.90(11)
N(2)-Zn(1)-N(1)	75.88(11)
N(1)#1-Zn(1)-N(1)	81.80(15)
C(1)-O(1)-Zn(1)	124.9(2)
O(1)-C(1)-C(2)	121.7(3)
O(1)-C(1)-C(6)	122.5(3)
C(2)-C(1)-C(6)	115.8(3)
C(3)-C(2)-C(1)	123.7(3)
C(3)-C(2)-I(1)	118.9(2)
C(1)-C(2)-I(1)	117.3(2)
C(2)-C(3)-C(4)	118.3(3)
C(3)-C(4)-C(5)	120.8(3)
C(3)-C(4)-I(2)	118.6(3)
C(5)-C(4)-I(2)	120.5(3)
C(4)-C(5)-C(6)	120.7(3)
C(5)-C(6)-C(1)	120.6(3)

C(5)-C(6)-C(7)	120.4(3)
C(1)-C(6)-C(7)	118.9(3)
N(1)-C(7)-C(6)	111.7(3)
N(1)-C(8)-C(8)#1	109.1(3)
N(1)-C(9)-C(10)	113.3(3)
C(9)-N(1)-C(8)	111.2(3)
C(9)-N(1)-C(7)	112.0(3)
C(8)-N(1)-C(7)	111.9(3)
C(9)-N(1)-Zn(1)	112.8(2)
C(8)-N(1)-Zn(1)	102.7(2)
C(7)-N(1)-Zn(1)	105.7(2)
N(2)-C(10)-C(11)	121.4(4)
N(2)-C(10)-C(9)	117.3(3)
C(11)-C(10)-C(9)	121.3(3)
C(12)-C(11)-C(10)	118.9(4)
C(11)-C(12)-C(13)	119.6(4)
C(14)-C(13)-C(12)	118.3(4)
N(2)-C(14)-C(13)	122.4(4)
C(10)-N(2)-C(14)	119.3(3)
C(10)-N(2)-Zn(1)	117.9(3)
C(14)-N(2)-Zn(1)	120.5(2)

Symmetry transformations used to generate equivalent atoms:
#1 -x+1,y,-z+3/2

Table C.8. Anisotropic displacement parameters (A^2 x 10^3) for **2**. The anisotropic displacement factor exponent takes the form: -2 pi^2 [h^2 a*^2 U11 + ... + 2 h k a* b* U12]

	U11	U22	U33	U23	U13	U12
I(1)	40(1)	24(1)	48(1)	9(1)	18(1)	11(1)
I(2)	32(1)	41(1)	33(1)	-6(1)	15(1)	2(1)
Zn(1)	31(1)	16(1)	22(1)	0	9(1)	0
O(1)	32(1)	20(1)	25(1)	0(1)	13(1)	2(1)
C(1)	26(2)	20(1)	22(2)	1(1)	5(1)	4(1)
C(2)	30(2)	21(1)	23(2)	1(1)	7(1)	4(1)
C(3)	30(2)	27(2)	25(2)	2(1)	8(1)	4(1)
C(4)	31(2)	32(2)	23(2)	-2(1)	10(1)	5(1)
C(5)	33(2)	25(2)	36(2)	-2(1)	8(2)	9(1)
C(6)	32(2)	24(2)	24(2)	2(1)	6(1)	7(1)
C(7)	40(2)	24(2)	28(2)	6(1)	9(2)	10(1)
C(8)	52(2)	16(1)	38(2)	1(1)	14(2)	3(2)
C(9)	45(2)	24(2)	29(2)	-8(1)	11(2)	3(2)
N(1)	37(2)	17(1)	30(2)	0(1)	9(1)	3(1)
C(10)	38(2)	22(2)	26(2)	-3(1)	9(2)	-3(1)
C(11)	52(3)	29(2)	26(2)	-6(2)	13(2)	-6(2)
C(12)	58(3)	37(2)	24(2)	-2(2)	4(2)	-4(2)
C(13)	44(2)	37(2)	34(2)	1(2)	0(2)	2(2)
C(14)	38(2)	29(2)	30(2)	-1(1)	8(2)	2(2)
N(2)	34(2)	25(1)	24(2)	-2(1)	8(1)	0(1)

Table C.9. Hydrogen coordinates (x 10^4) and isotropic displacement parameters (A^2 x 10^3) for **2**.

	x	y	z	U(eq)
H(3)	7631	6817	5794	32
H(5)	8052	2945	6340	37
H(11)	4973	2868	5271	42
H(12)	3870	4486	4876	48
H(13)	3137	5908	5553	46
H(14)	3471	5573	6598	38
H(7A)	6940(30)	2920(40)	7549(19)	16(10)
H(7B)	7240(30)	1970(40)	7136(18)	26(10)
H(8A)	5780(30)	490(40)	7283(18)	24(10)
H(8B)	5990(30)	1410(40)	7909(18)	20(9)
H(9A)	5970(30)	2160(40)	6290(20)	25(11)
H(9B)	5080(30)	1430(40)	6399(17)	22(10)

Table C.10. Torsion angles [deg] for **2**.

O(1)#1-Zn(1)-O(1)-C(1)	-143.4(3)
N(2)#1-Zn(1)-O(1)-C(1)	124.1(3)
N(2)-Zn(1)-O(1)-C(1)	-52.7(3)
N(1)#1-Zn(1)-O(1)-C(1)	85.2(4)
N(1)-Zn(1)-O(1)-C(1)	23.2(3)
Zn(1)-O(1)-C(1)-C(2)	134.5(3)
Zn(1)-O(1)-C(1)-C(6)	-45.2(5)
O(1)-C(1)-C(2)-C(3)	176.4(4)
C(6)-C(1)-C(2)-C(3)	-3.9(5)
O(1)-C(1)-C(2)-I(1)	-7.0(5)
C(6)-C(1)-C(2)-I(1)	172.7(3)
C(1)-C(2)-C(3)-C(4)	2.6(6)
I(1)-C(2)-C(3)-C(4)	-174.0(3)
C(2)-C(3)-C(4)-C(5)	-0.1(6)
C(2)-C(3)-C(4)-I(2)	176.8(3)
C(3)-C(4)-C(5)-C(6)	-0.8(6)
I(2)-C(4)-C(5)-C(6)	-177.6(3)
C(4)-C(5)-C(6)-C(1)	-0.7(6)
C(4)-C(5)-C(6)-C(7)	177.1(4)
O(1)-C(1)-C(6)-C(5)	-177.4(4)
C(2)-C(1)-C(6)-C(5)	2.9(5)
O(1)-C(1)-C(6)-C(7)	4.8(6)
C(2)-C(1)-C(6)-C(7)	-174.9(3)
C(5)-C(6)-C(7)-N(1)	-117.6(4)
C(1)-C(6)-C(7)-N(1)	60.3(5)
C(10)-C(9)-N(1)-C(8)	123.7(3)
C(10)-C(9)-N(1)-C(7)	-110.3(4)
C(10)-C(9)-N(1)-Zn(1)	8.9(4)
C(8)#1-C(8)-N(1)-C(9)	-73.6(4)
C(8)#1-C(8)-N(1)-C(7)	160.3(3)
C(8)#1-C(8)-N(1)-Zn(1)	47.4(4)
C(6)-C(7)-N(1)-C(9)	54.1(4)

C(6)-C(7)-N(1)-C(8)	179.7(3)
C(6)-C(7)-N(1)-Zn(1)	-69.3(3)
O(1)-Zn(1)-N(1)-C(9)	-92.6(3)
O(1)#1-Zn(1)-N(1)-C(9)	40.2(5)
N(2)#1-Zn(1)-N(1)-C(9)	177.2(3)
N(2)-Zn(1)-N(1)-C(9)	-0.1(3)
N(1)#1-Zn(1)-N(1)-C(9)	103.4(3)
O(1)-Zn(1)-N(1)-C(8)	147.6(3)
O(1)#1-Zn(1)-N(1)-C(8)	-79.6(4)
N(2)#1-Zn(1)-N(1)-C(8)	57.4(3)
N(2)-Zn(1)-N(1)-C(8)	-119.9(3)
N(1)#1-Zn(1)-N(1)-C(8)	-16.4(2)
O(1)-Zn(1)-N(1)-C(7)	30.2(2)
O(1)#1-Zn(1)-N(1)-C(7)	163.0(3)
N(2)#1-Zn(1)-N(1)-C(7)	-60.0(2)
N(2)-Zn(1)-N(1)-C(7)	122.7(2)
N(1)#1-Zn(1)-N(1)-C(7)	-133.8(3)
N(1)-C(9)-C(10)-N(2)	-18.2(5)
N(1)-C(9)-C(10)-C(11)	163.6(4)
N(2)-C(10)-C(11)-C(12)	-1.0(6)
C(9)-C(10)-C(11)-C(12)	177.1(4)
C(10)-C(11)-C(12)-C(13)	1.8(6)
C(11)-C(12)-C(13)-C(14)	-1.7(7)
C(12)-C(13)-C(14)-N(2)	0.8(6)
C(11)-C(10)-N(2)-C(14)	0.1(5)
C(9)-C(10)-N(2)-C(14)	-178.0(4)
C(11)-C(10)-N(2)-Zn(1)	-163.0(3)
C(9)-C(10)-N(2)-Zn(1)	18.9(4)
C(13)-C(14)-N(2)-C(10)	0.0(6)
C(13)-C(14)-N(2)-Zn(1)	162.6(3)
O(1)-Zn(1)-N(2)-C(10)	79.1(3)
O(1)#1-Zn(1)-N(2)-C(10)	-178.7(3)
N(2)#1-Zn(1)-N(2)-C(10)	-49.8(3)
N(1)#1-Zn(1)-N(2)-C(10)	-88.8(3)
N(1)-Zn(1)-N(2)-C(10)	-10.2(3)
O(1)-Zn(1)-N(2)-C(14)	-83.8(3)
O(1)#1-Zn(1)-N(2)-C(14)	18.4(3)
N(2)#1-Zn(1)-N(2)-C(14)	147.3(3)
N(1)#1-Zn(1)-N(2)-C(14)	108.3(3)
N(1)-Zn(1)-N(2)-C(14)	-173.1(3)

Symmetry transformations used to generate equivalent atoms:
#1 -x+1,y,-z+3/2

Least-squares planes (x,y,z in crystal coordinates) and deviations from them (* indicates atom used to define plane).

```
 9.4973 (0.0156) x + 2.9408 (0.0146) y + 13.0276 (0.0271) z = 16.7863 (0.0065)

*    0.0189 (0.0025)  C1
*   -0.0172 (0.0026)  C2
*    0.0035 (0.0027)  C3
*    0.0082 (0.0028)  C4
*   -0.0054 (0.0028)  C5
*   -0.0079 (0.0028)  C6
     0.0671 (0.0051)  O1
    -1.0474 (0.0063)  Zn1
    -0.0885 (0.0065)  C7
```

Rms deviation of fitted atoms = 0.0117

```
 10.5097 (0.0154) x + 6.4780 (0.0128) y - 1.4924 (0.0346) z = 6.2755 (0.0208)
```

Angle to previous plane (with approximate esd) = 44.15 (0.14)

```
*   -0.0007 (0.0026)  C10
*    0.0066 (0.0028)  C11
*   -0.0092 (0.0030)  C12
*    0.0058 (0.0030)  C13
*    0.0001 (0.0028)  C14
*   -0.0027 (0.0025)  N2
     0.5465 (0.0054)  Zn1
    -0.0500 (0.0065)  C9
```

Rms deviation of fitted atoms = 0.0053

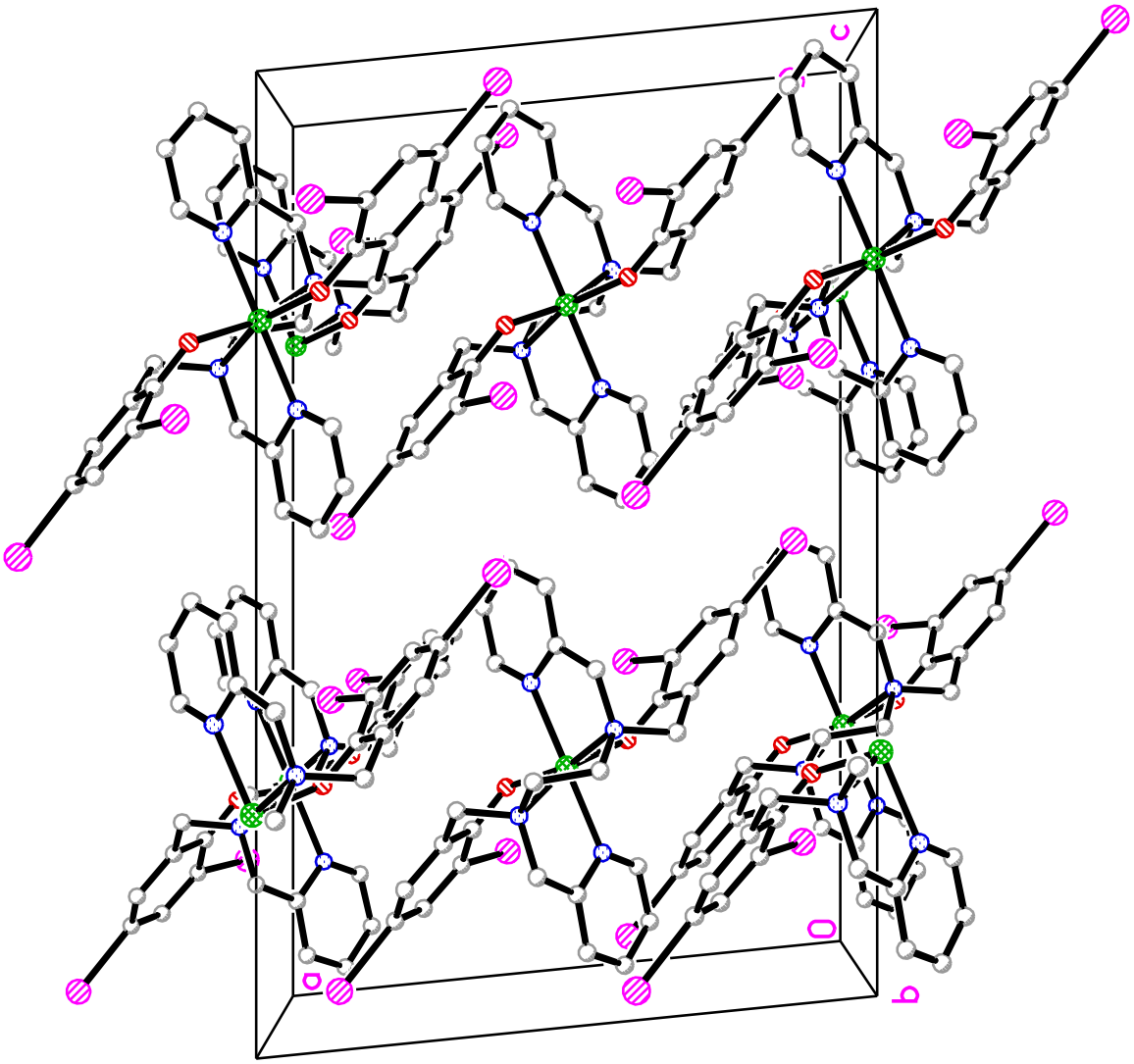

Figure C.1. Unit cell crystal structure for complex **2**.

APPENDIX D

Supplementary Material for Chapter 6

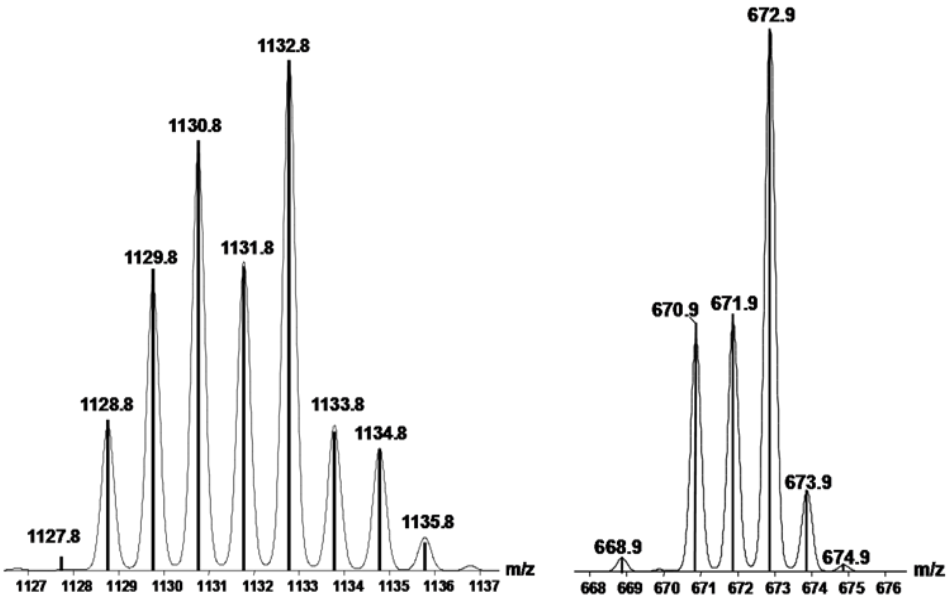

Figure D.6.2.1 Isotopic distribution for complex **3** (left) and **4** (right). Experimental results are represented by the bars, whereas simulated results are designated by the continuous spectra.

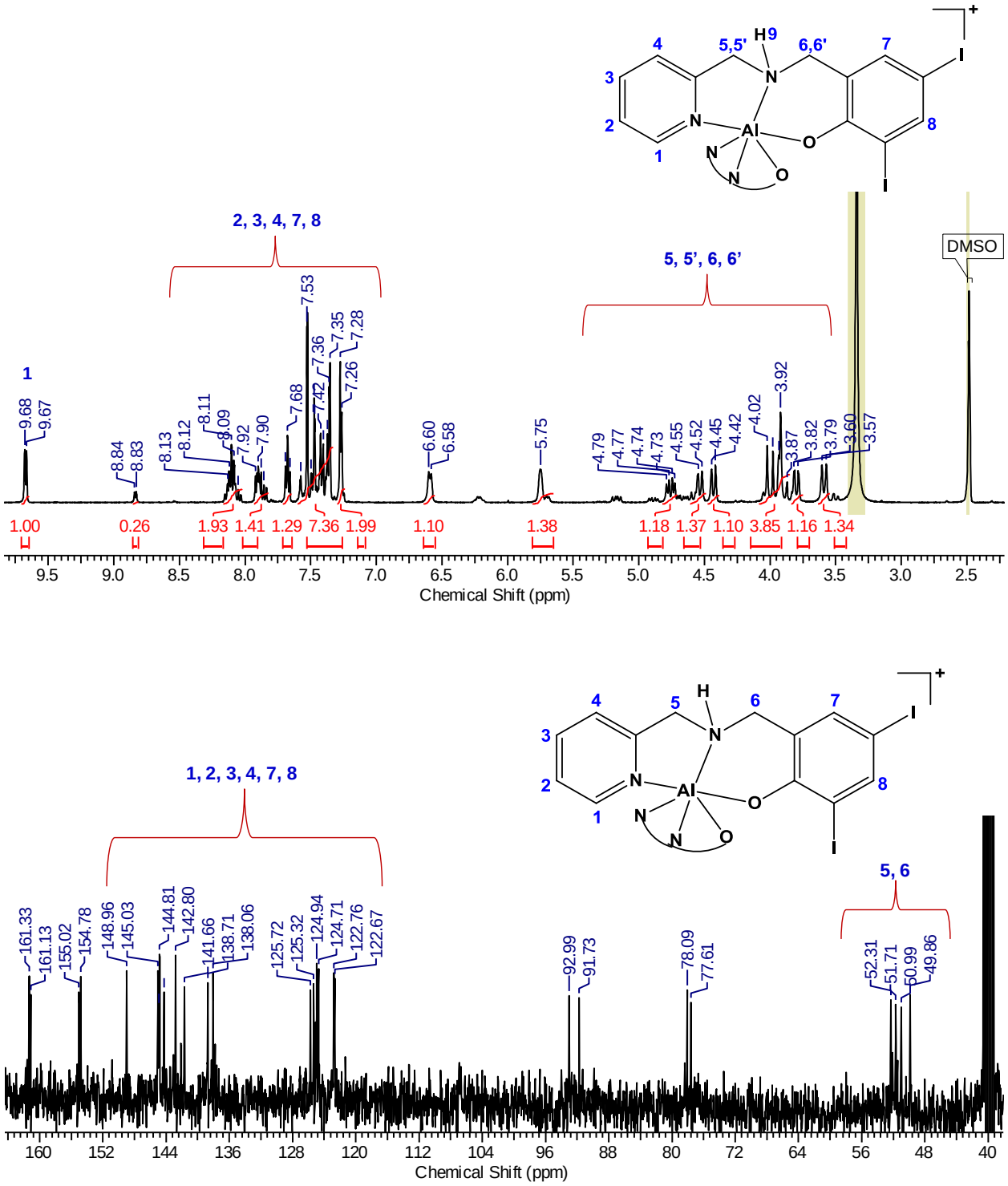

Figure D.6.2.3.1 ^{1}H- and ^{13}C-NMR spectra for complex **1** recorded in DMSO-d_6 at room temperature.

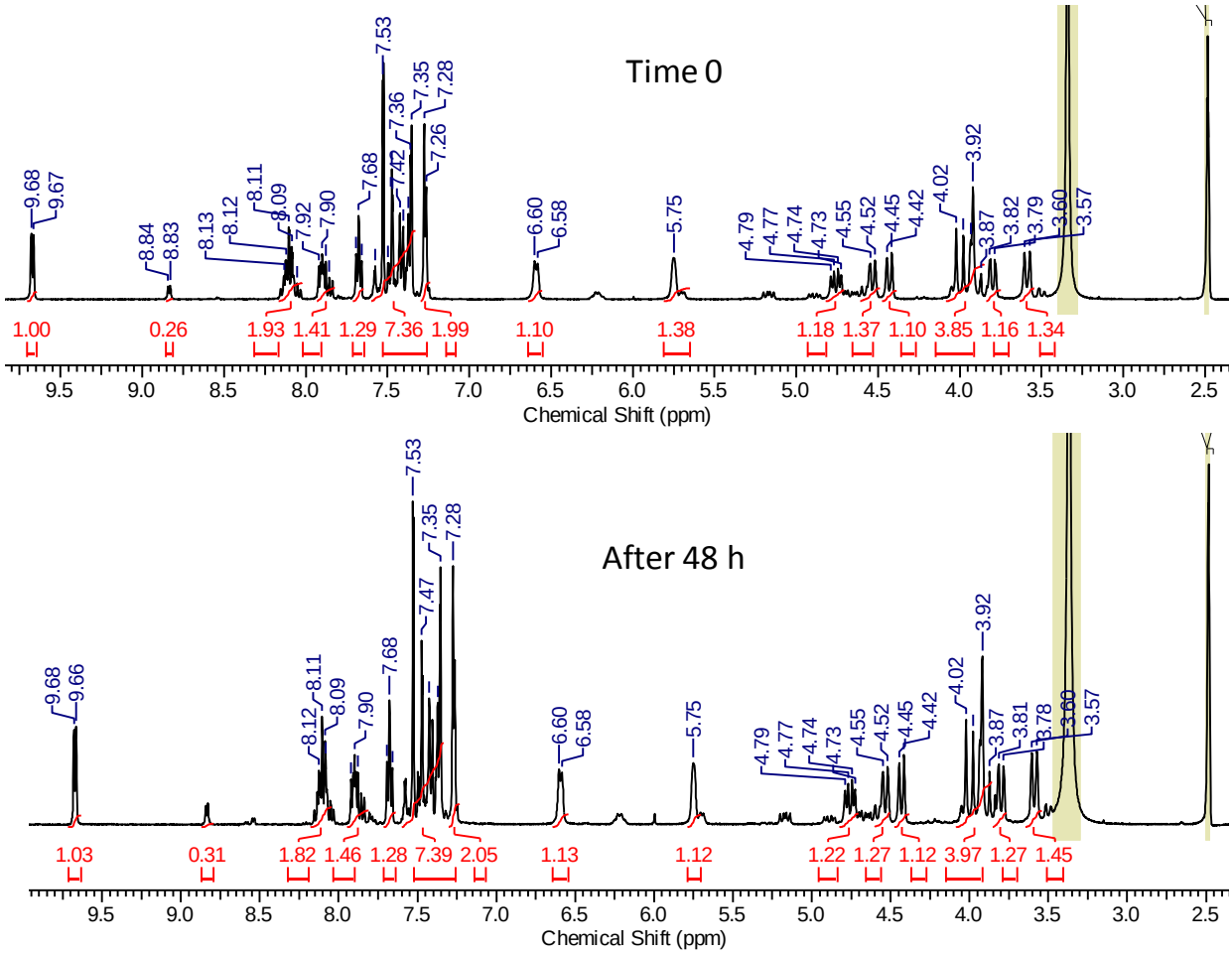

Figure D.6.2.3.2 Time dependent ^{1}H-NMR spectra for complex **1** recorded in DMSO-d_6 at room temperature.

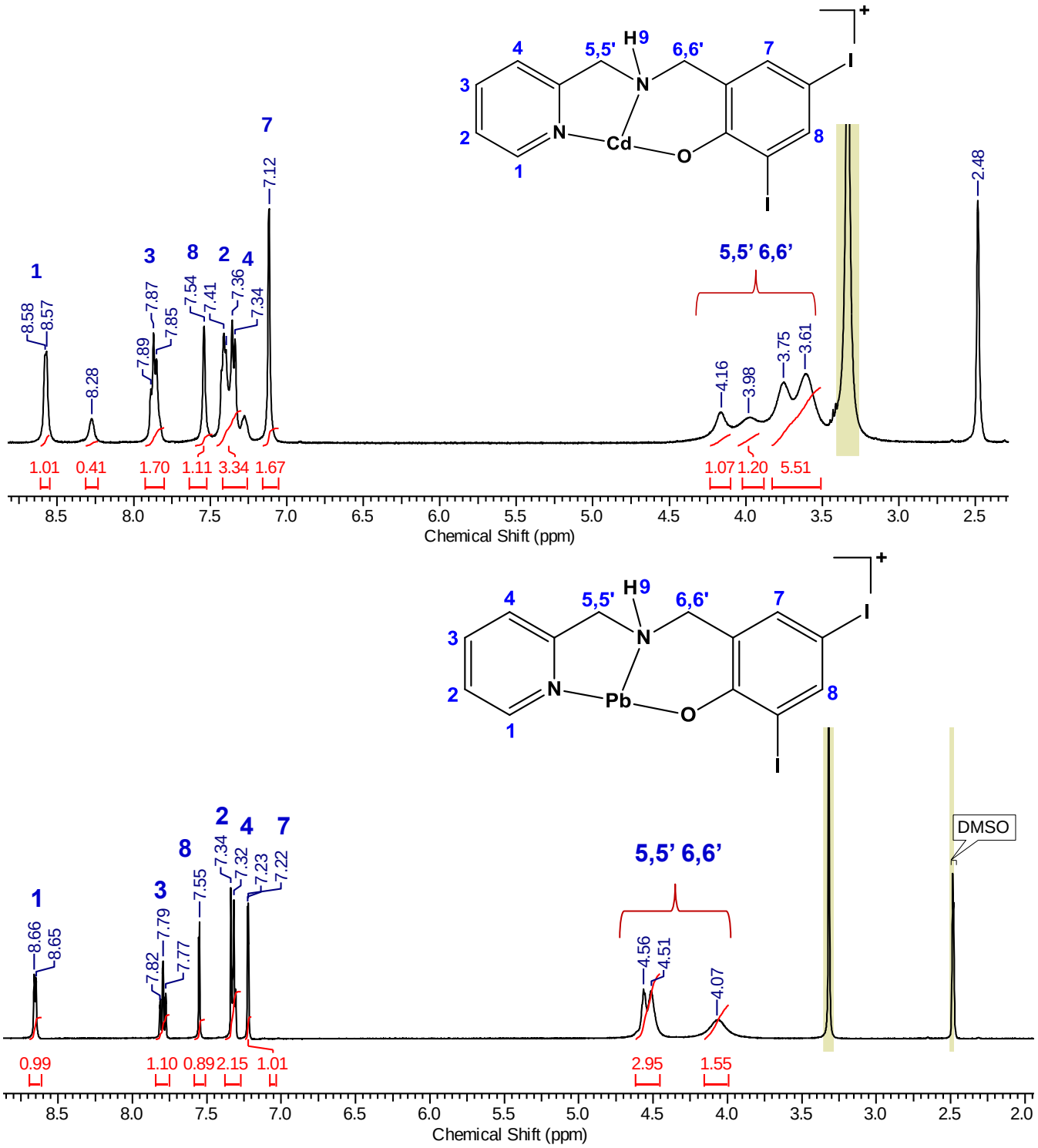

Figure D.6.2.3.3 ^{1}H-NMR spectra for complexes **2** (top) and **4** (bottom) in DMSO-d_6 at room temperature.

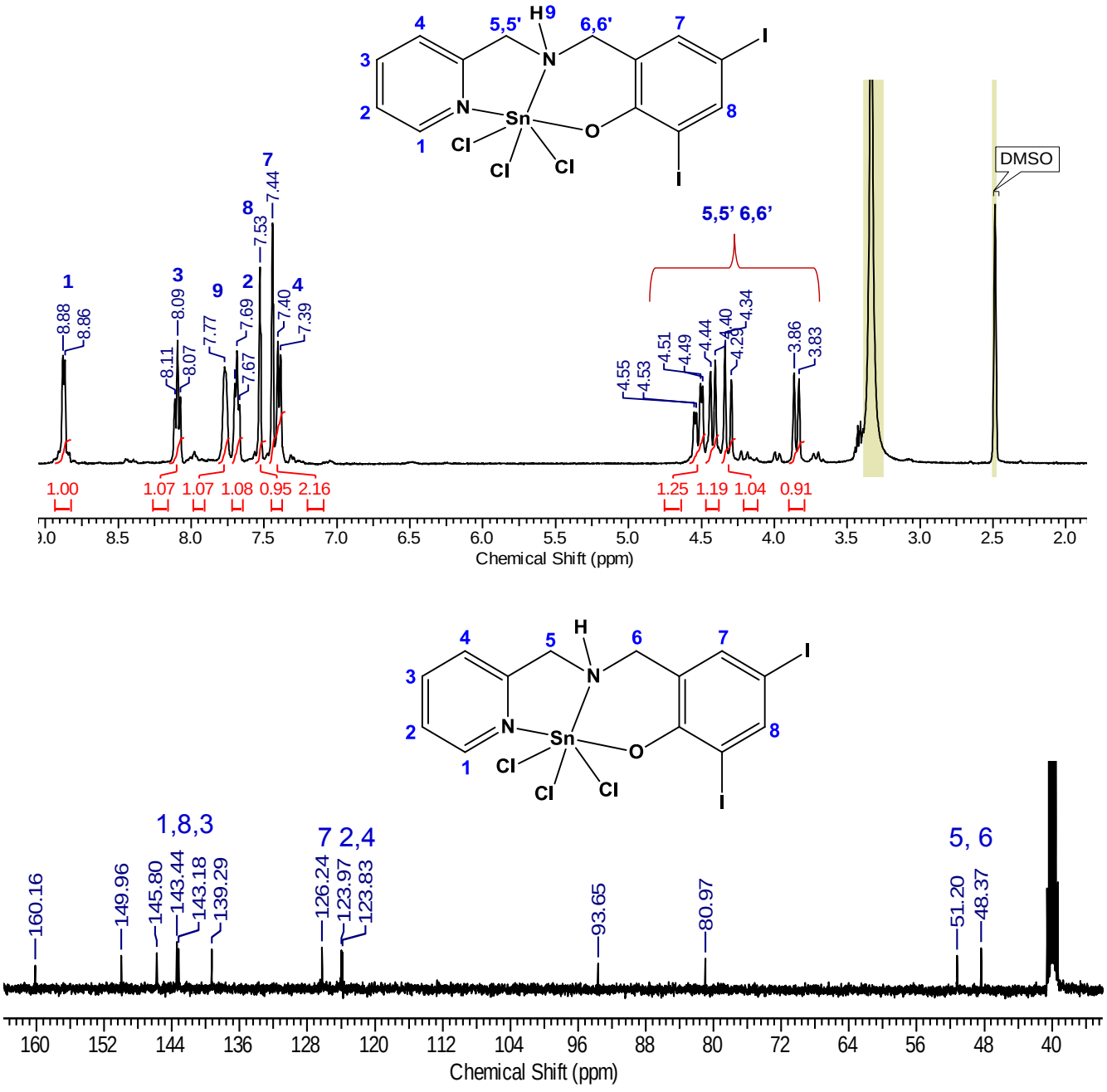

Figure D.6.2.3.4 ^{1}H- and ^{13}C-NMR spectra for complex **5** recorded in DMSO-d_6 at room temperature.

Crystal Structure Data for Complex 3

Table D.6.5.2.1 Atomic coordinates (x 10^4) and equivalent isotropic displacement parameters (A^2 x 10^3) for **3.** U(eq) is defined as one third of the trace of the orthogonalized Uij tensor.

	x	y	z	U(eq)
Hg(1)	5000	5000	5000	16(1)
I(1)	464(1)	1348(1)	4018(1)	24(1)
I(2)	3227(1)	4852(1)	768(1)	23(1)
N(1)	4209(2)	7004(2)	5971(2)	19(1)
C(1)	4375(3)	8209(3)	5643(3)	25(1)
C(2)	3859(3)	9204(3)	6306(3)	27(1)
C(3)	3152(3)	8947(3)	7344(3)	26(1)
C(4)	2972(3)	7701(3)	7676(3)	21(1)
C(5)	3512(3)	6756(3)	6967(3)	17(1)
C(6)	3408(3)	5350(3)	7333(3)	18(1)
N(2)	3399(2)	4710(2)	6288(2)	16(1)
C(7)	2050(3)	5212(3)	5598(3)	17(1)
C(8)	2032(3)	4504(3)	4571(3)	16(1)
C(9)	1457(3)	3481(3)	4730(3)	17(1)
C(10)	1394(3)	2844(3)	3769(3)	20(1)
C(11)	1892(3)	3239(3)	2627(3)	19(1)
C(12)	2477(3)	4244(3)	2486(3)	17(1)
C(13)	2606(3)	4919(3)	3431(3)	16(1)
O(1)	3177(2)	5843(2)	3285(2)	18(1)
S(1)	5052(1)	966(1)	8338(1)	24(1)
O(2)	4033(2)	1924(2)	7332(2)	23(1)
C(14)	5707(4)	1942(3)	9124(3)	32(1)
C(15)	6568(4)	320(4)	7583(4)	43(1)
S(2)	267(1)	1820(1)	9379(1)	31(1)
O(3)	1513(2)	631(2)	9824(2)	40(1)
C(16)	-389(4)	1545(3)	8017(3)	33(1)
C(17)	879(4)	3147(3)	8646(4)	35(1)

Table D.6.5.2.2 Bond lengths [A] and angles [deg] for **3**.

Hg(1)-N(2)#1	2.225(2)
Hg(1)-N(2)	2.225(2)
Hg(1)-N(1)	2.505(2)
Hg(1)-N(1)#1	2.505(2)
Hg(1)-O(1)#1	2.5063(19)
Hg(1)-O(1)	2.5063(19)
I(1)-C(10)	2.096(3)
I(2)-C(12)	2.095(3)
N(1)-C(5)	1.334(4)
N(1)-C(1)	1.335(4)
C(1)-C(2)	1.384(4)
C(2)-C(3)	1.378(5)
C(3)-C(4)	1.384(4)
C(4)-C(5)	1.383(4)
C(5)-C(6)	1.519(4)
C(6)-N(2)	1.462(4)

N(2)-C(7)	1.487(4)
C(7)-C(8)	1.495(4)
C(8)-C(9)	1.390(4)
C(8)-C(13)	1.432(4)
C(9)-C(10)	1.389(4)
C(10)-C(11)	1.390(4)
C(11)-C(12)	1.380(4)
C(12)-C(13)	1.419(4)
C(13)-O(1)	1.291(3)
S(1)-O(2)	1.509(2)
S(1)-C(15)	1.777(4)
S(1)-C(14)	1.779(3)
S(2)-O(3)	1.501(2)
S(2)-C(16)	1.775(4)
S(2)-C(17)	1.781(4)

N(2)#1-Hg(1)-N(2)	180.000(1)
N(2)#1-Hg(1)-N(1)	107.58(8)
N(2)-Hg(1)-N(1)	72.42(8)
N(2)#1-Hg(1)-N(1)#1	72.42(8)
N(2)-Hg(1)-N(1)#1	107.58(8)
N(1)-Hg(1)-N(1)#1	180.00(9)
N(2)#1-Hg(1)-O(1)#1	87.14(8)
N(2)-Hg(1)-O(1)#1	92.86(7)
N(1)-Hg(1)-O(1)#1	83.49(7)
N(1)#1-Hg(1)-O(1)#1	96.51(7)
N(2)#1-Hg(1)-O(1)	92.86(7)
N(2)-Hg(1)-O(1)	87.14(8)
N(1)-Hg(1)-O(1)	96.51(7)
N(1)#1-Hg(1)-O(1)	83.49(7)
O(1)#1-Hg(1)-O(1)	180.0
C(5)-N(1)-C(1)	118.8(3)
C(5)-N(1)-Hg(1)	110.67(17)
C(1)-N(1)-Hg(1)	130.5(2)
N(1)-C(1)-C(2)	122.3(3)
C(3)-C(2)-C(1)	119.1(3)
C(2)-C(3)-C(4)	118.4(3)
C(5)-C(4)-C(3)	119.3(3)
N(1)-C(5)-C(4)	122.0(3)
N(1)-C(5)-C(6)	116.6(2)
C(4)-C(5)-C(6)	121.3(3)
N(2)-C(6)-C(5)	114.2(2)
C(6)-N(2)-C(7)	112.4(2)
C(6)-N(2)-Hg(1)	110.61(17)
C(7)-N(2)-Hg(1)	109.96(16)
N(2)-C(7)-C(8)	112.0(2)
C(9)-C(8)-C(13)	121.6(3)
C(9)-C(8)-C(7)	120.1(3)
C(13)-C(8)-C(7)	118.2(2)
C(10)-C(9)-C(8)	120.7(3)
C(9)-C(10)-C(11)	120.1(3)
C(9)-C(10)-I(1)	119.8(2)
C(11)-C(10)-I(1)	120.0(2)
C(12)-C(11)-C(10)	118.6(3)
C(11)-C(12)-C(13)	124.5(3)
C(11)-C(12)-I(2)	119.0(2)
C(13)-C(12)-I(2)	116.5(2)
O(1)-C(13)-C(12)	123.5(3)
O(1)-C(13)-C(8)	122.2(3)
C(12)-C(13)-C(8)	114.3(2)
C(13)-O(1)-Hg(1)	103.89(15)
O(2)-S(1)-C(15)	105.92(15)
O(2)-S(1)-C(14)	107.61(14)

C(15)-S(1)-C(14)	95.48(18)
O(3)-S(2)-C(16)	106.34(16)
O(3)-S(2)-C(17)	105.60(16)
C(16)-S(2)-C(17)	97.48(17)

Symmetry transformations used to generate equivalent atoms:
#1 -x+1,-y+1,-z+1

Table D.6.5.2.3 Anisotropic displacement parameters (A^2 x 10^3) for **3**.
The anisotropic displacement factor exponent takes the form:
-2 pi^2 [h^2 a*^2 U11 + ... + 2 h k a* b* U12]

	U11	U22	U33	U23	U13	U12
Hg(1)	16(1)	21(1)	15(1)	-8(1)	1(1)	-8(1)
I(1)	23(1)	22(1)	34(1)	-12(1)	3(1)	-12(1)
I(2)	30(1)	27(1)	15(1)	-7(1)	1(1)	-13(1)
N(1)	25(1)	20(1)	15(1)	-5(1)	0(1)	-9(1)
C(1)	33(2)	23(2)	22(2)	-3(1)	-1(1)	-13(1)
C(2)	36(2)	16(1)	29(2)	-5(1)	-7(1)	-9(1)
C(3)	25(2)	20(2)	32(2)	-12(1)	-7(1)	-2(1)
C(4)	22(2)	23(2)	19(2)	-8(1)	-2(1)	-5(1)
C(5)	18(1)	17(1)	16(1)	-7(1)	-3(1)	-3(1)
C(6)	23(2)	18(1)	15(1)	-7(1)	2(1)	-9(1)
N(2)	20(1)	13(1)	15(1)	-3(1)	0(1)	-5(1)
C(7)	18(1)	20(1)	14(1)	-9(1)	1(1)	-6(1)
C(8)	14(1)	17(1)	17(1)	-6(1)	-1(1)	-2(1)
C(9)	14(1)	19(1)	19(2)	-6(1)	0(1)	-5(1)
C(10)	16(1)	18(1)	27(2)	-7(1)	-2(1)	-5(1)
C(11)	18(2)	19(1)	20(2)	-8(1)	-3(1)	-3(1)
C(12)	17(1)	20(1)	12(1)	-4(1)	-2(1)	-4(1)
C(13)	14(1)	15(1)	16(1)	-2(1)	-5(1)	-2(1)
O(1)	22(1)	18(1)	17(1)	-2(1)	-3(1)	-8(1)
S(1)	29(1)	16(1)	24(1)	-2(1)	-4(1)	-7(1)
O(2)	23(1)	16(1)	27(1)	-2(1)	-3(1)	-5(1)
C(14)	40(2)	26(2)	29(2)	-11(1)	-11(2)	-6(2)
C(15)	30(2)	52(2)	41(2)	-26(2)	-11(2)	7(2)
S(2)	27(1)	31(1)	28(1)	-1(1)	-1(1)	-4(1)
O(3)	34(1)	36(1)	36(2)	6(1)	-15(1)	-1(1)
C(16)	31(2)	28(2)	37(2)	-2(2)	-11(2)	-7(1)
C(17)	31(2)	31(2)	41(2)	-5(2)	-3(2)	-9(2)

Table D.6.5.2.4 Hydrogen coordinates (x 10^4) and isotropic displacement parameters (A^2 x 10^3) for **3**.

	x	y	z	U(eq)
H(1)	4864	8389	4930	30
H(2)	3991	10053	6050	32
H(3)	2795	9610	7820	31
H(4)	2483	7497	8383	26
H(6A)	4186	4779	7918	21
H(6B)	2564	5395	7777	21
H(2A)	3599	3793	6601	19
H(7A)	1821	6188	5249	20
H(7B)	1346	5082	6181	20
H(9)	1102	3214	5504	21
H(11)	1831	2826	1958	23
H(14A)	6020	2573	8516	39
H(14B)	6471	1348	9696	39
H(14C)	4989	2444	9591	39
H(15A)	6422	-257	7055	51
H(15B)	7308	-205	8207	51
H(15C)	6809	1066	7072	51
H(16A)	308	1445	7403	40
H(16B)	-1193	2312	7674	40
H(16C)	-644	726	8224	40
H(17A)	1262	3468	9279	42
H(17B)	126	3887	8172	42
H(17C)	1586	2816	8085	42

Table D.6.5.2.5 Torsion angles [deg] for **3**.

N(2)#1-Hg(1)-N(1)-C(5)	-164.42(18)
N(2)-Hg(1)-N(1)-C(5)	15.58(18)
N(1)#1-Hg(1)-N(1)-C(5)	-32(100)
O(1)#1-Hg(1)-N(1)-C(5)	-79.51(19)
O(1)-Hg(1)-N(1)-C(5)	100.49(19)
N(2)#1-Hg(1)-N(1)-C(1)	15.9(3)
N(2)-Hg(1)-N(1)-C(1)	-164.1(3)
N(1)#1-Hg(1)-N(1)-C(1)	148(100)
O(1)#1-Hg(1)-N(1)-C(1)	100.8(3)
O(1)-Hg(1)-N(1)-C(1)	-79.2(3)
C(5)-N(1)-C(1)-C(2)	0.6(5)
Hg(1)-N(1)-C(1)-C(2)	-179.8(2)
N(1)-C(1)-C(2)-C(3)	0.2(5)
C(1)-C(2)-C(3)-C(4)	-0.7(5)
C(2)-C(3)-C(4)-C(5)	0.4(4)
C(1)-N(1)-C(5)-C(4)	-0.8(4)
Hg(1)-N(1)-C(5)-C(4)	179.5(2)
C(1)-N(1)-C(5)-C(6)	-177.3(3)
Hg(1)-N(1)-C(5)-C(6)	3.0(3)
C(3)-C(4)-C(5)-N(1)	0.3(4)
C(3)-C(4)-C(5)-C(6)	176.7(3)

N(1)-C(5)-C(6)-N(2)	-31.5(4)
C(4)-C(5)-C(6)-N(2)	152.0(3)
C(5)-C(6)-N(2)-C(7)	-78.2(3)
C(5)-C(6)-N(2)-Hg(1)	45.2(3)
N(2)#1-Hg(1)-N(2)-C(6)	-166(100)
N(1)-Hg(1)-N(2)-C(6)	-30.91(16)
N(1)#1-Hg(1)-N(2)-C(6)	149.09(16)
O(1)#1-Hg(1)-N(2)-C(6)	51.34(17)
O(1)-Hg(1)-N(2)-C(6)	-128.66(17)
N(2)#1-Hg(1)-N(2)-C(7)	-42(100)
N(1)-Hg(1)-N(2)-C(7)	93.83(18)
N(1)#1-Hg(1)-N(2)-C(7)	-86.17(18)
O(1)#1-Hg(1)-N(2)-C(7)	176.08(17)
O(1)-Hg(1)-N(2)-C(7)	-3.92(17)
C(6)-N(2)-C(7)-C(8)	-177.2(2)
Hg(1)-N(2)-C(7)-C(8)	59.1(3)
N(2)-C(7)-C(8)-C(9)	100.7(3)
N(2)-C(7)-C(8)-C(13)	-80.0(3)
C(13)-C(8)-C(9)-C(10)	-1.4(4)
C(7)-C(8)-C(9)-C(10)	177.9(2)
C(8)-C(9)-C(10)-C(11)	-0.9(4)
C(8)-C(9)-C(10)-I(1)	-178.0(2)
C(9)-C(10)-C(11)-C(12)	1.7(4)
I(1)-C(10)-C(11)-C(12)	178.9(2)
C(10)-C(11)-C(12)-C(13)	-0.3(4)
C(10)-C(11)-C(12)-I(2)	-179.8(2)
C(11)-C(12)-C(13)-O(1)	178.9(3)
I(2)-C(12)-C(13)-O(1)	-1.6(3)
C(11)-C(12)-C(13)-C(8)	-1.8(4)
I(2)-C(12)-C(13)-C(8)	177.68(18)
C(9)-C(8)-C(13)-O(1)	-178.0(2)
C(7)-C(8)-C(13)-O(1)	2.6(4)
C(9)-C(8)-C(13)-C(12)	2.7(4)
C(7)-C(8)-C(13)-C(12)	-176.7(2)
C(12)-C(13)-O(1)-Hg(1)	-124.2(2)
C(8)-C(13)-O(1)-Hg(1)	56.6(3)
N(2)#1-Hg(1)-O(1)-C(13)	128.95(18)
N(2)-Hg(1)-O(1)-C(13)	-51.05(18)
N(1)-Hg(1)-O(1)-C(13)	-122.99(17)
N(1)#1-Hg(1)-O(1)-C(13)	57.01(17)
O(1)#1-Hg(1)-O(1)-C(13)	69(100)

Symmetry transformations used to generate equivalent atoms:
#1 -x+1,-y+1,-z+1

Table D.6.5.2.6 Hydrogen bonds for **3** [A and deg.].

Hydrogen bonds with H..A < r(A) + 2.000 Angstroms and <DHA > 110 deg.

D-H	d(D-H)	d(H..A)	<DHA	d(D..A)	A
N2-H2A	0.930	1.911	176.84	2.840	O2

Least-squares planes (x,y,z in crystal coordinates) and deviations from them (* indicates atom used to define plane)

```
 8.1882 (0.0081) x + 0.3929 (0.0136) y + 5.7482 (0.0118) z = 7.1494 (0.0147)

*    0.0044 (0.0019)  N1
*   -0.0010 (0.0022)  C1
*   -0.0031 (0.0022)  C2
*    0.0040 (0.0021)  C3
*   -0.0008 (0.0021)  C4
*   -0.0034 (0.0020)  C5
     0.0668 (0.0048)  C6
     0.0153 (0.0048)  Hg1
    -0.5669 (0.0052)  N2
```

Rms deviation of fitted atoms = 0.0031

```
 7.3811 (0.0080) x - 3.9666 (0.0109) y + 2.0290 (0.0119) z = 0.6539 (0.0078)
```

Angle to previous plane (with approximate esd) = 27.92 (0.14)

```
*   -0.0132 (0.0019)  C8
*    0.0002 (0.0019)  C9
*    0.0113 (0.0019)  C10
*   -0.0090 (0.0019)  C11
*   -0.0041 (0.0019)  C12
*    0.0147 (0.0018)  C13
    -0.0727 (0.0043)  C7
     0.0402 (0.0037)  O1
     2.0679 (0.0040)  Hg1
```

Rms deviation of fitted atoms = 0.0101

Crystal Structure Data for Complex 5

Table D.6.5.2.7 Atomic coordinates (x 10^4) and equivalent isotropic displacement parameters (A^2 x 10^3) for **5**. U(eq) is defined as one third of the trace of the orthogonalized Uij tensor.

	x	y	z	U(eq)
I(1)	4318(1)	2107(1)	7919(1)	24(1)
I(2)	-3230(1)	-769(1)	5830(1)	23(1)
Sn(1)	-1840(1)	-4119(1)	7998(1)	13(1)
N(1)	-218(3)	-3743(2)	6749(2)	15(1)
C(1)	-959(4)	-3690(3)	5620(2)	17(1)
C(2)	71(4)	-3212(3)	4931(3)	22(1)
C(3)	1878(4)	-2766(3)	5415(3)	24(1)
C(4)	2633(4)	-2807(3)	6582(3)	21(1)
C(5)	1536(4)	-3313(3)	7233(3)	17(1)
C(6)	2253(4)	-3458(3)	8487(3)	19(1)
N(2)	912(3)	-3276(2)	9185(2)	16(1)
C(7)	1039(4)	-1819(3)	9815(2)	19(1)
C(8)	852(4)	-929(3)	8937(2)	16(1)
C(9)	2282(4)	36(3)	8924(2)	19(1)
C(10)	2130(4)	756(3)	8035(2)	18(1)
C(11)	542(4)	537(3)	7168(3)	19(1)
C(12)	-905(4)	-414(3)	7188(2)	16(1)
C(13)	-784(4)	-1179(3)	8062(2)	15(1)
O(1)	-2151(3)	-2133(2)	8055(2)	16(1)
Cl(4)	-1029(1)	-6343(1)	7942(1)	19(1)
Cl(5)	-4489(1)	-5014(1)	6495(1)	23(1)
Cl(6)	-3034(1)	-4176(1)	9641(1)	20(1)

Table D.6.5.2.8 Bond lengths [A] and angles [deg] for **5**.

I(1)-C(10)	2.092(3)
I(2)-C(12)	2.079(3)
Sn(1)-O(1)	2.0564(18)
Sn(1)-N(1)	2.215(2)
Sn(1)-N(2)	2.243(2)
Sn(1)-Cl(5)	2.3479(7)
Sn(1)-Cl(6)	2.3561(7)
Sn(1)-Cl(4)	2.4227(7)
N(1)-C(5)	1.340(4)
N(1)-C(1)	1.351(4)
C(1)-C(2)	1.379(4)
C(2)-C(3)	1.377(5)
C(3)-C(4)	1.390(4)
C(4)-C(5)	1.391(4)
C(5)-C(6)	1.513(4)
C(6)-N(2)	1.489(4)
N(2)-C(7)	1.505(4)
C(7)-C(8)	1.503(4)
C(8)-C(9)	1.389(4)
C(8)-C(13)	1.413(4)

C(9)-C(10)	1.389(4)
C(10)-C(11)	1.384(4)
C(11)-C(12)	1.393(4)
C(12)-C(13)	1.407(4)
C(13)-O(1)	1.339(3)
O(1)-Sn(1)-N(1)	83.87(8)
O(1)-Sn(1)-N(2)	87.27(8)
N(1)-Sn(1)-N(2)	76.41(9)
O(1)-Sn(1)-Cl(5)	93.22(6)
N(1)-Sn(1)-Cl(5)	94.14(7)
N(2)-Sn(1)-Cl(5)	170.44(6)
O(1)-Sn(1)-Cl(6)	91.50(6)
N(1)-Sn(1)-Cl(6)	167.24(6)
N(2)-Sn(1)-Cl(6)	91.54(6)
Cl(5)-Sn(1)-Cl(6)	97.99(3)
O(1)-Sn(1)-Cl(4)	171.76(6)
N(1)-Sn(1)-Cl(4)	90.00(6)
N(2)-Sn(1)-Cl(4)	85.94(6)
Cl(5)-Sn(1)-Cl(4)	92.70(3)
Cl(6)-Sn(1)-Cl(4)	93.34(2)
C(5)-N(1)-C(1)	120.6(2)
C(5)-N(1)-Sn(1)	115.79(18)
C(1)-N(1)-Sn(1)	122.4(2)
N(1)-C(1)-C(2)	121.1(3)
C(3)-C(2)-C(1)	119.0(3)
C(2)-C(3)-C(4)	119.8(3)
C(3)-C(4)-C(5)	118.8(3)
N(1)-C(5)-C(4)	120.7(3)
N(1)-C(5)-C(6)	116.8(2)
C(4)-C(5)-C(6)	122.5(3)
N(2)-C(6)-C(5)	110.9(2)
C(6)-N(2)-C(7)	113.7(2)
C(6)-N(2)-Sn(1)	109.63(17)
C(7)-N(2)-Sn(1)	110.29(17)
C(8)-C(7)-N(2)	110.0(2)
C(9)-C(8)-C(13)	120.8(2)
C(9)-C(8)-C(7)	121.2(3)
C(13)-C(8)-C(7)	117.8(2)
C(8)-C(9)-C(10)	120.3(3)
C(11)-C(10)-C(9)	120.2(3)
C(11)-C(10)-I(1)	118.6(2)
C(9)-C(10)-I(1)	121.1(2)
C(10)-C(11)-C(12)	119.7(3)
C(11)-C(12)-C(13)	121.4(3)
C(11)-C(12)-I(2)	118.4(2)
C(13)-C(12)-I(2)	120.0(2)
O(1)-C(13)-C(12)	121.5(2)
O(1)-C(13)-C(8)	121.0(2)
C(12)-C(13)-C(8)	117.5(2)
C(13)-O(1)-Sn(1)	120.51(17)

Symmetry transformations used to generate equivalent atoms.

Table D.6.5.2.9 Anisotropic displacement parameters (A^2 x 10^3) for 5.
The anisotropic displacement factor exponent takes the form:
-2 pi^2 [h^2 a*^2 U11 + ... + 2 h k a* b* U12]

	U11	U22	U33	U23	U13	U12
I(1)	25(1)	22(1)	23(1)	5(1)	7(1)	-7(1)
I(2)	18(1)	23(1)	27(1)	13(1)	-2(1)	3(1)
Sn(1)	13(1)	13(1)	14(1)	6(1)	3(1)	0(1)
N(1)	19(1)	12(1)	18(1)	6(1)	6(1)	4(1)
C(1)	23(2)	14(1)	17(1)	6(1)	5(1)	5(1)
C(2)	34(2)	16(1)	19(1)	7(1)	9(1)	8(1)
C(3)	30(2)	20(1)	29(2)	11(1)	18(1)	5(1)
C(4)	20(2)	17(1)	29(2)	8(1)	11(1)	4(1)
C(5)	17(1)	13(1)	22(1)	7(1)	7(1)	4(1)
C(6)	13(1)	23(1)	23(1)	11(1)	3(1)	3(1)
N(2)	16(1)	17(1)	16(1)	7(1)	3(1)	2(1)
C(7)	21(2)	16(1)	17(1)	6(1)	0(1)	-1(1)
C(8)	17(1)	13(1)	16(1)	5(1)	2(1)	1(1)
C(9)	18(1)	17(1)	18(1)	3(1)	0(1)	-1(1)
C(10)	18(1)	13(1)	20(1)	5(1)	5(1)	-1(1)
C(11)	25(2)	12(1)	21(1)	8(1)	6(1)	3(1)
C(12)	16(1)	14(1)	18(1)	6(1)	2(1)	4(1)
C(13)	15(1)	13(1)	17(1)	4(1)	4(1)	1(1)
O(1)	14(1)	13(1)	23(1)	8(1)	5(1)	1(1)
Cl(4)	23(1)	15(1)	20(1)	9(1)	6(1)	5(1)
Cl(5)	19(1)	23(1)	22(1)	8(1)	-2(1)	-2(1)
Cl(6)	21(1)	22(1)	19(1)	8(1)	8(1)	2(1)

Table D.6.5.2.10 Hydrogen coordinates (x 10^4) and isotropic displacement parameters (A^2 x 10^3) for **5**.

	x	y	z	U(eq)
H(1)	-116	-4653	6539	18
H(1A)	-2209	-3985	5296	21
H(2)	-458	-3192	4134	26
H(3)	2605	-2431	4953	28
H(4)	3876	-2495	6928	25
H(6A)	2562	-4374	8466	23
H(6B)	3353	-2767	8878	23
H(7A)	86	-1763	10235	22
H(7B)	2205	-1495	10412	22
H(9)	3367	205	9526	23
H(11)	439	1032	6562	22

Table D.6.5.2.11 Torsion angles [deg] for **5**.

O(1)-Sn(1)-N(1)-C(5)	92.88(19)
N(2)-Sn(1)-N(1)-C(5)	4.21(18)
Cl(5)-Sn(1)-N(1)-C(5)	-174.32(18)
Cl(6)-Sn(1)-N(1)-C(5)	23.7(4)
Cl(4)-Sn(1)-N(1)-C(5)	-81.61(18)
O(1)-Sn(1)-N(1)-C(1)	-74.7(2)
N(2)-Sn(1)-N(1)-C(1)	-163.4(2)
Cl(5)-Sn(1)-N(1)-C(1)	18.1(2)
Cl(6)-Sn(1)-N(1)-C(1)	-143.9(2)
Cl(4)-Sn(1)-N(1)-C(1)	110.8(2)
C(5)-N(1)-C(1)-C(2)	1.1(4)
Sn(1)-N(1)-C(1)-C(2)	168.1(2)
N(1)-C(1)-C(2)-C(3)	-1.0(4)
C(1)-C(2)-C(3)-C(4)	0.2(4)
C(2)-C(3)-C(4)-C(5)	0.5(4)
C(1)-N(1)-C(5)-C(4)	-0.3(4)
Sn(1)-N(1)-C(5)-C(4)	-168.1(2)
C(1)-N(1)-C(5)-C(6)	-177.9(2)
Sn(1)-N(1)-C(5)-C(6)	14.3(3)
C(3)-C(4)-C(5)-N(1)	-0.5(4)
C(3)-C(4)-C(5)-C(6)	177.0(3)
N(1)-C(5)-C(6)-N(2)	-33.2(3)
C(4)-C(5)-C(6)-N(2)	149.2(3)
C(5)-C(6)-N(2)-C(7)	-89.6(3)
C(5)-C(6)-N(2)-Sn(1)	34.4(3)
O(1)-Sn(1)-N(2)-C(6)	-105.54(17)
N(1)-Sn(1)-N(2)-C(6)	-21.19(17)
Cl(5)-Sn(1)-N(2)-C(6)	-12.3(5)
Cl(6)-Sn(1)-N(2)-C(6)	163.03(16)
Cl(4)-Sn(1)-N(2)-C(6)	69.79(16)
O(1)-Sn(1)-N(2)-C(7)	20.37(17)
N(1)-Sn(1)-N(2)-C(7)	104.72(17)
Cl(5)-Sn(1)-N(2)-C(7)	113.6(4)
Cl(6)-Sn(1)-N(2)-C(7)	-71.06(16)
Cl(4)-Sn(1)-N(2)-C(7)	-164.30(16)
C(6)-N(2)-C(7)-C(8)	57.1(3)
Sn(1)-N(2)-C(7)-C(8)	-66.5(2)
N(2)-C(7)-C(8)-C(9)	-111.5(3)
N(2)-C(7)-C(8)-C(13)	63.6(3)
C(13)-C(8)-C(9)-C(10)	-1.1(4)
C(7)-C(8)-C(9)-C(10)	173.8(3)
C(8)-C(9)-C(10)-C(11)	1.3(4)
C(8)-C(9)-C(10)-I(1)	-175.3(2)
C(9)-C(10)-C(11)-C(12)	-0.3(4)
I(1)-C(10)-C(11)-C(12)	176.5(2)
C(10)-C(11)-C(12)-C(13)	-1.0(4)
C(10)-C(11)-C(12)-I(2)	-177.5(2)
C(11)-C(12)-C(13)-O(1)	-177.3(2)
I(2)-C(12)-C(13)-O(1)	-0.9(4)
C(11)-C(12)-C(13)-C(8)	1.2(4)
I(2)-C(12)-C(13)-C(8)	177.65(19)
C(9)-C(8)-C(13)-O(1)	178.4(2)
C(7)-C(8)-C(13)-O(1)	3.3(4)
C(9)-C(8)-C(13)-C(12)	-0.2(4)
C(7)-C(8)-C(13)-C(12)	-175.2(2)
C(12)-C(13)-O(1)-Sn(1)	122.5(2)
C(8)-C(13)-O(1)-Sn(1)	-56.0(3)
N(1)-Sn(1)-O(1)-C(13)	-39.33(19)
N(2)-Sn(1)-O(1)-C(13)	37.28(19)
Cl(5)-Sn(1)-O(1)-C(13)	-133.16(19)

Cl(6)-Sn(1)-O(1)-C(13)	128.75(19)
Cl(4)-Sn(1)-O(1)-C(13)	2.8(5)

Symmetry transformations used to generate equivalent atoms:

Table D.6.5.2.12 Hydrogen bonds for **5** [A and deg.].

Hydrogen bonds with H..A < r(A) + 2.000 Angstroms and <DHA > 110 deg.

D-H	d(D-H)	d(H..A)	<DHA	d(D..A)	A
N1-H1	0.930	2.746	117.64	3.283	Cl4

APPENDIX E

Permission/License Agreements for Copyrighted Material

ELSEVIER LICENSE
TERMS AND CONDITIONS

Jul 13, 2014

This is a License Agreement between Dajena Tomco ("You") and Elsevier ("Elsevier") provided by Copyright Clearance Center ("CCC"). The license consists of your order details, the terms and conditions provided by Elsevier, and the payment terms and conditions.

All payments must be made in full to CCC. For payment instructions, please see information listed at the bottom of this form.

Supplier	Elsevier Limited The Boulevard,Langford Lane Kidlington,Oxford,OX5 1GB,UK
Registered Company Number	1982084
Customer name	Dajena Tomco
Customer address	40425 Aynesley st CLINTON TOWNSHIP, MI 48038
License number	3405961257720
License date	Jun 11, 2014
Licensed content publisher	Elsevier
Licensed content publication	Journal of Inorganic Biochemistry
Licensed content title	Effects of tethered ligands and of metal oxidation state on the interactions of cobalt complexes with the 26S proteasome
Licensed content author	Dajena Tomco,Sara Schmitt,Bashar Ksebati,Mary Jane Heeg,Q. Ping Dou,Cláudio N. Verani
Licensed content date	December 2011
Licensed content volume number	105
Licensed content issue number	12
Number of pages	8
Start Page	1759
End Page	1766

Type of Use	reuse in a thesis/dissertation
Portion	full article
Format	both print and electronic
Are you the author of this Elsevier article?	Yes
Will you be translating?	No
Title of your thesis/dissertation	Proteasome Inhibition by Metal Complexes as a New Route for anticancer therapy
Expected completion date	Sep 2014
Estimated size (number of pages)	300
Elsevier VAT number	GB 494 6272 12
Permissions price	0.00 USD
VAT/Local Sales Tax	0.00 USD / 0.00 GBP
Total	0.00 USD
Terms and Conditions	

INTRODUCTION

1. The publisher for this copyrighted material is Elsevier. By clicking "accept" in connection with completing this licensing transaction, you agree that the following terms and conditions apply to this transaction (along with the Billing and Payment terms and conditions established by Copyright Clearance Center, Inc. ("CCC"), at the time that you opened your Rightslink account and that are available at any time at http://myaccount.copyright.com).

GENERAL TERMS

2. Elsevier hereby grants you permission to reproduce the aforementioned material subject to the terms and conditions indicated.

3. Acknowledgement: If any part of the material to be used (for example, figures) has appeared in our publication with credit or acknowledgement to another source, permission must also be sought from that source. If such permission is not obtained then that material may not be included in your publication/copies. Suitable acknowledgement to the source must be made, either as a footnote or in a reference list at the end of your publication, as follows:

"Reprinted from Publication title, Vol /edition number, Author(s), Title of article / title of chapter, Pages No., Copyright (Year), with permission from Elsevier [OR APPLICABLE SOCIETY COPYRIGHT OWNER]." Also Lancet special credit - "Reprinted from The Lancet, Vol. number, Author(s), Title of article, Pages No., Copyright (Year), with permission from Elsevier."

4. Reproduction of this material is confined to the purpose and/or media for which permission is hereby given.

5. Altering/Modifying Material: Not Permitted. However figures and illustrations may be altered/adapted minimally to serve your work. Any other abbreviations, additions, deletions and/or any other alterations shall be made only with prior written authorization of Elsevier Ltd. (Please contact Elsevier at permissions@elsevier.com)

6. If the permission fee for the requested use of our material is waived in this instance, please be advised that your future requests for Elsevier materials may attract a fee.

7. Reservation of Rights: Publisher reserves all rights not specifically granted in the combination of (i) the license details provided by you and accepted in the course of this licensing transaction, (ii) these terms and conditions and (iii) CCC's Billing and Payment terms and conditions.

8. License Contingent Upon Payment: While you may exercise the rights licensed immediately upon issuance of the license at the end of the licensing process for the transaction, provided that you have disclosed complete and accurate details of your proposed use, no license is finally effective unless and until full payment is received from you (either by publisher or by CCC) as provided in CCC's Billing and Payment terms and conditions. If full payment is not received on a timely basis, then any license preliminarily granted shall be deemed automatically revoked and shall be void as if never granted. Further, in the event that you breach any of these terms and conditions or any of CCC's Billing and Payment terms and conditions, the license is automatically revoked and shall be void as if never granted. Use of materials as described in a revoked license, as well as any use of the materials beyond the scope of an unrevoked license, may constitute copyright infringement and publisher reserves the right to take any and all action to protect its copyright in the materials.

9. Warranties: Publisher makes no representations or warranties with respect to the licensed material.

10. Indemnity: You hereby indemnify and agree to hold harmless publisher and CCC, and their respective officers, directors, employees and agents, from and against any and all claims arising out of your use of the licensed material other than as specifically authorized pursuant to this license.

11. No Transfer of License: This license is personal to you and may not be sublicensed, assigned, or transferred by you to any other person without publisher's written permission.

12. No Amendment Except in Writing: This license may not be amended except in a writing signed by both parties (or, in the case of publisher, by CCC on publisher's behalf).

13. Objection to Contrary Terms: Publisher hereby objects to any terms contained in any purchase order, acknowledgment, check endorsement or other writing prepared by you,

which terms are inconsistent with these terms and conditions or CCC's Billing and Payment terms and conditions. These terms and conditions, together with CCC's Billing and Payment terms and conditions (which are incorporated herein), comprise the entire agreement between you and publisher (and CCC) concerning this licensing transaction. In the event of any conflict between your obligations established by these terms and conditions and those established by CCC's Billing and Payment terms and conditions, these terms and conditions shall control.

14. Revocation: Elsevier or Copyright Clearance Center may deny the permissions described in this License at their sole discretion, for any reason or no reason, with a full refund payable to you. Notice of such denial will be made using the contact information provided by you. Failure to receive such notice will not alter or invalidate the denial. In no event will Elsevier or Copyright Clearance Center be responsible or liable for any costs, expenses or damage incurred by you as a result of a denial of your permission request, other than a refund of the amount(s) paid by you to Elsevier and/or Copyright Clearance Center for denied permissions.

LIMITED LICENSE

The following terms and conditions apply only to specific license types:

15. **Translation**: This permission is granted for non-exclusive world **English** rights only unless your license was granted for translation rights. If you licensed translation rights you may only translate this content into the languages you requested. A professional translator must perform all translations and reproduce the content word for word preserving the integrity of the article. If this license is to re-use 1 or 2 figures then permission is granted for non-exclusive world rights in all languages.

16. **Posting licensed content on any Website**: The following terms and conditions apply as follows: Licensing material from an Elsevier journal: All content posted to the web site must maintain the copyright information line on the bottom of each image; A hyper-text must be included to the Homepage of the journal from which you are licensing at http://www.sciencedirect.com/science/journal/xxxxx or the Elsevier homepage for books at http://www.elsevier.com; Central Storage: This license does not include permission for a scanned version of the material to be stored in a central repository such as that provided by Heron/XanEdu.

Licensing material from an Elsevier book: A hyper-text link must be included to the Elsevier homepage at http://www.elsevier.com . All content posted to the web site must maintain the copyright information line on the bottom of each image.

Posting licensed content on Electronic reserve: In addition to the above the following clauses are applicable: The web site must be password-protected and made available only to bona fide students registered on a relevant course. This permission is granted for 1 year

only. You may obtain a new license for future website posting.

For journal authors: the following clauses are applicable in addition to the above: Permission granted is limited to the author accepted manuscript version* of your paper.

***Accepted Author Manuscript (AAM) Definition:** An accepted author manuscript (AAM) is the author's version of the manuscript of an article that has been accepted for publication and which may include any author-incorporated changes suggested through the processes of submission processing, peer review, and editor-author communications. AAMs do not include other publisher value-added contributions such as copy-editing, formatting, technical enhancements and (if relevant) pagination.

You are not allowed to download and post the published journal article (whether PDF or HTML, proof or final version), nor may you scan the printed edition to create an electronic version. A hyper-text must be included to the Homepage of the journal from which you are licensing at http://www.sciencedirect.com/science/journal/xxxxx. As part of our normal production process, you will receive an e-mail notice when your article appears on Elsevier's online service ScienceDirect (www.sciencedirect.com). That e-mail will include the article's Digital Object Identifier (DOI). This number provides the electronic link to the published article and should be included in the posting of your personal version. We ask that you wait until you receive this e-mail and have the DOI to do any posting.

Posting to a repository: Authors may post their AAM immediately to their employer's institutional repository for internal use only and may make their manuscript publically available after the journal-specific embargo period has ended.

Please also refer to Elsevier's Article Posting Policy for further information.

18. **For book authors** the following clauses are applicable in addition to the above: Authors are permitted to place a brief summary of their work online only.. You are not allowed to download and post the published electronic version of your chapter, nor may you scan the printed edition to create an electronic version. **Posting to a repository:** Authors are permitted to post a summary of their chapter only in their institution's repository.

20. **Thesis/Dissertation**: If your license is for use in a thesis/dissertation your thesis may be submitted to your institution in either print or electronic form. Should your thesis be published commercially, please reapply for permission. These requirements include permission for the Library and Archives of Canada to supply single copies, on demand, of the complete thesis and include permission for UMI to supply single copies, on demand, of the complete thesis. Should your thesis be published commercially, please reapply for permission.

Elsevier Open Access Terms and Conditions

Elsevier publishes Open Access articles in both its Open Access journals and via its Open Access articles option in subscription journals.

Authors publishing in an Open Access journal or who choose to make their article Open Access in an Elsevier subscription journal select one of the following Creative Commons user licenses, which define how a reader may reuse their work: Creative Commons Attribution License (CC BY), Creative Commons Attribution – Non Commercial - ShareAlike (CC BY NC SA) and Creative Commons Attribution – Non Commercial – No Derivatives (CC BY NC ND)

Terms & Conditions applicable to all Elsevier Open Access articles:

Any reuse of the article must not represent the author as endorsing the adaptation of the article nor should the article be modified in such a way as to damage the author's honour or reputation.

The author(s) must be appropriately credited.

If any part of the material to be used (for example, figures) has appeared in our publication with credit or acknowledgement to another source it is the responsibility of the user to ensure their reuse complies with the terms and conditions determined by the rights holder.

Additional Terms & Conditions applicable to each Creative Commons user license:

CC BY: You may distribute and copy the article, create extracts, abstracts, and other revised versions, adaptations or derivative works of or from an article (such as a translation), to include in a collective work (such as an anthology), to text or data mine the article, including for commercial purposes without permission from Elsevier

CC BY NC SA: For non-commercial purposes you may distribute and copy the article, create extracts, abstracts and other revised versions, adaptations or derivative works of or from an article (such as a translation), to include in a collective work (such as an anthology), to text and data mine the article and license new adaptations or creations under identical terms without permission from Elsevier

CC BY NC ND: For non-commercial purposes you may distribute and copy the article and include it in a collective work (such as an anthology), provided you do not alter or modify the article, without permission from Elsevier

Any commercial reuse of Open Access articles published with a CC BY NC SA or CC BY NC ND license requires permission from Elsevier and will be subject to a fee.

Commercial reuse includes:

- Promotional purposes (advertising or marketing)
- Commercial exploitation (e.g. a product for sale or loan)
- Systematic distribution (for a fee or free of charge)

Please refer to Elsevier's Open Access Policy for further information.

21. **Other Conditions**:

v1.7

If you would like to pay for this license now, please remit this license along with your payment made payable to "COPYRIGHT CLEARANCE CENTER" otherwise you will be invoiced within 48 hours of the license date. Payment should be in the form of a check or money order referencing your account number and this invoice number 501325635. Once you receive your invoice for this order, you may pay your invoice by credit card. Please follow instructions provided at that time.

Make Payment To:
Copyright Clearance Center
Dept 001
P.O. Box 843006
Boston, MA 02284-3006

For suggestions or comments regarding this order, contact RightsLink Customer Support: customercare@copyright.com or +1-877-622-5543 (toll free in the US) or +1-978-646-2777.

Gratis licenses (referencing $0 in the Total field) are free. Please retain this printable license for your reference. No payment is required.

ELSEVIER LICENSE
TERMS AND CONDITIONS

Jul 13, 2014

This is a License Agreement between Dajena Tomco ("You") and Elsevier ("Elsevier") provided by Copyright Clearance Center ("CCC"). The license consists of your order details, the terms and conditions provided by Elsevier, and the payment terms and conditions.

All payments must be made in full to CCC. For payment instructions, please see information listed at the bottom of this form.

Supplier	Elsevier Limited The Boulevard,Langford Lane Kidlington,Oxford,OX5 1GB,UK
Registered Company Number	1982084
Customer name	Dajena Tomco
Customer address	40425 Aynesley st CLINTON TOWNSHIP, MI 48038
License number	3405970365264
License date	Jun 11, 2014
Licensed content publisher	Elsevier
Licensed content publication	Inorganica Chimica Acta
Licensed content title	Probing chemical reduction in a cobalt(III) complex as a viable route for the inhibition of the 20S proteasome
Licensed content author	Dajena Tomco,Fernando R. Xavier,Marco M. Allard,Cláudio N. Verani
Licensed content date	1 December 2012
Licensed content volume number	393
Licensed content issue number	None
Number of pages	7
Start Page	269
End Page	275
Type of Use	reuse in a thesis/dissertation
Intended publisher of new work	other
Portion	full article
Format	both print and electronic

Are you the author of this Elsevier article?	Yes
Will you be translating?	No
Title of your thesis/dissertation	Proteasome Inhibition by Metal Complexes as a New Route for anticancer therapy
Expected completion date	Sep 2014
Estimated size (number of pages)	300
Elsevier VAT number	GB 494 6272 12
Permissions price	0.00 USD
VAT/Local Sales Tax	0.00 USD / 0.00 GBP
Total	0.00 USD
Terms and Conditions	

INTRODUCTION

1. The publisher for this copyrighted material is Elsevier. By clicking "accept" in connection with completing this licensing transaction, you agree that the following terms and conditions apply to this transaction (along with the Billing and Payment terms and conditions established by Copyright Clearance Center, Inc. ("CCC"), at the time that you opened your Rightslink account and that are available at any time at http://myaccount.copyright.com).

GENERAL TERMS

2. Elsevier hereby grants you permission to reproduce the aforementioned material subject to the terms and conditions indicated.

3. Acknowledgement: If any part of the material to be used (for example, figures) has appeared in our publication with credit or acknowledgement to another source, permission must also be sought from that source. If such permission is not obtained then that material may not be included in your publication/copies. Suitable acknowledgement to the source must be made, either as a footnote or in a reference list at the end of your publication, as follows:

"Reprinted from Publication title, Vol /edition number, Author(s), Title of article / title of chapter, Pages No., Copyright (Year), with permission from Elsevier [OR APPLICABLE SOCIETY COPYRIGHT OWNER]." Also Lancet special credit - "Reprinted from The Lancet, Vol. number, Author(s), Title of article, Pages No., Copyright (Year), with permission from Elsevier."

4. Reproduction of this material is confined to the purpose and/or media for which permission is hereby given.

5. Altering/Modifying Material: Not Permitted. However figures and illustrations may be

altered/adapted minimally to serve your work. Any other abbreviations, additions, deletions and/or any other alterations shall be made only with prior written authorization of Elsevier Ltd. (Please contact Elsevier at permissions@elsevier.com)

6. If the permission fee for the requested use of our material is waived in this instance, please be advised that your future requests for Elsevier materials may attract a fee.

7. Reservation of Rights: Publisher reserves all rights not specifically granted in the combination of (i) the license details provided by you and accepted in the course of this licensing transaction, (ii) these terms and conditions and (iii) CCC's Billing and Payment terms and conditions.

8. License Contingent Upon Payment: While you may exercise the rights licensed immediately upon issuance of the license at the end of the licensing process for the transaction, provided that you have disclosed complete and accurate details of your proposed use, no license is finally effective unless and until full payment is received from you (either by publisher or by CCC) as provided in CCC's Billing and Payment terms and conditions. If full payment is not received on a timely basis, then any license preliminarily granted shall be deemed automatically revoked and shall be void as if never granted. Further, in the event that you breach any of these terms and conditions or any of CCC's Billing and Payment terms and conditions, the license is automatically revoked and shall be void as if never granted. Use of materials as described in a revoked license, as well as any use of the materials beyond the scope of an unrevoked license, may constitute copyright infringement and publisher reserves the right to take any and all action to protect its copyright in the materials.

9. Warranties: Publisher makes no representations or warranties with respect to the licensed material.

10. Indemnity: You hereby indemnify and agree to hold harmless publisher and CCC, and their respective officers, directors, employees and agents, from and against any and all claims arising out of your use of the licensed material other than as specifically authorized pursuant to this license.

11. No Transfer of License: This license is personal to you and may not be sublicensed, assigned, or transferred by you to any other person without publisher's written permission.

12. No Amendment Except in Writing: This license may not be amended except in a writing signed by both parties (or, in the case of publisher, by CCC on publisher's behalf).

13. Objection to Contrary Terms: Publisher hereby objects to any terms contained in any purchase order, acknowledgment, check endorsement or other writing prepared by you, which terms are inconsistent with these terms and conditions or CCC's Billing and Payment terms and conditions. These terms and conditions, together with CCC's Billing and Payment terms and conditions (which are incorporated herein), comprise the entire agreement between you and publisher (and CCC) concerning this licensing transaction. In

the event of any conflict between your obligations established by these terms and conditions and those established by CCC's Billing and Payment terms and conditions, these terms and conditions shall control.

14. Revocation: Elsevier or Copyright Clearance Center may deny the permissions described in this License at their sole discretion, for any reason or no reason, with a full refund payable to you. Notice of such denial will be made using the contact information provided by you. Failure to receive such notice will not alter or invalidate the denial. In no event will Elsevier or Copyright Clearance Center be responsible or liable for any costs, expenses or damage incurred by you as a result of a denial of your permission request, other than a refund of the amount(s) paid by you to Elsevier and/or Copyright Clearance Center for denied permissions.

LIMITED LICENSE

The following terms and conditions apply only to specific license types:

15. **Translation**: This permission is granted for non-exclusive world **English** rights only unless your license was granted for translation rights. If you licensed translation rights you may only translate this content into the languages you requested. A professional translator must perform all translations and reproduce the content word for word preserving the integrity of the article. If this license is to re-use 1 or 2 figures then permission is granted for non-exclusive world rights in all languages.

16. **Posting licensed content on any Website**: The following terms and conditions apply as follows: Licensing material from an Elsevier journal: All content posted to the web site must maintain the copyright information line on the bottom of each image; A hyper-text must be included to the Homepage of the journal from which you are licensing at http://www.sciencedirect.com/science/journal/xxxxx or the Elsevier homepage for books at http://www.elsevier.com; Central Storage: This license does not include permission for a scanned version of the material to be stored in a central repository such as that provided by Heron/XanEdu.

Licensing material from an Elsevier book: A hyper-text link must be included to the Elsevier homepage at http://www.elsevier.com . All content posted to the web site must maintain the copyright information line on the bottom of each image.

Posting licensed content on Electronic reserve: In addition to the above the following clauses are applicable: The web site must be password-protected and made available only to bona fide students registered on a relevant course. This permission is granted for 1 year only. You may obtain a new license for future website posting.

For journal authors: the following clauses are applicable in addition to the above: Permission granted is limited to the author accepted manuscript version* of your paper.

***Accepted Author Manuscript (AAM) Definition:** An accepted author manuscript (AAM) is the author's version of the manuscript of an article that has been accepted for publication and which may include any author-incorporated changes suggested through the processes of submission processing, peer review, and editor-author communications. AAMs do not include other publisher value-added contributions such as copy-editing, formatting, technical enhancements and (if relevant) pagination.

You are not allowed to download and post the published journal article (whether PDF or HTML, proof or final version), nor may you scan the printed edition to create an electronic version. A hyper-text must be included to the Homepage of the journal from which you are licensing at http://www.sciencedirect.com/science/journal/xxxxx. As part of our normal production process, you will receive an e-mail notice when your article appears on Elsevier's online service ScienceDirect (www.sciencedirect.com). That e-mail will include the article's Digital Object Identifier (DOI). This number provides the electronic link to the published article and should be included in the posting of your personal version. We ask that you wait until you receive this e-mail and have the DOI to do any posting.

Posting to a repository: Authors may post their AAM immediately to their employer's institutional repository for internal use only and may make their manuscript publically available after the journal-specific embargo period has ended.

Please also refer to Elsevier's Article Posting Policy for further information.

18. **For book authors** the following clauses are applicable in addition to the above: Authors are permitted to place a brief summary of their work online only.. You are not allowed to download and post the published electronic version of your chapter, nor may you scan the printed edition to create an electronic version. **Posting to a repository:** Authors are permitted to post a summary of their chapter only in their institution's repository.

20. **Thesis/Dissertation**: If your license is for use in a thesis/dissertation your thesis may be submitted to your institution in either print or electronic form. Should your thesis be published commercially, please reapply for permission. These requirements include permission for the Library and Archives of Canada to supply single copies, on demand, of the complete thesis and include permission for UMI to supply single copies, on demand, of the complete thesis. Should your thesis be published commercially, please reapply for permission.

Elsevier Open Access Terms and Conditions

Elsevier publishes Open Access articles in both its Open Access journals and via its Open Access articles option in subscription journals.

Authors publishing in an Open Access journal or who choose to make their article Open

Access in an Elsevier subscription journal select one of the following Creative Commons user licenses, which define how a reader may reuse their work: Creative Commons Attribution License (CC BY), Creative Commons Attribution – Non Commercial - ShareAlike (CC BY NC SA) and Creative Commons Attribution – Non Commercial – No Derivatives (CC BY NC ND)

Terms & Conditions applicable to all Elsevier Open Access articles:

Any reuse of the article must not represent the author as endorsing the adaptation of the article nor should the article be modified in such a way as to damage the author's honour or reputation.

The author(s) must be appropriately credited.

If any part of the material to be used (for example, figures) has appeared in our publication with credit or acknowledgement to another source it is the responsibility of the user to ensure their reuse complies with the terms and conditions determined by the rights holder.

Additional Terms & Conditions applicable to each Creative Commons user license:

CC BY: You may distribute and copy the article, create extracts, abstracts, and other revised versions, adaptations or derivative works of or from an article (such as a translation), to include in a collective work (such as an anthology), to text or data mine the article, including for commercial purposes without permission from Elsevier

CC BY NC SA: For non-commercial purposes you may distribute and copy the article, create extracts, abstracts and other revised versions, adaptations or derivative works of or from an article (such as a translation), to include in a collective work (such as an anthology), to text and data mine the article and license new adaptations or creations under identical terms without permission from Elsevier

CC BY NC ND: For non-commercial purposes you may distribute and copy the article and include it in a collective work (such as an anthology), provided you do not alter or modify the article, without permission from Elsevier

Any commercial reuse of Open Access articles published with a CC BY NC SA or CC BY NC ND license requires permission from Elsevier and will be subject to a fee.

Commercial reuse includes:

- Promotional purposes (advertising or marketing)
- Commercial exploitation (e.g. a product for sale or loan)
- Systematic distribution (for a fee or free of charge)

Please refer to Elsevier's Open Access Policy for further information.

21. **Other Conditions**:

v1.7

If you would like to pay for this license now, please remit this license along with your payment made payable to "COPYRIGHT CLEARANCE CENTER" otherwise you will be invoiced within 48 hours of the license date. Payment should be in the form of a check or money order referencing your account number and this invoice number 501325650. Once you receive your invoice for this order, you may pay your invoice by credit card. Please follow instructions provided at that time.

Make Payment To:
Copyright Clearance Center
Dept 001
P.O. Box 843006
Boston, MA 02284-3006

For suggestions or comments regarding this order, contact RightsLink Customer Support: customercare@copyright.com or +1-877-622-5543 (toll free in the US) or +1-978-646-2777.

Gratis licenses (referencing $0 in the Total field) are free. Please retain this printable license for your reference. No payment is required.

ELSEVIER LICENSE
TERMS AND CONDITIONS

Jul 13, 2014

This is a License Agreement between Dajena Tomco ("You") and Elsevier ("Elsevier") provided by Copyright Clearance Center ("CCC"). The license consists of your order details, the terms and conditions provided by Elsevier, and the payment terms and conditions.

All payments must be made in full to CCC. For payment instructions, please see information listed at the bottom of this form.

Supplier	Elsevier Limited The Boulevard,Langford Lane Kidlington,Oxford,OX5 1GB,UK
Registered Company Number	1982084
Customer name	Dajena Tomco
Customer address	40425 Aynesley st CLINTON TOWNSHIP, MI 48038
License number	3405970005082
License date	Jun 11, 2014
Licensed content publisher	Elsevier
Licensed content publication	Journal of Inorganic Biochemistry
Licensed content title	Inhibition of the 26S proteasome as a possible mechanism for toxicity of heavy metal species
Licensed content author	Dajena Tomco,Sara Schmitt,Mary Jane Heeg,Q. Ping Dou,Cláudio N. Verani
Licensed content date	March 2014
Licensed content volume number	132
Licensed content issue number	None
Number of pages	8
Start Page	96
End Page	103
Type of Use	reuse in a thesis/dissertation
Intended publisher of new work	other
Portion	full article
Format	both print and electronic

Are you the author of this Elsevier article?	Yes
Will you be translating?	No
Title of your thesis/dissertation	Proteasome Inhibition by Metal Complexes as a New Route for anticancer therapy
Expected completion date	Sep 2014
Estimated size (number of pages)	300
Elsevier VAT number	GB 494 6272 12
Permissions price	0.00 USD
VAT/Local Sales Tax	0.00 USD / 0.00 GBP
Total	0.00 USD
Terms and Conditions	

INTRODUCTION

1. The publisher for this copyrighted material is Elsevier. By clicking "accept" in connection with completing this licensing transaction, you agree that the following terms and conditions apply to this transaction (along with the Billing and Payment terms and conditions established by Copyright Clearance Center, Inc. ("CCC"), at the time that you opened your Rightslink account and that are available at any time at http://myaccount.copyright.com).

GENERAL TERMS

2. Elsevier hereby grants you permission to reproduce the aforementioned material subject to the terms and conditions indicated.

3. Acknowledgement: If any part of the material to be used (for example, figures) has appeared in our publication with credit or acknowledgement to another source, permission must also be sought from that source. If such permission is not obtained then that material may not be included in your publication/copies. Suitable acknowledgement to the source must be made, either as a footnote or in a reference list at the end of your publication, as follows:

"Reprinted from Publication title, Vol /edition number, Author(s), Title of article / title of chapter, Pages No., Copyright (Year), with permission from Elsevier [OR APPLICABLE SOCIETY COPYRIGHT OWNER]." Also Lancet special credit - "Reprinted from The Lancet, Vol. number, Author(s), Title of article, Pages No., Copyright (Year), with permission from Elsevier."

4. Reproduction of this material is confined to the purpose and/or media for which permission is hereby given.

5. Altering/Modifying Material: Not Permitted. However figures and illustrations may be

altered/adapted minimally to serve your work. Any other abbreviations, additions, deletions and/or any other alterations shall be made only with prior written authorization of Elsevier Ltd. (Please contact Elsevier at permissions@elsevier.com)

6. If the permission fee for the requested use of our material is waived in this instance, please be advised that your future requests for Elsevier materials may attract a fee.

7. Reservation of Rights: Publisher reserves all rights not specifically granted in the combination of (i) the license details provided by you and accepted in the course of this licensing transaction, (ii) these terms and conditions and (iii) CCC's Billing and Payment terms and conditions.

8. License Contingent Upon Payment: While you may exercise the rights licensed immediately upon issuance of the license at the end of the licensing process for the transaction, provided that you have disclosed complete and accurate details of your proposed use, no license is finally effective unless and until full payment is received from you (either by publisher or by CCC) as provided in CCC's Billing and Payment terms and conditions. If full payment is not received on a timely basis, then any license preliminarily granted shall be deemed automatically revoked and shall be void as if never granted. Further, in the event that you breach any of these terms and conditions or any of CCC's Billing and Payment terms and conditions, the license is automatically revoked and shall be void as if never granted. Use of materials as described in a revoked license, as well as any use of the materials beyond the scope of an unrevoked license, may constitute copyright infringement and publisher reserves the right to take any and all action to protect its copyright in the materials.

9. Warranties: Publisher makes no representations or warranties with respect to the licensed material.

10. Indemnity: You hereby indemnify and agree to hold harmless publisher and CCC, and their respective officers, directors, employees and agents, from and against any and all claims arising out of your use of the licensed material other than as specifically authorized pursuant to this license.

11. No Transfer of License: This license is personal to you and may not be sublicensed, assigned, or transferred by you to any other person without publisher's written permission.

12. No Amendment Except in Writing: This license may not be amended except in a writing signed by both parties (or, in the case of publisher, by CCC on publisher's behalf).

13. Objection to Contrary Terms: Publisher hereby objects to any terms contained in any purchase order, acknowledgment, check endorsement or other writing prepared by you, which terms are inconsistent with these terms and conditions or CCC's Billing and Payment terms and conditions. These terms and conditions, together with CCC's Billing and Payment terms and conditions (which are incorporated herein), comprise the entire agreement between you and publisher (and CCC) concerning this licensing transaction. In

the event of any conflict between your obligations established by these terms and conditions and those established by CCC's Billing and Payment terms and conditions, these terms and conditions shall control.

14. Revocation: Elsevier or Copyright Clearance Center may deny the permissions described in this License at their sole discretion, for any reason or no reason, with a full refund payable to you. Notice of such denial will be made using the contact information provided by you. Failure to receive such notice will not alter or invalidate the denial. In no event will Elsevier or Copyright Clearance Center be responsible or liable for any costs, expenses or damage incurred by you as a result of a denial of your permission request, other than a refund of the amount(s) paid by you to Elsevier and/or Copyright Clearance Center for denied permissions.

LIMITED LICENSE

The following terms and conditions apply only to specific license types:

15. **Translation**: This permission is granted for non-exclusive world **English** rights only unless your license was granted for translation rights. If you licensed translation rights you may only translate this content into the languages you requested. A professional translator must perform all translations and reproduce the content word for word preserving the integrity of the article. If this license is to re-use 1 or 2 figures then permission is granted for non-exclusive world rights in all languages.

16. **Posting licensed content on any Website**: The following terms and conditions apply as follows: Licensing material from an Elsevier journal: All content posted to the web site must maintain the copyright information line on the bottom of each image; A hyper-text must be included to the Homepage of the journal from which you are licensing at http://www.sciencedirect.com/science/journal/xxxxx or the Elsevier homepage for books at http://www.elsevier.com; Central Storage: This license does not include permission for a scanned version of the material to be stored in a central repository such as that provided by Heron/XanEdu.

Licensing material from an Elsevier book: A hyper-text link must be included to the Elsevier homepage at http://www.elsevier.com . All content posted to the web site must maintain the copyright information line on the bottom of each image.

Posting licensed content on Electronic reserve: In addition to the above the following clauses are applicable: The web site must be password-protected and made available only to bona fide students registered on a relevant course. This permission is granted for 1 year only. You may obtain a new license for future website posting.

For journal authors: the following clauses are applicable in addition to the above: Permission granted is limited to the author accepted manuscript version* of your paper.

***Accepted Author Manuscript (AAM) Definition:** An accepted author manuscript (AAM) is the author's version of the manuscript of an article that has been accepted for publication and which may include any author-incorporated changes suggested through the processes of submission processing, peer review, and editor-author communications. AAMs do not include other publisher value-added contributions such as copy-editing, formatting, technical enhancements and (if relevant) pagination.

You are not allowed to download and post the published journal article (whether PDF or HTML, proof or final version), nor may you scan the printed edition to create an electronic version. A hyper-text must be included to the Homepage of the journal from which you are licensing at http://www.sciencedirect.com/science/journal/xxxxx. As part of our normal production process, you will receive an e-mail notice when your article appears on Elsevier's online service ScienceDirect (www.sciencedirect.com). That e-mail will include the article's Digital Object Identifier (DOI). This number provides the electronic link to the published article and should be included in the posting of your personal version. We ask that you wait until you receive this e-mail and have the DOI to do any posting.

Posting to a repository: Authors may post their AAM immediately to their employer's institutional repository for internal use only and may make their manuscript publically available after the journal-specific embargo period has ended.

Please also refer to Elsevier's Article Posting Policy for further information.

18. **For book authors** the following clauses are applicable in addition to the above: Authors are permitted to place a brief summary of their work online only.. You are not allowed to download and post the published electronic version of your chapter, nor may you scan the printed edition to create an electronic version. **Posting to a repository:** Authors are permitted to post a summary of their chapter only in their institution's repository.

20. **Thesis/Dissertation**: If your license is for use in a thesis/dissertation your thesis may be submitted to your institution in either print or electronic form. Should your thesis be published commercially, please reapply for permission. These requirements include permission for the Library and Archives of Canada to supply single copies, on demand, of the complete thesis and include permission for UMI to supply single copies, on demand, of the complete thesis. Should your thesis be published commercially, please reapply for permission.

Elsevier Open Access Terms and Conditions

Elsevier publishes Open Access articles in both its Open Access journals and via its Open Access articles option in subscription journals.

Authors publishing in an Open Access journal or who choose to make their article Open

Access in an Elsevier subscription journal select one of the following Creative Commons user licenses, which define how a reader may reuse their work: Creative Commons Attribution License (CC BY), Creative Commons Attribution – Non Commercial - ShareAlike (CC BY NC SA) and Creative Commons Attribution – Non Commercial – No Derivatives (CC BY NC ND)

Terms & Conditions applicable to all Elsevier Open Access articles:

Any reuse of the article must not represent the author as endorsing the adaptation of the article nor should the article be modified in such a way as to damage the author's honour or reputation.

The author(s) must be appropriately credited.

If any part of the material to be used (for example, figures) has appeared in our publication with credit or acknowledgement to another source it is the responsibility of the user to ensure their reuse complies with the terms and conditions determined by the rights holder.

Additional Terms & Conditions applicable to each Creative Commons user license:

CC BY: You may distribute and copy the article, create extracts, abstracts, and other revised versions, adaptations or derivative works of or from an article (such as a translation), to include in a collective work (such as an anthology), to text or data mine the article, including for commercial purposes without permission from Elsevier

CC BY NC SA: For non-commercial purposes you may distribute and copy the article, create extracts, abstracts and other revised versions, adaptations or derivative works of or from an article (such as a translation), to include in a collective work (such as an anthology), to text and data mine the article and license new adaptations or creations under identical terms without permission from Elsevier

CC BY NC ND: For non-commercial purposes you may distribute and copy the article and include it in a collective work (such as an anthology), provided you do not alter or modify the article, without permission from Elsevier

Any commercial reuse of Open Access articles published with a CC BY NC SA or CC BY NC ND license requires permission from Elsevier and will be subject to a fee.

Commercial reuse includes:

- Promotional purposes (advertising or marketing)
- Commercial exploitation (e.g. a product for sale or loan)
- Systematic distribution (for a fee or free of charge)

Please refer to Elsevier's Open Access Policy for further information.

21. **Other Conditions**:

v1.7

If you would like to pay for this license now, please remit this license along with your payment made payable to "COPYRIGHT CLEARANCE CENTER" otherwise you will be invoiced within 48 hours of the license date. Payment should be in the form of a check or money order referencing your account number and this invoice number 501325643. Once you receive your invoice for this order, you may pay your invoice by credit card. Please follow instructions provided at that time.

Make Payment To:
Copyright Clearance Center
Dept 001
P.O. Box 843006
Boston, MA 02284-3006

For suggestions or comments regarding this order, contact RightsLink Customer Support: customercare@copyright.com or +1-877-622-5543 (toll free in the US) or +1-978-646-2777.

Gratis licenses (referencing $0 in the Total field) are free. Please retain this printable license for your reference. No payment is required.

ABSTRACT

PROBING PROTEASOME INHIBITON BY METAL COMPLEXES AS A NEW MECHANISM FOR ANTICANCER THERAPY

by

DAJENA TOMCO

December 2014

Advisor: Dr. Cláudio N. Verani

Major: Chemistry (Inorganic)

Degree: Doctor of Philosophy

The scope of this thesis is focused towards the development of metal-containing coordination compounds as potential therapeutic agents. Efforts of this research involve the design, synthesis, and purification of these complexes, as well as their evaluation by spectroscopic, spectrometric, and electrochemical characterization. The antineoplastic properties of these metal-containing pro-drugs are tested against the inhibition activity of the 26S proteasome. Selected metal ions ranging from transition to main group elements have been incorporated in various ligand systems containing phenolate and pyridyl donor sets. The mechanistic behavior of these complexes in solution has been thoroughly investigated along with their *in vitro* anticancer properties against the growth of prostate cancer PC-3 cells. It has been demonstrated that apoptosis induction of the PC-3 cells is due to the inhibition activity of the 26S proteasome upon treatment of various concentrations of these metal-based pro-drugs. The antiproliferative effects of these complexes are highly dependent on the charge, redox activity of the metal ions, as well as the nature of the chelating ligands.

AUTOBIOGRAPHICAL STATEMENT

DAJENA TOMCO

EDUCATION

Ph.D. Inorganic Chemistry, Wayne State University, Detroit, MI – 2014
Dissertation: "Probing Proteasome Inhibition by Metal Complexes as a New Mechanism for Anticancer Therapy." *Advisor: Cláudio N. Verani*

B.Sc. Chemistry, Wayne State University, Detroit, MI – August 2008

PUBLICATIONS

1. Tomco, D.; Schmitt, S.; Heeg, M. J.; Dou, Q. P.; Verani, C. N. "Inhibition of the 26S Proteasome as a Possible Mechanism for Toxicity of Heavy Metal Species." *J. Inorg. Biochem*. **2014**, *132*, 96 – 103.

2. Tomco, D.; Xavier, F. R.; Verani, C. N. "Probing Ligand Dissociation in Co(III) Complexes as Viable Mechanism for the Inhibition of the 20S Proteasome." *Inorg. Chim. Acta* **2012**, *393*, 269 – 275. *Special Issue: Metals in Medicine.*

3. Frezza, M.; Schmitt, S.; Tomco, D.; Chen, D.; Dou, Q. P.; Verani, C. N. "Inhibition of the Proteasome Activity by Gallium(III) Complexes." *Encyclopedia of Metalloproteins*, Springer, **2012**.

4. Tomco, D.; Schmitt, S.; Heeg, M. J.; Ksebati, B.; Dou, Q. P.; Verani, C. N. "Effects of Tethered Ligands and of Metal Oxidation State on the Interactions of Cobalt Complexes with the 26S Proteasome." *J. Inorg. Biochem*. **2011**, *105*, 1759 – 1766.

5. Frezza, M.; Hindo, S. S.; Chen, D.; Davenport, A.; Schmitt, S.; Tomco, D.; Dou, Q. P. "Novel Metals and Metal Complexes as Platforms for Cancer Therapy." *Curr. Pharm. Des.* **2010**, *16*, 1813 – 1825.

6. Frezza, M.; Hindo, S. S.; Tomco, D.; Allard, M.; Cui, Q. C.; Heeg, M. J.; Chen, D.; Dou, Q. P.; Verani, C. N. "Comparative Activities of Nickel(II) and Zinc(II) Complexes of Asymmetric [NN'O] Ligands as 26S Proteasome Inhibitors." *Inorg. Chem.* **2009**, *48*, 5928 – 5937.

7. Hindo, S. S.; Frezza, M.; Tomco, D.; Heeg, M. J.; Hryhorczuk, L.; McGarvey, B. R.; Dou, Q. P.; Verani, C. N. "Metals in Anticancer Therapy: Copper(II) Complexes as Inhibitors of the 26S Proteasome." *Eur. J. Med. Chem.* **2009**, *44*, 4353 – 4361.

8. Tomco, D.; Schmitt, S.; Heeg, M. J.; Dou, Q. P.; Verani, C. N. "*In Vitro* Studies of Gallium(III) and Zinc(II) Species on the Inhibition Activity of the 26S Proteasome." *In preparation.*

9. Yang, Zh.; Tomco, D.; Verani, C. N.; Rodger, M. T. "Molecular Level Probing of the Mechanism of Metal-based Anticancer Candidates by ESI FT-ICR Mass Spectrometry." *In preparation.*

AWARDS, HONORS, AND SCHOLARSHIPS

- Summer Dissertation Fellowship, May 2013 – August 2013
- Wayne State University, Graduate Exhibition 1st Prize Award for best poster presentation, March 2013
- Thomas C. Rumble University Graduate Fellowship, August 2012 – May 2013
- Graduate Research Fellowship, Office of the Vice President for Research, August 2011 – August 2012
- Esther & Stanley Kirschner General Chemistry Teaching Award, April 2011
- Pilot Grant Research Fellowship, Karmanos Cancer Institute, May 2010 – August 2010
- Graduate School Citation for Excellence in Teaching Award, April 2010
- Honor Citation for Teaching Service in Chemistry Award, April 2009
- Phi Lambda Upsilon Undergraduate Research Award, April 2008